Synthesis and Characterization of Novel Phosphorus Containing Anionic Compounds



Chenyang Hu

The Queen's College

University of Oxford

A thesis submitted for the degree of

Doctor of Philosophy

Hilary 2025

Abstract

Synthesis and Characterization of Phosphorus Containing Novel Anionic Compounds

Chenyang Hu — The Queen's College

DPhil Inorganic Chemistry — Hilary 2025

This thesis describes the synthesis and reactivity of two novel phosphorus containing anion, the cyapho(dicyano)methanide salt and the anionic imine supported phosphinidene oxide. The imine supported phosphinidene oxide can be further functionalized to amido supported phosphinidene oxide, which showed similar reactivity to organo-amide.

Chapter 1. An overview of multiple bonds between heavier p-block elements is presented, with a focus on key factors for their stabilization and their synthetic pathways. Recent advance in main group oxide is also detailed.

Chapter 2. The synthesis of a cyapho(dicyano)methanide salt, [K(18-crown-6)][$C(CN)_2(CP)$] was described. Subsequent reactivity studies reveal that that cyapho(dicyano)methanide ion is susceptible to protonation with strong acids to afford the parent acid $HC(CN)_2(CP)$. The reactivity of the cyaphide moiety in $[C(CN)_2(CP)]^-$ was explored through coordination to metal centers and in cycloaddition reactions with azides.

Chapter 3. Through both steric protection and electrostatic repulsion, an imine supported phosphinidene oxide $RNPO^-$ was isolated. DFT calculation and crystallographic data revealed a three-center-four-electron π-bond over the N–P–O moiety.

Chapter 4. The reactivity of imine supported phosphinidene oxide $RNPO^-$ was explored. Selective functionalization was achieved for all three atoms in the N–P–O moiety. When reacting with small electrophiles such as BnBr, the nitrogen atom is functionalized, affording

an amido phosphinidene oxide. Alternatively, when reacted with a bulky silyl group, *O*-functionalization occurs. Oxidants selectively react with P(III) center, leading to phosphorus(V) compounds.

Chapter 5. Phospha-(aza)-Wittig reaction is detailed. Amido phosphinidene oxide is able to replace the role of carbonyl compounds in Wittig reaction and react with phosphorus ylides, affording the corresponding phosphaalkene or phosphaimine.

Chapter 6. The isolation of a phosphinidene sulfide and a phosphinidene selenide is detailed. The amido phosphinidene oxide, as a heavier analogue of organo-amides, is able to react with Lawesson's reagent (LR) or Woollin's reagent (WR), yielding a dimer between phosphinidene chalcogenide and monomer of LR or WR. Addition of DMAP leads to the cleavage of the dimer, affording the phosphinidene chalcogenide monomers.

Acknowledgements

First and foremost, I would like to thank my supervisor, Professor Jose Goicoechea, for giving me the opportunity, resource and freedom to conduct research in his group. I couldn't achieve any of these without his trust, support and mentorship.

Thank you to all of the post-docs and D.Phil students who have I have had the pleasure of sharing this lab with over the years. The Goicoechea group has always been incredibly friendly and fun to work with, both in Oxford and Indiana University. Dr. Eric Yang, Dr. Joey Feld, Dr. Matt Reveley, Dr. Stephanie Urwin and Dr. Olie Townrow, thank you for showing me around the lab and teaching me how this group does synthetic chemistry. Dr. Josh Abbenseth, thank you for proof-reading my first Angewandte paper in the group. Dr. Lilian Szych for being my lab companion in nights and weekends, and all the ATS we had together for lunch. Dr. Aaron King and Alex Mapp, for all the drinks we shared, also the great times we had in San Sebastián together with Eric.

Special thanks to my IU labmates Dr. Álvaro García-Romero and Debanik Ray. We had a really hard but rewarding time setting up the new lab in Bloomington. It has been a pleasant journey working with you, and I will always remember all the chicken-kasu curry and AMF we had together.

I am also thankful to all the departmental stuff who offered help to me along the way. Especially to Dr. Maren Pink at IUMSC, thank you for sorting out all my complex crystals, and your trust on me to taking care of the instrument. I learned so much from you about both crystallographic and instrumental knowledge. Dr. Nick Rees and Dr. Arifuzzaman Tapash for helping me running NMR measurement.

Thank you to my parents for your continuous support and trust on me. Without you I wouldn't be who I am today. You provide me everything you had, and lift me up to see a bigger world.

Finally, special thanks to Miss. Yining Xia, thank you for trusting me with your life, and travelling around the world with me. I cannot imagine how my life would be without your emotional support and all the pleasure you bring to me. We have set our footprint around half of the earth, I am looking forward to explore the rest of world together with you.

List of Abbreviations

18-crown-6	1,4,7,10,13-pentaoxacyclopentadecane
Å	angstrom
Ad	1-adamantyl
anal.	analysis
ATR	attenuated total reflectance
au	atomic units
av	average
Bn	benzyl
BzK	benzylpotassium
calc	calculated
cm^{-1}	wavenumber
COD	cyclooctadiene
Cp	cyclopentadienyl
Cp*	pentamethylcyclopentadienyl
Cy	cyclohexyl
d	doublet
DFT	density functional theory
Dipp	2,6-diisopropylphenyl
DMAP	4-dimethylaminopyridine
Eind	1,1,3,3,5,5,7,7-octaethyl-s-hydrindacen-4-yl
FT	Fourier-transform
GIAO	gauge-independent atomic orbital
HIPTBr	5′-Bromo-2,2″,4,4″,6,6″-hexakis(1-methylethyl)-1,1′:3′,1″-terphenyl
HOMO	highest occupied molecular orbital
Hz	Hertz
HRMS	high-resolution Mass spectrometry

INT	intermediate
^{i}Pr	*iso*-propyl
IR	infrared
K	kelvin
KHMDS	potassium bis(trimethylsilyl)amide
KOTMS	potassium trimethylsilanolate
kcal	kilocalories
LUMO	lowest unoccupied molecular orbital
LR	Lawesson's reagent
LiHMDS	lithium hexamethyldisilazide
M	molar
MO	molecular orbital
m	multiplet
Me	Methyl
MeCN	Acetonitrile
Mes	2,4,6-$Me_3C_6H_2$
Mes*	2,4,6-$^{t}Bu_3C_6H_2$
mg	milligram
mL	millilitre
mol	mole
NaHMDS	sodium hexamethyldisilazide
NMR	nuclear magnetic resonance
NBO	natural bonding orbital
NRT	natural resonance theory
NPA	natural population analysis
OTf	triflate
Ph	phenyl

ppm	parts per million
PPN	bis(triphenylphosphine)iminium
r.t.	room temperature
s	singlet
sept	septet
t	triplet
Ter	terphenyl
TS	transition state
^{t}Bu	*tert*-butyl
TCM	tricyanomethanide
THF	tetrahydrofuran
TMS	trimethylsilyl
tol	toluene
z	charge
WR	Woollin's reagent
XRD	X-ray diffraction
δ	chemical shift

List of compounds

[Na(18-crown-6)]1	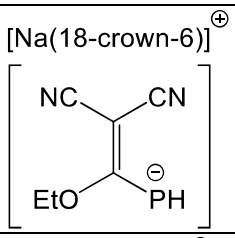
[K(18-cornw-6)]2	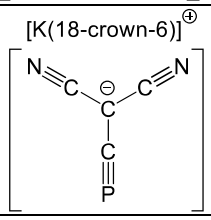
3	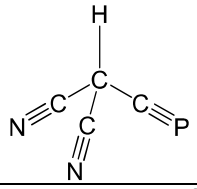
[K(18-crown-6)]4	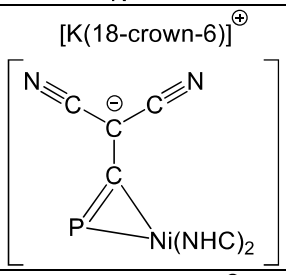
[K(18-crown-6)]5	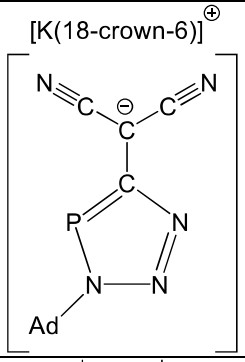
6	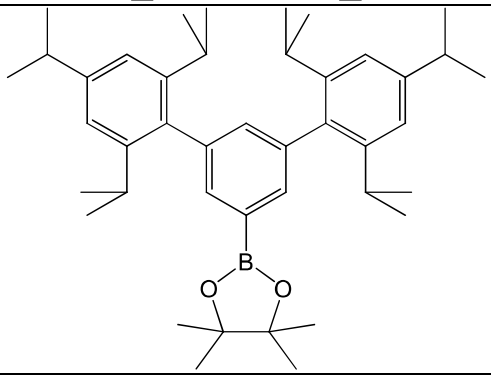

7	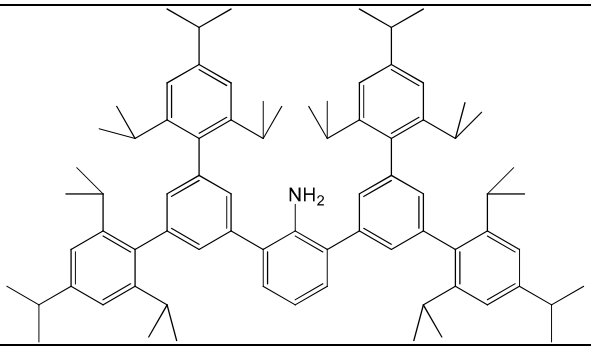
Ar	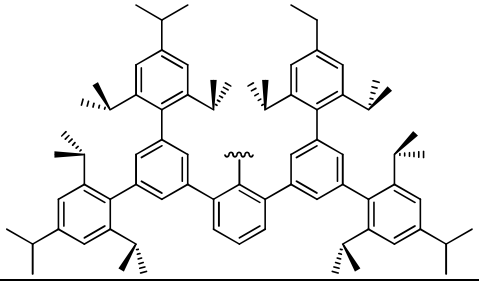
8	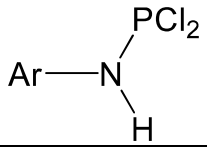
9	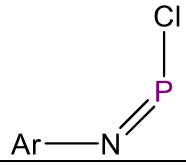
10	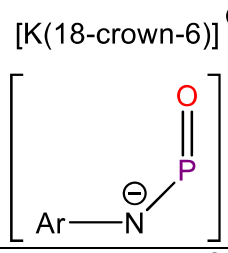
11	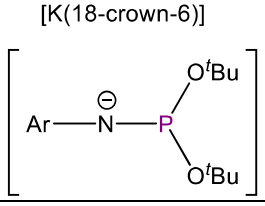
12	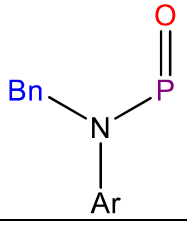

13	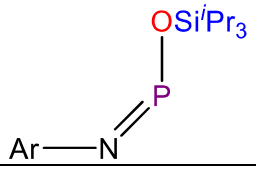
14	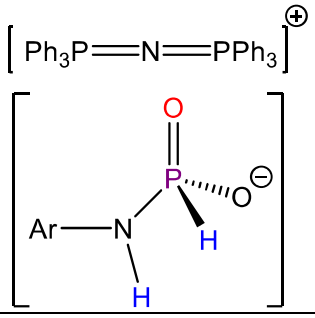
15	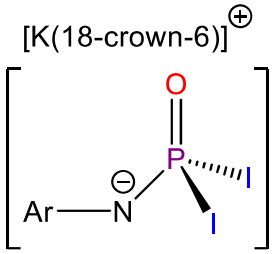
16	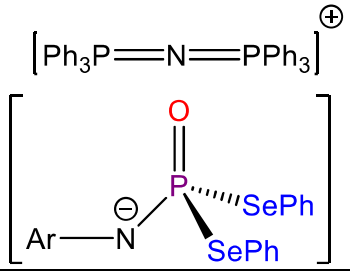
17	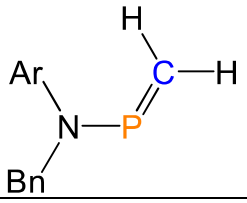
18-*E*	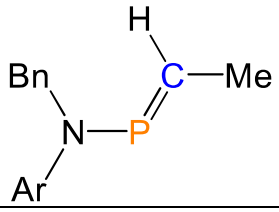
18-*Z*	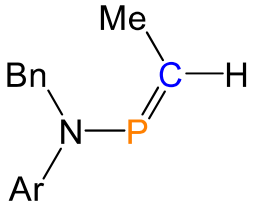

***trans*-19**	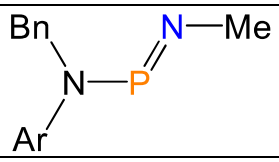
***cis*-19**	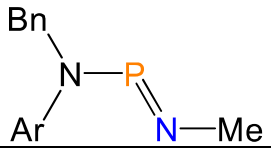
20	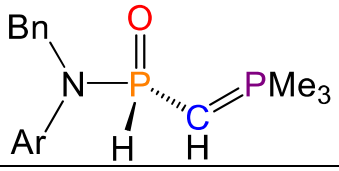
21	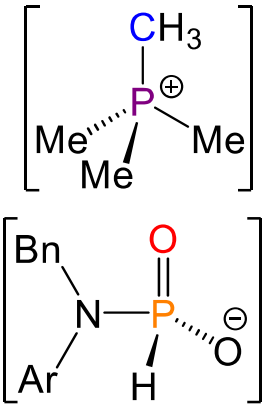
22	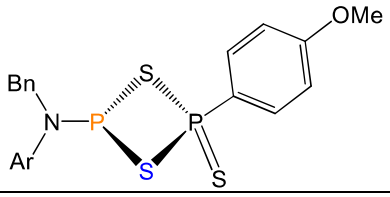
23	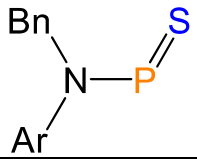
24	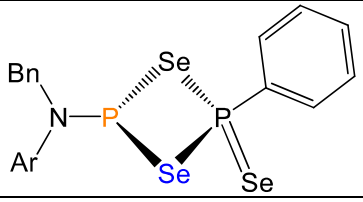
25	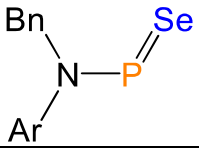

Table of content

1. Introduction 1

1.1 The double bond rule 2

1.2 Key factors to stabilize heavier multiple bonds 4

1.2.1 Steric hindrance—exemplified by the use of terphenyl ligands 4

1.2.2 London dispersion forces 6

1.2.3 Electrostatic repulsion 7

1.3 Main group elements oxides 9

1.3.1 Group 13 element oxide—oxoboryl 10

1.3.2 Group 14 element oxides—silanones and germanones 11

1.3.3 Group 15 element oxide—phosphinidene oxides 14

1.4 Phosphorus in main group multiple bonding 15

1.4.1 The isolobal analogy—phosphorus as a carbon copy 15

1.4.2 Phosphalkenes 16

1.4.3 Phosphalkynes 17

1.4.4 Phosphaketenes and the 2-phosphaethynolate ion 18

1.4.5 Iminophosphanes and iminophosphenium 20

1.5 Phosphinidene precursors and their use in multiple bonds synthesis 22

1.5.1 Phosphaketenes R–P=C=O 22

1.5.2 Phosphoranylidene-phosphines ($ArP{=}PMe_3$) 24

1.5.3 Arene fused phosphinidenes 26

1.6 Project aims 28

1.7 References 30

2. Synthesis, Structure and Reactivity of a Cyapho(dicyano)methanide Salt 37

2.1 Introduction 38

2.2 Rational design of a synthetic route towards a cyapho(dicyano)methanide salt $[C(CP)(CN)_2]^-$ 40

2.3 Synthesis and characterization of a cyapho(dicyano)methanide salt 41

2.4 DFT calculations 43

2.5 Reactivity studies 46

2.5.1 Protonation of **2** 46

2.5.2 Phosphaalkyne-like reactivities of **2** 49

2.6 Conclusions 52

2.7 Experimental section 52

2.7.1 Synthesis of **[Na(18-crown-6)]1** 52

2.7.2 Synthesis of **[K(18-crown-6)]2** 53

2.7.3 Synthesis of **3** 54

2.7.4 Synthesis of **[K(18-crown-6)]4** 55

2.7.5 Synthesis of **[K(18-crown-6)]5** 56

2.8 References 57

3. Isolation and Characterization of an Anionic Imine-Supported Two-Coordinate Phosphinidene Oxide 61

3.1 Introduction 62

3.2 Ligand design 64

3.3 Synthesis of an imine-stabilized phosphinidene oxide $RNPO^-$ 65

3.4 Mechanism of the reaction between **9** and KOTMS 66

3.4.1 1:1 Reaction between **9** and KOTMS 66

3.4.2 1:2 Reaction between **9** and KOTMS 67

3.4.3 1:2 Reaction between **9** and ^{t}BuOK 68

3.5 Crystal structure and DFT calculations of **10** 69

3.6 Conclusions 74

3.7 Experimental section 75

3.7.1 Synthesis of **6** 75

3.7.2 Synthesis of **7** 76

3.7.3 Synthesis of **8** 76

3.7.4 Synthesis of **9** 77

3.7.5 Synthesis of **10** 78

3.7.6 Synthesis of **11** 79

3.8 References 80

4. Functionalization of an Anionic Imine Phosphinidene Oxide $ArNPO^-$ 84

4.1 *N*-Functionalization with electrophiles 85

4.2 *O*-Functionalization with electrophiles 91

4.3 *P*-Functionalization with oxidants 94

4.3.1 Hydrolysis 94

4.3.2 Iodination with iodine 97

4.3.3 Oxidative addition of Se_2Ph_2 100

4.4 Conclusions 103

4.5 Experimental section 104

4.5.1 Synthesis of **12** 104
4.5.2 Synthesis of **13** 105
4.5.4 Synthesis of **15** 107
4.5.5 Synthesis of **16** 108
4.6 References 109
5. A New Twist on the Phospha-(Aza)-Wittig Reaction 111
5.1 Introduction 112
5.2 A phospha-Wittig reaction 114
5.3 A phospha-aza-Wittig reaction 119
5.4 Mechanistic studies of the phospha-Wittig reaction 124
5.5 Comparison between CH_2=PPh_3 and CH_2=PMe_3 128
5.6 Conclusions 130
5.7 Experimental section 130
5.7.1 Synthesis of **17** 130
5.7.2 Synthesis of **18** 131
5.7.3 Synthesis of **19** 132
5.7.4 Synthesis of **20** 133
5.7.5 Synthesis of **21** 135
5.8 References 136
6. Isolation of a Phosphinidene Sulfide and Selenide 139
6.1 Introduction 140
6.2 A phosphinidene sulfide 142
6.3 A phosphinidene selenide 149
6.4 Conclusions 153

6.5 Experimental section 154

6.5.1 Synthesis of **22** from **12** 154

6.5.2 One-pot synthesis of **23** 155

6.5.3 Synthesis of **22** from **23** 156

6.5.4 Independent synthesis of $ArPS_2$(DMAP) 156

6.5.5 Synthesis of **24** from **12** 157

6.5.6 One-pot synthesis of **25** 158

6.5.7 Synthesis of **24** from **25** 160

6.6 References 160

7. Conclusions and Future Work 164

7.1 Conclusions 165

7.2 Future work 166

7.3 Publications 168

7.4 References 168

8. Experimental Details 169

8.1 General synthetic procedures 170

8.2 Characterisation techniques 171

8.2.1 Single crystal X-ray diffraction 171

8.2.2 NMR spectroscopy 177

8.2.3 Elemental analysis 177

8.2.4 IR spectroscopy 177

8.2.5 High-resolution Mass spectroscopy 177

8.2.6 Computational detail 178

8.3 References 178

Chapter 1
Introduction

1.1 The double bond rule

In 1936, Kipping argued that compounds containing multiple bonds such as Si=O, Si=C, and Si=Si could not be isolated.[1] This conclusion was drawn from numerous unsuccessful experimental attempts to synthesize silicon-based analogues of common organic compounds, e.g. ketones and alkenes, using conventional organic synthetic techniques. Instead of forming the expected double bonds, these reactions primarily led to the synthesis of ring structures and oligomers with silicon single bonds. Consequently, the "double bond rule" was established, asserting that elements with a principal quantum number greater than two ($n > 2$) are unable to form stable multiple bonds.

Computational studies have revealed a significant decline in bonding energies for multiple bonds between heavier p-block elements. This phenomenon has been attributed to the heightened inner shell repulsion between the bonded atoms, a factor that remains negligible in light elements.[2] Additionally, s and p_π bonds are inherently weaker than p_σ bonds, making the formation of multiple single bonds energetically more favourable than $\sigma+\pi$ bond. This preference is evidenced in the strong tendency of silicon compounds to undergo oligomerization.[3] However, these observations primarily address the thermodynamic aspects of bond formation, without considering kinetic influences. By modifying the steric and electronic environment, chemists can effectively overcome these kinetic drawbacks, enabling the stabilization and isolation of reactive species containing heavier multiple bonds.

The double bond rule has been repeatedly debunked since the 1970s. The first isolable compounds with multiple bonds between heavier p-block elements were isolated by Ashe in 1971.[4] They demonstrated that the heavier analogue of pyridine, phosphabenzene (**II**) and arsabenzene (**III**), can be synthesized through transmetallation from a stanna-quinone (**I**; Scheme 1.1). The stability of the P=C and As=C double bonds is enhanced as both

phosphabenzene (**II**) and arsabenzene (**III**) have significant aromaticity, which brings extra stabilizing energy to the system.

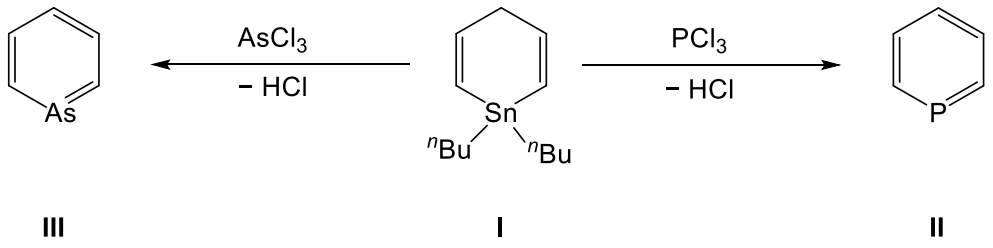

Scheme 1.1. Transmetallation to form a phosphabenzene (**II)** and an arsabenzene (**III)**.

Later, Yoshifuji and colleagues successfully synthesized the first stable compound featuring a phosphorus-phosphorus double bond, a diphosphorene (**IV**), via reduction of the corresponding phosphorus dichloride, followed by dimerization (Scheme 1.2).[5] In the same year, West and co-workers reported the first stable silicon-silicon double bond (**V**), marking another significant milestone in main-group multiple bonding (Scheme 1.2).[6] These two discoveries provided the first examples of homonuclear π-bonding between the heavier p-block elements, further challenging the validity of the "double bond rule." Notably, both diphosphene **IV** and disilene **V** were stabilized through extensive steric protection, employing Mes and Mes* groups, which played a crucial role in their isolation and stability.

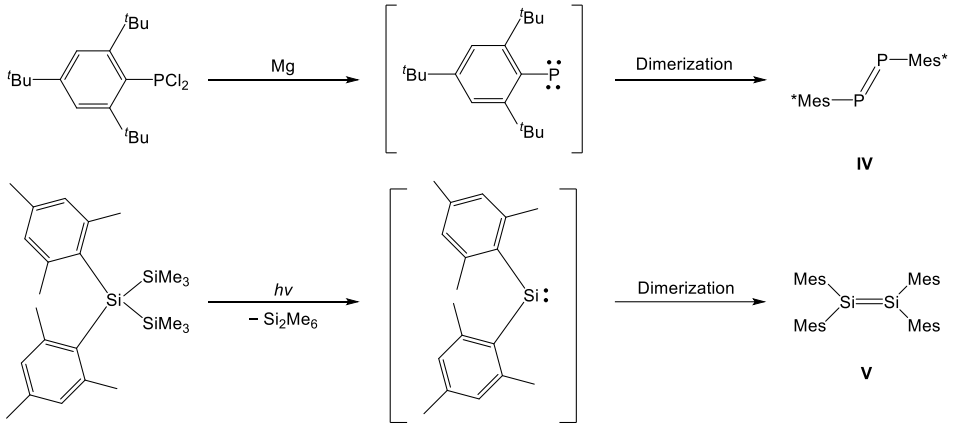

Scheme 1.2. Isolation of a diphosphene (**IV)** and a disilene (**V)**, Mes* = 2,4,6-^{t}Bu$_3$C$_6$H$_2$, Mes = 2,4,6-Me$_3$C$_6$H$_2$.

Whilst heavier main group multiple bonds were first studied out of curiosity, the insight gained through their synthesis and isolation has led to a broad field of research. Applications

range from accessing materials with unusual electronic properties, to mimicking transition metals in small molecule activation and catalysis.[7]

1.2 Key factors to stabilize heavier multiple bonds

1.2.1 Steric hindrance—exemplified by the use of terphenyl ligands

As with the aforementioned isolable diphosphene (**IV)** and disilene (**V)**, the majority of heavier main group multiple bonded species require significant steric protection to prevent dimerization or oligomerization.

The field of sterically stabilized main-group multiple bonding was largely pioneered by Philip P. Power, who introduced the use of terphenyl groups as sterically protecting ligands. By reducing the corresponding terphenyl-substituted main-group halides with alkali metals, Power and his team successfully isolated homonuclear dimers of nearly all p-block elements. These dimers encompass group 13–13 double bonds (**VI**–**IX**), group 15–15 double bonds (**XIII**–**XVI**), and group 14–14 single or triple bonds (**X**–**XII**).[8-15] For group 13 dimers, the presence of a low-lying LUMO often leads to over-reduction, particularly in the cases of aluminum and gallium, resulting in the formation of $[Ter–Al{\equiv}Al–Ter]^{2-}$ (**XVII**) and $[Ter–Ga{\equiv}Ga–Ter]^{2-}$ (**XVIII**), respectively. These anionic species are iso-electronic to alkynes, further expanding the understanding of multiple bonding in heavier main-group elements.[16, 17]

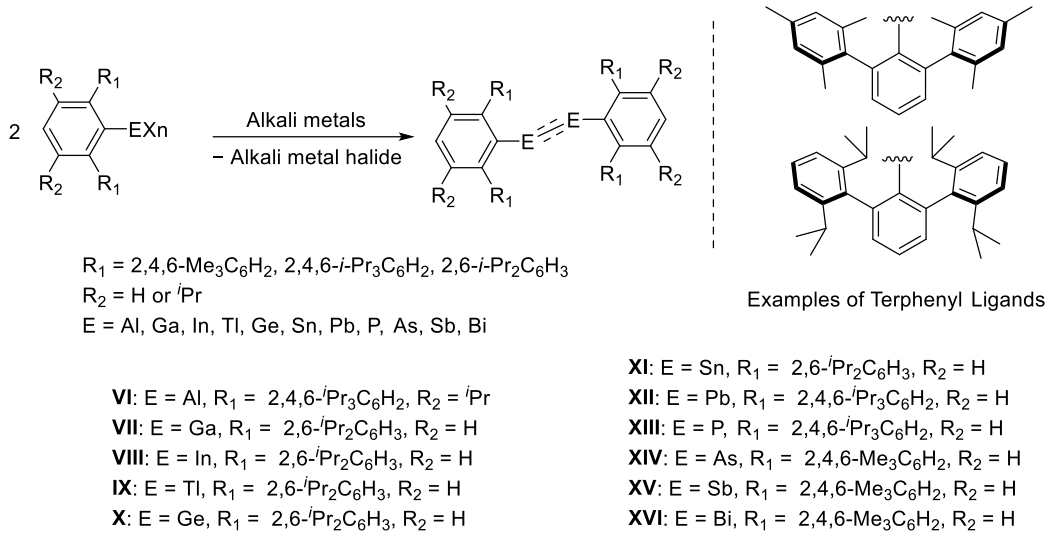

Scheme 1.3. Terphenyl ligand supported homonuclear main group element dimers.

Recently, the Goicoechea group reported the synthesis of terphenyl-ligand-supported heteronuclear dimers featuring Ter–P and Ter–Ga or Ter–In.[18] These P=Ga (**XIX**) and P=In (**XX**) bonds were generated through photolysis of a terphenyl phospha-Wittig reagent Ter–P=PMe_3 in the presence of terphenyl-substituted gallium(I) or indium(I) low-valent centers (Scheme 1.4). Although these compounds are iso-electronic to alkynes, they adopt a *trans*-bent geometry, in contrast to the linear structure of alkynes. This deviation in geometry is attributed to the low-energy, s-character lone pair on phosphorus, which is unable to effectively donate electron density into the empty p-orbital of the gallium or indium center.

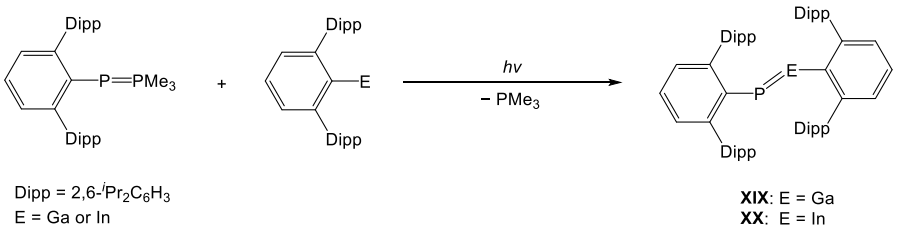

Scheme 1.4. Terphenyl ligand supported heteronuclear main group element dimers of P=Ga/In.

1.2.2 London dispersion forces

London dispersion forces arise from attractions between instantaneously induced dipoles on neighbouring atoms and are the weakest component of Van der Waals interactions. Due to their relative weakness for light atoms, they have been largely considered as a negligible factor in discussions of molecular stability and reactivity.[19]

However, the isolation of heavier main group multiple-bonded species often necessitates the use of highly bulky supporting ligands. As a result, short-range interactions between C–H moieties in the ancillary ligands, along with the overall molecular mass, are significantly enhanced compared to smaller organic molecules. This, in turn, leads to a substantial increase in the magnitude of London dispersion forces.

The introduction of a dispersion-correction in Density Functional Theory (DFT) calculations by Grimme, now allows for London dispersion forces to be quantitively evaluated.[20, 21] The stabilizing effect of London dispersion forces is best illustrated using the example of the dissociation of the group 14 ethylene analogues $[(Me_3Si)_2HC]_2E{=}E[CH(SiMe_3)_2]_2$ (E = Ge (**XXI**), Sn (**XXII**) or Pb (**XXIII**)) into their monomeric form $:E[CH(SiMe_3)_2]_2$.[22] When dispersion-correction is not applied in the DFT calculation, the dimeric form is only favoured by 2.1 kcal mol^{-1} for the tin species (**XXII**), whereas the monomeric form is favoured for the germanium (**XXI**) and lead (**XXIII**) derivatives. However, when employing the dispersion-corrected DFT-D3 method, the association process becomes much more favourable, with London dispersion stabilization energies ranging from 15.2–28.7 kcal mol^{-1} across the three systems in solution phase. These thermodynamic energy profiles indicate that dimerization of the germanium (**XXI**) and tin fragments (**XXII**) is energetically down-hill, in accordance with experimental observations.

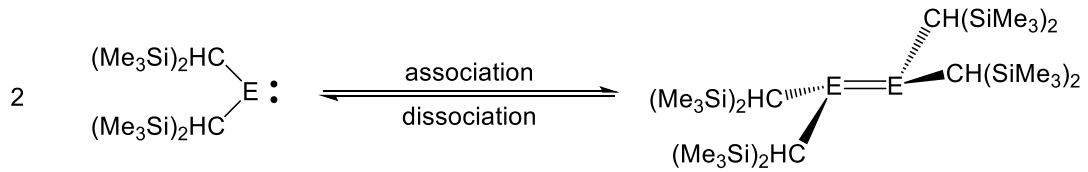

Scheme 1.5. London dispersion forces in the dissociation of group 14 analogues $[(Me_3Si)_2HC]_2E{=}E[CH(SiMe_3)_2]_2$.

The consideration of London dispersion forces has become a crucial factor in designing stable molecules with heavier main group elements multiple bonds now. Power reported a solution-stable distannene $R_2Sn{=}SnR_2$ (R = 2,4,6-Cy_3-C_6H_2) in 2021.[23] While the twelve cyclohexyl groups provide substantial London dispersion attraction between SnR_2 unit and subsequently stabilize the dimeric form, the use of less bulky 2,4,6-triphenylphenyl (2,4,6-Ph_3-C_6H_2) group afford the monomeric stannylene. This finding further underscores the importance of London dispersion forces in the isolation of heavier main group multiple bonds.

1.2.3 Electrostatic repulsion

An alternative strategy is to avoid oligomerization or polymerization of such species by synthesising charged compounds. Electrostatic repulsion can also be used to stabilise such molecules (Scheme 1.6).

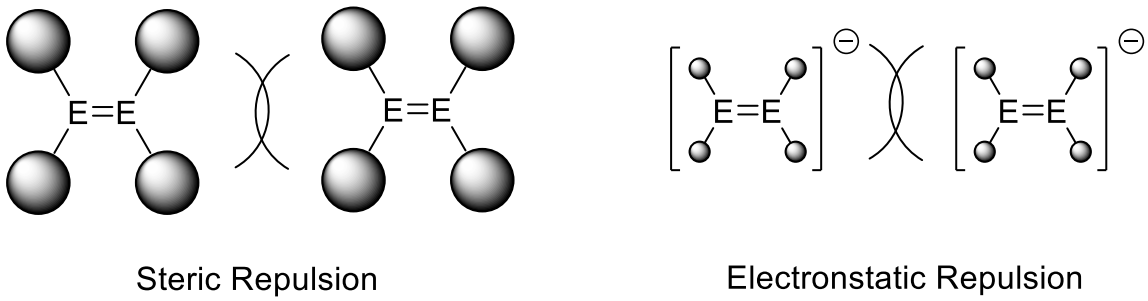

Scheme 1.6. Schematic illustration of the different strategies to stabilize compounds with multiple bonds between the main group elements.

The Goicoechea group has been working on the chemistry of the phosphaethynolate anion, PCO^-, for over a decade.[24] PCO^- is a heavy analogue of the cyanate ion, and it contains a very reactive carbon–phosphorus triple bond. Here, electrostatic repulsion prevents PCO^- from dimerization or oligomerization. Upon loss of the charge (through functionalization or oxidation, for example), the phosphaethynolate moiety will readily dimerize or trimerize. Based on this idea, the group synthesized a serious of small anions that contains multiple bonds between the heavier main group elements such as $AsCO^-$, $PCSe^-$, $AsCS^-$, $AsCSe^-$.[25, 26]

Following a similar synthetic route, the Goicoechea group reported the isolation of the cyapho-cyanamide salt $[Na(18\text{-crown-6})]^+[NCNCP]^-$ (**XXIV**).[27] The importance of electrostatic repulsion in stabilizing the $[NCNCP]^-$ anion is illustrated by the salt metathesis reaction with triphenyl germanium chloride Ph_3GeCl (Scheme 1.7). Upon losing the anionic charge after reaction, the neutral product was not observed. Instead, it directly reacted with another equivalent of $[N(CN)(CP)]^-$, forming a dimeric product **XXV**.

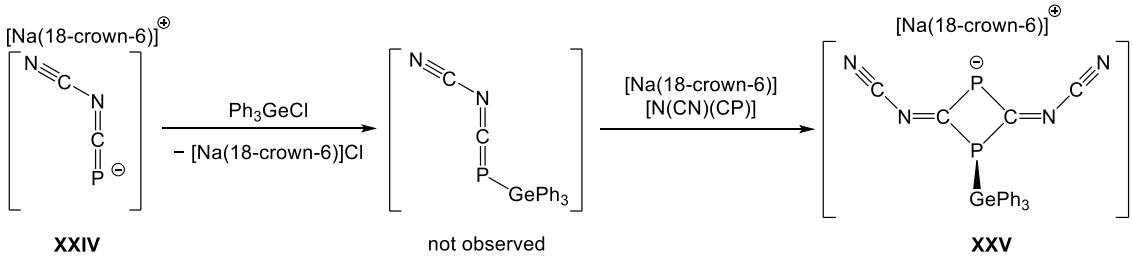

Scheme 1.7. Reaction of [Na(18-crown-6)][N(CN)(CP)] with 0.5 equivalents of Ph_3GeCl to afford a dimeric structure.

Synthesizing main-group multiple bonds in their anionic form can, in certain cases, provide additional electronic stabilization. Due to the inherently weak π-interactions between heavier main-group elements, the corresponding π* orbitals tend to be low in energy and readily accessible. In fact, for most main-group multiple-bonded species, the lowest unoccupied molecular orbital (LUMO) is predominantly composed of the π* orbital, making these species highly reactive. By generating these multiple bonds in their anionic form, the

LUMO energy can be effectively elevated, thereby reducing its accessibility and enhancing the overall stability of these otherwise reactive species.

The synthesis of the molecular aluminum oxide anion serves as another example of anionic charge stabilization in main-group multiple-bonded species. Attempts to isolate a neutral Al=O double bond have consistently resulted in either its oligomerization or the formation of coordinated complexes, where the Al=O moiety is stabilized through interactions with $B(C_6F_5)_3$ for example.[28, 29] However, Aldridge and co-workers successfully isolated an anionic aluminyl oxide species **XXVI** by reacting an aluminyl anion with nitrous oxide (N_2O; Scheme 1.8), demonstrating how anionic charge can be leveraged to stabilize otherwise elusive main-group multiple bonds.[30]

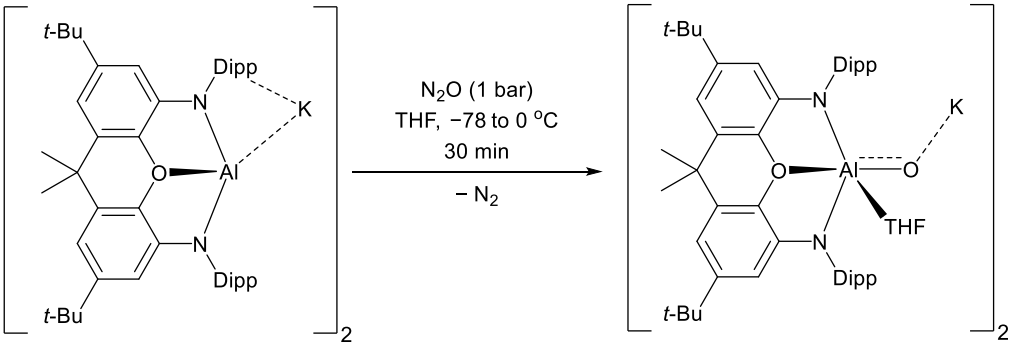

XXVI

Scheme 1.8. Trapping of the aluminyl oxide by the reaction of anionic aluminyl and nitrous oxide N_2O, Dipp = 2,6-$^{i}PrC_6H_3$.

1.3 Main group elements oxides

The synthesis of both homonuclear and heteronuclear multiple bonding between the heavier main group elements have seen significant advancement over the past 40 years; however, the isolation of main-group oxides still remains a significant challenge. As with the previously discussed aluminyl oxide, most main-group oxides exhibit a strong tendency toward dimerization or oligomerization. Two major obstacles hinder the isolation of

monomeric main-group oxides. First, oxygen, having one of the highest electronegativities of the p-block elements, induces a highly polarized π-bond with a main-group center, thereby weakening π-interactions and destabilizing such a species. Second, unlike other heavier main-group multiple-bonded compounds, which typically employ steric protection on both elements, main-group oxides feature a terminal oxygen atom, allowing steric protection to be applied to only one end of the molecule. This asymmetry significantly enhances the thermodynamic preference for oligomerization. Although coordination of Lewis acids or bases can mitigate the polarity of the main-group–oxygen bond, this approach fundamentally alters the electronic structure of the resulting oxide, leading to distinct reactivity profiles. In this thesis, the focus will be exclusively on acid- and base-free main-group oxides, exploring their isolation and intrinsic bonding characteristics.

1.3.1 Group 13 element oxide—oxoboryl

The only acid- and base-free neutral group 13 oxide reported to date is an oxoboryl complex **XXVII**, which was stabilized in the coordination sphere of platinum.[31] In this system, a B≡O triple bond is formed spontaneously via the elimination of bromotrimethylsilane (Me_3SiBr; Scheme 1.9). Theoretical calculations have predicted that the anionic BO^- ligand is iso-electronic to CO, possessing exceptionally strong σ-donating abilities while exhibiting poor π-acceptor characteristics.[32] This unique electronic configuration accounts for the remarkable stability of the sterically unprotected B≡O triple bond when coordinated to platinum.

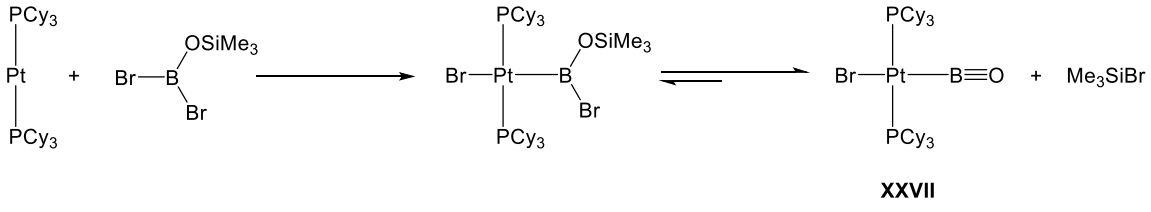

Scheme 1.9. Preparation of *trans*-[$(Cy_3P)_2BrPt(BO)$], Cy = cyclohexyl.

1.3.2 Group 14 elements oxides—silanones and germanones

Group 14 oxides, such as silanones ($R_2Si=O$) and germanones ($R_2Ge=O$), have garnered significant fundamental interest due to their structural and electronic relationship with organic ketones ($R_2C=O$), which represent one of the most important classes of compounds in both industry and biology. Unlike group 13 and 15 oxides, where only one steric protecting group can be incorporated, group 14 oxides benefit from the ability to accommodate two bulky substituents at the central element. As a result, isolable silanones and germanones are typically stabilized through substantial steric protection, which prevents oligomerization and enhances their stability. Furthermore, due to the relative accessibility of low-valent group 14 species, such as silylenes ($R_2Si:$) and germylenes ($R_2Ge:$), silanones and germanones are generally synthesized via oxygen atom transfer (OAT) reactions. These transformations commonly involve the reaction of low-valent silicon or germanium centers with oxygen atom transfer reagents such as N_2O, pyridine N-oxide, or trimethylamine N-oxide, providing a straightforward route to these intriguing main-group oxides.

The first isolated heavy ketone analogue featuring a terminal oxygen atom was a germanone (**XXVIII**), reported by Tamao.[33] To achieve steric stabilization, the Eind group (Eind = 1,1,3,3,5,5,7,7-octaethyl-s-hydrindacen-4-yl) was employed as a bulky protecting group. The Eind group contains four ethyl substituents oriented toward the terminal oxygen, effectively creating a cradle-like steric shield that prevents Ge=O oligomerization. This germanone (**XXVIII**) was synthesized via the reaction of the corresponding germylene with trimethylamine N-oxide ($ONMe_3$; Scheme 1.10). The crystal structure of the germanone (**XXVIII**) revealed a planar germanium center (Σ°: 359.8°) and a short Ge=O bond length (1.6468(5) Å), which is about 6% shorter than the typical Ge–O single-bond length (1.76 Å) found in tetracoordinate Ge(IV) compounds.[34] Notably, this bond length is also comparable to those observed in base-coordinated germanones (1.646(2)–1.672(3) Å).[35, 36] The relatively

small bond length contraction (~6%) suggests that the Ge=O bond exhibits only a modest degree of double-bond character, with a significant contribution from a charge-separated resonance form (Ge^{+}–O^{-}).

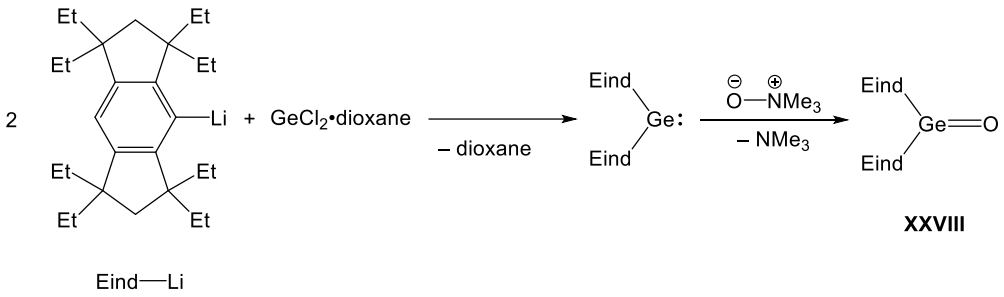

Scheme 1.10. Synthesis of a germanone from oxidation of germylene.

The first isolation of a silanone (**XXIX**) was achieved in the coordination sphere of chromium in 2013.[37] To break the Cr≡Si triple bond and restore the silene-like reactivity at the silicon(II) center, one equivalent of CO was introduced to the chromium complex. Subsequent addition of N_2O as an oxygen atom transfer reagent facilitated the formation of the desired silanone product **XXIX** (Scheme 1.11). Single-crystal X-ray diffraction analysis revealed a short Si=O bond length of 1.526(3) Å, which is slightly shorter than those observed in base-stabilized silanones (1.531–1.579 Å).[38-44] Density Functional Theory (DFT) calculations further indicate that the Si=O bond is highly polarized toward oxygen, with approximately 85% of the Natural Bond Orbital (NBO) density localized on the oxygen atom. This pronounced polarization suggests a strong contribution from the charge-separated resonance form (Si^{+}–O^{-}).

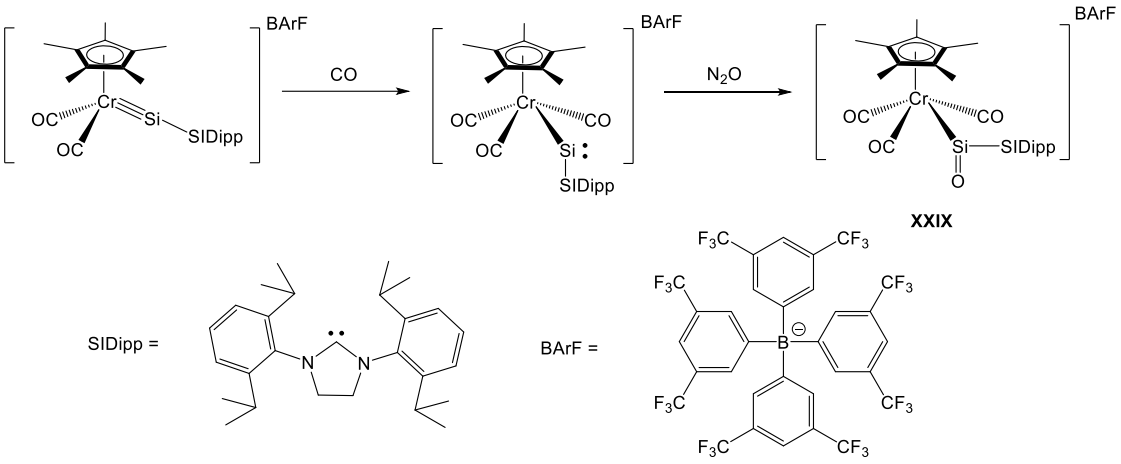

Scheme 1.11. Synthesis of a chromium stabilized silanone.

Subsequently, silanones with intramolecular π-donor were independently characterized by the Inoue group (**XXXI**) and the Kato group (**XXX**). Introducing a π-donor ligand at the silicon center effectively counteracts the electron-withdrawing effect of the oxygen atom, thereby reducing the polarity of the Si–O π-bond, as illustrated in Scheme 1.12. In the study by Kato's group, both an amino and a ylide group were employed as π-donor ligands, whereas Inoue's approach utilized a single N-heterocyclic imine (NHI) ligand.[45, 46] The NHI ligand, due to the presence of nitrogen atoms within the heterocyclic framework, possesses multiple lone pairs that can delocalize toward the silicon center, making it an exceptionally strong electron-donating ligand. Although the Si=O bond lengths in these systems are comparable to previously reported silanones, the notably shortened Si–ligand bond lengths indicate significant π-electron donation from the supporting ligands.

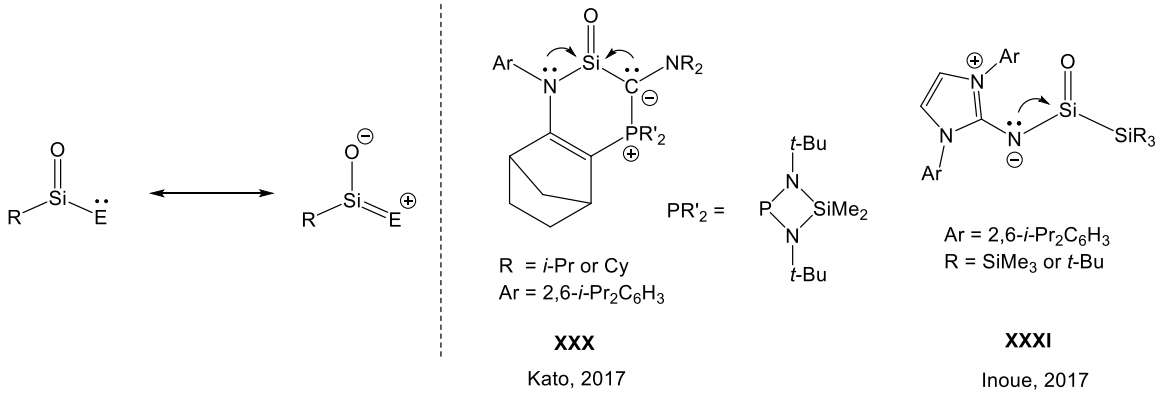

XXX
Kato, 2017

XXXI
Inoue, 2017

Scheme 1.12. Schematic illustration of the internal π-donor ligand stabilized silanones.

1.3.3 Group 15 elements oxide—phosphinidene oxides

The isolation of a two-coordinate phosphinidene oxide (P(III)=O) remains a significant challenge due to the lack of suitable phosphinidene precursors. To date, the only crystallographically characterized two-coordinate P(III)=O double bond is stabilized within the coordination sphere of a transition metal. In 1997, Cummins and co-workers reported a molybdenum complex featuring a terminal PO ligand (**XXXII**), obtained via oxidation of the corresponding molybdenum phosphide (Scheme 1.13).[47] Single-crystal X-ray diffraction analysis revealed a short P=O bond length of 1.49(2) Å, consistent with computed P=O double bond values.[48] Interestingly, the P–Mo bond length (2.079(5) Å) was shorter than that of the parent molybdenum phosphide (2.119(4) Å), which had previously been characterized as a Mo≡P triple bond.[49] The short P–Mo bond length and the nearly linear O–P–Mo geometry (177.6(8)°) suggest significant d_{π}–p_{π} interactions between the metal center and the phosphorus monoxide moiety. Despite the metal coordination, subsequent reactivity studies support the presence of multiple bonding between phosphorus and oxygen. Notably, an insertion reaction was observed between [Mo]–P=O (**XXXII**) and $Zr(Cp)_2Me_2$, wherein the Zr–Me bond was added across the P=O π-bond, yielding a three-coordinate molybdenum phosphide species **XXXIII** (Scheme 1.13).

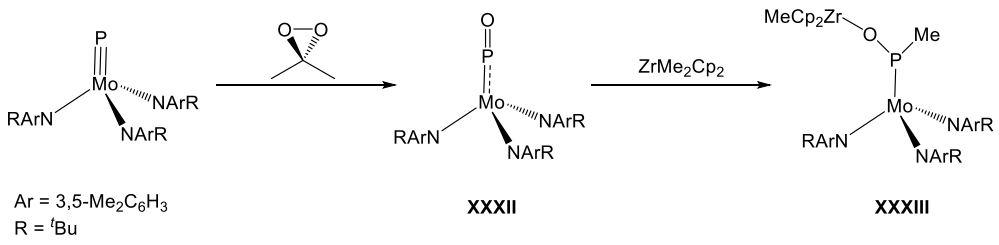

Scheme 1.13. Synthesis of the molybdenum complex with a terminal PO ligand, and its reactivity, Cp = C_5H_5.

Computational studies on organo-phosphinidene oxides suggest that, analogous to parent nitroso compounds (R–N=O), phosphinidene oxides are expected to adopt a bent geometry.[50] Experimental evidence from gas-phase matrix isolation studies of

phosphinidene oxides, including CH_3PO, CH_3OPO, and PhPO, further supports this bent structural preference.[51-53] The contrast between the expected bent geometry of phosphinidene oxides and the experimentally observed linear geometry in the molybdenum phosphide oxide complex suggests that these two species are electronically distinct. While the metal-coordinated [Mo]–P=O (**XXXII**) fragment exhibits a near-linear structure due to strong metal d_π–p_π interactions, free phosphinidene oxides are predicted to adopt a more polarized, bent configuration. Despite these insights, the isolation of a phosphinidene oxide in a free molecular form remains elusive, leaving its structural and electronic properties an open area for further investigation.

1.4 Phosphorus in main group multiple bonding

1.4.1 The isolobal analogy—phosphorus as a carbon copy

Nobel laureate Roald Hoffmann first introduced the isolobal principle as a guideline for linking complex organic and inorganic molecular fragments to well-understood compounds, aiming to provide insights into bonding behaviour. He defined fragments as isolobal when they share similarities—though not exact equivalence—in the number, symmetry, energy, and shape of their frontier orbitals.[54, 55] Originally, this concept was developed to relate organometallic fragments to simpler, better-characterized, organic species. However, its applicability extends across the entire periodic table. While the model offers a valuable conceptual framework, it does not take into account the kinetic or thermodynamic stability of molecules derived from isolobal argurments.

One of the most pertinent analogies in this context is the relationship between a phosphorus atom and a methine fragment (C–H; Scheme 1.14). The similarity in their partially occupied sp^3 orbitals suggests that phosphorus has the potential to replace methine units in organic molecules.

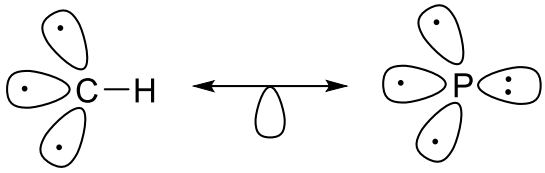

Scheme 1.14. The isolobal relationship between a methine fragment a phosphorus atom.

Beyond isolobality, the diagonal relationship between phosphorus and carbon further reinforces their comparable reactivity. This relationship arises from opposing periodic trends observed when moving across a period and down a group, leading to pairs of second- and third-period elements exhibiting similar characteristics.[56] Carbon and phosphorus form one such pair, sharing certain electronic and chemical properties. While the σ-electronegativity of phosphorus ($\chi_P = 2.19$) is lower than that of carbon ($\chi_C = 2.55$), it remains much closer to carbon than to its group neighbor, nitrogen ($\chi_N = 3.04$). Notably, their π-electronegativities are nearly identical.[57] These parallels in reactivity have paved the way for the development of phospha-organic chemistry. The phosphorus analogues of classic organic compounds such as alkenes, alkynes, imines and iso-nitriles have been documented, and their synthesis will be discussed in detail.

1.4.2 Phosphaalkenes

Phosphaalkenes are among the earliest and most extensively studied examples of unsaturated phospha-organic compounds, with their synthesis and reactivity having been reviewed extensively.[58] The first general strategy for phosphaalkene synthesis was introduced by Becker,[59] who reported the reaction of bis(trimethylsilyl)phosphine with an acyl chloride (Scheme 1.15). Driven by the strong oxophilicity of silicon, the resulting acyl phosphine **XXXIV** undergoes a 1,3-silyl migration from phosphorus to a neighbouring oxygen atom and generates the corresponding phosphaalkene **XXXV**. This characteristic migration has since been adapted to generate a series of phosphaalkenes via the reaction of bis(trimethylsilyl)phosphine with CO_2,[60] $S{=}CCl_2$,[61] and carbodiimides,[62] where silicon

preferentially bonds with oxygen, sulfur, or nitrogen rather than phosphorus. However, this strategy also has limitations, as the generated phosphaalkenes always have a silonate Me_3SiO^- substituting group, reducing the availability of functional groups.

The second widely used approach was first reported by Bickelhaupt in 1984 and involves a base-induced 1,2-elimination of HCl, providing a straightforward route to aryl-substituted phosphaalkenes **XXXVI**.[63] Over the years, other synthetic routes to access phosphaalkene have also been reported, such as a variety of phospha-Wittig reaction.[64-71]

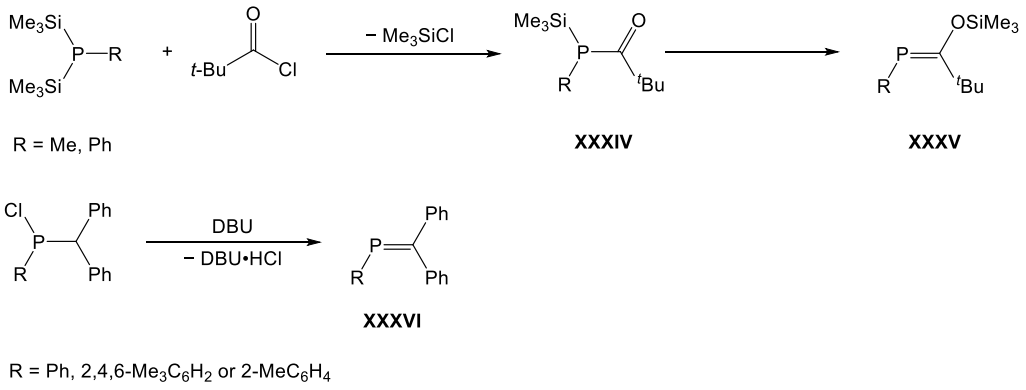

Scheme 1.15. Two general synthetic routes to phosphaalkenes, DBU = 1,8-diazabicyclo[5.4.0]undec-7-ene.

1.4.3 Phosphaalkynes

The parent phosphaalkyne, HC≡P, was first charactrized by Gier in 1961 via infrared spectroscopy and mass spectrometry in gas phase.[72] The first isolable phosphaalkyne was reported by Becker as a *tert*-butyl phosphaalkyne, ^{t}BuC≡P (**XXXVII**).[73] Based on the 1,3-silyl migration strategy for the synthesis of phosphaalkenes, addition of an external base, such as potassium *tert*-butoxide ^{t}BuOK, facilitates the elimination of hexamethyldisiloxane $O[Si(CH_3)_3]_2$, resulting in a C≡P triple bond (Scheme 1.16). Later, a general route to phosphaalkyne (**XXXVIII**) was documented by Guillemin and co-workers using base-induced salt elimination as shown in Scheme 1.16.[74, 75]

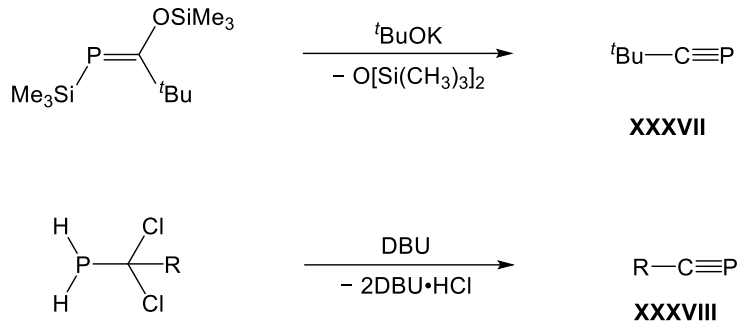

Scheme 1.16. Two general synthetic routes to phosphaalkynes, DBU = 1,8-diazabicyclo[5.4.0]undec-7-ene.

1.4.4 Phosphaketenes and the 2-phosphaethynolate ion

Phosphaketenes, R–P=C=O, are the heavier phosphorus analogues of ketenes $R_2C=C=O$ based on the diagonal rule. Before the discovery of stable salts of the 2-phosphaethynolate anion, phosphaketene chemistry was far less explored compared to phosphaalkenes and phosphaalkynes due to their instability under ambient conditions. The first phosphaketene characterized was *tert*-butyl phosphaketene ^{t}BuP=C=O (**IXL**), which exhibits thermal instability, remaining stable only below –60°C and rapidly undergoing dimerization upon warming to form diphosphekanedione.[76] However, increasing the steric bulk of the substituent from *tert*-butyl to 2,4,6-tri-*tert*-butylphenyl significantly enhanced stability, enabling the monomeric form **XL** to be isolated at room temperature.[77] The synthesis of both phosphaketenes was achieved through the reaction of bis(trimethylsilyl)phosphine with phosgene ($COCl_2$), which led to the elimination of two equivalents of trimethylsilyl chloride (Me_3SiCl) and the formation of the desired phosphaketene species (Scheme 1.17).

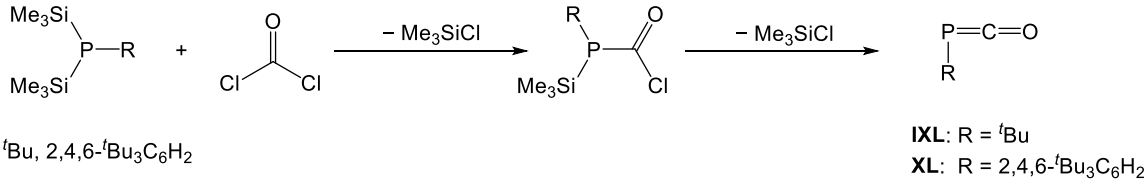

Scheme 1.17. Synthesis of organo-phosphaketenes.

While organo-substituted phosphaketenes are highly unstable and require substantial steric protection to prevent rapid decomposition, their anionic counterpart, the 2-phosphaethynolate anion (PCO^-), exhibits remarkable stability, remaining stable even upon exposure to air. This unexpected stability arises from electrostatic repulsion between anionic species, as previously discussed in Section 1.2.3. The first well-defined synthesis of the 2-phosphaethynolate anion was reported in 1992, when its lithium salt, $Li(DME)_2(PCO)$ (DME = 1,2-dimethoxyethane; **XLI**), was obtained via the reaction of lithium bis(trimethylsilyl)phosphide ($LiP[Si(CH_3)_3]_2$) with dimethyl carbonate (Scheme 1.18).[78] Although the anion was well-characterized, challenges associated with scaling up the synthesis and the instability of the lithium salt limited further studies on this species.

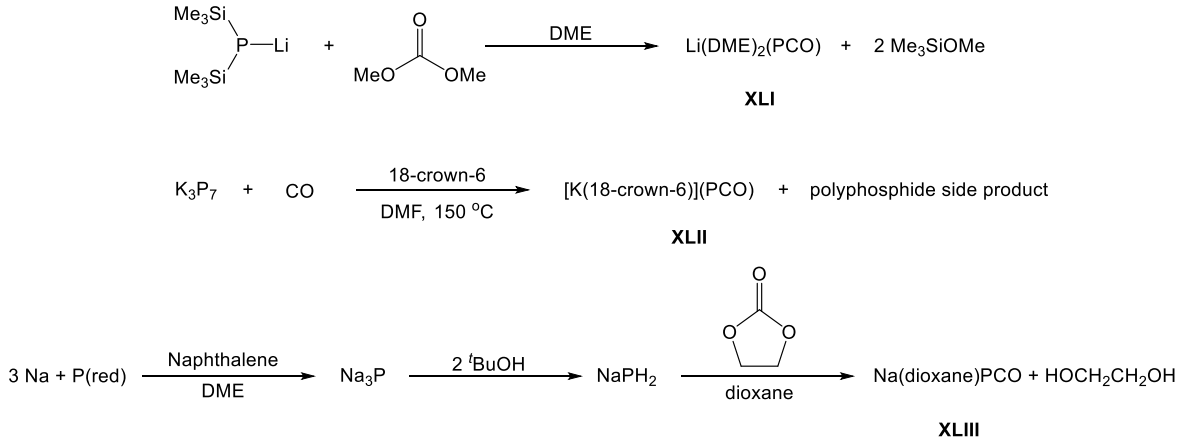

Scheme 1.18. Synthesis of 2-phosphaethynolate salts.

In 2013, the Goicoechea group reported a direct synthesis of the 2-phosphaethynolate ion (PCO^-; **XLII**) using the Zintl anion K_3P_7 and CO gas (Scheme 1.18).[79] The K_3P_7 anion can be conceptualized as a source of three P(–I) donor units coordinated to a P_4 fragment. Upon reaction with CO, the P(–I) species undergo transformation into PCO^-. However, despite its novelty, this method suffers from low atomic economy, making it impractical for large-scale synthesis of PCO^-. A major breakthrough came in 2014, when Grützmacher and co-workers developed a more scalable and practical route to sodium 2-phosphaethynolate, [Na(dioxane)][PCO] (**XLIII**; Scheme 1.18).[80] In this method, metallic sodium and red

phosphorus were used as starting materials, and the key step involved the reaction of *in situ* generated sodium phosphide ($NaPH_2$) with ethylene carbonate, leading to the formation of the corresponding alcohol and sodium 2-phosphaethynolate, with dioxane coordinating to the sodium cation [Na(dioxane)][PCO] (**XLIII**). This improved synthetic accessibility significantly expanded the applicability of 2-phosphaethynolate, establishing it as a versatile synthon for the development of novel organophosphorus compounds.[24]

1.4.5 Iminophosphanes and iminophosphenium

Iminophosphanes are compounds containing P(III)=N double bonds, representing the heavier analogues of imines (R_2C=NR). They are among the earliest isolated main-group species with multiple bonds, and their synthesis was first documented by Niecke in 1973.[81] Through salt metathesis between phosphorus trihalide and lithium bis(trimethylsilyl)amide Li[N($SiMe_3$)$_2$], an intermediate diaminophosphine halide was generated. Upon further heating, this intermediate eliminates one equivalent of trimethylsilylhalide, affording the iminophosphanes **XLIV** (Scheme 1.19). Although the *syn*-elimination of trimethylsilyl halide would theoretically lead to the *Z*-isomer of iminophosphanes, only the *E*-isomer is observed experimentally. This exclusive formation of the *E*-isomer is attributed to the low energy barrier for *E*-*Z* isomerization, allowing rapid interconversion to the thermodynamically more stable *E*-configuration.[82]

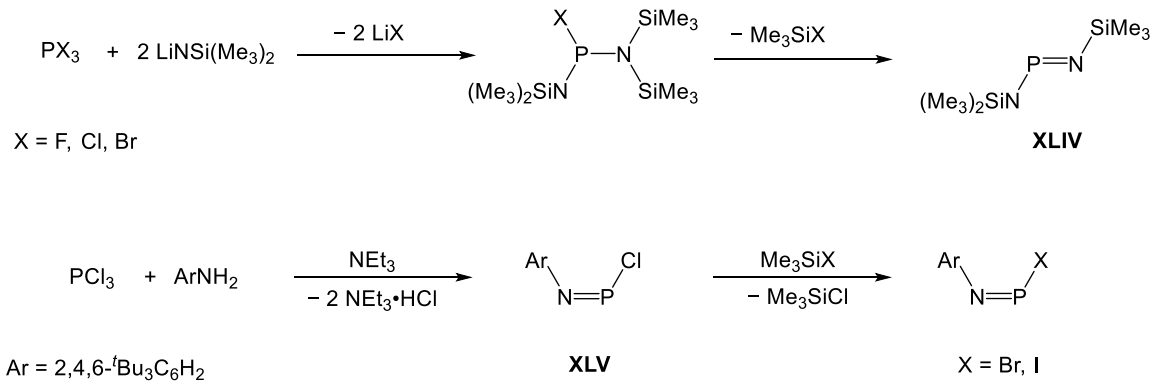

Scheme 1.19. Synthesis of iminophosphanes and imino(halogeno)phosphanes.

A particularly intriguing derivative of iminophosphanes was later synthesized, featuring a halide substituent on the phosphorus atom, giving rise to imino(halogeno)phosphanes (R–N=P–X; X = Cl, Br, I). These compounds can be obtained through hydrogen halide elimination between phosphorus trichloride and a bulky aniline, facilitated by triethylamine (NEt_3; Scheme 1.19).[83] Notably, the imino(chloro)phosphane (**XLV**) adopts a *Z*-geometry in the solid state, in contrast to the typical *E*-configuration observed in conventional iminophosphanes. This unusual *Z*-arrangement is attributed to a geometrically favored lone pair to σ* back-donation, as illustrated in Scheme 1.20. Due to the significant electronegativity difference between phosphorus and chloride, the σ* orbital of the P–Cl bond is highly polarized towards phosphorus, enabling the back-donation from the nitrogen lone pair to P–Cl σ* orbital. This back-donation effect is further corroborated by bond metrics. The N=P bond length is exceptionally short (1.495(4) Å), while the P–Cl bond length (2.142(4) Å) is longer than the expected value for a standard P–Cl single bond (2.10 Å).[84] This weakened P–Cl bond was easily cleaved with addition of Lewis acid such as $AlCl_3$, leading to the formation of an iminophosphenium ion **XLVI**, which features a formal N≡P triple bond (Scheme 1.20). Crystal structure of iminophosphenium **XLVI** revealed a N–P bond length of 1.475(8) Å, closely resembling the N=P bond length in the imino(chloro)phosphane **XLV**. This striking similarity further supports the presence of nitrogen lone pair to P–Cl σ* back donation.

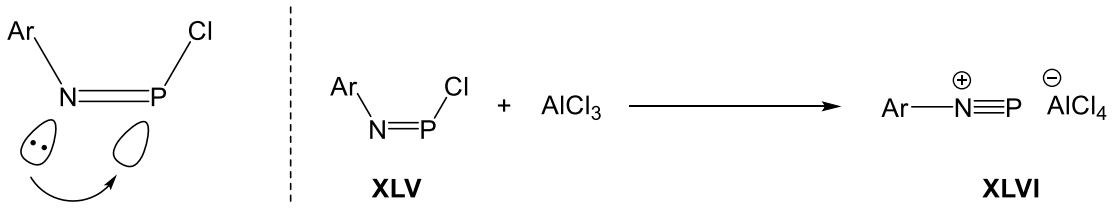

Scheme 1.20. Electonic structure of imino(chloro)phosphane and further conversion to an iminophosphenium.

1.5 Phosphinidene precursors and their use in multiple bonds synthesis

1.5.1 Phosphaketenes R–P=C=O

The decarbonylation of phosphaketenes was first reported by Cowley in 1992, in which Mes*PCO (**XL**) was subjected to photolysis under 254 or 300 nm UV light. This process led to the elimination of CO, generating a highly reactive phosphinidene species (Scheme 1.21).[85] However, the generated Mes*–P species exhibits a triplet ground state and is inherently unstable under ambient conditions, undergoing quantitative conversion to a C–H bond activation product **XLVII**.

In contrast, modifying the supporting ligand to a π-donating phosphino ligand, [P]PCO ([P] = 1,3-bis(2,6-diisopropylphenyl)-1,3,2-diazaphosphosphplidine; **XLVIII**), and photolysis successfully produces an isolable phosphinidene (**IL**) with a singlet ground state (Scheme 1.21).[86] Further research by the Bertrand group revealed that the [P]PCO fragment (**XLVIII**) can be conceptually regarded as a phosphino-phosphinidene coordinated by CO. This perspective suggests that ligand exchange can occur directly at the phosphinidene center, bypassing the need for photolysis.[87]

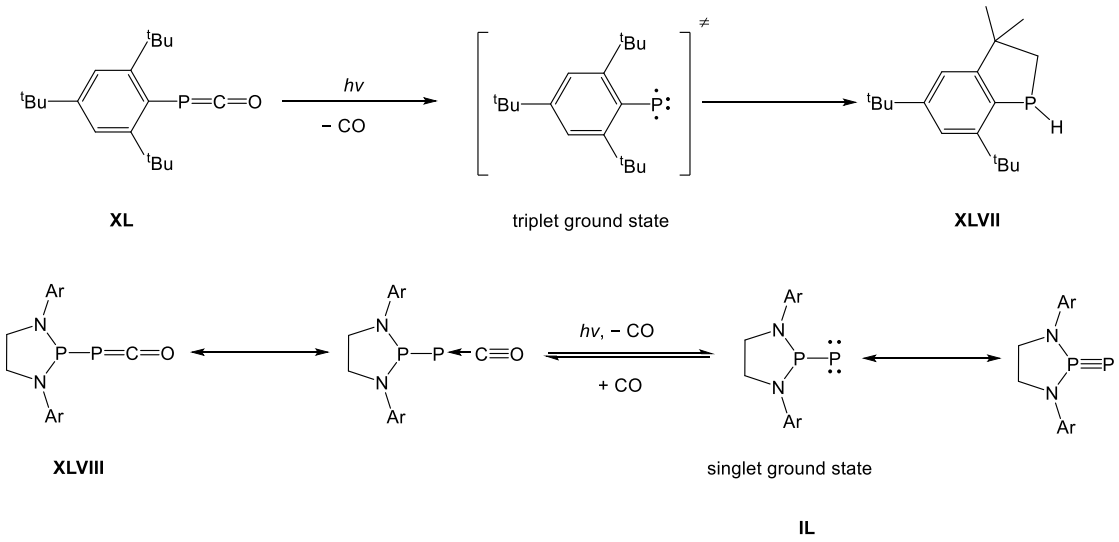

Scheme 1.21. Phosphinidene generated from photolysis of phosphaketenes.

These findings highlight the potential of phosphaketenes as phosphinidene (R–P) precursors, which can further react with low-valent main-group carbenoid species to generate phosphorus–main-group multiple bonds. Building upon this concept, the Goicoechea group reported the decarbonylation reaction between [P]PCO (**XLVII**) and Ga(NacNac) (NacNac = $HC[C(Me)NDipp]_2$), leading to the formation of a phosphagallene (a Ga=P double bond; **L**; Scheme 1.22).[88] A similar approach was employed by the Schulz group, who reported the reaction between (NacNac)(Cl)Ga–PCO and Ga(NacNac), leading to the formation of a Ga=P double bond.[89] Subsequently, the Goicoechea group expanded this strategy to the synthesis of a phosphagermene (P=Ge; **LI**) and a phosphaalumene (P=Al; **LII**) by reacting [P]PCO (**XLVII**) with $Ge[CH(SiMe_3)_2]_2$ or Al(NacNac) (Scheme 1.22). This work further demonstrated that phosphaketenes serve as versatile phosphinidene precursors, enabling the formation of phosphorus–main-group multiple bonds across a range of elements.[90, 91]

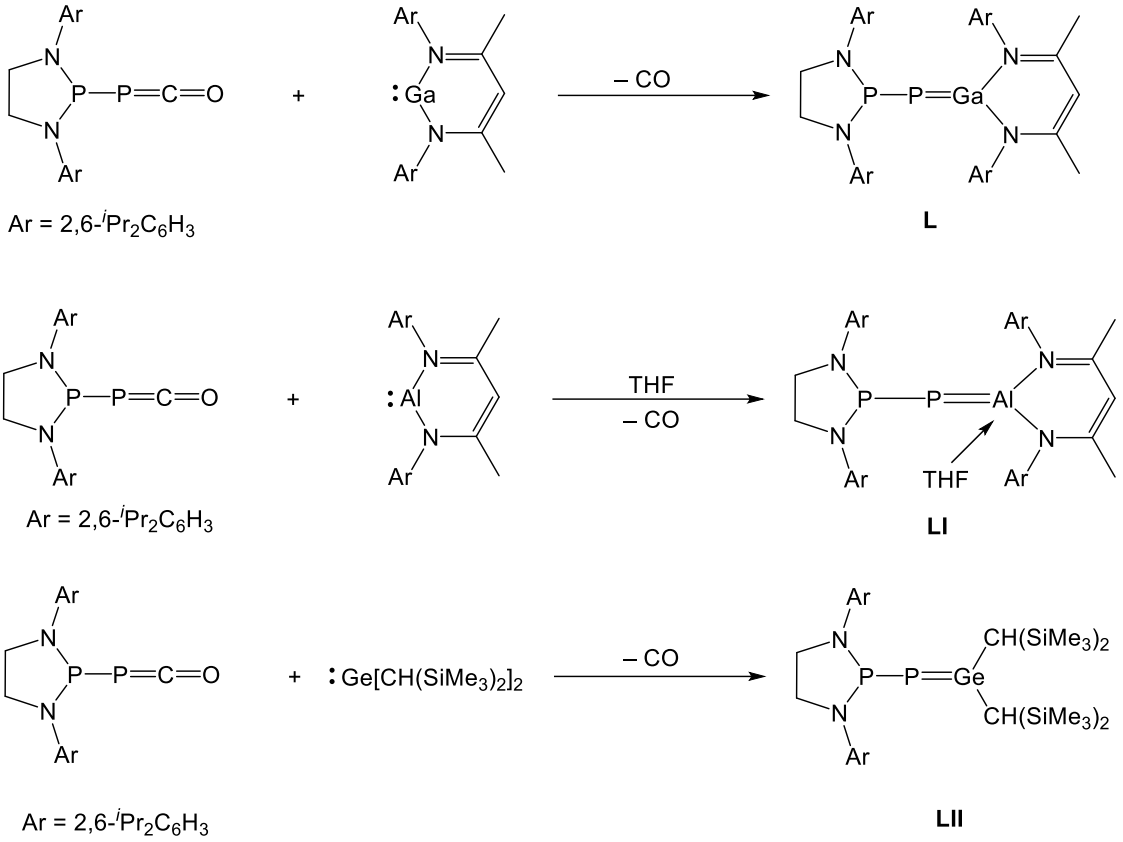

Scheme 1.22. Phosphaketenes reacting with low valent main group carbenoids.

1.5.2 Phosphoranylidene-phosphines (ArP=PMe$_3$)

Similar to phosphaketenes, which can be considered as phosphinidene–CO adducts, phosphoranylidene-phosphines (**LIII**) are regarded as phosphinidene–phosphine adducts. The photoinduced cleavage of phosphoranylidene-phosphines (**LIII**) has also been reported, generating phosphinidene species *in situ*, which subsequently undergo C–H bond activation, leading to the isolation of the corresponding C–H activation product (**XLVII**; Scheme 1.23).[92] According to the diagonal relationship, phosphoranylidene-phosphines are also recognized as the heavier analogues of phosphorus ylides ($R_2C{=}PR_3$). This conceptual analogy led to the report of the phospha-Wittig reaction in 1998, where ArP=PMe$_3$ was reacted with carbonyl compounds, yielding the corresponding phosphaalkenes (**LIV**; Scheme 1.23).[66, 70]

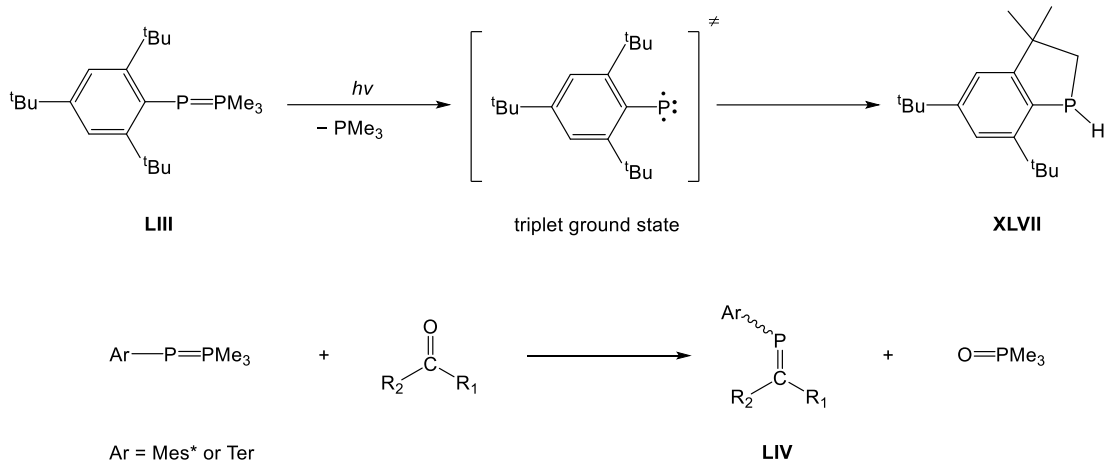

Scheme 1.23. Phosphoranylidene-phosphine as phosphinidene precursor and its phospha-Wittig reaction.

In 2021, Hering-Junghans and co-workers revisited the use of phosphoranylidene-phosphines as phosphinidene precursors. They demonstrated that these species could react with *in situ* generated Cp*Al(I), leading to the formation of a phosphaalumene (P=Al; **LV**; Scheme 1.24).[93] This work paved the way for the utilization of phosphoranylidene-phosphines as phosphinidene precursors for accessing heavier main-group elements multiple bonds. Following this breakthrough, additional reactions between phosphoranylidene-phosphines and low-valent main-group carbenoids, including Sn(II), Ge(II), Ga(I), and In(I), were reported, leading to the formation of the corresponding P=E double bonds (**XIX, XX, LVI**–**LVIII**; Scheme 1.24).[18, 94, 95]

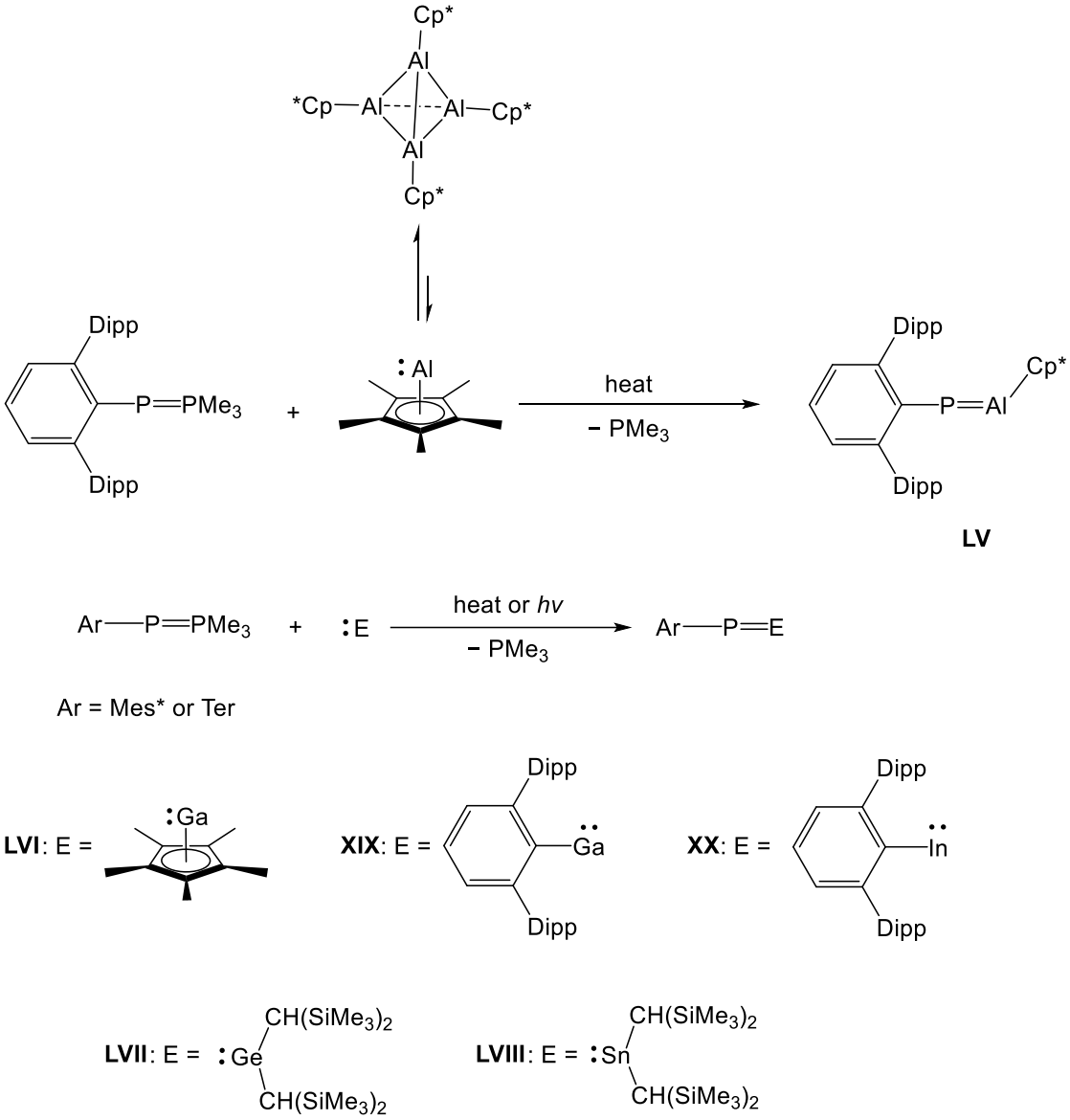

Scheme 1.24. Phosphoranylidene-phosphines as phosphinidene precursors to react with main group low valent carbenoids.

1.5.3 Arene fused phosphinidenes

Arene-fused phosphinidenes are less commonly utilized in the synthesis of phosphorus–main-group multiple bonds, primarily due to the difficulty in implementing effective steric protection at the phosphorus center. Nevertheless, some reports have explored their potential in main-group multiple bonding chemistry. One notable example is the dibenzo-7-phosphanorbornadiene (A–PR, A = anthracene) family, which represents a class of anthracene-stabilized phosphinidenes developed by Cummins and co-workers. Initial studies

demonstrated that R_2NP–A (**LIX**) is capable of transferring a phosphinidene (R_2NP) to various unsaturated substrates upon heating (Scheme 1.25).[96] A more versatile phosphinidene transfer reagent, ClP–A (**LX**), was also reported. Through salt metathesis reactions, the phosphinidene fragment (P–A) can be easily coupled with various fragments of interest, expanding its applicability in main-group chemistry. For instance, upon reaction with sodium azide (NaN_3), the azide-substituted species (N_3P–A; **LXI**) can be successfully isolated. Under photolytic or thermal conditions, N_3P–A (**LXI**) undergoes the elimination of both N_2 and anthracene, generating a free phosphorus mononitride (N≡P； **LXII**), which can be trapped *in situ* (Scheme 1.25).[97] ClP–A (**LX**) can also be considered a P(+1) donor, capable of transferring phosphinidene fragments to nucleophilic centers. Notably, the reaction of two equivalents of ClP–A (**LX**) with $[Fe(CO)_2(RNC)_2]^{2-}$ resulted in the formation of the first side-on coordinated P_2–transition metal complex (**LXIII**; Scheme 1.25).[98] Moreover, dibenzo-7-phosphanorbornadiene (A–PR) has also been used in the synthesis of phosphaalkynes and phosphinidene sulfides, further demonstrating its versatility as a phosphinidene transfer reagent.[99, 100]

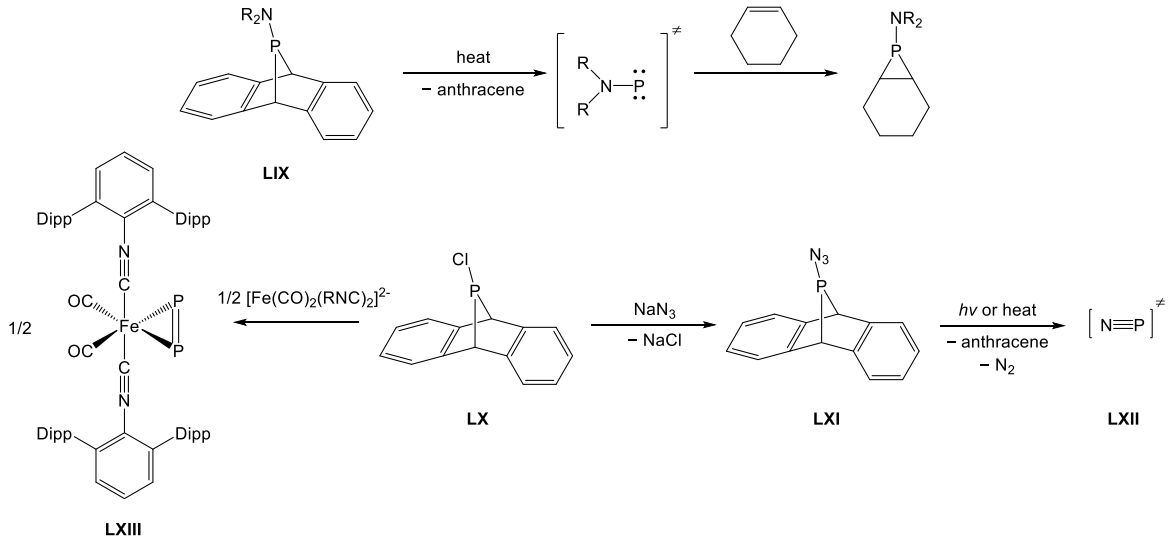

Scheme 1.25. Dibenzo-7-phosphanorbornadiene (RP–A) as phosphinidene precursor and its use in synthesizing main group multiple bonds.

In 2024, the Tilley group reported the synthesis of a ruthenophosphanorcaradiene (**LXIV**), generated via the decarbonylation of an *in situ* formed ruthenophosphaethynolate ([Ru]–PCO). This compound possesses the potential for accessing metal-substituted phosphorus–main-group multiple bonds.[101] Upon reaction with an organo-azide, the ruthenophosphanorcaradiene (**LXIV**) undergoes ligand re-aromatization, yielding a ruthenophosphaimine complex ([Ru]–P=N–R; **LXV**; Scheme 1.26). Further potential of ruthenophosphanorcaradiene (**LXIV**) as a metallophosphinidene synthon are under investigation.

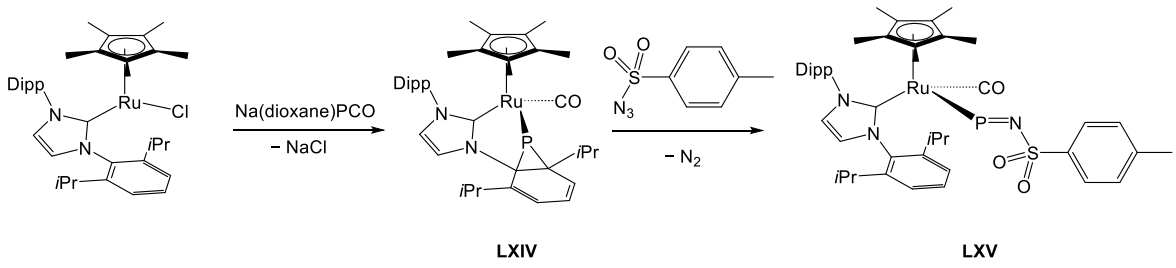

LXIV **LXV**

Scheme 1.26. Ruthenophosphanorcaradiene as metallophosphinidene synthon.

1.6 Project aims

This project primarily aimed to isolate novel classes of compounds with phosphorus–main group elements multiple bonds. As previously discussed, steric protection and electrostatic repulsion are critical factors in stabilizing such species. The first part of this project builds upon the concept of utilizing electrostatic repulsion to enhance stability, extending the work of the Goicoechea group on isolating heavier analogues of cyanate. Chapter 2 presents a detailed investigation into the synthesis, electronic structure, and reactivity of the cyapho(dicyano)methanide anion, $[C(CP)(CN)_2]^-$.

Building on the successful isolation of cyapho(dicyano)methanide, we aimed to further explore the application of electrostatic repulsion—complemented by steric protection—to

access more reactive main-group–phosphorus multiple bonds. A key objective was to target a phosphinidene oxide (P(III)=O), one of the most challenging multiple bonds due to its high polarity and lack of steric protection. Chapter 3 details the isolation of an anionic imine-supported phosphinidene oxide ($RNPO^{-}$), including the ligand design, synthesis, and electronic structure analysis using DFT calculations. Chapter 4 focuses on the reactivity of the aforementioned compound, particularly its alkylation at the nitrogen center, which leads to the formation of a neutral amino-supported phosphinidene oxide ($R_2NP=O$). Owing to the diagonal relationship between carbon and phosphorus, this species can be regarded as a heavier analogue of organic amides. Both theoretical and experimental data support this comparison.

Building on this understanding, we explored the use of our amino-supported phosphinidene oxide as a substitute for carbonyl compounds in the Wittig reaction. Chapter 5 introduces the phospha-Wittig reaction, wherein a phosphinidene oxide reacts with a phosphorus ylide, yielding the corresponding phosphaalkene alongside phosphine oxide as a byproduct. This transformation highlights the potential of phosphinidene oxide as a phosphinidene synthon in double-bond metathesis reactions, offering new avenues to access main group-phosphorus multiple bonds.

Carbonyl compounds are known to undergo reactions with Lawesson's reagent (LR) and Woollins' reagent (WR), leading to the formation of thiocarbonyl and selenocarbonyl derivatives, respectively. Given the structural and electronic parallels between carbonyl compounds and phosphinidene oxides, Chapter 6 explores the synthesis of a phosphinidene sulfide (P(III)=S) and a phosphinidene selenide (P(III)=Se) through the reaction of our phosphinidene oxide with LR or WR. Additionally, the electronic structures of these phosphinidene chalcogenides will be analysed to provide further insight into their bonding characteristics.

1.7 References

[1] F. S. Kipping, *Proc. R. Soc. A* **1937**, *159*, 139–148.

[2] K. S. Pitzer, *J. Am. Chem. Soc.* **1948**, *70*, 2140–2145.

[3] R. S. Mulliken, *J. Am. Chem. Soc.* **1950**, *72*, 4493–4503.

[4] A. J. Ashe, III, *J. Am. Chem. Soc.* **1971**, *93*, 3293–3295.

[5] M. Yoshifuji, I. Shima, N. Inamoto, K. Hirotsu, T. Higuchi, *J. Am. Chem. Soc.* **1981**, *103*, 4587–4589.

[6] R. West, M. J. Fink, J. Michl, *Science* **1981**, *214*, 1343–1344.

[7] P. P. Power, *Nature* **2010**, *463*, 171–177.

[8] A. Lehmann, J. D. Queen, C. J. Roberts, K. Rissanen, H. M. Tuononen, P. P. Power, *Angew. Chem. Int. Ed.* **2024**, *63*, e202412599.

[9] N. J. Hardman, R. J. Wright, A. D. Phillips, P. P. Power, *Angew. Chem. Int. Ed.* **2002**, *41*, 2842–2844.

[10] R. J. Wright, A. D. Phillips, N. J. Hardman, P. P. Power, *J. Am. Chem. Soc.* **2002**, *124*, 8538–8539.

[11] R. J. Wright, A. D. Phillips, S. Hino, P. P. Power, *J. Am. Chem. Soc.* **2005**, *127*, 4794–4799.

[12] M. Stender, A. D. Phillips, R. J. Wright, P. P. Power, *Angew. Chem. Int. Ed.* **2002**, *41*, 1785–1787.

[13] R. C. Fischer, L. Pu, J. C. Fettinger, M. A. Brynda, P. P. Power, *J. Am. Chem. Soc.* **2006**, *128*, 11366–11367.

[14] L. Pu, B. Twamley, P. P. Power, *J. Am. Chem. Soc.* **2000**, *122*, 3524–3525.

[15] B. Twamley, C. D. Sofield, M. M. Olmstead, P. P. Power, *J. Am. Chem. Soc.* **1999**, *121*, 3357–3367.

[16] R. J. Wright, M. Brynda, P. P. Power, *Angew. Chem. Int. Ed.* **2006**, *45*, 5953–5956.

[17] J. Su, X.-W. Li, R. C. Crittendon, G. H. Robinson, *J. Am. Chem. Soc.* **1997**, *119*, 5471–5472.

[18] Á. García-Romero, C. Hu, M. Pink, J. M. Goicoechea, *J. Am. Chem. Soc.* **2025**, *147*, 1231–1239.

[19] D. J. Liptrot, P. P. Power, *Nat. Rev. Chem.* **2017**, *1*, 0004.

[20] S. Grimme, *J. Comput. Chem.* **2006**, *27*, 1787–1799.

[21] S. Grimme, S. Ehrlich, L. Goerigk, *J. Comput. Chem.* **2011**, *32*, 1456–1465.

[22] J.-D. Guo, D. J. Liptrot, S. Nagase, P. P. Power, *Chem. Sci.* **2015**, *6*, 6235–6244.

[23] C. R. Stennett, M. Bursch, J. C. Fettinger, S. Grimme, P. P. Power, *J. Am. Chem. Soc.* **2021**, *143*, 21478–21483.

[24] J. M. Goicoechea, H. Grützmacher, *Angew. Chem. Int. Ed.* **2018**, *57*, 16968–16994.

[25] A. Hinz, J. M. Goicoechea, *Angew. Chem. Int. Ed.* **2016**, *55*, 8536–8541.

[26] F. Tambornino, A. Hinz, R. Köppe, J. M. Goicoechea, *Angew. Chem. Int. Ed.* **2018**, *57*, 8230–8234.

[27] D. Ergöçmen, J. M. Goicoechea, *Angew. Chem. Int. Ed.* **2021**, *60*, 25286–25289.

[28] R. J. Wehmschulte, P. P. Power, *J. Am. Chem. Soc.* **1997**, *119*, 8387–8388.

[29] D. Neculai, H. W. Roesky, A. M. Neculai, J. Magull, B. Walfort, D. Stalke, *Angew. Chem. Int. Ed.* **2002**, *41*, 4294–4296.

[30] J. Hicks, A. Heilmann, P. Vasko, J. M. Goicoechea, S. Aldridge, *Angew. Chem. Int. Ed.* **2019**, *58*, 17265–17268.

[31] H. Braunschweig, K. Radacki, A. Schneider, *Science* **2010**, *328*, 345–347.

[32] A. W. Ehlers, E. J. Baerends, F. M. Bickelhaupt, U. Radius, *Chem. Eur. J.* **1998**, *4*, 210–221.

[33] L. Li, T. Fukawa, T. Matsuo, D. Hashizume, H. Fueno, K. Tanaka, K. Tamao, *Nat. Chem.* **2012**, *4*, 361–365.

[34] F. Allen, *Acta Crystallogr. B* **2002**, *58*, 380–388.

[35] S. Yao, Y. Xiong, W. Wang, M. Driess, *Chem. Eur. J.* **2011**, *17*, 4890–4895.

[36] S. Yao, Y. Xiong, M. Driess, *Chem. Commun.* **2009**, 6466–6468.

[37] A. C. Filippou, B. Baars, O. Chernov, Y. N. Lebedev, G. Schnakenburg, *Angew. Chem. Int. Ed.* **2014**, *53*, 565–570.

[38] Y. Xiong, S. Yao, M. Driess, *J. Am. Chem. Soc.* **2009**, *131*, 7562–7563.

[39] Y. Xiong, S. Yao, R. Müller, M. Kaupp, M. Driess, *Nat. Chem.* **2010**, *2*, 577–580.

[40] R. S. Ghadwal, R. Azhakar, H. W. Roesky, K. Pröpper, B. Dittrich, S. Klein, G. Frenking, *J. Am. Chem. Soc.* **2011**, *133*, 17552–17555.

[41] T. Muraoka, K. Abe, Y. Haga, T. Nakamura, K. Ueno, *J. Am. Chem. Soc.* **2011**, *133*, 15365–15367.

[42] Y. Xiong, S. Yao, M. Driess, *Angew. Chem. Int. Ed.* **2013**, *52*, 4302–4311.

[43] R. Rodriguez, T. Troadec, D. Gau, N. Saffon-Merceron, D. Hashizume, K. Miqueu, J.-M. Sotiropoulos, A. Baceiredo, T. Kato, *Angew. Chem. Int. Ed.* **2013**, *52*, 4426–4430.

[44] R. Rodriguez, D. Gau, T. Troadec, N. Saffon-Merceron, V. Branchadell, A. Baceiredo, T. Kato, *Angew. Chem. Int. Ed.* **2013**, *52*, 8980–8983.

[45] I. Alvarado-Beltran, A. Rosas-Sánchez, A. Baceiredo, N. Saffon-Merceron, V. Branchadell, T. Kato, *Angew. Chem. Int. Ed.* **2017**, *56*, 10481–10485.

[46] Wendel, D. Reiter, A. Porzelt, P. J. Altmann, S. Inoue, B. Rieger, *J. Am. Chem. Soc.* **2017**, *139*, 17193–17198.

[47] M. J. A. Johnson, A. L. Odom, C. C. Cummins, *Chem. Commun.* **1997**, 1523–1524.

[48] P. Pyykkö, M. Atsumi, *Chem. Eur. J.* **2009**, *15*, 12770–12779.

[49] C. E. Laplaza, W. M. Davis, C. C. Cummins, *Angew. Chem., Int. Ed. Engl.* **1995**, *34*, 2042–2044.

[50] O. Krahe, F. Neese, R. Streubel, *Chem. Eur. J.* **2009**, *15*, 2594–2601.

[51] X. Chu, Y. Yang, B. Lu, Z. Wu, W. Qian, C. Song, X. Xu, M. Abe, X. Zeng, *J. Am. Chem. Soc.* **2018**, *140*, 13604–13608.

[52] X. Zhao, X. Chu, G. Rauhut, C. Chen, C. Song, B. Lu, X. Zeng, *Angew. Chem. Int. Ed.* **2019**, *58*, 12164–12169.

[53] A. Mardyukov, F. Keul, P. R. Schreiner, *Angew. Chem. Int. Ed.* **2020**, *59*, 12445–12449.

[54] R. Hoffmann, *Angew. Chem., Int. Ed. Engl.* **1982**, *21*, 711–724.

[55] M. Elian, M. M. L. Chen, D. M. P. Mingos, R. Hoffmann, *Inorg. Chem.* **1976**, *15*, 1148–1155.

[56] D. M. P. Mingos, *Essential trends in inorganic chemistry*, Oxford University Press, **1998**.

[57] T. Renner, *Quantities, units and symbols in physical chemistry*, Royal Society of Chemistry, **2007**.

[58] A. C. Gaumont, J. M. Denis, *Chem. Rev.* **1994**, *94*, 1413–1439.

[59] G. Recker, *Z. Anorg. Allg. Chem.* **1976**, *423*, 242–254.

[60] R. Appel, B. Laubach, M. Siray, *Tetrahedron Lett.* **1984**, *25*, 4447–4448.

[61] R. Appel, P. Fölling, L. Krieger, M. Siray, F. Knoch, *Angew. Chem., Int. Ed. Engl.* **1984**, *23*, 970–971.

[62] K. Issleib, H. schmidt, H. Meyer, *J. Organomet. Chem* **1980**, *192*, 33–39.

[63] T. C. Klebach, R. Lourens, F. Bickelhaupt, *J. Am. Chem. Soc.* **1978**, *100*, 4886–4888.

[64] A. Marinetti, F. Mathey, *Angew. Chem., Int. Ed. Engl.* **1988**, *27*, 1382–1384.

[65] A. Marinetti, S. Bauer, L. Ricard, F. Mathey, *Organometallics* **1990**, *9*, 793–798.

[66] S. Shah, J. D. Protasiewicz, *Coord. Chem. Rev.* **2000**, *210*, 181–201.

[67] C. C. Cummins, R. R. Schrock, W. M. Davis, *Angew. Chem., Int. Ed. Engl.* **1993**, *32*, 756–759.

[68] T. L. Breen, D. W. Stephan, *J. Am. Chem. Soc.* **1995**, *117*, 11914–11921.

[69] B. F. Wicker, J. Scott, J. G. Andino, X. Gao, H. Park, M. Pink, D. J. Mindiola, *J. Am. Chem. Soc.* **2010**, *132*, 3691–3693.

[70] S. Shah, J. D. Protasiewicz, *Chem. Commun.* **1998**, 1585–1586.

[71] A. M. Borys, E. F. Rice, G. S. Nichol, M. J. Cowley, *J. Am. Chem. Soc.* **2021**, *143*, 14065–14070.

[72] T. E. Gier, *J. Am. Chem. Soc.* **1961**, *83*, 1769–1770.

[73] G. Becker, G. Gresser, W. Uhl, *Z. Naturforsch. B* **1981**, *36*, 16–19.

[74] J.-C. Guillemin, T. Janati, J.–M. Denis, *J. Org. Chem.* **2001**, *66*, 7864–7868.

[75] J.-C. Guillemin, T. Janati, J.–M. Denis, *J. Chem. Soc., Chem. Commun.* **1992**, 415–416.

[76] R. Appel, W. Paulen, *Tetrahedron Lett.* **1983**, *24*, 2639–2642.

[77] R. Appel, W. Paulen, *Angew. Chem., Int. Ed. Engl.* **1983**, *22*, 785–786.

[78] G. Becker, W. Schwarz, N. Seidler, M. Westerhausen, *Z. Anorg. Allg. Chem.* **1992**, *612*, 72–82.

[79] A. R. Jupp, J. M. Goicoechea, *Angew. Chem. Int. Ed.* **2013**, *52*, 10064–10067.

[80] D. Heift, Z. Benkő, H. Grützmacher, *Dalton Trans.* **2014**, *43*, 831–840.

[81] E. Niecke, W. Flick, *Angew. Chem., Int. Ed. Engl.* **1973**, *12*, 585–586.

[82] E. Niecke, D. Gudat, *Angew. Chem., Int. Ed. Engl.* **1991**, *30*, 217–237.

[83] E. Niecke, M. Nieger, F. Reichert, *Angew. Chem., Int. Ed. Engl.* **1988**, *27*, 1715–1716.

[84] P. Pyykkö, M. Atsumi, *Chem. Eur. J.* **2009**, *15*, 186–197.

[85] A. H. Cowley, F. Gabbai, R. Schluter, D. Atwood, *J. Am. Chem. Soc.* **1992**, *114*, 3142–3144.

[86] L. Liu, David A. Ruiz, D. Munz, G. Bertrand, *Chem* **2016**, *1*, 147–153.

[87] M. M. Hansmann, G. Bertrand, *J. Am. Chem. Soc.* **2016**, *138*, 15885–15888.

[88] D. W. N. Wilson, J. Feld, J. M. Goicoechea, *Angew. Chem. Int. Ed.* **2020**, *59*, 20914–20918.

[89] M. K. Sharma, C. Wölper, G. Haberhauer, S. Schulz, *Angew. Chem. Int. Ed.* **2021**, *60*, 6784–6790.

[90] J. Feld, E. S. Yang, S. J. Urwin, J. M. Goicoechea, *Chem. Eur. J.* **2024**, *30*, e202401736.

[91] L. S. Szych, L. Denker, J. Feld, J. M. Goicoechea, *Chem. Eur. J.* **2024**, *30*, e202401326.

[92] S. Shah, M. C. Simpson, R. C. Smith, J. D. Protasiewicz, *J. Am. Chem. Soc.* **2001**, *123*, 6925–6926.

[93] M. Fischer, S. Nees, T. Kupfer, J. T. Goettel, H. Braunschweig, C. Hering-Junghans, *J. Am. Chem. Soc.* **2021**, *143*, 4106–4111.

[94] T. Taeufer, F. Dankert, D. Michalik, J. Pospech, J. Bresien, C. Hering-Junghans, *Chem. Sci.* **2023**, *14*, 3018–3023.

[95] M. J. Reveley, J. Feld, D. Temerova, E. S. Yang, J. M. Goicoechea, *Chem. Eur. J.* **2023**, *29*, e202301542.

[96] W. J. Transue, A. Velian, M. Nava, C. García-Iriepa, M. Temprado, C. C. Cummins, *J. Am. Chem. Soc.* **2017**, *139*, 10822–10831.

[97] A. K. Eckhardt, M.-L. Y. Riu, M. Ye, P. Müller, G. Bistoni, C. C. Cummins, *Nat. Chem.* **2022**, *14*, 928–934.

[98] S. Wang, J. D. Sears, C. E. Moore, A. L. Rheingold, M. L. Neidig, J. S. Figueroa, *Science* **2022**, *375*, 1393–1397.

[99] W. J. Transue, J. Yang, M. Nava, I. V. Sergeyev, T. J. Barnum, M. C. McCarthy, C. C. Cummins, *J. Am. Chem. Soc.* **2018**, *140*, 17985–17991.

[100] W. J. Transue, M. Nava, M. W. Terban, J. Yang, M. W. Greenberg, G. Wu, E. S. Foreman, C. L. Mustoe, P. Kennepohl, J. S. Owen, S. J. L. Billinge, H. J. Kulik, C. C. Cummins, *J. Am. Chem. Soc.* **2019**, *141*, 431–440.

[101] T. G. Saint-Denis, T. A. Wheeler, Q. Chen, G. Balázs, N. S. Settineri, M. Scheer, T. D. Tilley, *J. Am. Chem. Soc.* **2024**, *146*, 4369–4374.

Chapter 2

Synthesis, Structure and Reactivity of a Cyapho(dicyano)methanide Salt

---

The contents of this chapter have been published:

C. Hu, J. M. Goicoechea, *Angew. Chem. Int. Ed.* **2022**, 61, e202208921.

2.1 Introduction

Tricyanomethane (or cyanoform; $HC(CN)_3$) is a highly unstable acid ($pK_a = -5.1$ in water) that was first observed by microwave spectroscopy in the gas phase,[1–3] and only recently isolated in solution by Kornath and co-workers.[4] By contrast, its conjugate base, tricyanomethanide (TCM), is a well-established weak organic base first synthesized from the reaction of potassium cyanate and malononitrile by Schmidtmann in 1896.[5] Due to its extended conjugated π-system, TCM is a resonance stabilized pseudo-halide with a planar geometry.[6] The lone pairs on the three nitrogen atoms allows TCM to coordinate to metal centers, a property which has seen it used as a building block in coordination polymers.[7–11] Coordination to main group Lewis acids can also be used to access weakly coordinating anions.[12] Moreover, the high stability and delocalized charge of this ion allows access to ionic liquids in which TCM is combined with a bulky counter-cation. Such ionic liquids have been used in a number of applications including CO_2 separation, the synthesis of dye-sensitized solar cells and the extraction of aromatic hydrocarbons.[13–19]

Nitrile-containing inorganic anions of generic formula $[E(CN)_n]^-$ (E = p-block element; Figure 2.1) are a relatively large family, many of which are stable on account of the electron-withdrawing properties of the cyano-group and its ability to stabilize a multitude of resonance structures. For example, the TCM ion can be thought of as being composed of a central group 14 element (a carbon atom) surrounded by three cyano-groups. An analogous compound with a central group 15 element would be dicyanamide, $[N(CN)_2]^-$, which was first synthesized by Madelung and Kern in 1922.[20] Like TCM, dicyanamide has also found use in coordination polymers and ionic liquids.[10, 21–23] A group 16 version of this class of ions is cyanate $[OCN]^-$, which is an archetypal inorganic anion with a myriad of applications, synthesized industrially by heating of a mixture of sodium carbonate and urea.[24] Due to the importance of these nitrile-containing small anions, the synthesis of heavier analogues in

which one or more of the nitrogen atoms is replaced by a heavier pnictogen element has attracted significant interest. For example, Becker first synthesized the lithium salt of the 2-phosphaethynolate anion, OCP^-, in 1992,[25] and in recent years this ion has been shown to be a valuable building block for the synthesis of an incredibly broad range of phosphorus-containing compounds.[26] Heavier analogues of this ion, such as ECP^- (E = S, Se),[27,28] and $OCAs^-$, have also been synthesized.[29] Analogues of the dicyanamide ion where one of the nitrogen atoms has been replaced by heavier elements have also been reported. The dicyanophosphide ion, $[P(CN)_2]^-$, was first synthesized by Schmidpeter in 1977.[30,31] However, due to difficulties associated with its synthesis, its reactivity was not explored until forty years later when Macdonald and Liu separately discovered new synthetic routes towards this ion.[32,33] More recently, (cyapho)cyanamide, $[N(CN)(CP)]^-$, was also synthesized by our group.[34] The fact that heavier phosphorus-containing analogues of the cyanate and dicyanamide ion are now synthetically available prompted us to explore the synthesis of a phosphorus-containing tricyanomethanide ion. Herein, we describe the synthesis of the cyapho(dicyano)methanide $[C(CN)_2(CP)]^-$ anion employing a similar synthetic protocol as used for the synthesis of (cyapho)cyanamide $[N(CN)(CP)]^-$ and the 2-phosphaethynolate anion (PCO^-).[34–36]

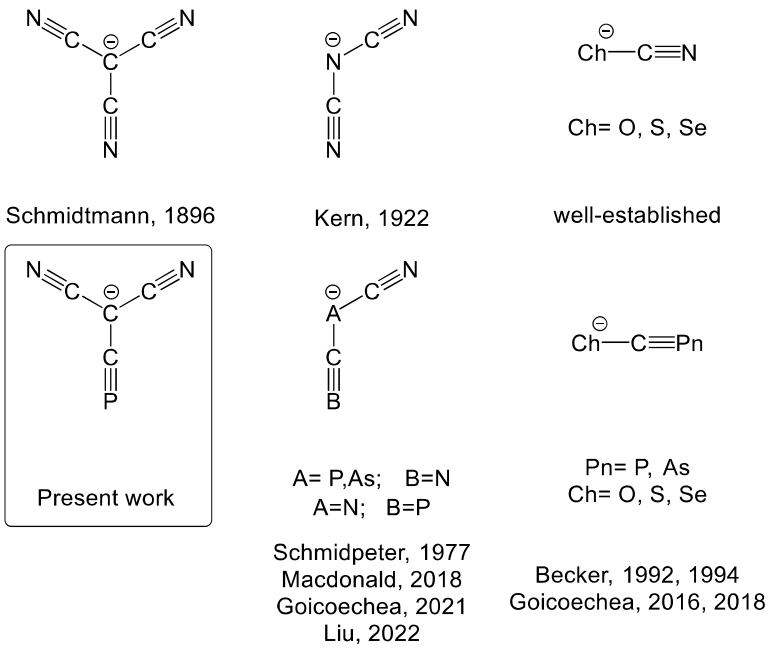

Figure 2.1. Selected nitrile-containing inorganic anions and their heavier analogues.

2.2 Rational design of a synthetic route towards a cyapho(dicyano)methanide salt $[C(CP)(CN)_2]^-$

The synthesis of the 2-phosphaethynolate anion, (OCP^-), and (cyapho)cyanamide, $[N(CN)(CP)]^-$ are closely related. They all involve reaction of sodium phosphide, $NaPH_2$, with a carbonate or carbonate analogue (Scheme 2.1). The reaction involves nucleophilic addition of PH_2^- to the polarized C=E double bonds (E = O, S, Se, N(CN)), followed by the proton transfer from phosphorus to oxygen and subsequent elimination of two equivalents of the corresponding alcohol to generate the C≡P triple bond. Depending on the electron withdrawing effect of the E group, in some cases an intermediate could be isolated. For E = chalcogenide, due to their high electronegativity, the intermediate will spontaneously eliminate the second equivalent of alcohol, directly affording the desired 2-phosphaethynolate anion and its heavier analogues, $PCCh^-$. For less electron-withdrawing groups such as E = N(CN), the intermediate was isolated, which is still unstable and

undergoes alcohol elimination upon extended standing at room temperature. Addition of external base such as LiHMDS facilities the elimination as well.

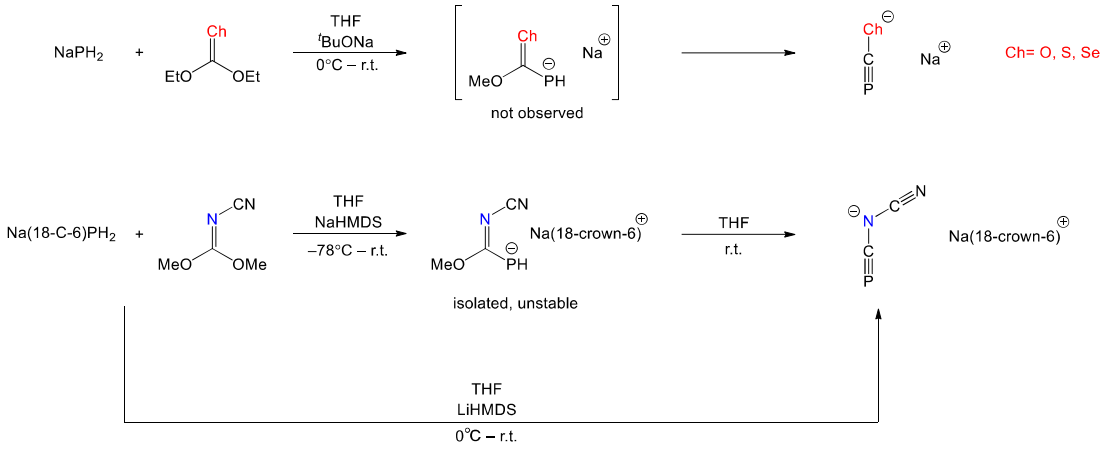

Scheme 2.1. Synthesis of 2-phosphaethynolate anion, OCP^-, and (cyapho)cyanamide, $[N(CN)(CP)]^-$.

For the synthesis of cyapho(dicyano)methanide, we decide to adopt a similar synthetic route to OCP^- and $[N(CN)(CP)]^-$ and identified 1,1-diethoxy-2,2-dicyanoethylene $(EtO)_2C{=}C(CN)_2$ as a viable precursor. The nitrile substituents on the ethylene also serve to polarize the C=C bond making it susceptible to nucleophilic attack by sodium phosphanide, $NaPH_2$, as would be expected in a Michael addition. Elimination of two equivalents of ethanol following the Michael addition would generate our desired ion.

2.3 Synthesis and characterization of a cyapho(dicyano)methanide

Reaction of a THF solution of $[Na(18\text{-crown-}6)][PH_2]$ and $(EtO)_2C{=}C(CN)_2$ at –78 °C (Scheme 2.2) gave rise to a yellow solution after allowing the reaction mixture to slowly warm to room temperature overnight. *In situ* ^{31}P NMR spectroscopy revealed a doublet at –66.3 ppm with a $^1J_{H–P}$ coupling constant of 166.5 Hz corresponding to $[Na(18\text{-crown-}6)][HP\{C(OEt)C(CN)_2\}]^-$ ([Na(18-crown-6)]**1**). **1** is a relatively weak anionic phosphide and

can co-exist with the ethanol that is generated in the reaction mixture. In contrast to other related species, such as the precursor to the (cyapho)cyanamide ion,[34] **1** does not undergo further elimination of ethanol on standing. It decomposes before eliminating ethanol when heated to 50 °C for 6 hours. However, treatment of [Na(18-crown-6)]**1** with KHMDS (potassium hexamethyl disilazide) at 0 °C for 2 days afforded the target compound [K(18-crown-6)][C(CN)$_2$(CP)] ([K(18-crown-6)]**2**; Scheme 2.1), which features a singlet in its ^{31}P NMR spectrum at 27.1 ppm. [K(18-crown-6)]**2** is soluble in polar solvents (e.g. THF) and moderately soluble apolar aromatics such as toluene and benzene.

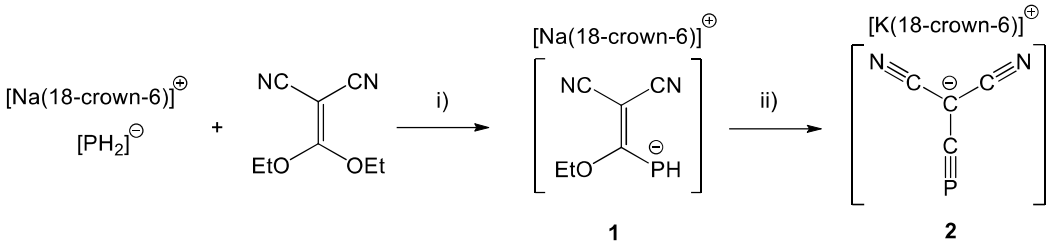

Scheme 2.2. Synthesis of compound [Na(18-crown-6)]**1** and [K(18-crown-6)]**2**. i) THF, −78 °C to r.t. (yield 63%); ii) THF, KHMDS, −78 °C to 0 °C (yield 64%).

The structures of [Na(18-crown-6)]**1**·THF and [K(18-crown-6)]**2**·THF were confirmed by single crystal X-ray diffraction (Figure 2.2). Both of the ions exhibit a planar geometry about the central carbon atom (Σ°: 360.0 for both **1** and **2**). The most notable structural change on going from **1** to **2** is the significant shortening of the C−P bond length which contracts from 1.742(2) to 1.553(2) Å, in line with the formation of a C≡P triple bond.[37] The C−C bond lengths in **2** (1.390(3), 1.418(3) and 1.419(3) Å) all lie within the range of C–C single and C=C double bonds.[38] Taken together, these bond metric data are indictive of high degree of conjugation. It is worth noting that the counter ion for **2** has changed from [Na(18-crown-6)]$^+$ to [K(18-crown-6)]$^+$. This is because KHMDS is used to facilitate the loss of an additional molecule of ethanol from **1**, and 18-crown-6 preferentially binds K^+ over other alkali metal cations.[40]

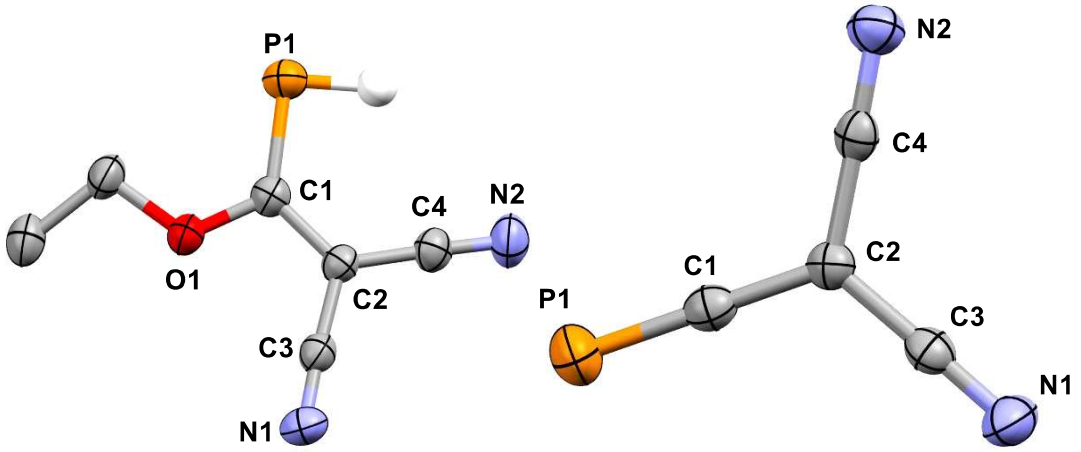

Figure 2.2. Single crystal X-ray structures of the anionic components in [Na(18-crown-6)]**1**·THF (left) and [K(18-crown-6)]**2**·THF (right). Anisotropic displacement ellipsoids pictured at 50% probability. Selected bond lengths (Å) and angles (°) **1**: P1–C1, 1.742(2); C1–C2 1.432(2); C1–O1, 1.355(2); C2–C3, 1.410(2); C2–C4, 1.404(2); C3–N1, 1.154(2); C4–N2, 1.150(2); P1-C1-O1, 121.67(12); P1-C1-C2, 127.78(13); C2-C1-O1, 110.55(14). **2**: P1–C1, 1.553(2); C1–C2 1.390(3); C2–C3, 1.418(3), C2–C4, 1.419(3), C3–N1, 1.149(3), C4–N2, 1.151(3); C1-C2-C3, 120.79(18), C1-C2-C4, 121.19(18); C3-C2-C4, 117.98(18).

2.4 DFT calculations

In order to further understand the electronic structure of **2**, density functional theory (DFT) calculations (M06-2X/def2-SVP) were performed. The optimized geometry is in good agreement with the bond metrics obtained by X-ray crystallography (e.g. P1–C2: 1.567 Å; C1–C2: 1.396 Å). Natural resonance theory (NRT) as implemented in NBO 7.0 confirmed extensive π-orbital delocalization in **2**. All four major contributing resonance structures have a similar weighting (Figure 2.3). The heteroallene-like structure with negative charge at the terminal phosphorus atom has the greatest contribution (15.9%). This is in line with the

experimental observation that the C1−C2 bond length (1.390(3) Å) is slightly shorter than C2–C3 and C2–C4 (1.418(3) and 1.419(3) Å, respectively). This implies greater C–C double bond character between C1 and C2 than between C2–C3 and C2–C4. Second-order perturbation theory suggests a back-donation energy E(2) = 142.7 kcal mol^{-1} from the lone pair of C2 to the CP π* orbital, which is almost twice as strong than it is into the into CN π* orbitals (E(2) = 79.8 kcal mol^{-1}; Figure 2.4). The nitrile group has long been known as a competent stabilizing functionality for a negative charge in an α position, but in this case, theory suggests that cyaphide group is moderately better at delocalizing negative charge, due to its lower lying C–P π* orbital.

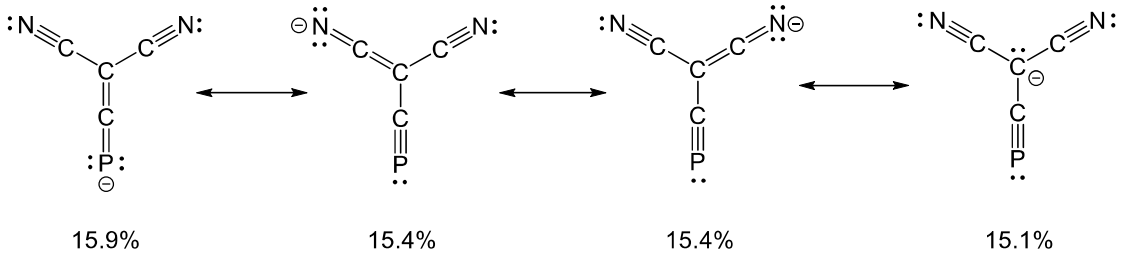

Figure 2.3. The four major resonance structures of **2** and their weighting as predicted by natural resonance theory (NRT).

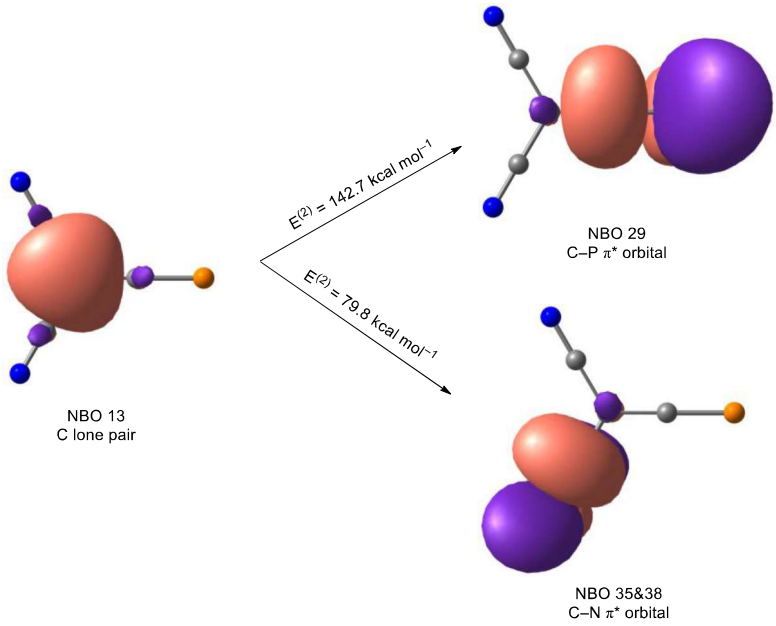

Figure 2.4. Selected NBOs of $[C(CN)_2(CP)]^-$ from second-order perturbation theory analysis.

A detailed comparison based on NBO calculations between **2** and the parent structure tricyanomethanide $[C(CN)_3]^-$ was performed. Unlike $[C(CP)(CN)_2]^-$, the resonance structure of $[C(CN)_3]^-$ with a lone pair on the central carbon atom (and a formal negative charge) has the greatest contribution to the overall electronic structure (Figure 2.5). This is consistent with our findings that the cyaphide moiety can delocalize negative charge better than a nitrile group. Here, without the cyaphide moiety, more negative charge accumulates on the central carbon atom, causing this resonance structure to become the most significant one. But since the cyaphide moiety is only slightly better at delocalizing negative charge, the weight of each of the other resonance structures is similar to those calculated for $[C(CP)(CN)_2]^-$.

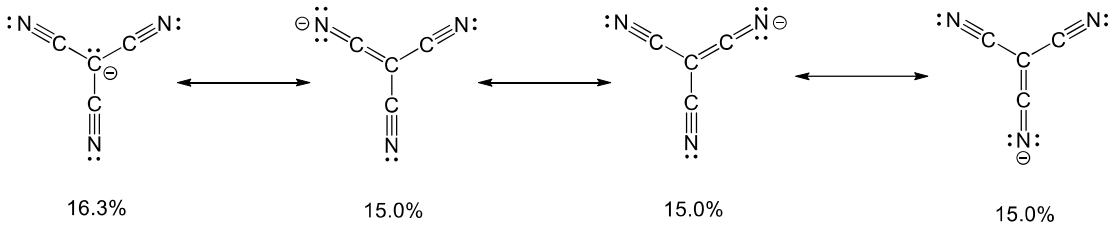

Figure 2.5. The four major resonance structures of $[C(CN)_3]^-$ as predicted by natural resonance theory (NRT).

Table 2.1. NPA charge of $[C(CP)(CN)_2]^-$ and $[C(CN)_3]^-$.

Atom type	$[C(CP)(CN)_2]^-$	$[C(CN)_3]^-$
Central C	−0.57	−0.61
N	−0.44	−0.44
CN Moiety	−0.12	−0.13
P	+0.22	
CP Moiety	−0.20	

The NPA charges show that the central carbon in $[C(CN)_3]^-$ carries more negative charge than in $[C(CP)(CN)_2]^-$. This finding, again, agrees with our hypothesis that cyaphide moiety can delocalize negative charge better than a nitrile group.

2.5 Reactivity studies

The reactivity of **2** was further explored with the aim of experimentally probing these bonding arguments. Due to the high degree of negative charge delocalization, **2** is a poor nucleophile compared to other phosphorus containing anions such as PCO^- or $[N(CN)(CP)]^-$.[26,34] It is inert towards moderate strength electrophiles such as Ph_3GeCl and 1,3,2-diazaphosphochloride $[(CH_2)NDipp]_2PCl$. Reactions with strong electrophiles such as $^{i}Pr_3SiOTf$ or Ge(^{Dipp}NacNac)OTf at room temperature were found to decompose to intractable, insoluble precipitates. [K(18-crown-6)]**2** is also unreactive towards carbodiimides, which are known to readily undergo [2+2] cycloaddition reactions with PCO^- and $AsCO^-$.[26,29]

2.5.1 Protonation of 2

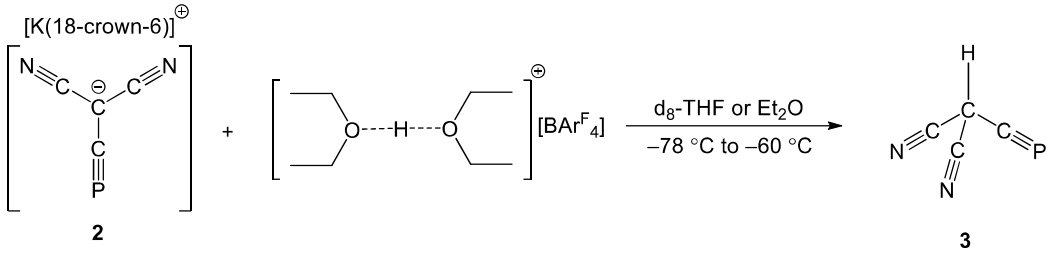

Scheme 2.3. Synthesis of **3**.

Nevertheless, protonation of [K(18-crown-6)]**2** with Brookhart's acid[40] at –78 °C in THF (or Et_2O) afforded a solution of (cyapho)dicyano-methane $HC(CN)_2(CP)$, **3**, which is stable for more than 12 hours at –60 °C (Scheme 2.3). It is worth noting, however, that **3** decomposes within minutes on warming to –30 °C. No additional compounds could be

observed by ^{31}P NMR spectroscopy at this temperature, suggesting the formation of insoluble decomposition products. The existence of **3** was confirmed by multi-element NMR spectroscopy at –60 °C. The ^{31}P NMR spectrum of the reaction mixture revealed a doublet ($^{3}J_{P–H}$ = 13.8 Hz) at –50.9 ppm (Figure 2.6). A doublet in the ^{1}H NMR spectrum could also be observed with same coupling constant at 6.03 ppm. This resonance collapses to a singlet in the ^{1}H{^{31}P} NMR spectrum. Resonances for all three magnetically inequivalent carbon atoms in **3** could be detected by ^{13}C–^{1}H 2D NMR spectroscopy. The central methine carbon was observed as a doublet at 23.92 ppm with $^{2}J_{C–P}$ = 22.7 Hz. The chemical shifts for the cyanide and cyaphide moieties were observed by ^{13}C{^{1}H} and HMBC NMR spectroscopy at 110.86 and 145.06 ppm, respectively. These values are in good agreement with computed chemical shifts (Table 2.2). These findings all are all consistent with the *in situ* generation of cyapho(dicyano)methane, and with protonation at the central carbon position. Indeed, calculations also suggest that cyapho(dicyano)methane is the most thermodynamically stable acid (by at least 5.0 kcal mol^{-1}) when compared to the other isomers that could be formed on protonation of **2** (Figure 2.7). These data are in line with the values reported by Kornath for tricyanomathine.[4]

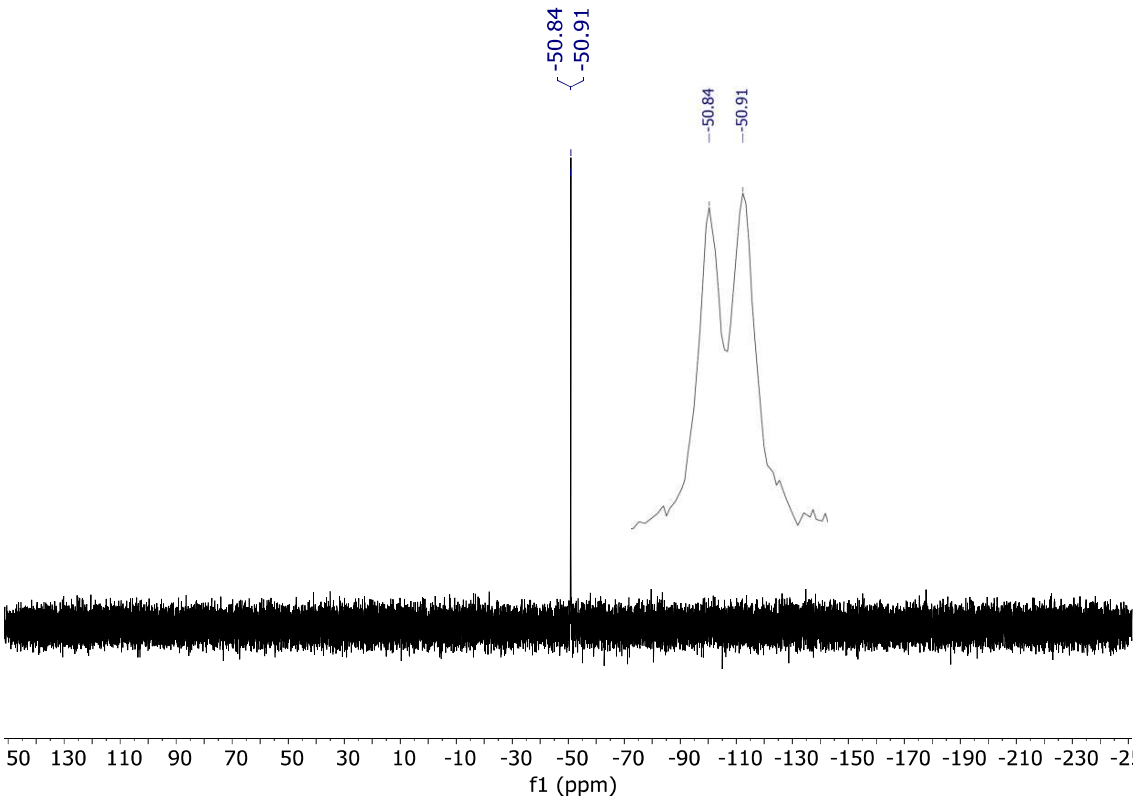

Figure 2.6. ^{31}P NMR spectrum of **3** at −60 °C (202 MHz, d_8-THF).

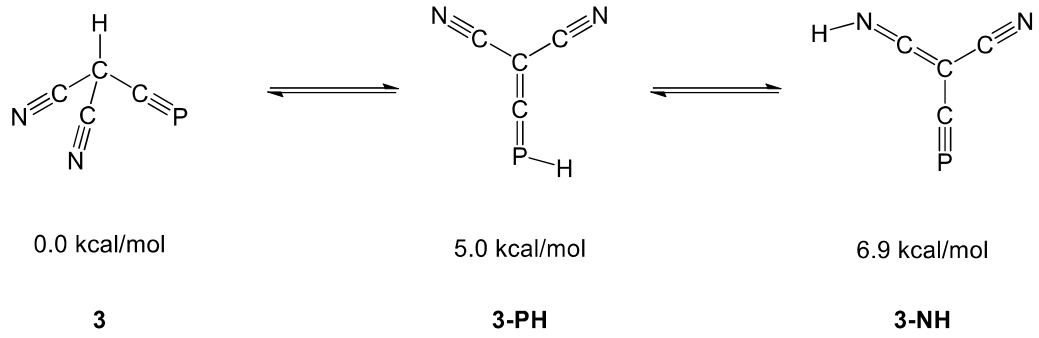

Figure 2.7. Relative energy of **3** and its isomers.

Table 2.2. NMR data for cyapho(dicyano)methane (**3**). Chemical shift values in ppm, coupling constants in Hz. (Calculated NMR shifts are referenced relative to ^{t}BuCP [$\delta(^{31}P) = -69.2$ ppm; $\delta(^{13}C$ *C*P moiety) = 184.8 ppm].[41]

Nucleus	Experimental	Computed[a]
$\delta(^{31}P)$ ($^3J_{P-H}$)	–50.1 (13.8) in d_8-THF	−39.8
	–43.7 (13.7) in Et_2O	
$\delta(^{13}C)$ of cyaphide	145.06 in d_8-THF	142.3
$\delta(^{13}C)$ of methine	23.92 in d_8-THF	15.2
$\delta(^{13}C)$ of cyanide	110.86 in d_8-THF	103.5

[a] GIAO-PBE1PBE/6-311G(d,p)].

2.5.2 Phosphaalkyne-like reactivities of 2

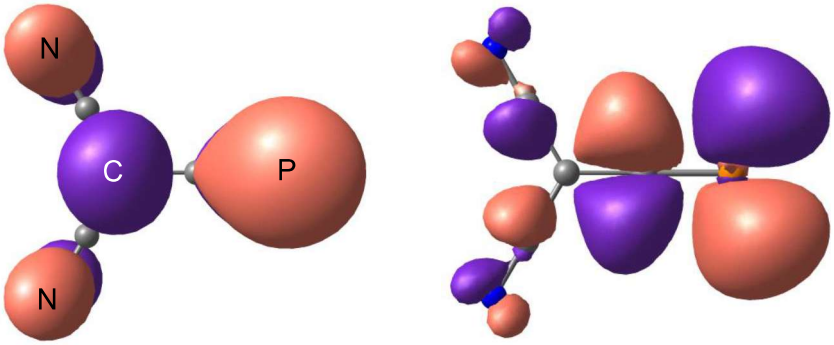

HOMO (−2.19 eV) **LUMO (3.86 eV)**

Figure 2.8. Kohn-Sham orbital depictions of the HOMO and LUMO of $[C(CN)_2(CP)]^-$ rendered at an isovalue of 0.03.

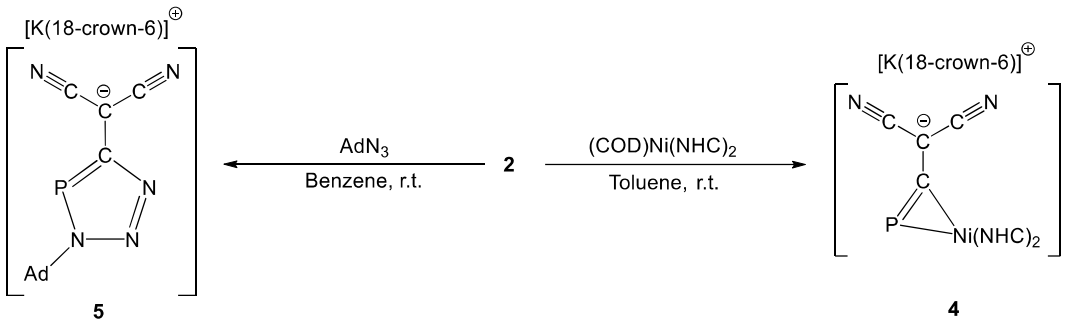

Scheme 2.4. Reactivity of **2** leading to **4** and **5**. [K(18-crown-6)]**4** and [K(18-crown-6)]**5** were isolated in 40 and 49% yield, respectively.

Having established that **2** is capable of reacting through the methanide carbon atom, we turned our attention to the reactivity of the cyaphide moiety. DFT calculations reveal that the lowest unoccupied molecular orbital (LUMO) of **2** has a significant contribution from an out-of-plane C−P π* interaction (Figure 2.8), which implies that reactions with the C≡P triple bond should be accessible. As phosphaalkynes are known to bind to transition metals complexes,[42] we reasoned that reaction of **2** with an electron-rich transition metal fragment should allow access to the cyaphide moiety through LUMO-driven reactivity.[43] Treatment of **2** with [Ni(COD)(^{Me}IPr)$_2$] (^{Me}IPr = C[N^{t}PrCMe]$_2$) in toluene afforded complex **4** (Scheme 2.4), which features a singlet in its ^{31}P NMR spectrum at 45.4 ppm. The solid-state molecular structure of [K(18-crown-6]**4**·1.5tol was determined by single crystal X-ray diffraction (Figure 2.9, left), which revealed a structure containing C–P–Ni three-membered ring as expected. The bond length of C–P bond length (1.672(2) Å) is significantly elongated compared to that of **2** (1.553(2) Å), consistent with significant back-donation from the nickel center to the C–P π* orbital. The cyapho(dicyano)-methanide moiety in **4** still retains its planar geometry (Σ°: 359.8°), indicating that the molecule is still highly conjugated. Of note is that the P1–C1–C2 bond angle is now significantly bent (143.8(1)°) relative to that of **2** (179.6(2)°). This geometry is very similar to that observed for [Ni(IMes)(CO)(η^2-PC^{t}Bu)] reported by Wolf in 2019,[44] which has a C–P bond of 1.626(2) Å and a P–C–C bond angle of 146.1(2)°.

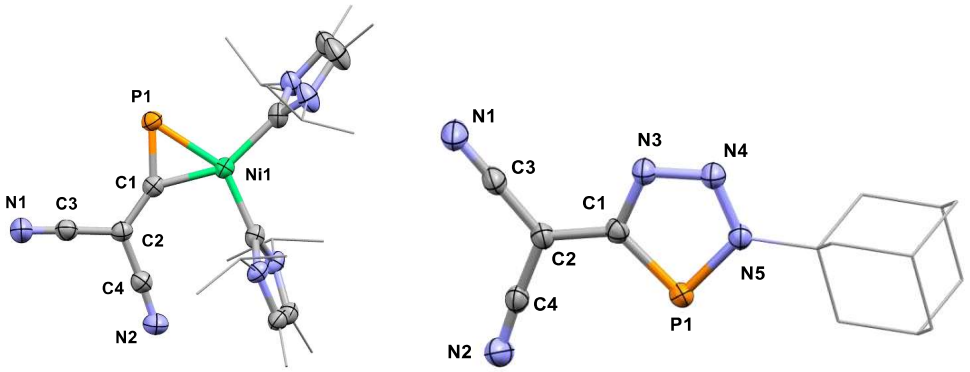

Figure 2.9. Single crystal X-ray structures of the anionic components in [K(18-crown-6]**4**·1.5tol (left) and [K(18-crown-6)]**5** (right). Anisotropic displacement ellipsoids pictured at 50% probability. Carbon atoms of Me, ^{i}Pr and Ad groups pictured using wireframe mode. Selected bond lengths (Å) and angles (°) **4**: P1–C1, 1.672(2); C1–C2 1.416(2); C2–C3, 1.414(2), C2–C4, 1.418(2), C3–N1, 1.159(2), C4–N2, 1.157(2), P1–Ni1, 2.210(1); P1–C1, 1.672(2); C1-C2-C3, 123.6(2), C1-C2-C4, 123.4(2); C3-C2-C4, 112.8(2); C2-C1-P2, 143.8(1); Ni1-C1-P1, 76.8(1); C1–Ni1–P1, 47.4(1); Ni1–P1–C1 55.7(1). **5**: P1–C1, 1.740(2); C1–C2 1.442(2); C2–C3, 1.409(2), C2–C4, 1.403(2), C3–N1, 1.160(2), C4–N2, 1.158(2), C1–N3, 1.364(2); N3–N4, 1.316(2); N4–N5, 1.331(2); P1–N5, 1.706(1); C1-C2-C3, 122.3(2), C1-C2-C4, 118.4(2); C3-C2-C4, 119.3(2); C2-C1-P1, 126.3(1); C1-N3-N4, 113.1(2); N3–N4–N5, 112.1(1); N4–N5–P1 116.0(1); N5–P1–C1 86.1(1).

Prompted by the phosphaalkyne-like nature of the bonding in **4**, we decided to explore other reactions of the C−P bond. Cyclisation reactions between azides and phosphaalkynes are known to yield triazaphospholes,[45–50] however, to the best of our knowledge, no such reactivity has been reported for *anions* that contain a cyaphide moiety such as PCO^{-} or $[N(CN)(CP)]^{-}$. Given the extensive delocalization present in **2**, it seemed viable that [3+2] cyclisation reactions might indeed take place with azides due to the relatively small degree of negative charge located on the cyaphide moiety (Table 2.1). Reaction of **2** with adamantyl azide revealed the formation of a new compound by ^{31}P NMR spectroscopy with a singlet at 136.5 ppm. This is comparable to other known trizaphospholes such as 3,5-di-*tert*-butyl-1,2,3,4-triazaphosphole which has a ^{31}P chemical shift at 161.8 ppm.[47] The structure of the resulting product, [K(18-crown-6)]**5**, was confirmed by single crystal X-ray diffraction (Figure 2.9, right). The most notable aspect of this structure is the fact that the

triazaphosphole and dicyanomethanide moieties are co-planar (mean deviation from plane 0.0156 Å), which is once again indicative of extensive delocalization of negative charge throughout the anion. As expected, on cyclisation the C−P bond elongates significant to 1.740(2) Å (cf. 1.553(2) Å for **2**).

2.6 Conclusions

In summary, we have developed a synthetic route to access a novel cyaphide-containing anion, (cyapho)dicyano-methanide $[C(CN)_2CP]^-$ (**2**) from the reaction of 1,1-diethoxy-2,2-dicyanoethylene $(EtO)_2C{=}C(CN)_2$ with $[Na(18\text{-crown-6})][PH_2]$. An intermediate, $[HP\{C(OEt){=}C(CN)_2\}]^-$, was isolated after the first Michael addition-elimination step, and with the help of a non-nucleophilic base (KHMDS), this intermediate could further be converted to the target anion. DFT calculations reveal that **2** possesses a highly delocalized π-system and that the cyaphide moiety is just as (if not more) effective at negative charge stabilization than a nitrile group. The parent acid, (cyapho)dicyanomethane could also be synthesized and characterized at −60 °C by multi-element NMR spectroscopic studies. Further reactivity studies revealed that the C≡P triple bond in **2** is chemically accessible by reaction with transition metal nucleophiles and azides. These findings suggest that, as with TCM, this novel anion may find use as a component in coordination polymers.

2.7 Experimental section

2.7.1 Synthesis of [Na(18-crown-6)]1

A THF solution (3 mL) of 1,1-diethoxy-2,2-dicyanoethylene, $(EtO)_2C{=}C(CN)_2$, (150 mg, 0.90 mmol, 1.00 eq.) was added dropwise to a stirring THF solution (10 mL) of $[Na(18\text{-crown-6})][PH_2]$ (289 mg, 0.90 mmol, 1.00 eq.) at −78 °C. The reaction was allowed to slowly warm to room temperature overnight. All volatiles were removed *in vacuo*, and the

resulting yellow oil was re-dissolved in minimal amount of THF (5 ml) and layered with pentane (THF:pentane = 1:1) at room temperature. Yellow, needle-like crystals were collected after 1 day and these were washed with toluene (2 × 2 mL) and pentane (2 × 2 mL) and dried under a dynamic vacuum to yield [Na(18-crown-6)]**1** (250 mg, 0.57 mmol; 63% yield). Single crystals of [Na(18-crown-6)]**1**·THF suitable for X-ray diffraction were obtained by slow diffusion of pentane into a concentrated THF solution of the product at –35°C for 3 days. Anal. Calcd. for $C_{18}H_{30}N_2NaO_7P$ (M.W. 440.38 g mol^{-1}): C, 49.09; H, 6.87; N, 6.36; Found: C 48.98; H, 6.82; N, 6.60.

^{1}H NMR (600 MHz, d$_8$-THF): δ (ppm) 1.27 (t, $^{3}J_{H–H}$ = 7.0 Hz, 3H; C*H*$_3$), 3.14 (d, $^{1}J_{P–H}$ = 166.5 Hz, 1H; P*H*), 3.62 (s, 24H; 18-crown-6), 4.11 (dq, $^{4}J_{P–H}$ = 2.6 Hz, $^{3}J_{H–H}$ = 7.0 Hz, 2H; C*H*$_2$).

^{13}C{^{1}H} NMR (151 MHz, d$_8$-THF): δ (ppm) 15.00 (s; *C*H$_3$), 47.20 (d, $^{2}J_{P–C}$ = 11.9 Hz; (CN)$_2$*C*), 65.75 (d, $^{3}J_{P–C}$ = 37.1 Hz; O*C*H$_2$), 70.54 (s; 18-crown-6), 120.65 (br; *C*N), 124.86 (br; *C*N), 215.61 (d, $^{1}J_{P–C}$ = 62.0 Hz; *C*(PH)).

^{31}P NMR (162 MHz, d$_8$-THF): δ (ppm) −66.3 (d, $^{1}J_{P–H}$ = 166.5 Hz).

^{31}P{^{1}H} NMR (162 MHz, d$_8$-THF): δ (ppm) −66.7 (s).

2.7.2 Synthesis of [K(18-crown-6)]2

A THF solution (3 mL) of KHMDS (67.8 mg, 0.34 mmol, 1.00 eq.) was slowly added to a THF solution (10 mL) of [Na(18-crown-6)]**1** (150 mg, 0.34 mmol, 1.00 eq.) at –78 °C. After stirring for 3 hours at –78 °C, the solution was warmed up to 0 °C and kept stirring at this temperature for 2 days. The reaction was monitored by ^{31}P NMR spectroscopy until all of the starting material was completed consumed. The solution was filtered using a filter cannula to remove NaOEt. The solution was concentrated to half of the original volume under vacuum at –35 °C and then layered with cold pentane. [Note: Treatment of this solution

above –30 °C was found to give rise to product decomposition]. The THF/pentane mixture was shaken vigorously at –35 °C to form a brown precipitate, and the solvent removed by filtration. The remaining brown powder was dried *in vacuo* to yield [K(18-crown-6)]**2** (90 mg, 0.22 mmol; yield: 64%). Single crystals of [K(18-crown-6)]**2**·THF suitable for X-ray diffraction were obtained by slow diffusion of pentane into a THF solution of the product at –35 °C for 3 days. Anal. Calcd. for $C_{16}H_{24}KN_2O_6P$ (M.W. 410.42 g mol^{-1}): C, 46.82; H, 5.89; N, 6.83; Found: C 47.54; H, 6.04; N, 6.61.

^{1}H NMR (500 MHz, d$_8$-THF): δ (ppm) 3.62 (s, 18-crown-6).

^{13}C{^{1}H} NMR (125 MHz, d$_8$-THF): δ (ppm) 34.94 (d, $^{2}J_{P–C}$=19.3 Hz; *C*$(CN)_2$), 70.91 (s, 18-crown-6), 122.59 (d, $^{3}J_{P–C}$ = 4.8 Hz; *C*N), 171.00 (d, $^{1}J_{P–C}$ = 27.5 Hz; *C*P).

^{31}P NMR (162 MHz, d$_8$-THF): δ (ppm) 27.1 (s).

FTIP (ATR): ν(cm^{-1}) 1554.6 (vs, PCC stretch), 2151.7 (vs, NCC_{asymm} stretch), 2183.1 (vs, NCC_{symm} stretch).

2.7.3 Synthesis of 3

[K(18-crown-6)]**2** (5 mg, 0.012 mmol, 1.00 eq.) and Brookhart's acid (12.3 mg, 0.012 mmol, 1.00 eq.) were weighed into an NMR tube equipped with an air-tight tap inside a glovebox. 0.4 ml of d$_8$-THF (or Et_2O) were vacuum transferred into the NMR tube and the solvent was allowed to thaw in an acetone-dry ice bath. A Bruker AVIII HD 500 MHz (w/ detect ^{13}C cryoprobe) spectrometer was pre-cooled to –60 °C before the reaction mixture was inserted into the instrument. All NMR data were recorded at this temperature. Based on the integration of ^{1}H NMR spectrum, around 40% conversion was achieved at –60 °C.

^{1}H NMR (500 MHz, d$_8$-THF, –60 °C): δ (ppm) 3.56 (s; 18-crown-6), 6.03 (d, $^{3}J_{P–H}$ = 13.8 Hz, 0.4H; *H*C$(CN)_2$(CP)), 1.10 (t, $^{3}J_{H–H}$ = 6.4 Hz, 12H; C*H*$_3$ Et_2O), 3.35 (q, $^{3}J_{H–H}$ = 6.4 Hz,

8H; CH_2 Et_2O), 7.70 (s, 4H; ArH $BAr^F{}_4$), 7.86 (s, 8H; ArH $BAr^F{}_4$), 13.10 (s broad, 0.6 H; H^+).

$^{13}C\{^1H\}$ NMR (125 MHz, d_8-THF, –60 °C): δ (ppm) 23.92 (d, $^2J_{P–C}$ = 22.7 Hz; HC(CN)$_2$(CP)), 70.80 (s, 18-crown-6) 110.86 (s; CN), 145.06 (CP), 15.73 (s; CH$_3$ Et_2O), 66.46 (s; CH$_2$ Et_2O), 118.23 (s; ArC $BAr^F{}_4$), 125.21 (q, $^1J_{C–F}$ = 273.0 Hz; CF$_3$ $BAr^F{}_4$), 129.72 (q, $^2J_{C–F}$ = 31.8 Hz; ArC $BAr^F{}_4$), 135.16 (s; ArC $BAr^F{}_4$), 162.75 (q, $^1J_{C–B}$ = 49.5 Hz; ArC $BAr^F{}_4$).

^{31}P NMR (202 MHz, d_8-THF, –60 °C): δ (ppm) −50.9 (d, $^3J_{P–H}$=13.8 Hz).

^{31}P{^{1}H} NMR (202 MHz, d_8-THF, –60 °C): δ (ppm) −50.1 (s).

^{31}P NMR (202 MHz, Et_2O, –60 °C): δ (ppm) −43.7 (d, $^3J_{P–H}$=13.7 Hz).

^{31}P{^{1}H} NMR (202 MHz, Et_2O, –60 °C): δ (ppm) −43.6 (s).

2.7.4 Synthesis of [K(18-crown-6]4

A toluene solution (0.6 mL) of [Ni(COD)(^{Me}IPr)$_2$] (12.8 mg, 0.024mmol, 1.00 eq.) was slowly added to a toluene solution (0.6 mL) of [K(18-crown-6)]**2** (10 mg, 0.024mmol, 1.00 eq.). The mixture was stirred for 10 minutes before filtering. The resulting dark-brown solution was layered with pentane at −35 °C. Orange crystals were collected after 3 days and washed with pentane (2 × 1 mL), then dried *in vacuo* to afford [K(18-crown-6)]**4** (8 mg, 0.01 mmol; yield: 40%). Single crystal of [K(18-crown-6)]**4**·1.5tol suitable for X-ray diffraction were obtained by slow diffusion of pentane into a concentrated toluene/THF solution of the product at room temperature overnight. Anal. Calcd for $C_{38}H_{64}KN_6NiO_6P$·0.5tol (M.W. 875.73 g mol^{-1}): C, 56.91; H, 7.83; N, 9.60; Found: C 56.30; H, 8.21; N, 9.28.

^{1}H NMR (600 MHz, C_6D_6): δ (ppm) 1.28 (d, $^3J_{H–H}$ = 7.1 Hz, 6H; CH(CH_3)$_2$), 1.32 (d broad, $^3J_{H–H}$ = 7.0 Hz, 12H, CH(CH_3)$_2$), 1.91 (s, 6H; CH_3), 2.04 (s, 6H; CH_3), 3.31 (s, 24H; 18-

crown-6), 6.07 (sept, $^{3}J_{H–H}$ = 7.0 Hz, 2H; C*H*$(CH_3)_2$), 6.21 (sept, $^{3}J_{H–H}$ = 7.0 Hz, 2H; C*H*$(CH_3)_2$).

$^{13}C\{^{1}H\}$ NMR (151 MHz, C_6D_6): δ (ppm) 10.58 (s; *C*H_3), 10.86 (s; *C*H_3), 22.06 (s; CH(*C*$H_3)_2$), 22.42 (s; CH(*C*$H_3)_2$), 22.51 (s; CH(*C*$H_3)_2$), 42.68 (s; *C*$(CN)_2$(CP)), 52.10 (s; *C*H$(CH_3)_2$), 52.21 (s; *C*H$(CH_3)_2$), 70.37 (s; 18-crown-6), 123.27 (s; *C*(CH_3)), 124.01 (s; *C*(CH_3)), 132.54 (s; *C*N), 201.16 (s; carbene *C*), 203.60 (s; carbene *C*), 219.20 (d, $^{1}J_{P–C}$ = 88.3 Hz; *C*P).

^{31}P NMR (162 MHz, C_6D_6): δ (ppm) 45.4 (s).

2.7.5 Synthesis of [K(18-crown-6)]5

A benzene solution (0.3 mL) of AdN_3 (4.4 mg, 0.024 mmol, 1.00 eq.) was slowly added to a benzene solution (0.3 mL) of [K(18-crown-6)]**2** (10 mg, 0.024 mmol, 1.00 eq.). The mixture was stirred for 24 hours before all volatiles were removed *in vacuo* to obtain a dark brown oil. The oil was re-dissolved in THF and filtered to remove insoluble impurities. The THF solution was layered with pentane and placed in a −35 °C freezer. A brown powder was collected after 3 days and washed with pentane (2 × 1 mL), then dried *in vacuo* to afford [K(18-crown-6)]**5** (7 mg, 0.012 mmol; yield: 49%). Single crystal of [K(18-crown-6)]**5** suitable for X-ray diffraction were obtained by slow diffusion hexane into a concentrated benzene and THF solution of the product at room temperature. Anal. Calcd. for $C_{26}H_{39}KN_5O_6P$ (M.W. 587.65 g mol^{-1}): C, 53.13; H, 6.69; N, 11.92; Found: C 53.56; H, 6.67; N, 11.30.

^{1}H NMR (600 MHz, C_6D_6): δ (ppm) 1.50 (m, 6H; CH_2 Ad), 1.91 (s, 3H; C*H* Ad), 2.26 (d, $^{4}J_{P–H}$ = 2.3 Hz, 6H; CH_2 Ad), 3.24 (s, 24H; 18-crown-6).

$^{13}C\{^{1}H\}$ NMR (151 MHz, C_6D_6): δ (ppm) 29.05 (d, $^{2}J_{P-C}$ = 38.3 Hz; *C*$(CN)_2$), 30.30 (s; *C*H Ad), 36.47 (s; *C*H_2 Ad), 45.40 (d, $^{3}J_{P-C}$ = 6.8 Hz; *C*H_2 Ad), 60.80 (d, $^{2}J_{P-C}$ = 7.9 Hz; *C* Ad), 70.19 (s, 18-crown-6), 126.58 (d, $^{3}J_{P-C}$ = 3.4 Hz; *C*N), 186.88 (d, $^{1}J_{P-C}$ = 50.8 Hz; *C*P)

^{31}P NMR (162 MHz, C_6D_6): δ (ppm) 136.5 (s).

2.8 References

[1] R. H. Boyd, *J. Phys. Chem.* **1963**, *67*, 737−744.

[2] E. Raamat, K. Kaupmees, G. Ovsjannikov, A. Trummal, A. Kütt, J. Saame, I. Koppel, I. Kaljurand, L. Lipping, T. Rodima, V. Pihl, I. A. Koppel, I. Leito, *J. Phys. Org. Chem.* **2013**, *26*, 162−170.

[3] B. Bak, H. Svanholt, *J. Mol. Struct.* **1977**, *37*, 153−156.

[4] T. Soltner, J. Häusler, A. J. Kornath, *Angew. Chem. Int. Ed.* **2015**, *54*, 13775−13776.

[5] H. Schmidtmann, *Ber. Dtsch. Chem. Ges.* **1896**, *29*, 1168.

[6] H. Brand, A. Schulz, A. Villinger, *Z. Anorg. Allg. Chem.* **2007**, *633*, 22−35.

[7] B. F. Abrahams, S. R. Batten, B. F. Hoskins, R. Robson, *Inorg. Chem.* **2003**, *42*, 2654−2664.

[8] H. B. Wineinger, V. Smetana, A. Nayak, F. Qu, A.-V. Mudring, R. D. Rogers, *Cryst. Growth Des.* **2022**, *22*, 2372−2381

[9] J. Kohout, L. Jäger, M. Hvastijová, J. Kožíšek, *J. Coord. Chem.* **2000**, *51*, 169−218.

[10] S. R. Batten, K. S. Murray, *Coord. Chem. Rev.* **2003**, *246*, 103−130.

[11] R. Srinivasan, S. Tragl, H.-J. Meyer, *Z. Anorg. Allg. Chem.* **2005**, *631*, 1075−1078.

[12] A. Bernsdorf, H. Brand, R. Hellmann, M. Köckerling, A. Schulz, A. Villinger, K. Voss, *J. Am. Chem. Soc.* **2009**, *131*, 8958–8970.

[13] L. C. Tomé, M. Isik, C. S. R. Freire, D. Mecerreyes, I. M. Marrucho, *J. Membr. Sci.* **2015**, *483*, 155−165.

[14] L. C. Tomé, D. C. Guerreiro, R. M. Teodoro, V. D. Alves, I. M. Marrucho, *J. Membr. Sci.* **2018**, *549*, 267−274.

[15] A. S. L. Gouveia, E. Bumenn, K. Rohtlaid, A. Michaud, T. M. Vieira, V. D. Alves, L. C. Tomé, C. Plesse, I. M. Marrucho, *Sep. Purif. Technol.* **2021**, *274*, 118437.

[16] M. Marszalek, Z. Fei, D.-R. Zhu, R. Scopelliti, P. J. Dyson, S. M. Zakeeruddin, M. Grätzel, *Inorg. Chem.* **2011**, *50*, 11561−11567.

[17] M. Bidikoudi, T. Stergiopoulos, V. Likodimos, G. E. Romanos, M. Francisco, B. Iliev, G. Adamová, T. J. S. Schubert, P. Falaras, *J. Mater. Chem. A* **2013**, *1*, 10474−10486.

[18] G. W. Meindersma, A. B. De Haan, *Sci. China Chem.* **2012**, *55*, 1488−1499.

[19] M. Larriba, N. Delgado-Mellado, P. Navarro, R. Alcover, C. Moya, J. Palomar, J. García, F. Rodríguez, *Energy Fuels* **2018**, *32*, 5650−5658.

[20] W. Madelung, E. Kern, *Liebigs Ann.* **1922**, *427*, 1−26.

[21] J. S. Miller, J. L. Manson, *Acc. Chem. Res.* **2001**, *34*, 563−570.

[22] D. R. MacFarlane, J. Golding, S. Forsyth, M. Forsyth, G. B. Deacon, *Chem. Commun.* **2001**, 1430−1431.

[23] Y. Yoshida, K. Muroi, A. Otsuka, G. Saito, M. Takahashi, T. Yoko, *Inorg. Chem.* **2004**, *43*, 1458−1462.

[24] N. N. Greenwood, A. Earnshaw, *Chemistry of the Elements*, Elsevier, 2012.

[25] G. Becker, W. Schwarz, N. Seidler, M. Westerhausen, *Z. Anorg. Allg. Chem.* **1992**, *612*, 72−82.

[26] J. M. Goicoechea, H. Grützmacher, *Angew. Chem. Int. Ed.* **2018**, *57*, 16968−16994.

[27] G. Becker, K. Hübler, *Z. Anorg. Allg. Chem.* **1994**, *620*, 405−417.

[28] F. Tambornino, A. Hinz, R. Köppe, J. M. Goicoechea, *Angew. Chem. Int. Ed.* **2018**, *57*, 8230−8234.

[29] A. Hinz, J. M. Goicoechea, *Angew. Chem. Int. Ed.* **2016**, *55*, 8536–8541.

[30] A. Schmidpeter, F. Zwaschka, *Angew. Chem. Int. Ed. Engl.* **1977**, *16*, 704−705.

[31] W. S. Sheldrick, J. Kroner, F. Zwaschka, A. Schmidpeter, *Angew. Chem. Int. Ed. Engl.* **1979**, *18*, 934−935.

[32] J. F. Binder, S. C. Kosnik, P. B. J. St Onge, C. L. B. Macdonald, *Chem. Eur. J.* **2018**, *24*, 14644−14648.

[33] Y. Mei, Z. Yan, L. L. Liu, *J. Am. Chem. Soc.* **2022**, *144*, 1517−1522.

[34] D. Ergöçmen, J. M. Goicoechea, *Angew. Chem. Int. Ed.* **2021**, *60*, 25286−25289.

[35] F. F. Puschmann, D. Stein, D. Heift, C. Hendriksen, Z. A. Gal, H.-F. Grützmacher, H. Grützmacher, *Angew. Chem. Int. Ed.* **2011**, *50*, 8420–8423.

[36] D. Heift, Z. Benkő, H. Grützmacher, *Dalton Trans.* **2014**, *43*, 831–840.

[37] A. M. Arif, A. R. Barron, A. H. Cowley, S. W. Hall, *J. Chem. Soc., Chem. Commun.* **1988**, 171−172.

[38] P. Pyykkö, M. Atsumi, *Chem. Eur. J.* **2009**, *15*, 186−197.

[39] L. X. Dang, *J. Am. Chem. Soc.* **1995**, *117*, 6954−6960.

[40] M. Brookhart, B. Grant, A. F. Volpe, *Organometallics* **1992**, *11*, 3920−3922.

[41] G. Becker, G. Gresser, W. Uhl, *Z. Naturforsch. B* **1981**, *36*, 16−19.

[42] J. F. Nixon, *Coord. Chem. Rev.* **1995**, *145*, 201−258.

[43] For similar reactivity in the context of bridging cyaphide ligands see: E. S. Yang, J. M. Goicoechea, *Angew. Chem. Int. Ed.* DOI: 10.1002/anie.202206783.

[44] G. Hierlmeier, P. Coburger, M. Bodensteiner, R. Wolf, *Angew. Chem. Int. Ed.* **2019**, *58*, 16918−16922.

[45] W. Rösch, M. Regitz, *Angew. Chem. Int. Ed. Engl.* **1984**, *23*, 900−901.

[46] Y. Y. C. Y. L. Ko, R. Carrié, A. Muench, G. Becker, *J. Chem. Soc., Chem. Commun.* **1984**, 1634−1635.

[47] W. Rösch, T. Facklam, M. Regitz, *Tetrahedron* **1987**, *43*, 3247−3256.

[48] J. A. W. Sklorz, S. Hoof, N. Rades, N. De Rycke, L. Könczöl, D. Szieberth, M. Weber, J. Wiecko, L. Nyulászi, M. Hissler, C. Müller, *Chem. Eur. J.* **2015**, *21*, 11096−11109.

[49] M. Papke, L. Dettling, J. A. W. Sklorz, D. Szieberth, L. Nyuläszi, C. Müller, *Angew. Chem. Int. Ed.* **2017**, *56*, 16484–16489.

[50] T. Görlich, D. S. Frost, N. Boback, N. T. Coles, B. Dittrich, P. Müller, W. D. Jones, C. Müller, *J. Am. Chem. Soc.* **2021**, *143*, 19365−19373.

Chapter 3
Isolation and Characterization of an Anionic Imine-Supported Two-Coordinate Phosphinidene Oxide

---

The contents of this chapter have been published:

C. Hu, N. H. Rees, M. Pink and J. M. Goicoechea, *Nat. Chem.* **2024**, 16, 1855–1860.

3.1. Introduction

Nitroso compounds, R–N=O, are nitrogen(III) oxides with a bent geometry and a stereochemically active lone pair on the nitrogen atom. They are key intermediates in several important organic transformations such as the hetero Diels-Alder (HDA) and nitroso-aldol reactions.[1,2] Despite the propensity of nitrosoarenes to dimerize, many monomeric *C*- and *N*-nitroso compounds are stable at ambient temperature and commercially available. By contrast, analogous phosphorus(III) oxides, R–P=O (phosphanones or phosphinidene oxides), are highly unstable. Compounds such as CH_3PO,[3] CH_3OPO,[4] and PhPO[5] can only be observed at extremely low temperatures (3–15 K) in inert gas matrices. Despite their highly reactive nature, these compounds are of enormous fundamental importance. For example, metaphosphorous acid (*cis*-HOPO) is proposed to be a key intermediate in the oxidation of organic phosphorus compounds such as phosphines.[6–9] The aforementioned studies point at the difficulties associated with the isolation of phosphorus(III) oxides, which are prone to intermolecular polymerization pathways on account of their diminished π-bond energies when compared to their nitrogen analogues.

A common strategy for the isolation of highly reactive molecules is to trap these in the coordination sphere of metals. For example, work by Cummins has shown that phosphorus monoxide can be employed as a terminal ligand for the formation of a molybdenum complex with a terminal Mo–P=O bond (Figure 3.1, **A**).[10] This species exhibits a short Mo–P bond (2.079(5) Å) and a linear Mo-P-O bond angle (177.6(8)°), both of which imply significant d_π–p_π interactions between the metal center and phosphorus monoxide moiety. To our knowledge, the synthesis of an isolable phosphinidene oxide with a bent structure such as that predicted for R–P=O, (R = OH, CH_3, OCH_3, Ph) has not been achieved to date despite various attempts to characterize such compounds in the condensed phase.[11–16] The first direct

observation of a phosphenite RO–P=O (R = 2,6-di-*tert*-butyl-4-methylphenyl; **B**) was accomplished by pyrolyzing its cyclic trimer. This species was identified by $^{31}P\{^{1}H\}$ NMR spectroscopy (singlet resonance at 238 ppm) and IR spectroscopy ($\nu_{P=O}$ = 1235 cm^{-1}).[17] However, the monomer rapidly reverted to the starting material upon warming up to 272 K. Phosphinidene oxides have been stabilized when coordinated to transition metal centers or through interactions with main group Lewis acids/bases. The first isolable phosphinidene oxide complex was stabilized within the coordination sphere of chromium, as reported by Niecke and colleagues in 1980 (**C**), and several group six metal stabilized cases were reported later.[18–22] More recently, Stephen and Liu successfully isolated a donor-acceptor stabilized phosphinidene oxide compound (**D**).[23] Compounds stabilized exclusively by an external donor would come several years later with Braunschweig describing an N-heterocyclic carbene adduct of phosphinidene oxide,[24] while Nikonov and co-workers reported a phosphine stabilized congener (**E**).[25]

The availability of phosphinidene oxides stabilized by external Lewis bases prompted us to explore whether the use of an internal π-donor substituent would allow access to an isolable variant. In addition to the electronic stabilization offered by such a ligand, significant steric bulk would be required to circumvent the aforementioned oligomerization pathways. Herein, we describe the synthesis of an anionic imine stabilized phosphinidene oxide $RNPO^{-}$ which can be further functionalized into a neutral amido-functionalized phosphinidene oxide R(R')NPO (detailed in Chapter 4). These species represent the first examples of isolable two coordinate phosphorus(III) oxides.

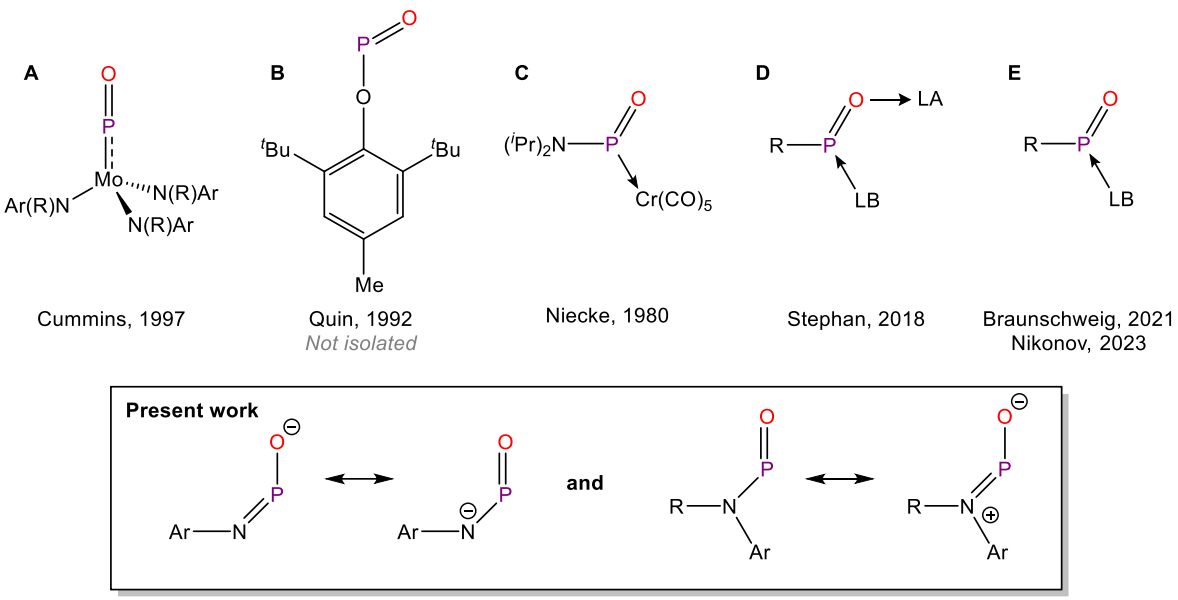

Figure 3.1. Phosphinidene oxides and their complexes.

3.2. Ligand design

In contrast to other kinetically stabilized main group species with multiple bonds, phosphinidene oxides R–P=O present a unique challenge. The use of steric protection is only viable at one end of the molecule, thus necessitating the presence of an R group capable of providing long-range steric shielding to prevent oligomerization. Inspired by the work of Goto and co-workers, in which they adopted *meta*-substituted terphenyl group to protect nitroso-selenocysteine (R–SeNO) and selenenic acids (R–SeOH),[26–29] we synthesized compound **7** as an N-terminal protecting group (Scheme 3.1) through a Suzuki-Miyaura cross-coupling reaction. In addition to the kinetic stabilization offered by steric bulk, the corresponding phosphinidene oxide precursors R–NPO$^-$ are viable targets for compounds with P^{III}=O double bond character on account of their anionic charge. Electrostatic repulsion can effectively deter oligomerization or polymerization of such species. An exemplary case of this strategy is the isolation of the 2-phosphaethynolate anion PCO$^-$ and its

analogues.[30–34] However, it is crucial to note that upon losing the charge (through protonation, for instance), these anions readily oligomerize.[35]

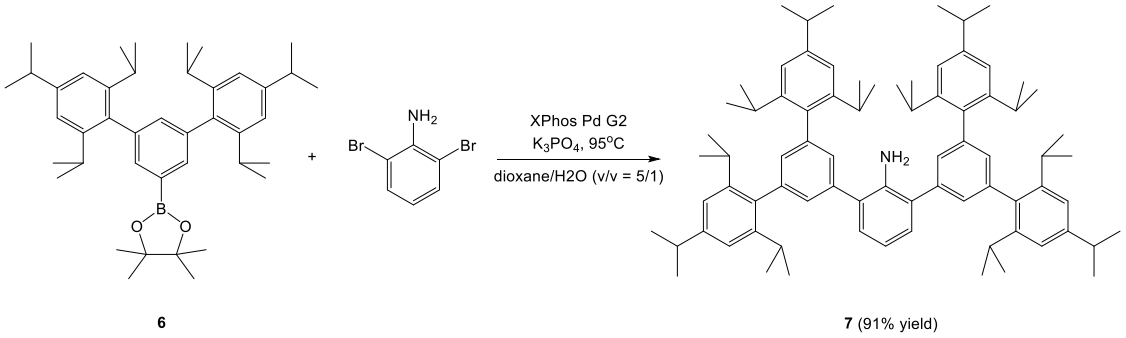

Scheme 3.1. Synthesis of **7**, herein abbreviated as $ArNH_2$, through Suzuki-Miyaura cross-coupling reaction.

3.3. Synthesis of an imine-stabilized phosphinidene oxide RNPO$^-$

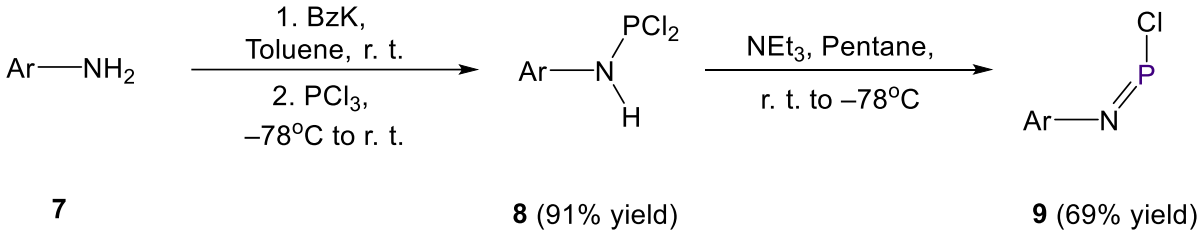

Scheme 3.2. Synthesis of **8** and **9** according to a modified literature procedure.

To achieve our goal, we synthesized the chloro(imino)phosphane **9** through a doubly hydrogen chloride elimination (Scheme 3.2), according to a modified literature procedure.[36] As Cl^- is iso-electronic to O^{2-}, exchange of the chloride ion in **9** could lead to the imine-stabilized anionic phosphinidene oxide RNPO$^-$. We identified KOTMS as a potential O^{2-} transfer reagent, due to the semi-labile Si–O bond in KOTMS which can be cleaved by another molecule of KOTMS. Upon treatment of **9** with 2.5 equivalents of KOTMS in tetrahydrofuran (THF), *in situ* $^{31}P\{^1H\}$ NMR spectroscopy revealed a distinct singlet at 237.2 ppm, corresponding to the formation of **10** (Scheme 3.3).

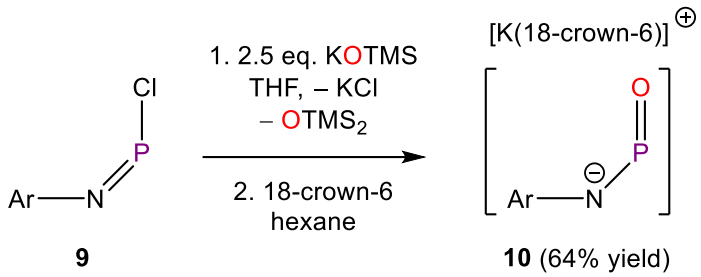

Scheme 3.3. Synthesis of **10**.

3.4. Mechanism of the reaction between 9 and KOTMS

Interestingly, this reaction did not proceed via the expected intermediate, R–N=P–OTMS, followed by desilylation. Instead, it proceeds via a three-coordinate phosphite K[R–N–P(OTMS)$_2$], facilitated by the excess KOTMS, ultimately leading to the elimination of hexamethyldisiloxane OTMS$_2$. Evidence is provided by controlling the stoichiometry of KOTMS with **9**.

3.4.1 1:1 Reaction between 9 and KOTMS

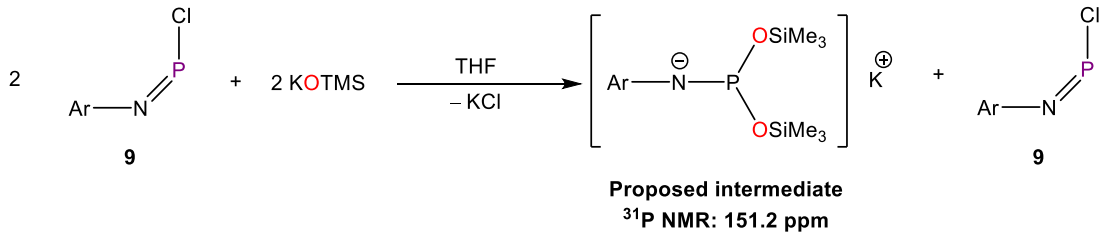

Scheme 3.4. 1:1 Reaction between **9** and KOTMS.

To a solid mixture of **9** (10 mg, 0.009 mmol, 1.0 eq.) and KOTMS (1.1 mg, 0.009 mmol, 1 eq.), THF (0.5 ml) was added (Scheme 3.4). The mixture was stirred vigorously for 5 min before the *in situ* measurement of the ^{31}P NMR spectrum. A 1:1 mixture was observed in the ^{31}P NMR spectrum with one of the components being unconsumed starting material **9** (Figure 3.2). Based on this finding, we proposed a 1:2 reaction between **9** and KOTMS, generating [ArNP(OTMS)$_2$]$^-$K$^+$ as an intermediate.

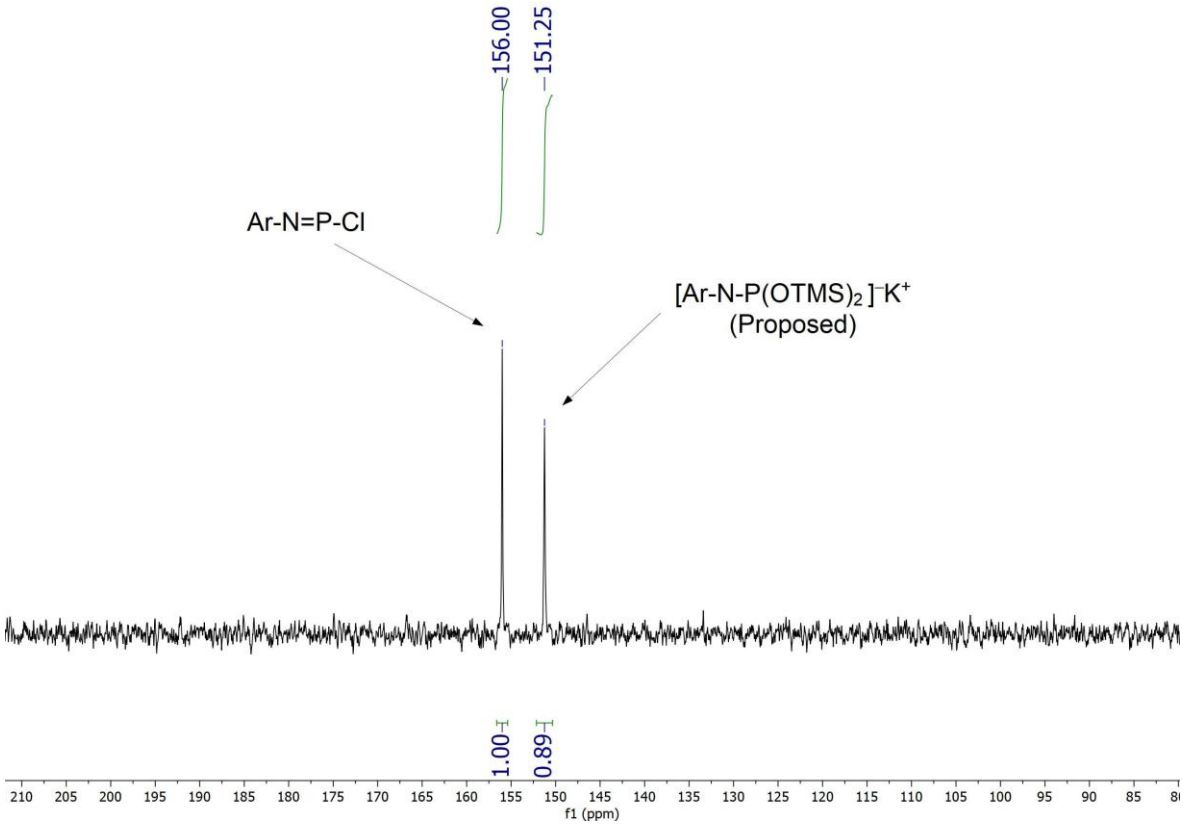

Figure 3.2. *In situ* ^{31}P NMR spectrum of 1:1 reaction between **9** and KOTMS (162 MHz, THF).

3.4.2 1:2 Reaction between 9 and KOTMS

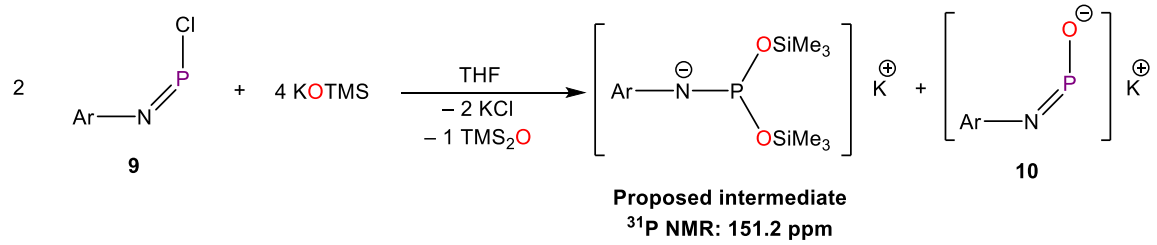

Scheme 3.5. 1:2 Reaction between **9** and KOTMS.

To a solid mixture of **9** (10 mg, 0.009 mmol, 1.0 eq.) and KOTMS (2.2 mg, 0.018 mmol, 2 eq.), THF (0.5 ml) was added (Scheme 3.5). The mixture was stirred vigorously for 5 min before collection of its ^{31}P NMR spectrum measurement. A 1:1 mixture was observed in the ^{31}P NMR spectrum again, with one of the component being the final product **10**, and the other component the intermediate at 151.2 ppm, which we proposed to be $[ArNP(OTMS)_2]^-K^+$ (Figure 3.3). Excess KOTMS was then added to the reaction mixture, after which only

the final product **10** can be observed in the ^{31}P NMR spectrum. Therefore, we propose that the reaction mixture between **9** and KOTMS first went through the $[ArNP(OTMS)_2]^-K^+$ intermediate. The following elimination of the hexamethyldisiloxane (TMS_2O) was assisted by excess KOTMS.

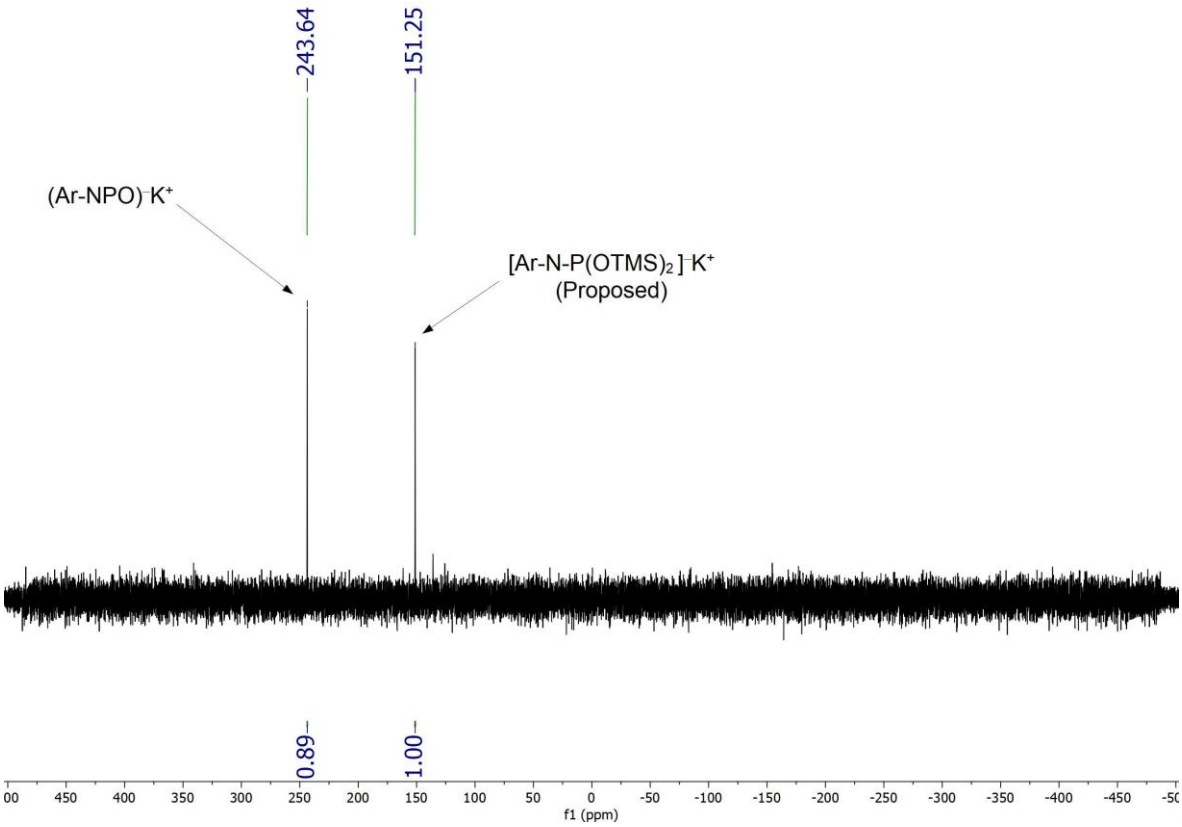

Figure 3.3. *In situ* ^{31}P NMR spectrum of 1:2 reaction between **9** and KOTMS (162 MHz, THF).

3.4.3 1:2 Reaction between 9 and ^{t}BuOK

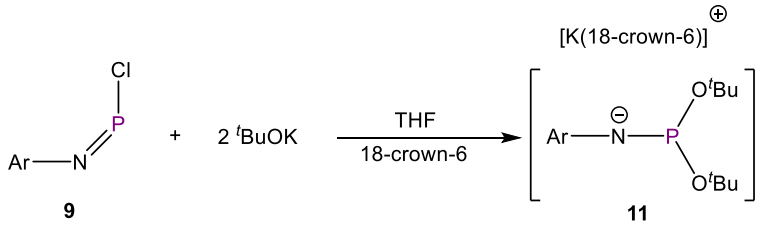

Scheme 3.6. 1:2 Reaction between **9** and ^{t}BuOK.

Due to the inertness of the C–O bond, when the reagent changed from KOTMS to ^{t}BuOK, the generated product $[ArNP(O^tBu)_2]^-K^+$ did not go through the elimination of di-

tert-butyl ether ($^{t}Bu_2O$; Scheme 3.6). Upon addition of 18-crown-6, **11** can be isolated in a 75% yield. The structure of **11** was confirmed through single crystal X-ray diffraction (Figure 3.4), further supporting the formation of $[ArNP(OTMS)_2]^{-}K^{+}$, in the reaction involving KOTMS.

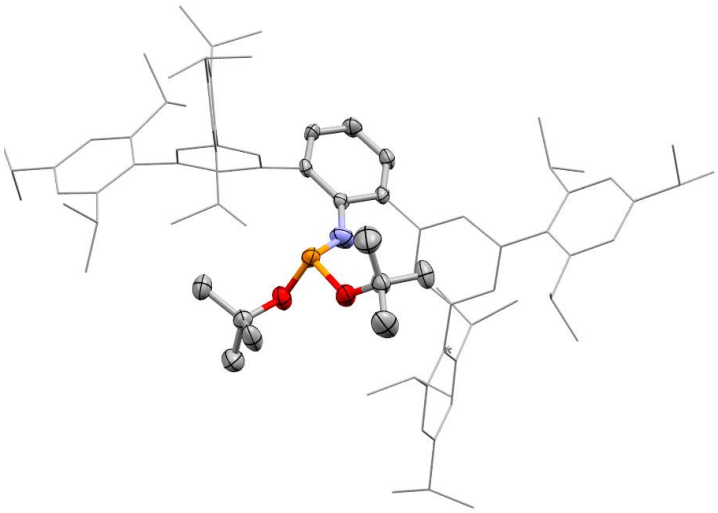

Figure 3.4. Single crystal X-ray structure of **11**. Selected carbon atoms for backbones are depicted with an arbitrary radius; thermal ellipsoids of heteroatoms pictured at 50% probability level. Solvent of crystallization, hydrogen atoms, $[K(18\text{-crown-6})(THF)_2]^{+}$ counter cation, and minor disordered components are removed for clarity.

3.5. Crystal structure and DFT calculations of 10

Structural confirmation of compounds **9** and **10** was obtained through single crystal X-ray diffraction analysis (Figure 3.5). The crystal structure of **10** reveals a bent N-P-O moiety (116.85(11)°) and a P–O bond length of 1.501(2) Å. Notably, this P–O bond length closely resembles those observed in phosphinidene oxides stabilized by either acids or bases.[18,24–25] The P–N bond elongates from 1.497(2) Å in **9** to 1.5822(19) Å. These bond lengths suggest that there is π-bonding character between both P–O and P–N. In fact, the anionic moiety in

10 can be rationalized as a heavier analogue of nitrite (NO_2^-), exhibiting phosphorus-centered three-center-four-electron (3c-4e) bonding. The oxygen atom of the anionic moiety exhibits a short electrostatic interaction with the $[K(18\text{-crown-6})]^+$ counteraction with an O···K interatomic distance of 2.634(2) Å.

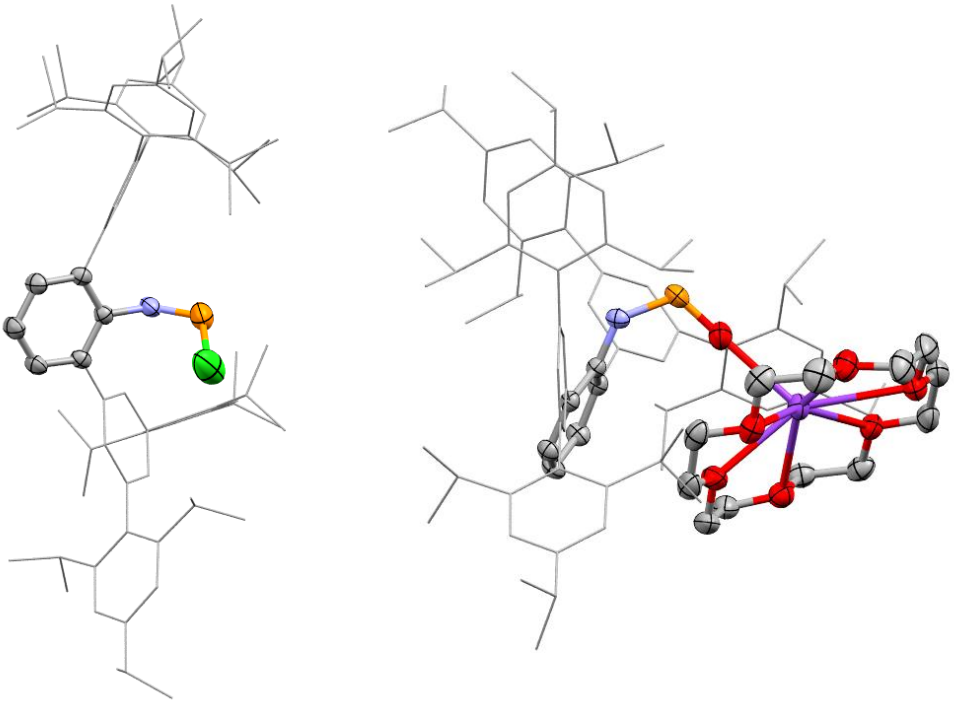

Figure 3.5. Single crystal X-ray structures of **9** (left) and **10** (right). Selected carbon atoms for backbones are depicted with wireframe mode. Thermal ellipsoids pictured at 50% probability level. Solvent of crystallization and hydrogen atoms are removed for clarity.

Table 3.1. Bond metric data comparison between computed structure and crystal structure.

Bond length/angle	N–P (Å)	P–O (Å)	K–O (Å)	N–P–O (°)
Crystal structure	**1.5822 (19)**	**1.501 (2)**	**2.634 (2)**	**116.85(11)**
$[ArNPO]^-$	**1.601**	**1.522**	**N.A.**	**115.79**
[K(18-crown-6)][ArNPO] (3)	**1.596**	**1.532**	**2.518**	**113.54**

DFT calculations were conducted to elucidate the electronic structure of **10**. The optimized geometries of both the free ion ($[ArNPO]^-$) and the ion-paired salt (**10**) were computed at the M06-2X/Def2-svp level of theory (a comparison is provided in Table 3.1). For the simplicity, the free ion ($[ArNPO]^-$) is used in the analysis discussed herein. The computed structural metrics and are in good agreement with those obtained by X-ray crystallography (e.g. N1–P1: 1.601 Å; O1–P1: 1.522 Å for $[ArNPO]^-_{DFT}$). Natural bond orbital (NBO) analysis revealed the presence of a three-center-four-electron (3c-4e) bonding interaction, with the N–P double bond contributing 57.3% to the system and the P–O double bond contributing 42.7% (refer to the resonance forms in Figure 3.6a). This is supported by Wiberg bond indices (WBIs), which indicate similar bond orders for the N–P (1.25) and P–O (1.24) bonds. Mayer bond indices indicate a slightly higher bond order for the P–O bond (1.64) compared to the N–P bond (1.40). Nevertheless, both bond indices collectively confirm the existence of multiple bonding character within the N–P–O moiety. Remarkably, in both the WBIs and Mayer bond indices, the N–O bond showed a non-negligible bond order (0.16 in WBIs and 0.07 in Mayer). This observation underscores the delocalized nature of the N–P–O bonding interaction, with N–O exhibiting some degree of π bonding. Indeed, three molecular orbitals can be located in a simplified model ($MeNPO^-$), representing a classic three-center-four-electron system (Figure 3.6b). The Natural Population Analysis (NPA) showed that both N (–1.06 a.u.) and O (–1.10 a.u.) carry significant negative charge, indicating both atoms can be used for further functionalization. To gain further insight into the reactive sight, a conceptual DFT calculation was conducted. The dual descriptor iso-surface showed that N1 has a larger negative $\Delta f(r)$ compared O1, which implies that N1 is a more nucleophilic center (Figure 3.6c).[37–39] The nucleophilicity of N1 and O1 in **10** is probed through reactivities studies detailed in Chapter 4.

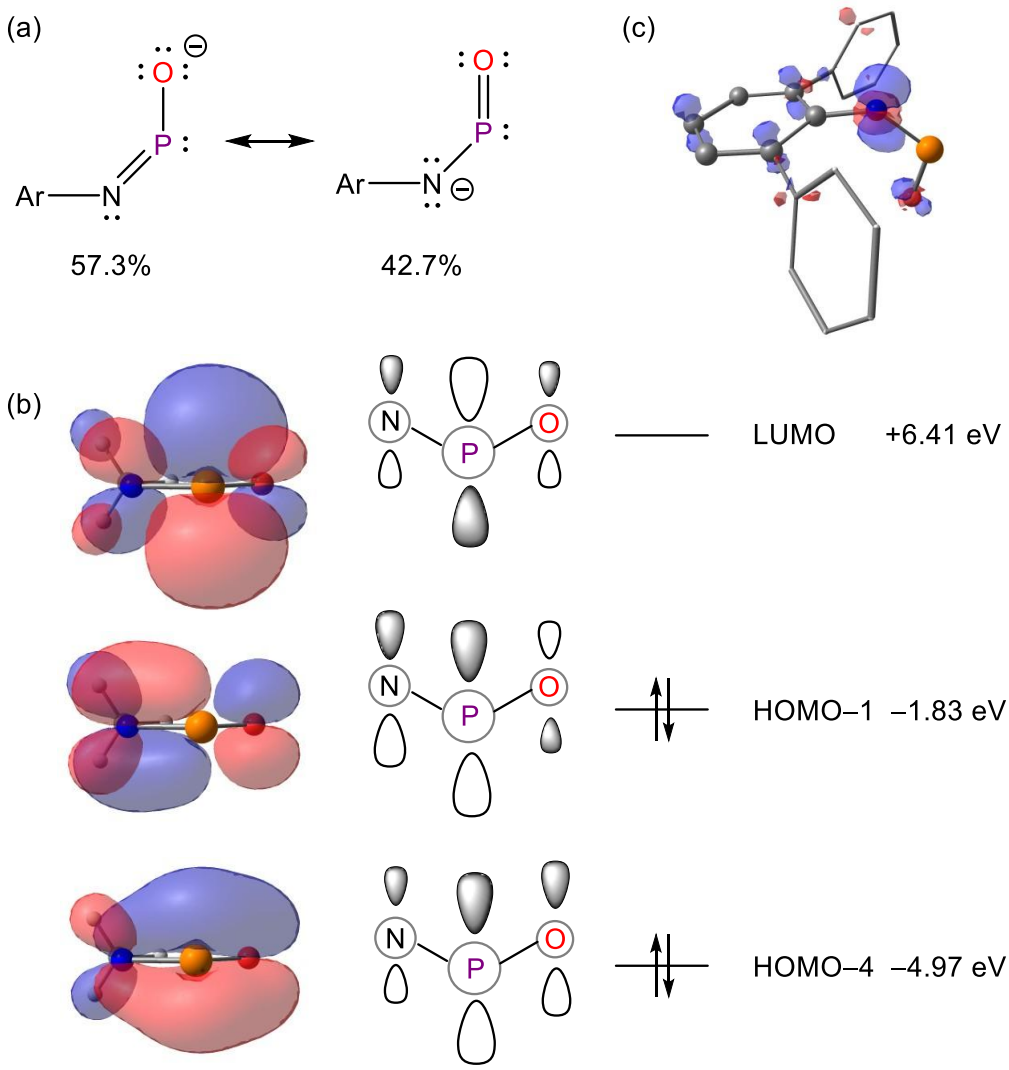

Figure 3.6. a) Resonance forms and NBO analysis of **10**; b) Selected Kohn-Sham molecular orbitals and a simplified MO diagram for the three-center-four-electron bonding interaction present in **10**; c) Dual descriptor iso-surface model.

The crystal structure of **10** reveals a *cis*-geometry comparable to that of **9** and other reported chloro(imino)phosphanes.[36,40] However, calculations on the cation-free moiety $[ArNPO]^-$ showed that *trans*-isomer is thermodynamically more stable than the *cis*-isomer by 1.1 kcal with a low energy barrier of interconversion (6.5 kcal mol^{-1}; Figure 3.7). When calculating the full ion pair [K(18-crown-6)][ArNPO] the two optimized geometries showed a significant energy difference, with the *cis*-isomer being lower in energy by 4.6 kcal mol^{-1}.

This can be rationalized by the fact that the *cis*-isomer exhibits a shorter K···O interatomic distance (2.518 Å versus 2.587 Å or 2.637 Å in an unfavored geometry), which offers greater electrostatic stabilization. In this case, the *cis*-isomer showed less steric hindrance, because the $[K(18\text{-crown-6})]^+$ counter-cation can occupy the void below the bulky ligand. While the low energy barrier suggests rapid isomerization at room temperature, the much more thermodynamically stable *cis*-isomer is formed predominantly (as observed by X-ray diffraction).

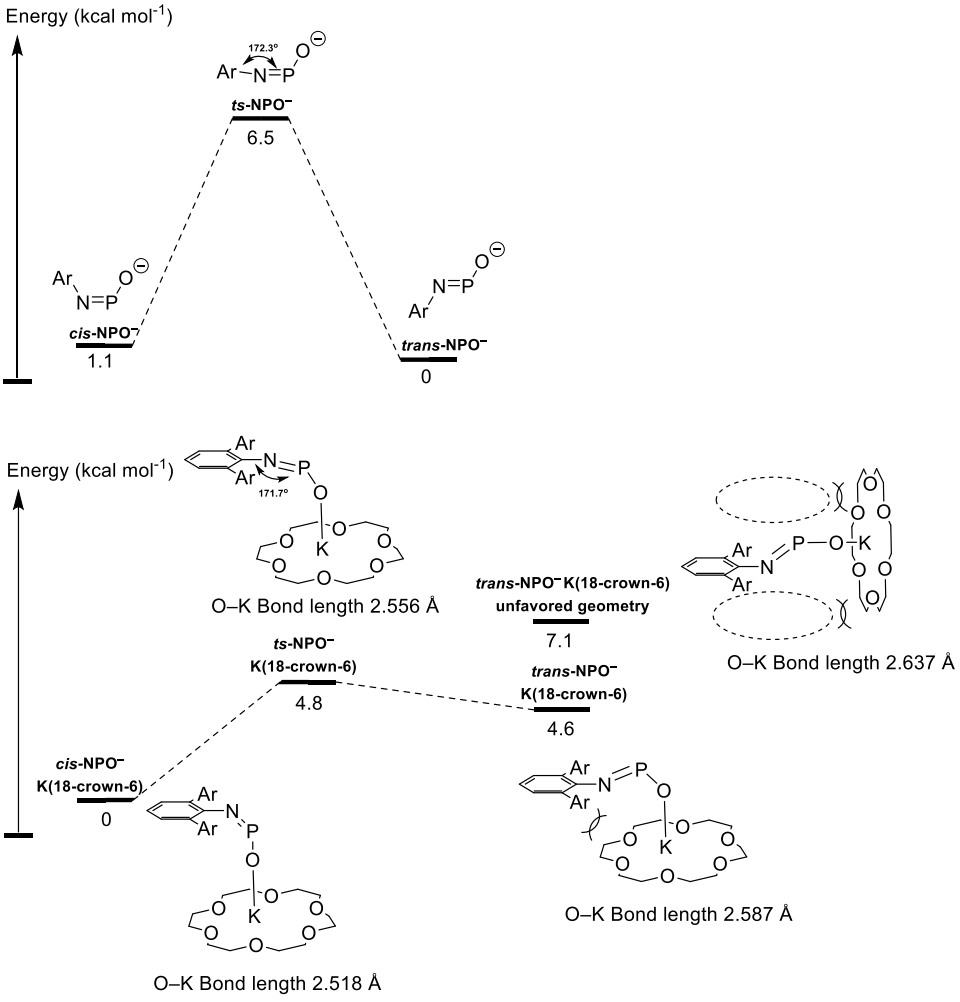

Figure 3.7. Energy plots for the *cis*-*trans* isomerization processes computed for $[ArNPO]^-$ (top) and [K(18-crown-6)][ArNPO] (bottom).

3.6. Conclusions

In summary, we have developed a synthetic route to access a novel anionic imine supported phosphinidene **10** from the reaction of chloro(imino)phosphane **9** and excess KOTMS. The rection proceed through an unexpected phosphite K[R–N–P(OTMS)$_2$], which was characterized by *in situ* ^{31}P NMR spectroscopy. Facilitated by excess KOTMS, the intermediate undergoes elimination of hexamethyldisiloxane OTMS$_2$, affording the desired phosphinidene oxide product **10**. This phosphinidene oxide is stabilized through both steric protection by the extremely bulky meta-substituted aryl group as well as electrostatic repulsion, preventing it from dimerization or oligomerization. Similar to the parent ion NO_2^-, a three-center-four-electron (3c-4e) interaction was detected within the N–P–O moiety, with the N=P double bond contributing most to the system. This finding is supported by both crystallographic data and DFT calculations. A classic 3c-4e molecular orbital pattern was also found in the simplified model $MeNPO^-$. DFT calculations also suggest that both N1 and O1 in **10** possess significant negative charge, indicating both atoms can be functionalized through electrophilic reactions. This hypothesis will be further explored in Chapter 4.

3.7. Experimental section

3.7.1. Synthesis of 6

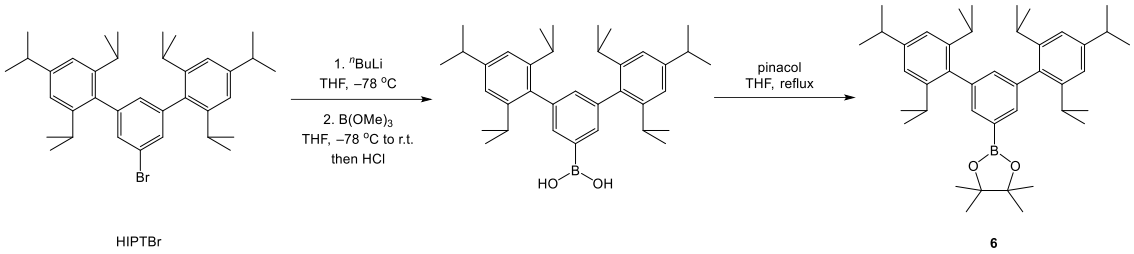

Scheme 3.7. Synthesis of **6**.

5′-Bromo-2,2″,4,4″,6,6″-hexakis(1-methylethyl)-1,1′:3′,1″-terphenyl (HIPTBr) was synthesized based on reported literature procedure.[41] ^{n}BuLi (1.6M in hexane, 8.26 ml, 13.3 mmol, 1.07 eq.) was added dropwise to a stirring THF solution (150 ml) of HIPTBr (7 g, 12.46 mmol, 1.00 eq.) at –78 ˚C. The reaction was allowed to stir at this temperature for 2 h before $B(OMe)_3$ (4.2 ml, 37.4 mmol, 3.00 eq.) was added to the solution dropwise. The reaction was allowed to slowly warm to room temperature overnight, then treated a 1M HCl (60 ml) and stirred for 2 h. The mixture was extracted with Et_2O and the combined organic layer was dried over $MgSO_4$. All volatiles were removed *in vacuo*, and to the resulting oily solid was added a THF solution (100 ml) of pinacol (1.484 g, 12.6 mmol, 1.01 eq.). The mixture was heated to reflux overnight, and solvent evaporated afterwards. The crude mixture was purified by silica gel column chromatography (PE:$CHCl_3$ = 4:1) to give **6** (6.05g, 9.96mmol; 80% yield) as a white powder. Anal. Calcd. for $C_{42}H_{61}B_1O_2$ (M.W. 608.76 g mol^{-1}): C, 82.87; H, 10.10; Found: C 83.05; H, 10.21.

^{1}H NMR (500 MHz, $CDCl_3$): δ (ppm) 1.03 (d, $^3J_{H–H}$ = 6.9 Hz, 12H; $CH(CH_3)_2$), 1.14 (d, $^3J_{H–H}$ = 6.8 Hz, 12H; $CH(CH_3)_2$), 1.29 (d, $^3J_{H–H}$ = 6.9 Hz, 12H; $CH(CH_3)_2$), 1.33 (s, 12H; CH_3), 2.71 (sept, $^3J_{H–H}$ = 6.8 Hz, 4H; $CH(CH_3)_2$), 2.92 (sept, $^3J_{H–H}$ = 6.8 Hz, 2H; $CH(CH_3)_2$), 7.02 (s, 4H; Ar*H*), 7.13 (t, $^4J_{H–H}$ = 1.7 Hz, 1H; Ar*H*), 7.59 (d, $^4J_{H–H}$ = 1.7 Hz, 2H; Ar*H*).

$^{13}C\{^1H\}$ NMR (125 MHz, $CDCl_3$): δ (ppm) 24.18, 24.63, 25.17 (s; $CH(CH_3)_2$), 24.27 (s; $OC(CH_3)_2$), 30.50, 34.46 (s; $CH(CH_3)_2$), 83.77 (s; $OC(CH_3)_2$), 120.48, 134.13, 134.34, 137.13, 139.86, 146.65, 147.81 (s; Ar*C*).

3.7.2. Synthesis of 7

To a solid mixture of **6** (6.0 g, 9.858 mmol, 2.02 eq.), 2,6-dibromoaniline (1.224 g, 4.878 mmol, 1.0 eq.), XPhos Pd G2 (100 mg) and K_3PO_4 (4.06 g, 19.13 mmol, 3.92 eq.), a degassed mixture of dioxane (100 ml) and H_2O (20 ml) was added. The mixture was stirred at 95 °C overnight. After cooling back to room temperature, the mixture was extracted with EtOAc (200 ml) and the combined organic layer was dried over $MgSO_4$. All volatiles were removed *in vacuo*, and the residue was purified by silica gel column chromatography (PE:$CHCl_3$ = 10:1) to give **7** (4.7 g, 4.46 mmol; 91% yield) as a white powder. Anal. Calcd. for $C_{78}H_{103}N$ (M.W. 1054.69 g mol^{-1}): C, 88.83; H, 9.84; N, 1.33; Found: C 88.46; H, 9.80; N, 1.32.

^1H NMR (600 MHz, C_6D_6): δ (ppm) 1.17 (d, $^3J_{H–H}$ = 6.8 Hz, 24H; $CH(CH_3)_2$), 1.26 (d, $^3J_{H–H}$ = 6.8 Hz, 24H; $CH(CH_3)_2$), 1.31 (d, $^3J_{H–H}$ = 6.8 Hz, 24H; $CH(CH_3)_2$), 2.90 (sept, $^3J_{H–H}$ = 6.8 Hz, 4H; $CH(CH_3)_2$), 3.06 (sept, $^3J_{H–H}$ = 6.8 Hz, 8H; $CH(CH_3)_2$), 3.95 (s, 2H; N*H*), 6.80 (t, $^3J_{H–H}$ = 7.6 Hz, 1H; Ar*H*), 7.09 (t, $^4J_{H–H}$ = 1.6 Hz, 2H; Ar*H*), 7.21 (s, 8H; Ar*H*), 7.37 (d, $^3J_{H–H}$ = 7.6 Hz, 2H; Ar*H*), 7.61 (d, $^4J_{H–H}$ = 1.6 Hz, 4H; Ar*H*).

$^{13}C\{^1H\}$ NMR (151 MHz, C_6D_6): δ (ppm) 24.41, 24.47, 25.71 (s; $CH(CH_3)_2$), 31.10, 34.93 (s; $CH(CH_3)_2$), 119.33, 120.84, 129.13, 130.66, 130.78, 137.38, 140.00, 141.37, 141.91, 146.88, 148.58 (s; Ar*C*).

HRMS (*m*/*z*): $[M+H]^+$ calcd. For $C_{78}H_{104}N$, 1054.8163; found 1054.8119.

3.7.3. Synthesis of 8

To a solid mixture of **7** (2.0 g, 1.896 mmol, 1.0 eq.) and BzK (248 mg, 1.896 mmol, 1.0 eq.), toluene (80 ml) was added. The mixture was stirred at room temperature for 2 h before

cooling to –78 °C. PCl_3 (0.2 ml, 2.29 mmol, 1.2 eq.) was added dropwise at this temperature, after which the mixture was allowed to slowly warm up to room temperature overnight. All volatiles were removed *in vacuo*, and the residue was re-dissolved in hexane (100 ml). The solution was filtered using a filter cannula to remove KCl. All volatiles were removed *in vacuo* again to give **8** (1.95 g, 1.73 mmol; 91% yield) as a white powder. Note: due to the identical solubility of **7** and **8**, **8** cannot be isolated as a pure sample, the product always contains ~5% of **7**.

^{1}H NMR (500 MHz, C_6D_6): δ (ppm) 1.24 (d, $^3J_{H–H}$ = 6.8 Hz, 24H; CH(C*H*$_3$)$_2$), 1.28-1.31 (m, 48H; CH(C*H*$_3$)$_2$), 2.89 (sept, $^3J_{H–H}$ = 6.8 Hz, 4H; C*H*(CH$_3$)$_2$), 3.10 (sept, $^3J_{H–H}$ = 6.8 Hz, 8H; C*H*(CH$_3$)$_2$), 6.24 (s, 1H; N*H*), 6.84 (td, $^3J_{H–H}$ = 7.5 Hz, $^6J_{P–H}$ = 2.5 Hz, 1H; Ar*H*), 7.21-7.25 (m, 12H; Ar*H*), 7.34 (d, $^4J_{H–H}$ = 1.5 Hz, 4H; Ar*H*).

^{13}C{^{1}H} NMR (125 MHz, C_6D_6): δ (ppm) 24.45, 24.54, 24.83 (s; CH(*C*H$_3$)$_2$), 31.02, 34.92 (s; *C*H(CH$_3$)$_2$), 120.88, 125.16 (d, $^3J_{P–C}$ = 3.2 Hz), 129.68 (d, $^4J_{P–C}$ = 2.5 Hz), 130.94 (d, $^4J_{P–C}$ = 2.9 Hz), 131.90, 135.07, 136.72 (d, $^2J_{P–C}$ = 4.8 Hz), 139.36 (d, $^5J_{P–C}$ = 1.7 Hz), 136.99, 142.33, 146.94, 148.74 (s; Ar*C*).

^{31}P{^{1}H} NMR (202 MHz, C_6D_6): δ (ppm) 168.3 (s)

3.7.4. Synthesis of 9

To a pentane solution (80 ml) of **8** (500 mg, 0.44 mmol, 1.0 eq.), NEt_3 (0.5 ml, 3.58 mmol, 8.14 eq.) was added at room temperature. The mixture was slowly cooled to –78 °C, and then kept at this temperature and stirred for 4 h. The solution was filtered using a filter cannula under –78 °C. (This reaction is under dynamic equilibrium, and product is favoured at low temperature) The filtrate was allowed to warm up to room temperature, after which all volatiles were removed *in vacuo* to give **9** (342 mg, 0.306 mmol; 69% yield) as a yellow powder. Note: due to the identical solubility of **7**, **8** and **9**, **9** cannot be isolated as a

compositionally pure sample, the product always contains ~5% of **7** and trace amount of **8**. Single crystals of **9** suitable for X-ray diffraction were obtained by slow evaporation of a concentrated hexane solution of the product at room temperature.

^{1}H NMR (500 MHz, C_6D_6): δ (ppm) 1.22–1.24 (m, 48H; CH(C*H*$_3$)$_2$), 1.30 (d, $^{3}J_{H–H}$ = 6.8 Hz, 24H; CH(C*H*$_3$)$_2$), 2.89 (sept, $^{3}J_{H–H}$ = 6.8 Hz, 4H; C*H*(CH$_3$)$_2$), 3.07 (sept, $^{3}J_{H–H}$ = 6.8 Hz, 8H; C*H*(CH$_3$)$_2$), 6.90 (t, $^{3}J_{H–H}$ = 6.5 Hz, 1H; Ar*H*), 7.09 (t, $^{4}J_{H–H}$ = 1.5 Hz, 2H; Ar*H*), 7.21 (s, 8H; Ar*H*), 7.37 (d, $^{3}J_{H–H}$ = 6.5 Hz, 2H; Ar*H*), 7.46 (d, $^{4}J_{H–H}$ = 1.5 Hz, 4H; Ar*H*).

^{13}C{^{1}H} NMR (125 MHz, C_6D_6): δ (ppm) 24.46, 24.57, 24.76 (s; CH(*C*H$_3$)$_2$), 31.03, 34.93 (s; *C*H(CH$_3$)$_2$), 120.84, 126.19, 129.44, 130.04, 131.14, 133.00 (d, $^{2}J_{P–C}$ = 10.6 Hz), 137.35, 139.86, 141.43, 146.92, 148.59, 148.74 (s; Ar*C*).

^{31}P NMR (202 MHz, C_6D_6): δ (ppm) 161.5 (s).

HRMS (*m*/*z*): [M+H]$^{+}$ calcd. For $C_{78}H_{102}NPCl$, 1118.7444; found 1118.7840.

3.7.5. Synthesis of 10

To a solid mixture of **9** (150 mg, 0.134 mmol, 1.0 eq.) and KOTMS (42.5 mg, 0.331 mmol, 2.5 eq.), THF (15 ml) was added. The mixture was stirred vigorously for 5 min before all volatiles were removed *in vacuo*. Hexane (10 ml) was added to the residue, and the solution was filtered using a filter cannula. To the filtrate, a solution of 18-crown-6 (35 mg, 0.132 mmol; 0.99 eq.) in hexane (10 ml) was added, and the mixture was left standing overnight. **10** precipitated out of solution over the course of 24 h, the suspension was filtered, and the resulting solid was washed with hexane (10 ml × 2) then dried *in vacuo* to afford **10** (120 mg, 0.086 mmol; yield: 64%) as a reddish white powder. Single crystals of **10** suitable for X-ray diffraction were obtained by slowly evaporating a concentrated toluene/hexane mixed solution of **10** in a –35 °C freezer for a week. Anal. Calcd for $C_{90}H_{125}KNO_7P$ (M.W. 1403.06 g mol^{-1}): C, 77.05; H, 8.98; N, 1.00; Found: C 75.49; H, 8.78; N, 1.12. m.p. 204 °C.

^{1}H NMR (600 MHz, C_6D_6): δ (ppm) 1.29 (d, $^{3}J_{H–H}$ = 6.8 Hz, 24H; CH(C*H*$_3$)$_2$), 1.30 (d, $^{3}J_{H–H}$ = 6.8 Hz, 24H; CH(C*H*$_3$)$_2$), 1.33 (d, $^{3}J_{H–H}$ = 6.8 Hz, 24H; CH(C*H*$_3$)$_2$), 2.88 (sept, $^{3}J_{H–H}$ = 6.8 Hz, 4H; C*H*(CH$_3$)$_2$), 3.00 (s, 24H; 18-crown-6), 3.42 (sept, $^{3}J_{H–H}$ = 6.8 Hz, 8H; C*H*(CH$_3$)$_2$), 6.79 (t, $^{3}J_{H–H}$ = 7.8 Hz, 1H; Ar*H*), 7.12 (t, $^{4}J_{H–H}$ = 1.6 Hz, 2H; Ar*H*), 7.20 (s, 8H; Ar*H*), 7.44 (d, $^{3}J_{H–H}$ = 7.8 Hz, 2H; Ar*H*), 7.86 (d, $^{4}J_{H–H}$ = 1.6 Hz, 4H; Ar*H*).

^{13}C{^{1}H} NMR (151 MHz, C_6D_6): δ (ppm) 24.56, 24.72, 25.11 (s; CH(*C*H$_3$)$_2$), 30.77, 34.89 (s; *C*H(CH$_3$)$_2$), 69.87 (s; 18-crown-6), 117.11, 120.60, 129.15, 129.19, 130.33, 134.75 (d, $^{3}J_{P–C}$ = 8.6 Hz), 138.97, 139.41, 144.62, 147.41, 147.59 (s; Ar*C*), 150.21 (d, $^{2}J_{P–C}$ = 23.7 Hz; Ar*C*).

^{31}P NMR (162 MHz, C_6D_6): δ (ppm) 237.2 (s).

HRMS (*m*/*z*): [Anion+H_2O]$^{+}$ calcd. For $C_{78}H_{103}NPO_2$, 1116.7721; found 1116.7736.

FTIR (ATR): ν(cm^{-1}) 1077 (s, PO stretch).

3.7.6. Synthesis of 11

To a solid mixture of **9** (24 mg, 0.02 mmol, 1.0 eq.) and ^{t}BuOK (4.4 mg, 0.04 mmol, 2 eq.), THF (0.5 ml) was added. The mixture was stirred vigorously for 5 min before all volatiles were removed *in vacuo*. Hexane (10 ml) was added to the residue, and the solution was filtered. The filtrate was dried under vacuum, and THF (0.3 ml) was added to redissolve the residue. A solution of 18-crown-6 (5.3 mg, 0.02 mmol, 1.0 eq.) in THF (0.3 ml) was then added to the mixture, and stirred for 2 h. Hexane was then layered on top of the THF solution, and left for 24 h before supernatant was removed and the remaining crystals dried *in vacuo* to afford **11** (23 mg, 0.015 mmol; yield: 75%) as a yellow powder. Single crystals of **11** suitable for X-ray diffraction were obtained by slow diffusion of hexane into a concentrated THF solution of the product at room temperature. Anal. Calcd. for $C_{98}H_{143}NO_8PK$ (M.W. 1533.29 g mol^{-1}): C, 76.77; H, 9.40; N, 0.91; Found: C 73.55; H, 8.48; N, 0.83.

^{1}H NMR (500 MHz, d$_8$-THF): δ (ppm) 1.02–1.04 (m, 42H; CH(C*H*$_3$)$_2$ and OC(C*H*$_3$)$_3$), 1.16 (d, $^{3}J_{H–H}$ = 6.8 Hz, 24H; CH(C*H*$_3$)$_2$), 1.24 (d, $^{3}J_{H–H}$ = 6.8 Hz, 24H; CH(C*H*$_3$)$_2$), 2.86 (sept, $^{3}J_{H–H}$ = 6.8 Hz, 4H; C*H*(CH$_3$)$_2$), 3.11 (sept, $^{3}J_{H–H}$ = 6.8 Hz, 8H; C*H*(CH$_3$)$_2$), 3.52 (s, 24H; 18-crown-6), 5.97 (t, $^{3}J_{H–H}$ = 7.4 Hz, 1H; Ar*H*), 6.55 (s, 2H; Ar*H*), 6.76 (d, $^{3}J_{H–H}$ = 7.4 Hz, 2H; Ar*H*), 6.98 (s, 8H; Ar*H*), 7.58 (d, $^{3}J_{H–H}$ = 7.6 Hz, 2H; Ar*H*), 7.63 (s, 4H; Ar*H*).

^{13}C{^{1}H} NMR (125 MHz, d$_8$-THF): 24.45, 24.68, 30.61, 32.26, 32.33, 35.17 (s; *C*H(*C*H$_3$)$_2$ and OC(*C*H$_3$)$_3$), 71.02 (s; 18-crown-6), 71.60 (d, $^{2}J_{P–C}$ = 2.4 Hz; O*C*(CH$_3$)$_3$), 120.42, 120.82, 127.55, 130.83 (d, $^{3}J_{P–C}$ = 3.7 Hz), 131.12, 134.21 (d, $^{2}J_{P–C}$ = 5.0 Hz), 138.49, 139.98, 147.07, 147.11, 147.50, 148.35 (s; Ar*C*).

^{31}P{^{1}H} NMR (162 MHz, C$_6$D$_6$): δ (ppm) 139.4 (br).

HRMS (*m*/*z*): not detected

3.8. References

[1] B. G. Gowenlock, G. B. Richter-Addo, *Chem. Rev.* **2004**, 104, 3315–3340.

[2] P. Bianchi, J. C. M. Monbaliu, *Org. Chem. Front.* **2022**, 9, 223–26.

[3] X. X. Chu, Y. Yang, B. Lu, Z. Wu, W. Y. Qian, C. Song, X. F. Xu, M. Abe, X. Q. Zeng, *J. Am. Chem. Soc.* **2018**, 140, 13604–13608.

[4] X. F. Zhao, X. X. Chu, G. Rauhut, C. Y. Chen, C. Song, B. Lu, X. Q. Zeng, *Angew. Chem. Int. Ed.* **2019**, 58, 12164–12169.

[5] A. Mardyukov, F. Keul, P. R. Schreiner, *Angew. Chem. Int. Ed.* **2020**, 59, 12445–12449.

[6] X. Chu, W. Qian, B. Lu, L. Wang, J. Qin, J. Li, G. Rauhut, T. Trabelsi, J. S. Francisco, X. Q. Zeng *Angew. Chem. Int. Ed.* **2020**, 59, 21949–21953.

[7] D. E. Fast, M. Zalibera, A. Lauer, A. Eibel, C. Schweigert, A.-M. Kelterer, M. Spichty, D. Neshchadin, D. Voll, H. Ernst, Y. Liang, K. Dietliker, A. N. Unterreiner, C. Barner-Kowollik, H. Grützmacher, G. Gescheidt, *Chem. Commun.* **2016**, 52, 9917–9920.

[8] S. Liang, P. Hemberger, N. M. Neisius, A. Bodi, H. Grützmacher, J. Levalois-Grützmacher, S. Gaan, *Chem. Eur. J.* **2015**, 21, 1073–1080.

[9] W. Y. Qian, X. X. Chu, C. Song, Z. Wu, M. Q. Jiao, H. W. Liu, B. Zou, G. Rauhut, D. P. Tew, L. N. Wang, X. Q. Zeng, *Chem. Eur. J.* **2020**, *26*, 8205–8209.

[10] M. J. A. Johnson, A. L. Odom, C. C. Cummins, *Chem. Commun.* **1997**, 1523–1524 .

[11] J. K. Stille, J. L. Eichelberger, J. Higgins, M. E. Freeburger, *J. Am. Chem. Soc.* **1972**, 94, 4761–4763.

[12] M. Yoshifuji, S. Nakayama, R. Okazaki, N. Inamoto, *J. Chem. Soc., Perkin Trans.* **1973**, 2065–2068.

[13] N. Shigenobu, Y. Masaaki, O. Renji, I. Naoki, *Bull. Chem. Soc. Jpn.* **1975**, 48, 546–548.

[14] E. Niecke, H. Zorn, B. Krebs, G. Henkel, *Angew. Chem., Int. Ed. Engl.* **1980**, 19, 709–710.

[15] A. H. Cowley, F. P. Gabbaï, S. Corbelin, A. Decken, *Inorg. Chem.* **1995**, 34, 5931–5932.

[16] P. P. Gaspar, H. Qian, A. M. Beatty, D. A. d'Avignon, J. L. F. Kao, J. C. Watt, N. P. Rath, *Tetrahedron* **2000**, 56, 105–119.

[17] L. D. Quin, S. Jankowski, A. G. Sommese, P. M. Lahti, D. B. Chesnut, *J. Am. Chem. Soc.* **1992**, 114, 11009–11010.

[18] E. Niecke, M. Engelmann, H. Zorn, B. Krebs, G. Henkel, *Angew. Chem., Int. Ed. Engl.* **1980**, 19, 710–712.

[19] M. Alonso, M. E. García, M. A. Ruiz, H. Hamidov, J. C. Jeffery, *J. Am. Chem. Soc.* **2004**, 126, 13610–13611.

[20] M. Alonso, M. A. Alvarez, M. E. García, M. A. Ruiz, H. Hamidov, J. C. Jeffery, *J. Am. Chem. Soc.* **2005**, 127, 15012–15013.

[21] M. Alonso, M. A. Alvarez, M. E. García, D. García-Vivó, M. A. Ruiz, *Inorg. Chem.* **2010**, 49, 8962–8976.

[22] M. Alonso, M. A. Alvarez, M. E. García, M. A. Ruiz, H. Hamidov, J. C. Jeffery, *Inorg. Chem.* **2010**, 49, 11595–11605.

[23] L. L. Liu, D. W. Stephan, *Chem. Commun.* **2018**, 54, 1041–1044.

[24] D. Dhara, P. K. Pal, R. Dolai, N. Chrysochos, H. Rawat, B. J. Elvers, I. Krummenacher, H. Braunschweig, C. Schulzke, V. Chandrasekhar, U. D. Priyakumar, A. Jana, *Chem. Commun.* **2021**, 57, 9546–9549.

[25] A. G. Baradzenka, S. F. Vyboishchikov, M. Pilkington, G. I. Nikonov, *Chem. Eur. J.* **2023**, 29, e202301842.

[26] K. Goto, G. Yamamoto, B. Tan, R. Okazaki, *Tetrahedron Lett.* **2001**, 42, 4875–4877.

[27] K. Shimada, K. Goto, T. Kawashima, N. Takagi, Y.-K. Choe, S. Nagase, *J. Am. Chem. Soc.* **2004**, 126, 13238–13239.

[28] R. Masuda, R. Kimura, T. Karasaki, S. Sase, K. Goto, *J. Am. Chem. Soc.* **2021**, 143, 6345–6350.

[29] R. Masuda, S. Kuwano, K. Goto, *J. Am. Chem. Soc.* **2023**, 145, 14184–14189.

[30] J. M. Goicoechea, H. Grützmacher, *Angew. Chem. Int. Ed.* **2018**, 57, 16968–16994.

[31] A. Hinz, J. M. Goicoechea, *Angew. Chem. Int. Ed.* **2016**, 55, 8536–8541.

[32] F. Tambornino, A. Hinz, R. Köppe, J. M. Goicoechea, *Angew. Chem. Int. Ed.* **2018**, 57, 8230–8234.

[33] D. Ergöçmen, J. M. Goicoechea, *Angew. Chem. Int. Ed.* **2021**, 60, 25286–25289.

[34] C. Hu, J. M. Goicoechea, *Angew. Chem. Int. Ed.* **2022**, 61, e202208921.

[35] A. Hinz, R. Labbow, C. Rennick, A. Schulz, J. M. Goicoechea, *Angew. Chem. Int. Ed.* **2017**, 56, 3911–3915.

[36] E. Niecke, M. Nieger, F. Reichert, *Angew. Chem. Int. Ed. Engl.* **1988**, 27,1715–1716.

[37] C. Morell, A. Grand, A. Toro-Labbé, *J. Phys. Chem. A* **2005**, 109, 205–212.

[38] T. Lu, F. Chen, *J. Comput. Chem.* **2012**, 33, 580–592.

[39] T. Lu, Q. Chen, *Conceptual Density Functional Theory* (Liu, S.-B. Ed.) pp. 631–647 (Wiley-VCH: Weinheim, Germany, 2022).

[40] J. Vrána, V. Němec, M. A. Samsonov, A. Růžička, *Dalton Transactions* **2021**, 50, 14352-14361.

[41] D. V. Yandulov, R. R. Schrock, *J. Am. Chem. Soc.* **2002**, 124, 6252-6253.

Chapter 4
Functionalization of an Anionic Imine Phosphinidene Oxide $ArNPO^-$

The contents of this chapter have been published:

C. Hu, N. H. Rees, M. Pink and J. M. Goicoechea, *Nat. Chem.* **2024**, 16, 1855–1860.

4.1 *N*-Functionalization with electrophiles

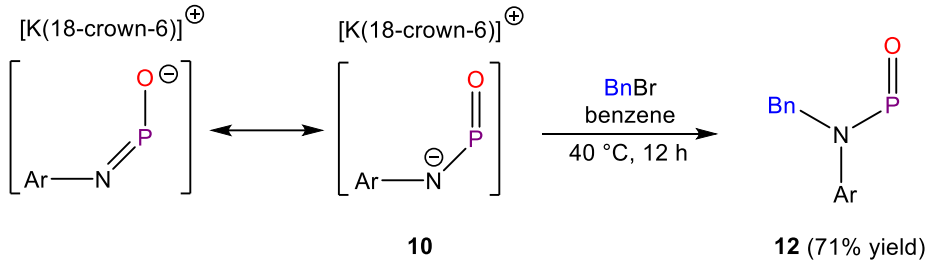

Scheme 4.1. Synthesis of **12** from **10**.

Based on the DFT calculations discussed in Chapter 3, the nitrogen atom in compound **10** is more nucleophilic than the oxygen. To probe this, benzyl bromide was selected as an electrophile, and was heated with **10** at 40 °C for 12 h (Scheme 4.1). Monitoring the reaction mixture by *in situ* $^{31}P\{^{1}H\}$ NMR spectroscopy revealed two new singlet resonances at 284.4 and 286.3 ppm.

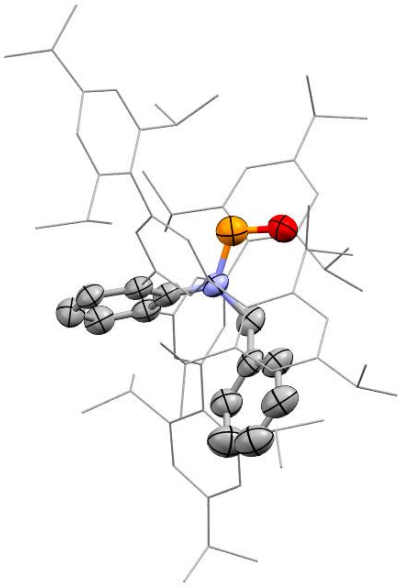

Figure 4.1. Single crystal X-ray structure of **12**. Selected carbon atoms for backbones are depicted with wireframe mode. Thermal ellipsoids pictured at 50% probability level. Solvent of crystallization and hydrogen atoms are removed for clarity.

The structure of the resulting product, compound **12**, was confirmed by single crystal X-ray diffraction (Figure 4.1). Crystallographic analysis confirms functionalization at the nitrogen atom, yielding a neutral amido-phosphinidene oxide. Notably, the P–O bond in **12**

shortens significantly (1.447(6) Å), compared to that in compound **10** (1.501(2) Å). Additionally, the N–P bond in **12** elongated to 1.667(6) Å relative to **10** (1.5822(19) Å). This extended N–P bond length, while shorter than the standard N–P single bond predicted by Pyykkö (1.82 Å),[1] indicates strong π donation from the nitrogen atom lone pair to the P–O π* bond. This π donation is further supported by the trigonal planar geometry of nitrogen (Σ°: 360.0°). In the context of the diagonal relationship between phosphorus and carbon,[2] compound **12** can be regarded as a heavier analogue of an amide (Scheme 4.2), as it exhibits strikingly similar geometric characteristics to such compounds, including shorter N–C bonds and a trigonal planar nitrogen center. An IR band corresponding the $\nu_{P=O}$ stretch for **12** was observed at 1186 cm^{-1} (cf. 1077 cm^{-1} for **10**; Figure 4.2 and 4.3) suggesting an increase in the multiple bond character of the P–O bond. The blue-shift in the $\nu_{P=O}$ absorption aligns with the observation of a shorter P–O bond in the crystal structure, reinforcing the structural changes brought about by the chemical functionalization. These absorptions are slightly blue-shifted from reported vibrations for Mes*–O–P=O (1252.6 and 1292.2 cm^{-1}),[3] in line with the greater electron donating ability of imine and amide groups over an oxyl functionality.

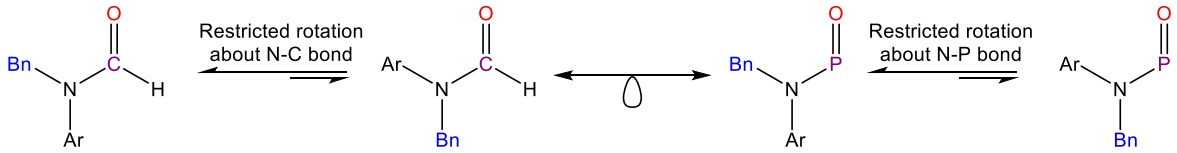

Scheme 4.2. Comparison between **12** and an organo-amide.

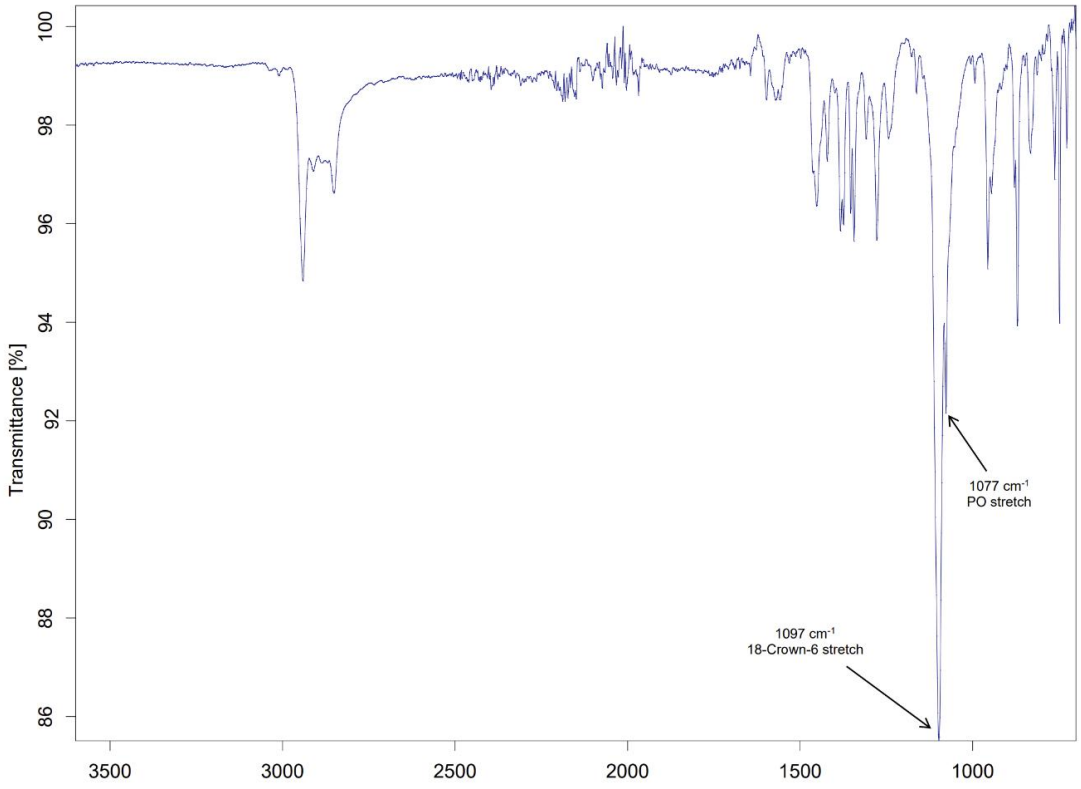

Figure 4.2. FTIR spectrum of **10**.

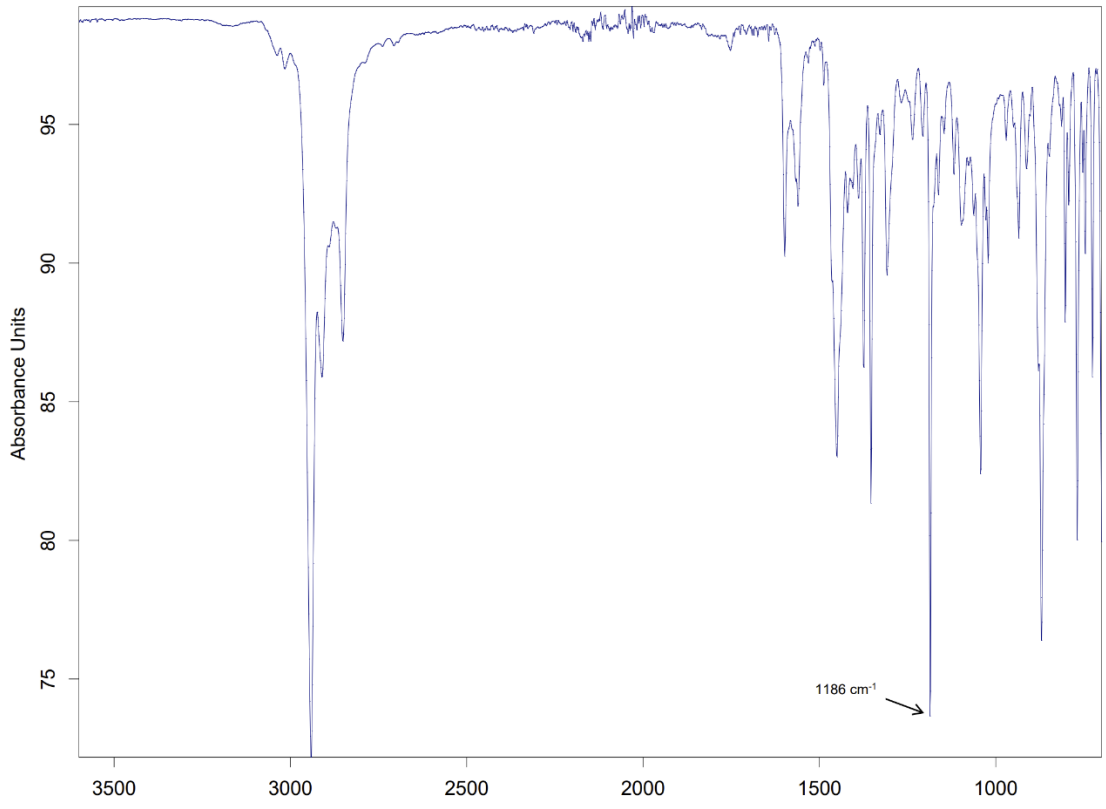

Figure 4.3. FTIR spectrum of **12**.

The origin of the two singlets observed in the $^{31}P\{^{1}H\}$ NMR spectrum of **12** was attributed to *cis-trans* isomerization about the N–P bond (Scheme 4.2) and was further investigated using Saturation Transfer Differential NMR spectroscopy (STD-NMR). In toluene solution at ambient temperature, **12** exists in two forms in a 1:6 ratio as shown by the ^{31}P NMR spectrum (Figure 4.4a). To prove that these two species are in exchange and to ascertain the exchange rate, a series of ^{31}P 1D-EXSY experiments (Figure 4.4b) were performed over a range of temperatures, the obtained rate constants are listed in Table 4.1. These results are summarized in the Eyring plot (Figure 4.4c) from which $\Delta H^* = 19(2)$ kcal mol^{-1}, $\Delta S^* = 3.8(60)$ cal mol^{-1} K^{-1} and $\Delta G^*(298\ K) = 18(2)$ kcal mol^{-1} can be calculated for the exchange process.

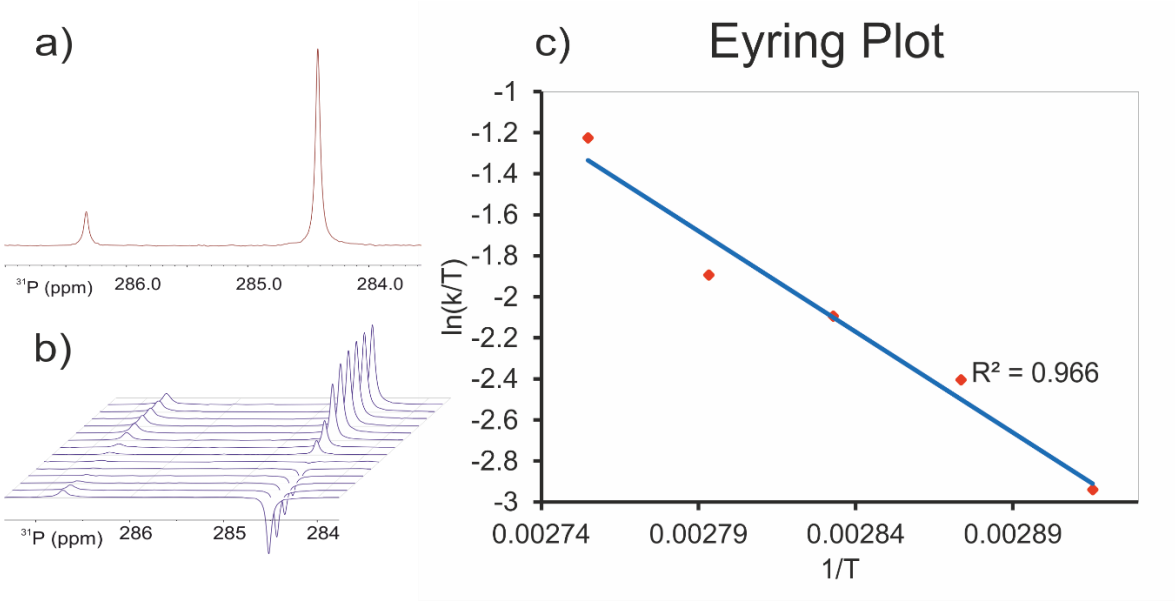

Figure 4.4. a) ^{31}P NMR spectrum of **12** at 298 K, b) ^{31}P 1D-EXSY spectrum at 353 K, c) Eyring plot.

Table 4.1. Data determined from ^{31}P 1D-EXSY NMR studies and used for an Eyring analysis.

Temp/K	**1/T**	***k***	**ln(*k*/T)**
343	0.00293	18.1	–2.94
348	0.00287	31.4	–2.41

353	0.00283	43.5	–2.09
358	0.00279	53.9	–1.89
363	0.00276	106.6	–1.23

DFT calculations were carried out to gain a deeper understanding of the electronic structure of **12**. Natural bond orbital (NBO) analysis revealed a three-center-four-electron (3c-4e) interaction within the N–P–O moiety, with the P=O interaction contributing more significantly to the overall electronic structure (65.3%) than the N=P component (34.7%) (see resonance forms in Figure 4.5a). This observation was consistent with calculated Mayer bond indices, which revealed a bond order of 1.06 for N–P bond and 1.83 for P–O bond. Notably, both σ-bonding and π-bonding orbitals were identified in NBO orbital between phosphorus and oxygen (see Figures 4.5b and 4.5c), providing further evidence of the double bond character of the P=O moiety in **12**. Second order perturbation theory analysis, reveals strong donation from the lone pair of the nitrogen atom into the P–O π* orbital (E(2) = 41.1 kcal mol^{-1}). This donation aligns with the presence of the 3c-4e π bond in the NPO fragment, corroborating the structural evidence from crystallography. Energy calculations using the SMD-M062X/def2-TZVP//M062X/def2-SVP level of theory indicated that the *trans*-isomer represents the ground state, with the *cis*-isomer being 1.2 kcal mol^{-1} higher in energy. The energy barrier for the isomerization process was determined to be 21.8 kcal mol^{-1}. These computational findings are in excellent agreement with the experimental observations obtained through STD-NMR, as the experimental measured energy barrier is 18(2) kcal mol^{-1}. Based on the predicted ground state, as well as the *trans*-geometry observed by crystallography, we can confidently assign the singlet at 284.4 ppm in ^{31}P NMR spectrum to be the *trans*-isomer, while the peak at 286.3 ppm corresponds to the *cis*-isomer.

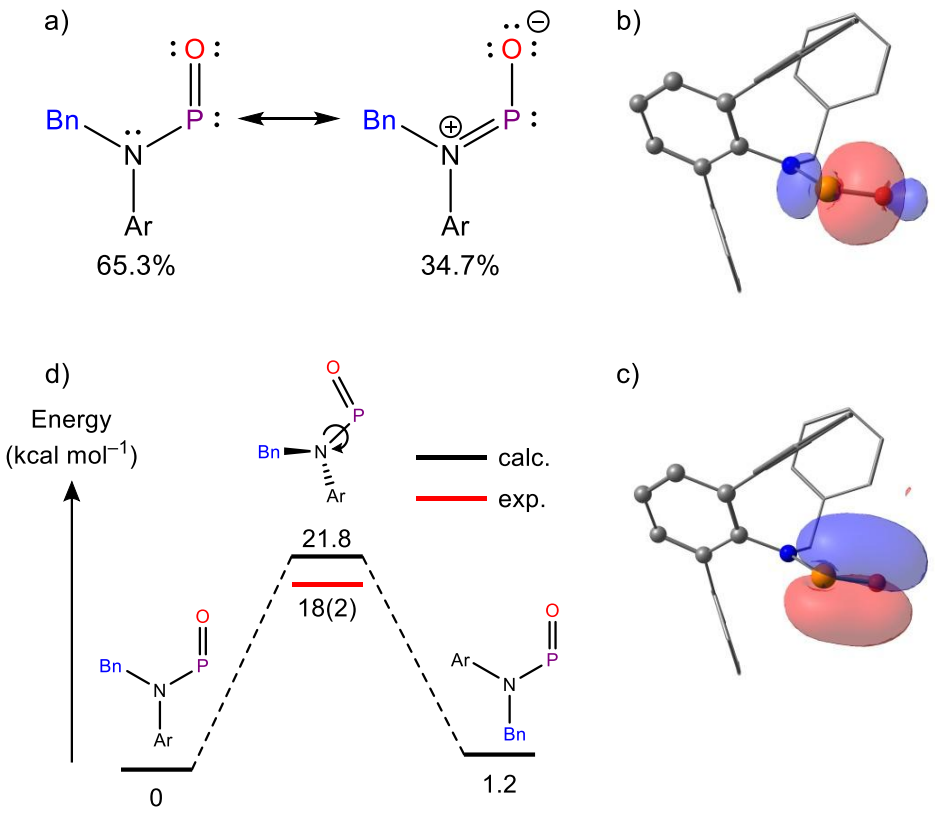

Figure 4.5. a) Resonance forms and NBO analysis of **12**; b) Natural Bonding Orbital representing the σ-bonding orbital interaction between P–O; c) Natural Bonding Orbital representing the π-bonding orbital interaction between P–O; d) Computed energy barrier for interconversion of *trans*- and *cis*-isomers of **12**.

For comparison, here we have calculated the *cis-trans* isomerization barrier for an amide with same substituent as **12** (Figure 4.6). The energy barrier was determined to be 25.7 kcal mol^{-1}, while conventional amides have energy barriers of 19–20 kcal mol^{-1}.[4] This increased energy barrier may be attributed to the extremely bulky *meta*-substituted terphenyl ligand. Compared to the calculated energy barrier for **12** (21.8 kcal mol^{-1}), the amide analogue has a slightly higher energy barrier indicating that the N–P π bond is of a comparable order with the N–C π bond in amides, but slightly weaker.

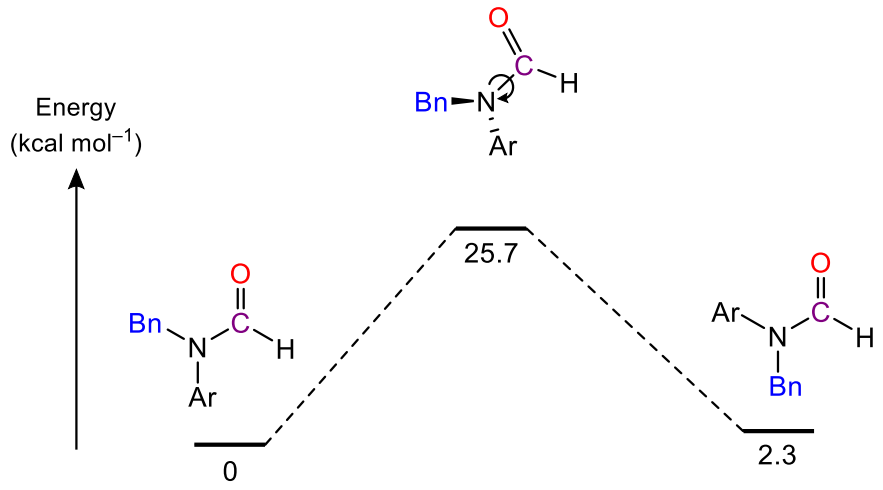

Figure 4.6. Energy plot for *cis-trans* isomerization of an amide.

4.2 *O*-Functionalization with electrophiles

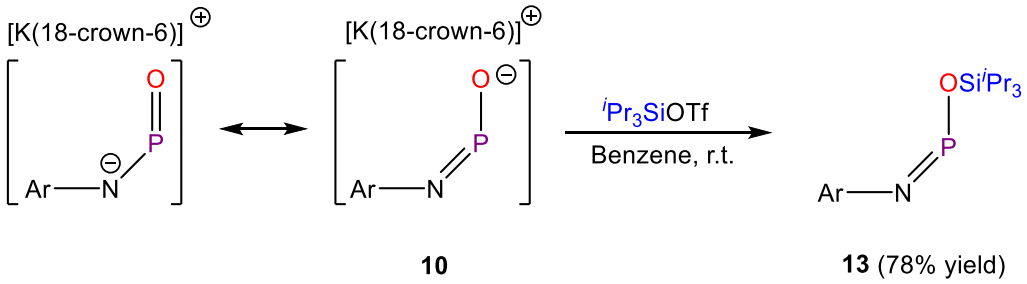

Scheme 4.3. Synthesis of **13** from **10**.

While the nitrogen atom in compound **10** is the most nucleophilic position based on the dual descriptor analysis, it is noteworthy that the oxygen atom also carries a significant amount of negative charge. Given that the oxygen atom is less sterically hindered, we postulated that bulky electrophiles could be employed to access oxygen functionalized compounds. Treatment of **10** with $^{i}Pr_3SiOTf$ in benzene afforded **13**, which features a singlet in its $^{31}P\{^{1}H\}$ NMR spectrum at 169.0 ppm (Scheme 4.3). The solid-state molecular structure of **13** was determined by single crystal X-ray diffraction (Figure 4.7). This analysis revealed the presence of a silanolate-substituted N=P double bond with a N–P bond length of 1.544(2)

Å. **13** exhibits comparable bond metrics to related compounds of general formula of R–N=P–OR′.[5–11]

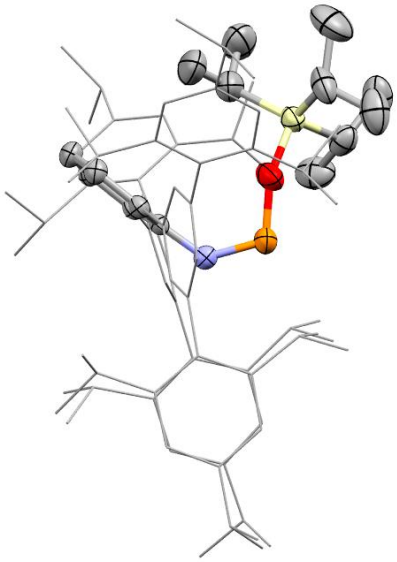

Figure 4.7. Single crystal X-ray structures of **13**. Selected carbon atoms for backbones are depicted with wireframe mode. Thermal ellipsoids pictured at 50% probability level. Solvent of crystallization and hydrogen atoms are removed for clarity.

Following silylation, the Mayer bond order for N–P increased from 1.40 in **10** to 1.79 in **13**, while P–O bond order decreased from 1.64 to 1.01. A detailed comparison of bond orders between **10**, **12** and **13** is given below in Table 4.2 and Table 4.3.

Table 4.2. Calculated Wiberg Bond Orders (WBI) for $[ArNPO]^-$, **12** and **13**.

Compound	N–P	P–O	N–O
$[ArNPO]^-$	**1.25**	**1.24**	**0.16**
12	**0.88**	**1.40**	**0.11**
13	**1.55**	**0.75**	**0.09**

Table 4.3. Calculated Mayer Bond Orders for [ArNPO]$^-$, **12** and **13**.

Compound	N–P	P–O	N–O
[ArNPO]$^-$	**1.40**	**1.64**	**0.07**
12	**1.06**	**1.83**	**0.06**
13	**1.79**	**1.01**	**Not detected**

In compound **12**, due to the functionalization of the nitrogen atom, a formal P=O double bond is formed, which leads to an increase of bond order for the P–O bond, and a concomitant decrease of bond order for the N–P bond. The N–O bond order also decreases, which can be reasoned by the greater localization of the lone pair on the nitrogen atom leading to poorer delocalization of the 3c-4e bond. Similarly, in compound **13**, upon functionalization of the oxygen atom, a formal N=P double bond is formed, resulting in an increase of the N–P bond order, as well as a decrease of the P–O bond order. The Mayer bond order for the N–O bond was not detected because there is no delocalized 3c-4e bond in compound **13**. Infrared spectroscopy of **13** also showed no obvious vibration band within the expected region for P=O vibration (1100–1200 cm^{-1}), contrasting to **10** and **12**.

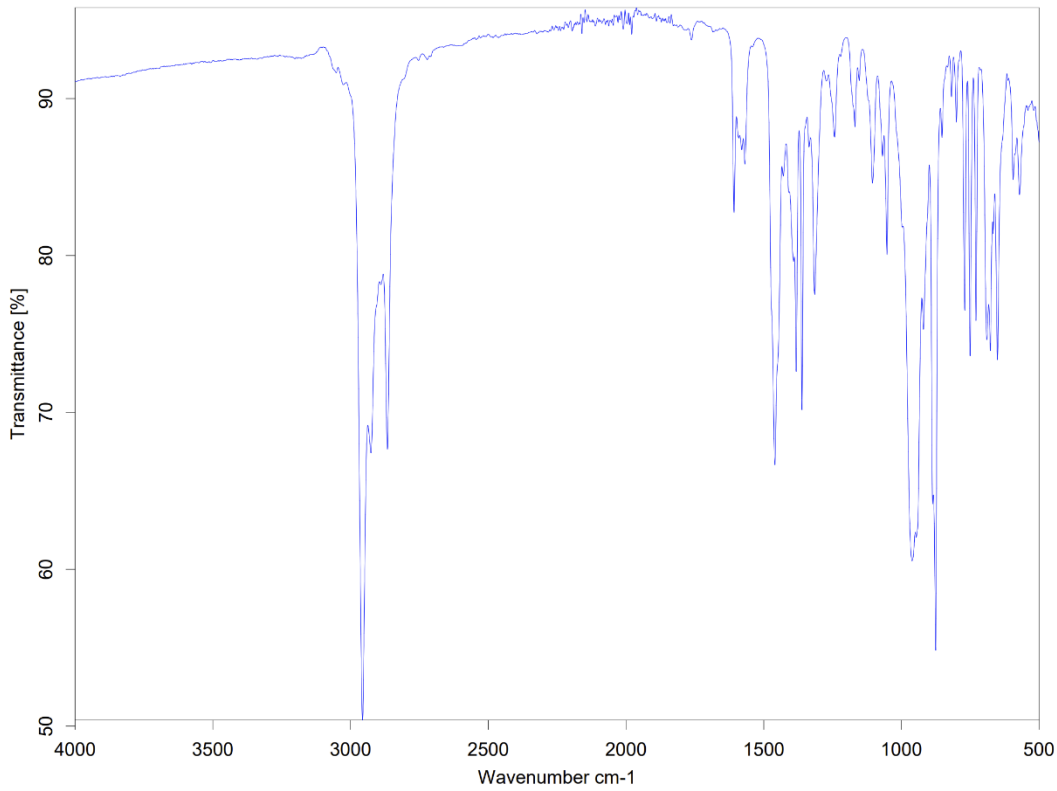

Figure 4.8. FTIR spectrum of **13**.

4.3 *P*-Functionalization with oxidants

4.3.1 Hydrolysis

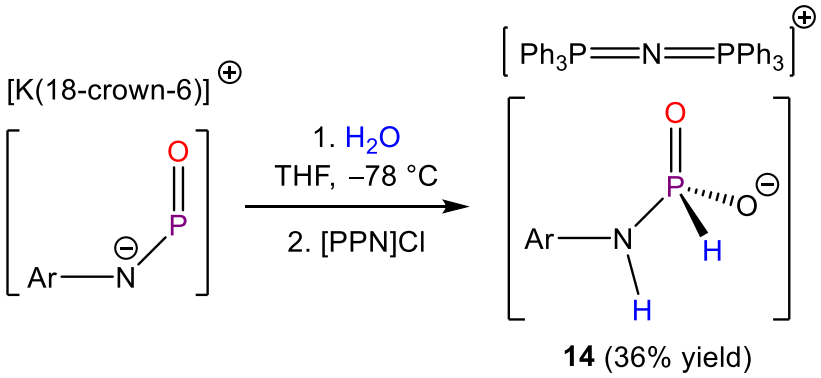

14 (36% yield)

Scheme 4.4. Synthesis of **14** from **10**.

While **10** is stable at ambient, or even elevated, temperature in both solution and the solid-state under an inert atmosphere, it readily reacts with trace amounts of moisture

(Scheme 4.4). Upon exposing to one equivalent of H_2O at –78 °C, **10** undergoes conversion to a phosphorous acid derivative **14**, which exhibits a doublet in its ^{31}P NMR spectrum at –3.5 ppm ($^1J_{P–H}$ = 572.4 Hz). The connectivity was confirmed by single crystal X-ray diffraction (Figure 4.9). Compound **14** is structurally and electronically related to a base-stabilized dioxophosphorane recently reported by Vidović and co-workers.[12] The most intriguing aspect of the structure is the protonation of the nitrogen atom instead of oxygen, with the anionic charge being delocalized solely between two oxygen atoms. This conclusion is supported by several key structural features, including the elongation of the N1–P1 bond length (1.719(2) Å) and the nearly identical P–O bond lengths (P1–O1: 1.473(3) Å and P1–O2: 1.487(3) Å), which fall within the typical range for a P=O double bond.[1] Protonation of N1 was further confirmed by the observation of a resonance at 5.64 ppm in the ^1H NMR spectrum, and by NOESY NMR spectroscopy, which revealed correlation between the N–H resonance and the benzylic C–H adjacent to the central phenyl ring (Figure 4.10). This reactivity showcases that **10** represents a novel mononuclear phosphorous acid anhydride, distinguishing it from the previously known tetranuclear phosphorous acid anhydride P_4O_6.[13]

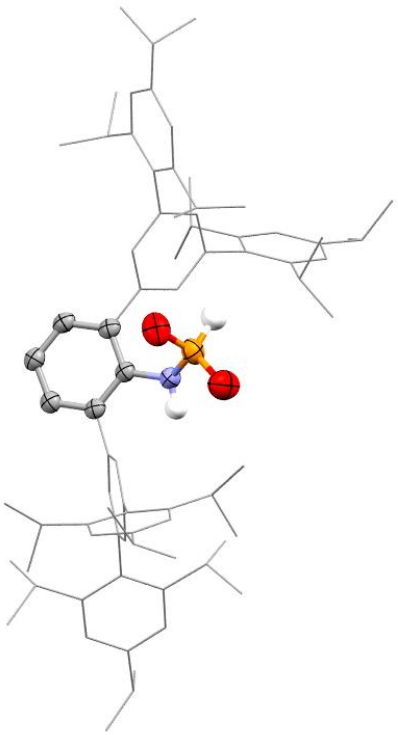

Figure 4.9. Single crystal X-ray structures of **14**. Selected carbon atoms for backbones are depicted with wireframe mode. Counter cations, solvent of crystallization and hydrogen atoms (expect for H1N and H1P) are removed for clarity.

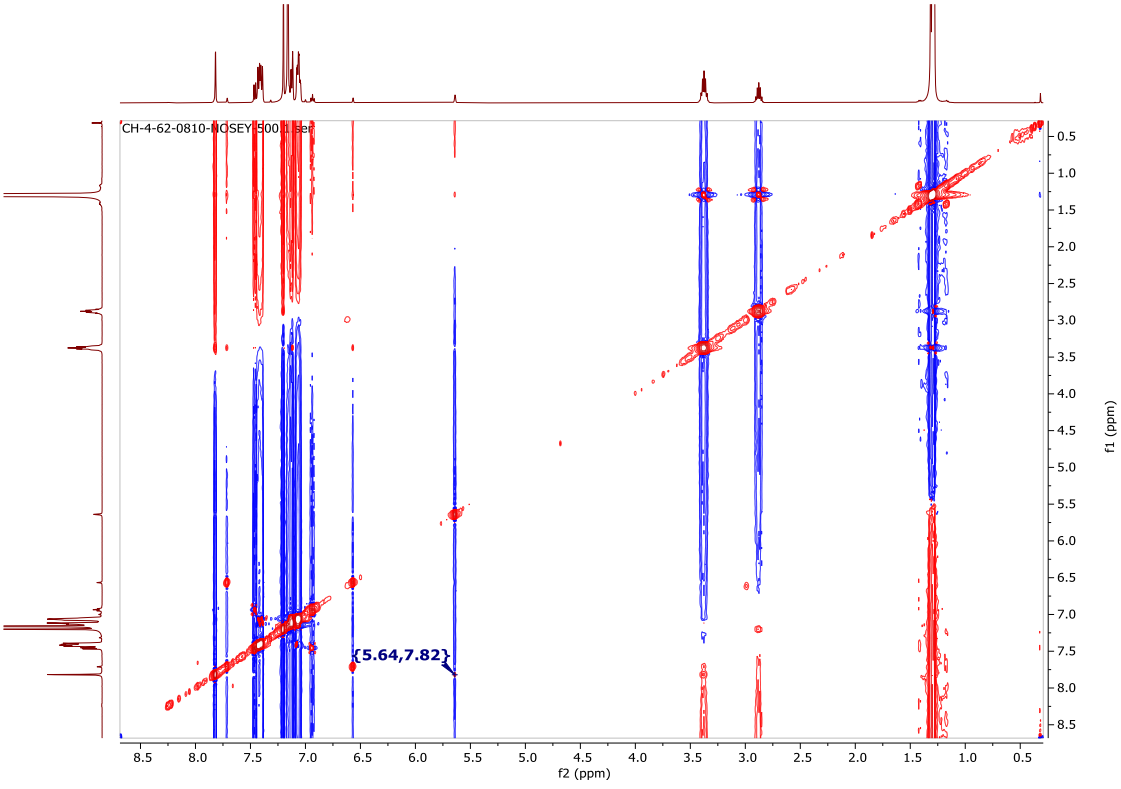

Figure 4.10. ^{1}H-^{1}H NOESY NMR spectrum of **14** (500 MHz, C_6D_6).

4.3.2 Iodination with iodine

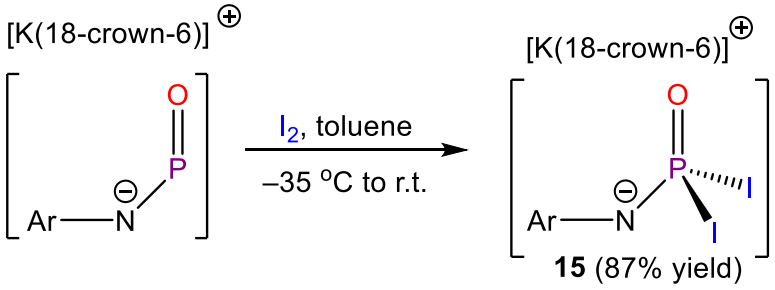

Scheme 4.5. Synthesis of **15** from **10**.

In addition to hydrolysis, as a phosphorus(III) center, **10** can also undergo oxidative processes to form phosphorus(V) compounds. Reaction of a toluene solution of **10** and iodine I_2 at –35 °C gave rise to a light-yellow solution (Scheme 4.5). *In situ* $^{31}P\{^1H\}$ NMR spectroscopy revealed a broad singlet at –147.8 ppm corresponding to **15**. Single crystals of **15** can be obtained by slow evaporation of a toluene/hexane solution. Single crystal X-ray diffraction allowed for structural authentication of this compound (Figure 4.10), revealing a di-iodide substituted phosphorus(V) center with short N1–P1 (1.560(5) Å) and O1–P1 bonds (1.457(6) Å). These bond lengths imply that the anionic charge remains delocalized between N1 and O1. Notably, the P–I bond lengths (mean bond length: 2.529 Å) are longer than any reported P(V)–I bond lengths, which typically range from 2.33 to 2.45 Å. While the synthesis of OPI_3 was reported in 1973,[14] this compound remains poorly characterized. To date, no crystallographic data are available for OPI_3 or its derivatives. The closest known compound is a Lewis acid-stabilized OPI_3 moiety reported by the Krossing group in 2006.[15] Compound **15** represents the first crystallographically characterized OPI_2R derivative, shedding light on the structural properties of this class of molecules.

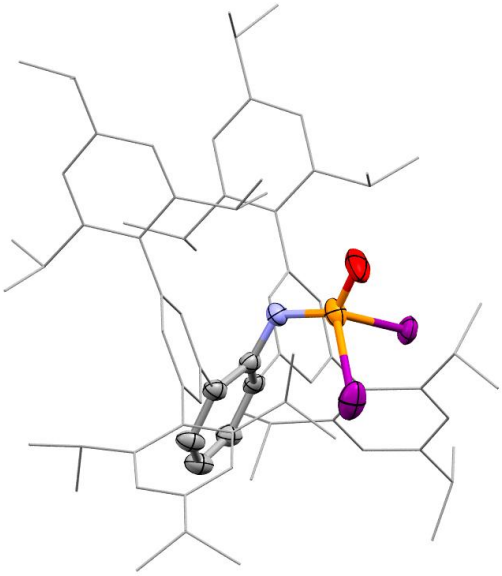

Figure 4.10. Single crystal X-ray structures of **15**. Selected carbon atoms for backbones are depicted with wireframe mode; thermal ellipsoids of heteroatoms pictured at 50% probability level. Counter cations, solvent of crystallization and hydrogen atoms are removed for clarity.

The elongated P–I bond and the shortened N–P and O–P bonds can be attributed to strong back donation from the lone pairs of nitrogen and/or oxygen to the P–I σ* orbitals, a phenomenon arising from the inherent weakness of the P–I bond. NBO calculation further supported this explanation. Second-order perturbation theory analysis revealed multiple back donations from nitrogen and oxygen lone pairs to P–I σ* orbital, with a E(2) energies ranging from 1.7 to 50.1 kcal mol^{-1} (Figure 4.11).

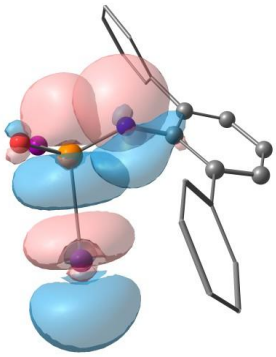

Lone pair(1) of N donating to P(1)–I(1) σ* orbital
E(2)=26.0 kcal mol^{-1}

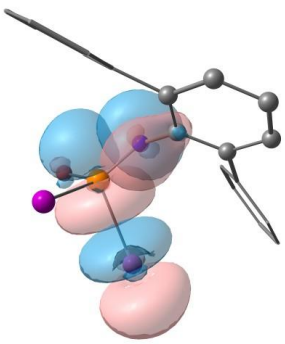

Lone pair(1) of N donating to P(1)–I(2) σ* orbital
E(2)=1.7 kcal mol^{-1}

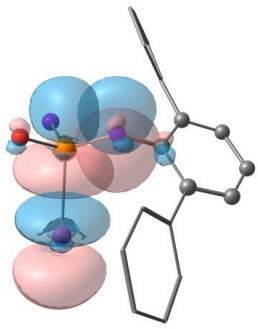

Lone pair(2) of N donating to P(1)–I(1) σ* orbital
E(2)=16.0 kcal mol^{-1}

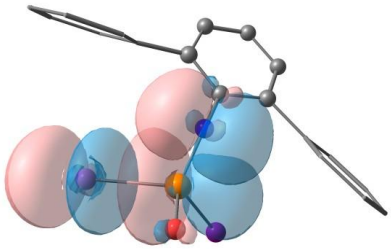

Lone pair(2) of N donating to P(1)–I(2) σ* orbital
E(2)=50.1 kcal mol^{-1}

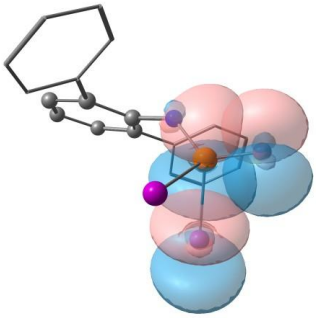

Lone pair(1) of O donating to P(1)–I(1) σ* orbital
E(2)=13.8 kcal mol^{-1}

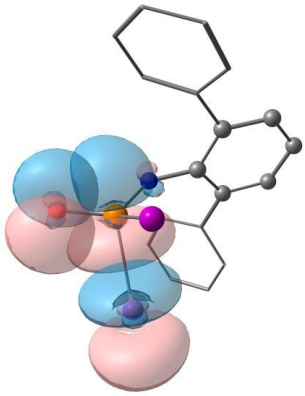

Lone pair(1) of O donating to P(1)–I(2) σ* orbital
E(2)=17.4 kcal mol^{-1}

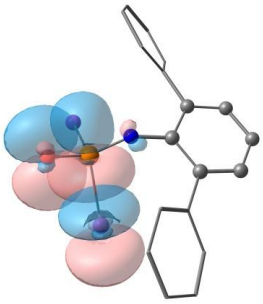

Lone pair(2) of O donating to P(1)–I(1) σ* orbital
E(2)=32.9 kcal mol^{-1}

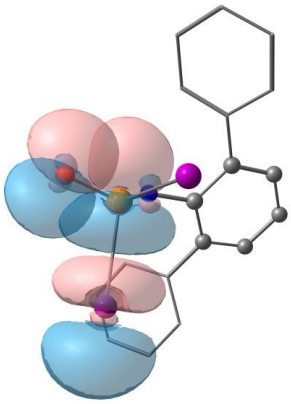

Lone pair(2) of O donating to P(1)–I(2) σ* orbital
E(2)=28.6 kcal mol^{-1}

Figure 4.11. Selected NBOs of **15** from second-order perturbation theory analysis.

Due to the strong donation from lone pair electrons of the nitrogen and oxygen atoms to the two P–I σ* orbitals, the electron occupancy for them is significantly lower than the expected, as shown in Table 4.4. Consequently, both P–I σ* orbitals are also partially filled.

Table 4.4. Selected NBOs of **15** and their electron occupancy.

NBO orbital	Electron occupancy
Lone pair (1) of N	1.72
Lone pair (2) of N	1.70
Lone pair (1) of O	1.80
Lone pair (2) of O	1.77
P(1)–I(1) σ* orbital	0.36
P(1)–I(2) σ* orbital	0.38

4.3.3 Oxidative addition of Se_2Ph_2

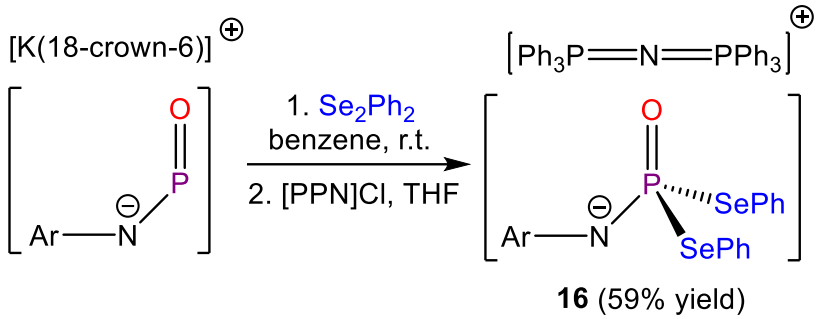

Scheme 4.6. Synthesis of **16** from **10**.

The aforementioned oxidative process observed for **10** is not limited to iodine. When treated with one equivalent of diphenyl diselenide Se_2Ph_2 (Scheme 4.6), a new species **16** was detected by *in situ* $^{31}P\{^1H\}$ NMR spectroscopy. Compound **16** exhibits a singlet at –23.2 ppm in its $^{31}P\{^1H\}$ NMR spectrum, with a P–Se coupling constant of 398.7 Hz. A doublet at 512.7 ppm was also detected in its ^{77}Se NMR spectrum with a coupling constant of 398.7 Hz. The single crystal X-ray structure of **16** reveals a four-coordinate P(V) center (Figure 4.12). Structurally, **16** closely resembles **15**, with relatively short N–P (1.557(2) Å) and P–O (1.474(2) Å) bonds. The P–Se bonds in **16** (mean bond length: 2.310 Å) are slightly elongated compared to the standard P–Se single bond (2.27 Å).[1] Again, this elongation can be attributed to the delocalization of the anionic charge and back donation to the P–Se σ* orbital. However, the back donation in **16** is slightly weaker than that in **15**, presumably due to the higher electronegativity of iodine. A second-order perturbation theory analysis

revealed multiple back donation interactions (Figure 4.13), the strongest of which has an E(2) energy of 33.8 kcal mol^{-1}, while the highest computed for compound **15** is 50.1 kcal mol^{-1}. Similarly, the occupancy for nitrogen and oxygen lone pairs was found to be higher than for **15**, while the occupancy for P–Se σ* orbital is lower (Table 4.5).

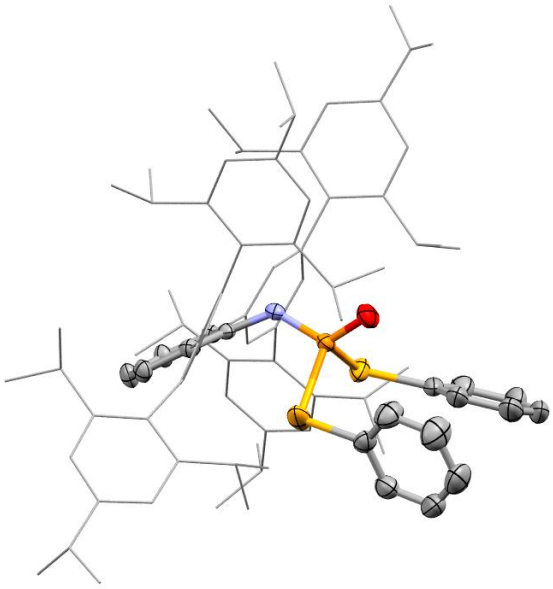

Figure 4.12. Single crystal X-ray structures of **16**. Selected carbon atoms for backbones are depicted with wireframe mode; thermal ellipsoids of heteroatoms pictured at 50% probability level. Counter cations, solvent of crystallization and hydrogen atoms are removed for clarity.

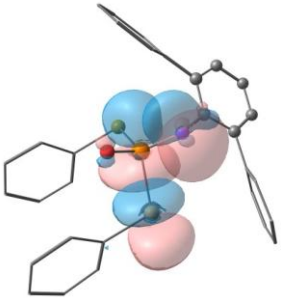

Lone pair(1) of N donating to P(1)–Se(1) σ* orbital
E(2)=9.51 kcal mol^{-1}

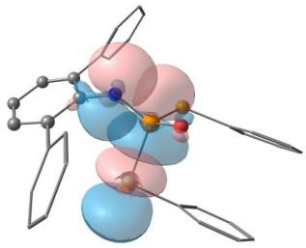

Lone pair(1) of N donating to P(1)–Se(2) σ* orbital
E(2)=25.24 kcal mol^{-1}

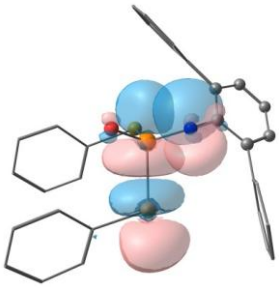

Lone pair(2) of N donating to P(1)–Se(1) σ* orbital
E(2)=20.72 kcal mol^{-1}

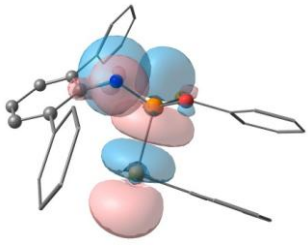

Lone pair(2) of N donating to P(1)–Se(2) σ* orbital
E(2)=0.62 kcal mol^{-1}

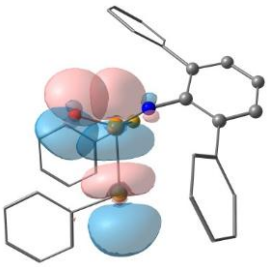

Lone pair(1) of O donating to P(1)–Se(1) σ* orbital
E(2)=21.79 kcal mol^{-1}

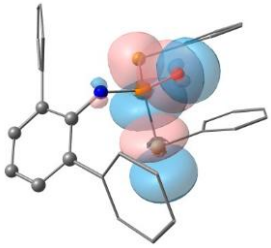

Lone pair(1) of O donating to P(1)–Se(2) σ* orbital
E(2)=2.41 kcal mol^{-1}

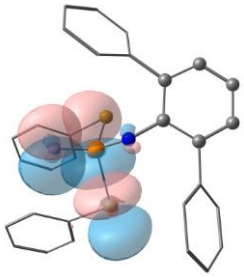

Lone pair(2) of O donating to P(1)–Se(1) σ* orbital
E(2)=13.63 kcal mol^{-1}

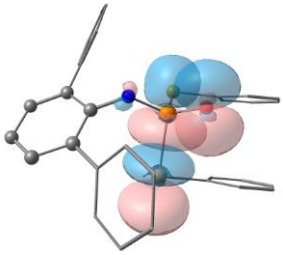

Lone pair(2) of O donating to P(1)–Se(2) σ* orbital
E(2)=33.79 kcal mol^{-1}

Figure 4.13. Selected NBOs of **16** from second-order perturbation theory analysis.

Table 4.5. Selected NBOs of **16** and their electron occupancy.

NBO orbital	Electron occupancy
Lone pair (1) of N	1.76811
Lone pair (2) of N	1.70788
Lone pair (1) of O	1.80961
Lone pair (2) of O	1.79340
P(1)–Se(1) σ* orbital	0.28540
P(1)–Se(2) σ* orbital	0.27671

4.4 Conclusions

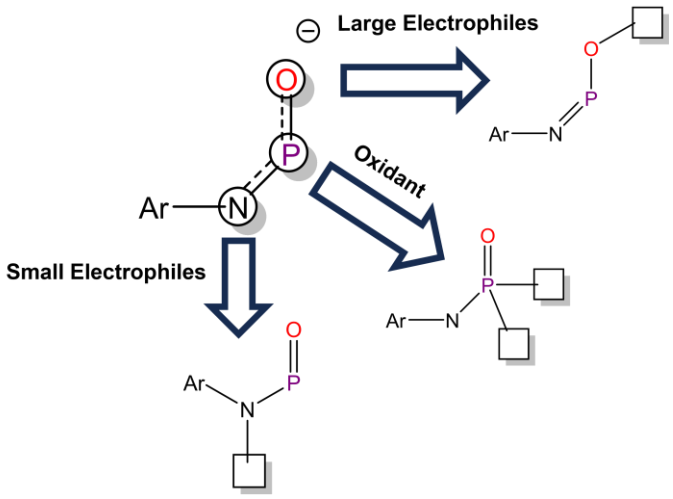

Figure 4.14. Selective functionalization of N, P and O in **10**.

Due to the delocalization of the anionic charge between nitrogen and oxygen atom in **10**, both atoms can be selectively functionalized depending on the electrophile employed. With small alkyl groups, *N*-functionalization takes place giving rise to the formation of an amido phosphinidene oxide **12**, the first structurally authenticated compound of its class, which can be considered a heavier analogue of amide. The restricted N–P bond rotation closely resembles the restricted N–C bond rotation of an amide, leading to a pair of *cis*-*trans* isomers. Alternatively, when reacted with a bulky silyl group, *O*-functionalization occurs, resulting in the generation of a silanolate-substituted N=P double-bonded species **13**. Moreover, compound **10** displays versatility in its reactivity, as it can also undergo functionalization through oxidative transformations, as exemplified by reactions with water, iodine and diphenyl diselenide. At this point, all three atoms in the N–P–O moiety have been functionalized individually, showcasing the potential of **10** as a synthon to access various phosphorus-containing structures.

4.5 Experimental Section

4.5.1 Synthesis of 12

A benzene solution (0.2 mL) of BnBr (1.3 mg, 0.0076 mmol, 1.07 eq.) was slowly added to a benzene solution (0.3 mL) of **10** (10 mg, 0.0071 mmol, 1.00 eq.). The mixture was heated for 12 hours in a sealed NMR tube before all volatiles were removed *in vacuo*. Hexane (0.5 ml) was added to the residue, and the mixture was filtered to obtain the filtrate. The solution was evaporated under vacuum to obtain a colorless oily residue, which was then triturated with MeCN to give **12** (6 mg, 0.0050 mmol; yield: 71%) as a white powder. Single crystals of **12** suitable for X-ray diffraction were obtained by slow evaporation of a concentrated hexane solution of **12** at room temperature. Anal. Calcd. for $C_{85}H_{108}NOP$ (M.W. 1190.78 g mol^{-1}): C, 85.74; H, 9.14; N, 1.18; Found: C 84.32; H, 8.97; N, 1.28. m.p. 158 ºC.

^{1}H NMR (600 MHz, C_6D_6): δ (ppm) 1.17–1.20 (m, 24H; CH(C*H*$_3$)$_2$), 1.23 (d, $^{3}J_{H–H}$ = 6.8 Hz, 12H; CH(C*H*$_3$)$_2$), 1.27–1.30 (m, 36H; CH(C*H*$_3$)$_2$), 2.86 (sept, $^{3}J_{H–H}$ = 6.8 Hz, 4H; C*H*(CH$_3$)$_2$), 2.99 (sept, $^{3}J_{H–H}$ = 6.8 Hz, 8H; C*H*(CH$_3$)$_2$), 5.03 (s, 2H; NC*H*$_2$Ph), 6.61 (t, $^{3}J_{H–H}$ = 7.4 Hz, 2H; Ar*H*), 6.77 (t, $^{3}J_{H–H}$ = 7.4 Hz, 1H; Ar*H*), 6.89-6.94 (m, 3H; Ar*H*), 7.11 (s, 2H; Ar*H*), 7.17–7.21 (m, 12H; Ar*H*), 7.32 (d, $^{3}J_{H–H}$ = 7.4 Hz, 2H; Ar*H*).

^{13}C{^{1}H} NMR (125 MHz, C_6D_6): δ (ppm) 24.23, 24.42, 24.67, 25.06 (s; CH(*C*H$_3$)$_2$), 30.97, 34.88 (s; *C*H(CH$_3$)$_2$), 47.96 (s; N*C*H$_2$Ph), 120.75, 130.87, 131.47, 131.73, 132.09, 133.53, 135.98, 137.03, 137.24, 139.98, 140.44, 141.17, 141.80, 146.88, 148.63 (s; Ar*C*).

^{31}P{^{1}H} NMR (162 MHz, C_6D_6): δ (ppm) 284.4 (s; *trans*-isomer), 286.3 (s; *cis*-isomer).

HRMS (*m*/*z*): $[M+H_3O]^+$ calcd. For $C_{85}H_{111}NPO_2$, 1208.8347; found 1208.8295.

FTIR (ATR): ν(cm^{-1}) 1186 (s, PO stretch).

4.5.2 Synthesis of 13

A benzene solution (0.2 mL) of $^{i}Pr_3SiOTf$ (2.4 mg, 0.0078 mmol, 1.10 eq.) was slowly added to a benzene solution (0.3 mL) of **10** (10 mg, 0.0071 mmol, 1.00 eq.). The mixture was stirred for 1 min and filtered to obtain the filtrate. MeCN (5 ml) was added to the filtrate and the mixture was left in a in a –35 °C freezer overnight. The supernatant was removed and the resulting solid was dried *in vacuo* to afford **13** (7 mg, 0.0057 mmol; 78% yield) as a light yellow powder. Single crystals of **13** suitable for X-ray diffraction were obtained by slow evaporation of a concentrated hexane solution of **13** at room temperature. Anal. Calcd. for $C_{87}H_{122}NOPSi$ (M.W. 1257.00 g mol^{-1}): C, 83.13; H, 9.78; N, 1.11; Found: C 83.13; H, 9.39; N, 1.05. m.p. > 240 ºC.

^{1}H NMR (600 MHz, C_6D_6): δ (ppm) 0.83–0.84 (m, 21H; SiC*H*(CH_3)$_2$), 1.24 (d, $^{3}J_{H–H}$ = 6.8 Hz, 24H; CH(CH_3)$_2$), 1.27 (d, $^{3}J_{H–H}$ = 6.8 Hz, 24H; CH(CH_3)$_2$), 1.33 (d, $^{3}J_{H–H}$ = 6.8 Hz, 24H; CH(CH_3)$_2$), 2.91 (sept, $^{3}J_{H–H}$ = 6.8 Hz, 4H; C*H*(CH_3)$_2$), 3.12 (sept, $^{3}J_{H–H}$ = 6.8 Hz, 8H; C*H*(CH_3)$_2$), 6.94 (t, $^{3}J_{H–H}$ = 7.6 Hz, 1H; Ar*H*), 7.08 (t, $^{4}J_{H–H}$ = 1.6 Hz, 2H; Ar*H*), 7.24 (s, 8H; Ar*H*), 7.49 (d, $^{3}J_{H–H}$ = 7.6 Hz, 2H; Ar*H*), 7.91 (d, $^{4}J_{H–H}$ = 1.6 Hz, 4H; Ar*H*).

^{13}C{^{1}H} NMR (151 MHz, C_6D_6): δ (ppm) 12.31 (s; Si*C*H(CH_3)$_2$), 17.44 (s; SiCH(*C*H_3)$_2$), 24.49, 24.55, 25.13 (s; CH(*C*H_3)$_2$), 30.93, 34.94 (s; *C*H(CH_3)$_2$), 120.89, 123.18, 129.48, 130.59, 130.76, 131.96 (d, $^{3}J_{P–C}$ = 9.6 Hz), 137.78, 140.63, 140.73, 141.55 (d, $^{2}J_{P–C}$ = 27.8 Hz), 147.06, 148.39 (s; Ar*C*).

^{31}P{^{1}H} NMR (162 MHz, C_6D_6): δ (ppm) 169.0 (s).

HRMS (*m*/*z*): $[M+H]^+$ calcd. For $C_{87}H_{123}NPOSi$, 1256.9112; found 1256.9060.

4.5.3 Synthesis of 14

To a solid mixture of **9** (30 mg, 0.0268 mmol, 1.0 eq.) and KOTMS (8.5 mg, 0.066 mmol, 2.5 eq.), THF (5 ml) was added. The mixture was stirred vigorously for 5 min before all

volatiles were removed *in vacuo*. Hexane (10 ml) was added to the residue, and the solution was filtered using a filter cannula, and the filtrate was dried *in vacuo* again. THF (5 ml) was added to the residue and the solution was cooled to –78 °C before a THF solution of H_2O (5 mg/ml, 0.12 ml, 0.033 mmol, 1.25 eq.) was added dropwise. The mixture was stirred for 20 min at –78 °C then slowly warmed up to room temperature. (PPN)Cl (30.7 mg, 0.0536 mmol, 2 eq.) was then added to the mixture. The mixture was sonicated for 5 min and stirred for another 2 h before filtering to remove insoluble salts. The filtrate was dried under vacuum, and toluene (3 ml) was added to dissolve the residue. The solution was then stored in a –35 °C freezer for three days to crystallize. The supernatant was removed and the resulting solid was dried *in vacuo* to afford **14** (16 mg, 0.00966 mmol; 36% yield) as a white powder. Single crystals of **14** suitable for X-ray diffraction were obtained by slow diffusion of hexane into a concentrated THF solution of the product at room temperature. Anal. Calcd. for $C_{87}H_{122}NOPSi$ (M.W. 1656.25 g mol^{-1}): C, 82.67; H, 8.09; N, 1.69; Found: C 81.43; H, 7.77; N, 1.71. m.p. 210 °C.

^{1}H NMR (500 MHz, C_6D_6): δ (ppm) 1.28–1.31 (m, 72H; CH(C*H*$_3$)$_2$), 2.88 (sept, $^3J_{H–H}$ = 6.8 Hz, 4H; C*H*(CH$_3$)$_2$), 3.38 (sept, $^3J_{H–H}$ = 6.8 Hz, 8H; C*H*(CH$_3$)$_2$), 5.64 (s, 1H; N*H*), 6.94 (t, $^3J_{H–H}$ = 7.4 Hz, 1H; Ar*H*), 7.04–7.08 (m, 12H; Ar*H*), 7.12–7.15 (m, 8H; ArH), 7.14 (d, $^1J_{P–H}$ = 572.4 Hz, 1H; P*H*), 7.21 (s, 8H; Ar*H*), 7.39-7.43 (m, 12H; Ar*H*), 7.47 (d, $^3J_{H–H}$ = 7.4 Hz, 2H; Ar*H*), 7.82 (d, $^4J_{H–H}$ = 1.1 Hz, 4H; Ar*H*).

^{13}C{^{1}H} NMR (151 MHz, C_6D_6): δ (ppm) 24.56, 24.86, 25.90 (s; CH(*C*H$_3$)$_2$), 30.96, 34.93 (s; *C*H(CH$_3$)$_2$), 119.23, 120.55, 126.54 (d, $J_{P–C}$ = 2.3 Hz), 127.39 (d, $J_{P–C}$ = 2.5 Hz), 129.74–129.89, 130.31, 130.60, 132.68, 132.72, 132.77, 133.60, 135.34, 138.67, 140.53, 143.41, 147.60, 147.63 (s; Ar*C*).

^{31}P NMR (202 MHz, C_6D_6): δ (ppm) –3.5 (d, $^1J_{P–H}$ = 572.4 Hz), 21.2 (s, Ph$_3$*P*=N=*P*Ph$_3$).

^{31}P{^{1}H} NMR (202 MHz, C_6D_6): δ (ppm) –3.5 (s), 21.2 (s, Ph$_3$*P*=N=*P*Ph$_3$).

HRMS (*m*/*z*): [Anion]$^+$ calcd. For $C_{78}H_{103}NPO_2$, 1116.7732; found 1116.7732.

FTIR (ATR): ν(cm^{-1}) 1063 (s, $PO_{2\ symm}$ stretch), 1114 (s, PNP stretch).

4.5.4 Synthesis of 15

A toluene solution (3 mL) of I_2 (18 mg, 0.07 mmol, 1.00 eq.) was slowly added to a toluene solution (5 mL) of **10** (100 mg, 0.07 mmol, 1.00 eq.) dropwise at –35 ºC. The mixture was stirred for 5 min before all volatiles were removed *in vacuo*. The oily yellow residue was then triturated with hexane to give **15** (102 mg, 0.0062 mmol; yield: 87%) as a brown powder. Single crystals of **15** suitable for X-ray diffraction were obtained by slow evaporation of a concentrated hexane/toluene solution of **15** at room temperature. Anal. Calcd. for $C_{90}H_{125}NO_7PI_2$ (M.W. 1641.84 g mol^{-1}): C, 65.11; H, 7.49; N, 0.85; Found: C 61.65; H, 7.24; N, 0.72. m.p. sample decomposes above 166 ºC.

^{1}H NMR (500 MHz, C_6D_6): δ (ppm) 1.30 (d, $^3J_{H–H}$ = 6.8 Hz, 24H; CH(C*H*$_3$)$_2$), 1.33 (d, $^3J_{H–H}$ = 6.8 Hz, 24H; CH(C*H*$_3$)$_2$), 1.35 (d, $^3J_{H–H}$ = 6.8 Hz, 24H; CH(C*H*$_3$)$_2$), 2.95 (sept, $^3J_{H–H}$ = 6.8 Hz, 4H; C*H*(CH$_3$)$_2$), 3.26 (s, 24H; 18-crown-6), 3.47 (sept, $^3J_{H–H}$ = 6.8 Hz, 8H; C*H*(CH$_3$)$_2$), 7.09 (d, $^4J_{H–H}$ = 1.1 Hz, 2H; Ar*H*), 7.21 (t, $^3J_{H–H}$ = 7.5 Hz, 1H; Ar*H*), 7.29 (s, 8H; Ar*H*), 7.58 (d, $^3J_{H–H}$ = 7.6 Hz, 2H; Ar*H*), 8.07 (d, $^4J_{H–H}$ = 1.1 Hz, 4H; Ar*H*).

^{13}C{^{1}H} NMR (125 MHz, C_6D_6): δ (ppm) 24.59, 25.03, 25.59 (s; CH(*C*H$_3$)$_2$), 30.82, 35.01 (s; *C*H(CH$_3$)$_2$), 70.06 (s; 18-crown-6), 120.72, 129.51, 131.43, 132.93 (d, $^2J_{P–C}$ = 9.0 Hz), 138.06, 138.87, 139.82, 144.60, 146.98, 147.47, 147.75, 148.55 (s; Ar*C*).

^{31}P{^{1}H} NMR (162 MHz, C_6D_6): δ (ppm) –147.8 (br).

HRMS (*m*/*z*): [M+H]$^+$ calcd. For $C_{78}H_{101}NPOI_2$, 1352.5716; found 1352.5701.

FTIR (ATR): ν(cm^{-1}) 1105 (s, 18-crown-6 stretch).

4.5.5 Synthesis of 16

A benzene solution (0.2 mL) of Se_2Ph_2 (2.2 mg, 0.007 mmol, 1.00 eq.) was added to a benzene solution (0.3 mL) of **10** (10 mg, 0.007 mmol, 1.00 eq.). The mixture was stirred for 24 h before all volatiles were removed *in vacuo*. THF (0.5 ml) was added to the residue together with (PPN)Cl (8 mg, 0.014 mmol, 2.00 eq.). The mixture was sonicated for 5 min and then stirred for 2 h before filtered to remove insoluble salts. The filtrate was layered with hexane (6 ml) and left for 24 h before removing the supernatant. The remaining crystals were dried *in vacuo* to afford **16** (8 mg, 0.0041 mmol; yield: 59%) as a yellow powder. Single crystals of **16** suitable for X-ray diffraction were obtained by slow diffusion of hexane into a concentrated THF solution of the product at room temperature. Anal. Calcd. for $C_{126}H_{141}N_2OP_3Se_2$ (M.W. 1950.39 g mol^{-1}): C, 77.59; H, 7.29; N, 1.44; Found: C 77.16; H, 6.96; N, 1.42. m.p. 199 °C.

^{1}H NMR (400 MHz, d$_8$-THF): δ (ppm) 0.98 (d, $^3J_{H–H}$ = 7.0 Hz, 24H; CH(C*H*$_3$)$_2$), 1.10 (d, $^3J_{H–H}$ = 7.0 Hz, 24H; CH(C*H*$_3$)$_2$), 1.22 (d, $^3J_{H-H}$ = 7.0 Hz, 24H; CH(C*H*$_3$)$_2$), 2.83 (sept, $^3J_{H–H}$ = 7.0 Hz, 4H; C*H*(CH$_3$)$_2$), 3.22 (sept, $^3J_{H–H}$ = 7.0 Hz, 8H; C*H*(CH$_3$)$_2$), 6.61–6.67 (m, 8H; Ar*H*), 6.95 (s, 8H; Ar*H*), 7.08 (dd, $^3J_{H–H}$ = 7.6 Hz, $^4J_{H–H}$ = 1.5 Hz, 2H; Ar*H*), 7.33 (d, $^3J_{H–H}$ = 7.6 Hz, 4H; Ar*H*), 7.43–7.48 (m, 13H; Ar*H*), 7.54–7.60 (m, 16H; Ar*H*), 7.66 (td, $^3J_{H–H}$ = 7.6 Hz, $^4J_{H–H}$ = 1.5 Hz, 6H; Ar*H*).

^{13}C{^{1}H} NMR (151 MHz, d$_8$-THF): δ (ppm) 24.47, 24.71, 25.23 (s; CH(*C*H$_3$)$_2$), 30.70, 35.20 (s; *C*H(CH$_3$)$_2$), 118.21 (d, $J_{P–C}$ = 5.5 Hz), 120.43 (d, $J_{P–C}$ = 2.1 Hz), 128.64 (d, $J_{P–C}$ = 11.6 Hz), 128.83, 128.86, 128.94, 129.43, 130.12–130.25 (m), 130.34 (d, $J_{P–C}$ = 4.5 Hz), 130.73, 131.30 (d, $J_{P–C}$ = 2.3 Hz), 132.03 (d, $J_{P–C}$ = 2.7 Hz), 132.47, 132.59 (d, $J_{P–C}$ = 2.6 Hz), 132.65 (d, $J_{P–C}$ = 2.1 Hz), 132.97–133.08 (m), 134.51, 135.57 (d, $J_{P–C}$ = 2.0 Hz), 135.96 (d, $J_{P–C}$ = 5.5 Hz), 138.70 (d, $J_{P–C}$ = 10.7 Hz), 139.52 (d, $J_{P–C}$ = 6.3 Hz), 144.96, 146.97 (d, $J_{P–C}$ = 5.5 Hz), 147.23, 147.88 (s; Ar*C*).

^{77}Se NMR (95.4 MHz, d_8-THF): δ (ppm) 512.7 (d, $J_{P–Se}$ = 398.7 Hz).

^{31}P{^{1}H} NMR (162 MHz, C_6D_6): δ (ppm) –23.2 with two satellites at –24.5 and –22.0 (s, $J_{P–Se}$ = 398.7 Hz), 21.0 (s, Ph_3P=N=$P$$Ph_3$).

HRMS (*m*/*z*): [Anion]$^+$ calcd. For $C_{90}H_{111}NPOSe_2$, 1412.6739; found 1412.6758.

FTIR (ATR): ν(cm^{-1}) 1115 (s, PNP stretch).

4.6 References

[1] P. Pyykkö, M. Atsumi, *Chem. Eur. J.* **2009**, 15, 186–197.

[2] G. Rayner-Canham, *Found. Chem.* **2011**, 13, 121–129.

[3] L. D. Quin, S. Jankowski, A. G. Sommese, P. M. Lahti, D. B. Chesnut, *J. Am. Chem. Soc.* **1992**, 114, 11009–11010.

[4] X. Hu, W. Zhang, I. Carmichael, A. S. Serianni, *J. Am. Chem. Soc.* **2010**, 132, 4641−4652.

[5] A. N. Chernega, M. Y. Antipin, Y. T. Struchkov, A. V. Ruban, V. D. Romanenko, *J. Struct. Chem.* **1989**, 30, 957–962.

[6] A. I. Chernega, M. Y. Antipin, Y. T. Struchkov, A. V. Ruban, V. D. Romanenko, *J. Struct. Chem.* **1990**, 31, 301–306.

[7] E. Niecke, R. Detsch, M. Nieger, F. Reichert, W. Schoeller, *Bull. Soc. Chim. Fr.* **1993**, 130, 25–31.

[8] N. Pötschke, D. Barion, M. Nieger, E. Niecke, *Tetrahedron* **1995**, 51, 8993–8996.

[9] A. N. Chernega, V. D. Romanenko, *J. Struct. Chem.* **1996**, 37, 364–366.

[10] M. Kuprat, R. Kuzora, M. Lehmann, A. Schulz, A. Villinger, R. Wustrack, *J. Organomet. Chem.* **2010**, 695, 1006–1011.

[11] A. K. Eckhardt, M.-L. Y. Riu, P. Müller, C. C. Cummins, *J. Am. Chem. Soc.* **2021**, 143, 21252–21257.

[12] Z. Liu, A. I. McKay, L. Zhao, C. M. Forsyth, V. Jevtović, M. Petković, G. Frenking, D. Vidović, *J. Am. Chem. Soc.* **2022**, 144, 7357–7365.

[13] N. N. Greenwood, A. Earnshaw, *Chemistry of the Elements* (2nd ed.) (Elsevier Butterworth-Heineman: Oxford, 2005).

[14] V. Kostina, N. Feshchenko, A. Kirsanov, *Zh. Obs. Khim.* **1973**, 43, 209.

[15] M. Gonsior, L. Müller, I. Krossing, I. *Chem. Eur. J.* **2006**, 12, 5815–5822.

Chapter 5
A New Twist on the Phospha-(Aza)-Wittig Reaction

5.1 Introduction

In its narrowest definition, the Wittig reaction involves the reaction of a phosphorus ylide (i.e. a Wittig reagent) with an organic carbonyl (an aldehyde or a ketone) to afford an alkene and a phosphine oxide (Figure 5.1a).[1–6] This formal metathesis reaction is widely regarded as one of the most practical and versatile transformations in organic chemistry. It finds use in both academic research and industry due to its high chemo- and regio-selectivity and broad functional group tolerance.[7–10] Historically, the Wittig reaction was limited to carbonyl substrates such as ketones or aldehydes. However, more recent studies have demonstrated that phosphorus ylides can react with electron-deficient amides or esters to produce the corresponding alkenes. This transformation has been referred to the "non-classical" Wittig reaction.[11,12] Despite extensive investigations, the exact mechanistic details of the Wittig reaction remain a subject of debate. While the concerted [2+2] cycloaddition followed by a retro-[2+2] elimination mechanism is widely accepted, alternative pathways have also been proposed. Specifically, evidence suggests that the initial [2+2] cycloaddition may proceed via a stepwise mechanism, involving the formation of a betaine intermediate through nucleophilic attack of the phosphorus ylide on the carbonyl group.[13]

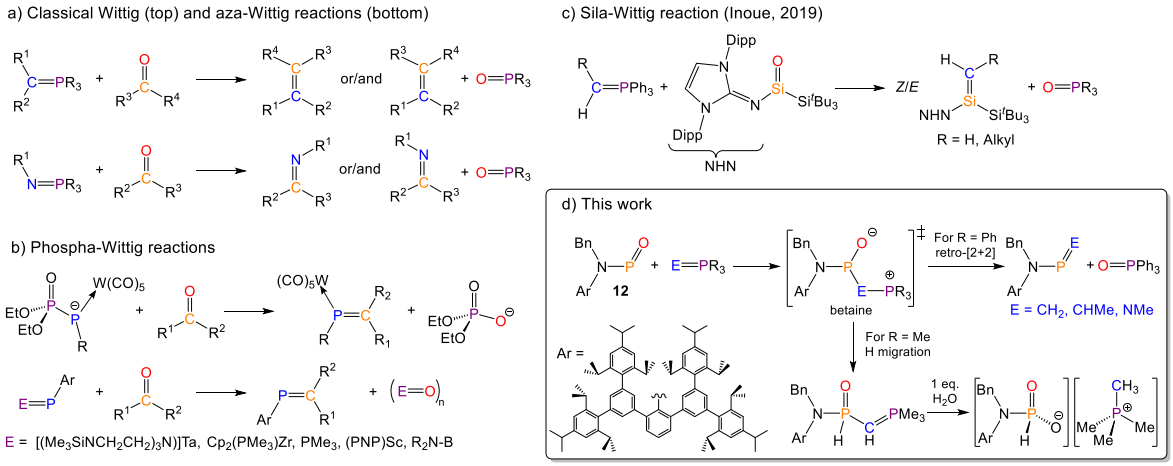

Figure 5.1. The Wittig reaction and related transformations.

Mechanistically related transformations involving other heteroatoms also fall under the broader definition of a Wittig reaction. A representative example is the aza-Wittig reaction; instead of using a phosphorus ylide as the nucleophile, this reaction involves the use of a phosphine imide (or iminophosphorane).[5,14] The iminophophorane reacts with an organic carbonyl to generate the corresponding imine (and a phosphine oxide by-product).[15] Heavier analogues of imines, phosphaalkenes, can also be prepared via the phospha-Wittig reaction (Figure 5.1b). This concept was pioneered by Mathey, who employed anionic phosphorus-containing reagents as *nucleophiles* to react with carbonyl compounds, yielding phosphaalkenes.[16,17] Mathey's "phospha-Wittig reagents" can be regarded as "push-pull" stabilized phosphinidenes, where the reactive phosphinidene moiety (P–R) is stabilized by coordination to a Lewis acid and a Lewis base. In the years following these reports, several other phosphinidene transfer reagents have proven to be effective at this transformation.[18] Several terminal transition-metal phosphinidene complexes – e.g. Schrock's $[(Me_3SiNCH_2CH_2)_3N]Ta{=}PR$ (R = Ph, Cy, ^{t}Bu), Stephan's $Cp_2(PMe_3)Zr{=}PMes^*$ and Mindiola's (PNP)Sc=P(DMP)·LiBr – have been shown to react with ketones or aldehydes, giving rise to phosphaalkenes and the corresponding metal oxide (which may further oligomerize).[19–21]

More closely related to "classical" Wittig transformations is the reaction between phosphoranylidene-phosphines ($ArP{=}PMe_3$) and organic carbonyls, which has been shown to yield phosphaalkenes and trimethylphosphine oxide.[22] In 2021, Cowley and co-workers introduced the phospha-bora-Wittig reaction, where they used a transient phosphaborene $Mes^*P{=}BNR_2$ as nucleophile and reacted it with carbonyl compounds, resulting in phosphaalkenes.[23] While the choice of *nucleophiles* in the Wittig reaction has been studied extensively, significantly fewer investigations have focused on replacing carbonyl compounds with other E=O *electrophiles*. This paucity of research is largely attributed to the challenges associated with isolating suitable main-group oxides, which are typically highly

reactive and prone to oligomerization. In 2019, Inoue and co-workers reported a sila-Wittig reaction (Figure 5.1c), where they used a silanone, $R_2Si{=}O$, as a heavier analogy of ketone and reacted it with phosphorus ylides. Reactions with non-stabilized ylides were found to generate the corresponding silaolefins as a mixture of E/Z isomers.[24]

This prompted us to explore the use of other main-group oxides as the electrophilic partners in Wittig-type transformations. We detailed the isolation of a two-coordinate amino-phosphinidene oxide (BnArNP=O; **12**) in Chapter 4 and demonstrated that its electronic structure closely resembles that of organic amides, as both *cis* and *trans* isomers were observed due to restricted N–P bond rotation.[25] This structural and electronic similarity inspired us to investigate the potential of this species as an *electrophile* in Wittig-type reactions (Figure 5.1d).

5.2 A phospha-Wittig reaction

We started our investigation using the prototypical phosphorus ylide, methylene-triphenylphosphorane $CH_2{=}PPh_3$ (Scheme 5.1). Adding benzene to a solid mixture of **12** and $H_2C{=}PPh_3$ at room temperature leads to instantaneous conversion to two new products. *In-situ* ^{31}P NMR spectroscopy revealed a doublet of doublets at 269.6 ppm with two $^2J_{P–H}$ coupling constants of 21.2 and 8.1 Hz, indicative of the formation of a primary phosphaalkene **17**. Additionally, the generation of triphenylphosphine oxide $O{=}PPh_3$ (a singlet with a characteristic chemical shift at 24.8 ppm) was also confirmed by ^{31}P NMR spectroscopy.[24] These observations support successful metathesis between the oxo- and methylene groups in **12** and $H_2C{=}PPh_3$, respectively.

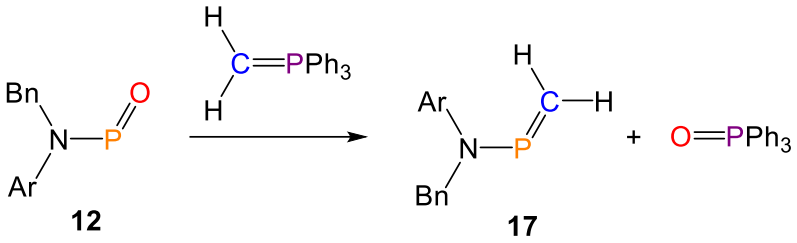

Scheme 5.1. Synthesis of compounds **17** from reaction of ylides with **12**.

Structural confirmation of **17** was obtained by single-crystal X-ray diffraction analysis (Figure 5.2). The crystallographic data revealed a short P=CH_2 bond length of 1.644(4) Å, as expected for a P=C double bond, and consistent with the values reported for other primary phosphaalkenes.[26,27] The first phosphaalkene with a terminal methylene group was reported in 1984,[28] however since then, no other primary phosphaalkenes have been reported. It is also worth highlighting that **17** has a *cis*-arrangement of substituents along the N–P bond, contrasting with the *trans*-geometry observed in the precursor **12**. However, due to positional disorder within the asymmetric unit, a more nuanced analysis of bond metric data for **17** is not viable.

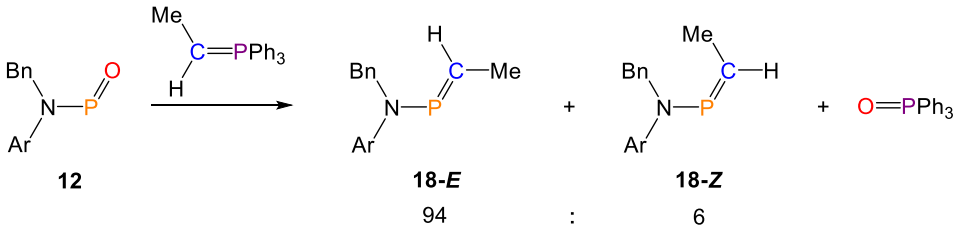

Scheme 5.2. Synthesis of compounds **18** from reaction of ylides with **12**.

To investigate the *E*/*Z* selectivity of this reaction, ethylidene-triphenylphosphorane HMeC=PPh_3 was employed as the ylide. Addition of benzene to a solid mixture of **12** and HMeC=PPh_3 leads to the generation of O=PPh_3 along with two other products **18-*E*** and **18-*Z***, as determined by multielement NMR spectroscopy. It is worth noting that the reaction takes 3 h to reach full conversion, which is significantly slower compared to the reaction of **12** with H_2C=PPh_3. *In-situ* ^{31}P NMR spectroscopy revealed two multiplets corresponding to **18-*E*** at 252.2 ppm and **18-*Z*** at 239.5 ppm. Integration of these resonances indicated a *E*/*Z*

ratio of 94:6. Upon proton decoupling, both multiplets collapsed to singlets. Due to their similar solubility, these two isomers cannot be isolated in pure form.

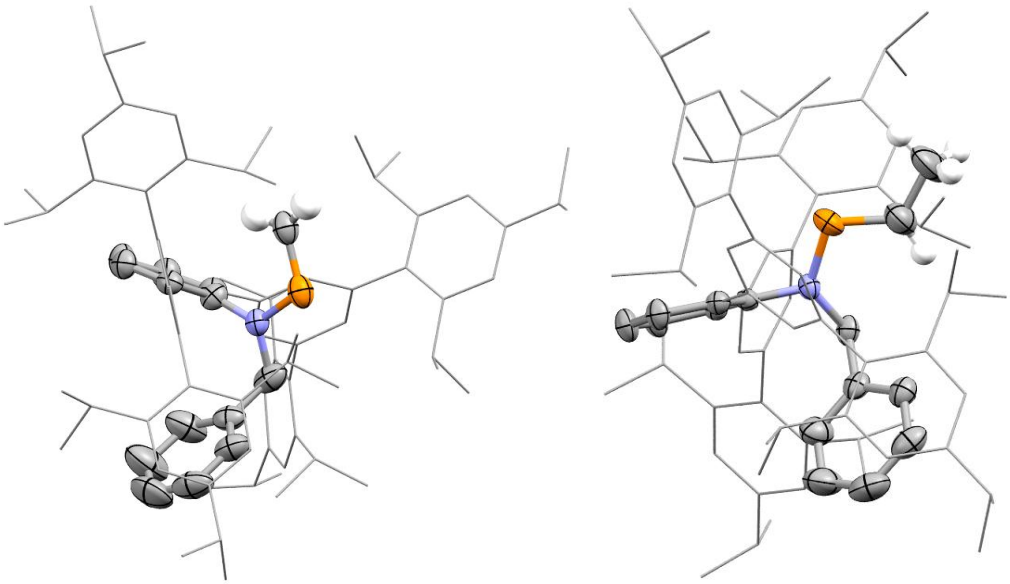

Figure 5.2. Single-crystal X-ray structures of **17** (left) and **18** (right). Selected carbon atoms for backbones are depicted with wireframe mode. Thermal ellipsoids pictured at 50% probability level. Solvent of crystallization, positional disorder and hydrogen atoms (except for those associated with the methylene and ethylidene fragments) are removed for clarity.

Single crystals suitable for X-ray analysis support that the major isomer in the mixture is **18-*E*** (Figure 5.2). The P=C bond length was found to be 1.642(3) Å, which is in good agreement with that observed for **17** (1.644(4) Å). The crystal structure further revealed a *trans*-geometry about the N–P bond, in contrast with the *cis*-geometry found in **17**. The crystal quality of **18** was significantly better than that of **17**, enabling a more detailed analysis of bond metrics. Notably, the nitrogen atom retains a planar geometry ($\Sigma_N°$: 360.0°), indicating that the lone pair is still engaged in a π-interaction with the P=C π* orbital. This planar geometry at nitrogen has been observed for other amino phosphaalkenes.[29,30] The N–P bond length in **18-*E*** (1.679(2) Å) is comparable to that of **17** (1.678(3) Å) suggesting a comparable degree of donation interaction into the P=C π* orbital. These are both somewhat

longer than in the phosphinidene oxide precursor, **12**, which exhibits a P–N bond length of 1.667(6) Å. This subtle structural difference is also manifested in the ^{31}P NMR spectra of these compounds. While compound **12** exhibited two distinct signals corresponding to the *cis* and *trans* isomer pairs relative to the N–P bond (284.4 and 286.3 ppm),[25] compound **18-*E*** displays only a single resonance, indicating that the N–P bond in **18-*E*** can rotate freely on the NMR timescale.

Density functional theory (DFT) calculations were conducted on **17** to probe its electronic structure. The optimized geometry at the M06-2X/Def2-SVP level of theory is in good agreement with that determined by X-ray crystallography (e.g. P–C: 1.655 Å, N–P: 1.710 Å; Σ_N°: 359.3°). Natural bond orbital (NBO) analysis provides insights into intramolecular electronic interactions. Second-order perturbation theory calculations on **17** reveal a back-donation energy, E(2), of 21.2 kcal mol^{-1}, for the nitrogen lone pair donating into the P=C π* orbital. This value is notably lower than that computed for compound **12** (41.1 kcal mol^{-1}). This can be attributed to the greater electronegativity of oxygen, which causes the P–O π* orbital to have a greater orbital contribution from phosphorus (Figure 5.3). NBO orbital analysis further supports this observation: the P–O π* NBO orbital of **12** has a phosphorus contribution of 78.92%, while for the P–C π* NBO orbital of **17**, the phosphorus contribution decreases to 60.03%. Additionally, the energy of the lowest unoccupied molecular orbital (LUMO) in **17** (–0.32 eV, P=C π* orbital, Figure 5.4) is also higher compared to the LUMO energy in **12** (–0.86 eV, P=O π* orbital, Figure 5.4). This further supports weaker back-donation in **17**. Energy calculations at SMD-M062X/def2-TZVP//M062X/def2-SVP level of theory revealed that the energy barrier for N–P bond rotation in **17** is 12.1 kcal mol^{-1}, significantly lower than the barrier in **12** (21.8 kcal mol^{-1}). This reduced rotation barrier aligns with the experimental observation by NMR spectroscopy and is in line with the weaker back-donation arguments described above.

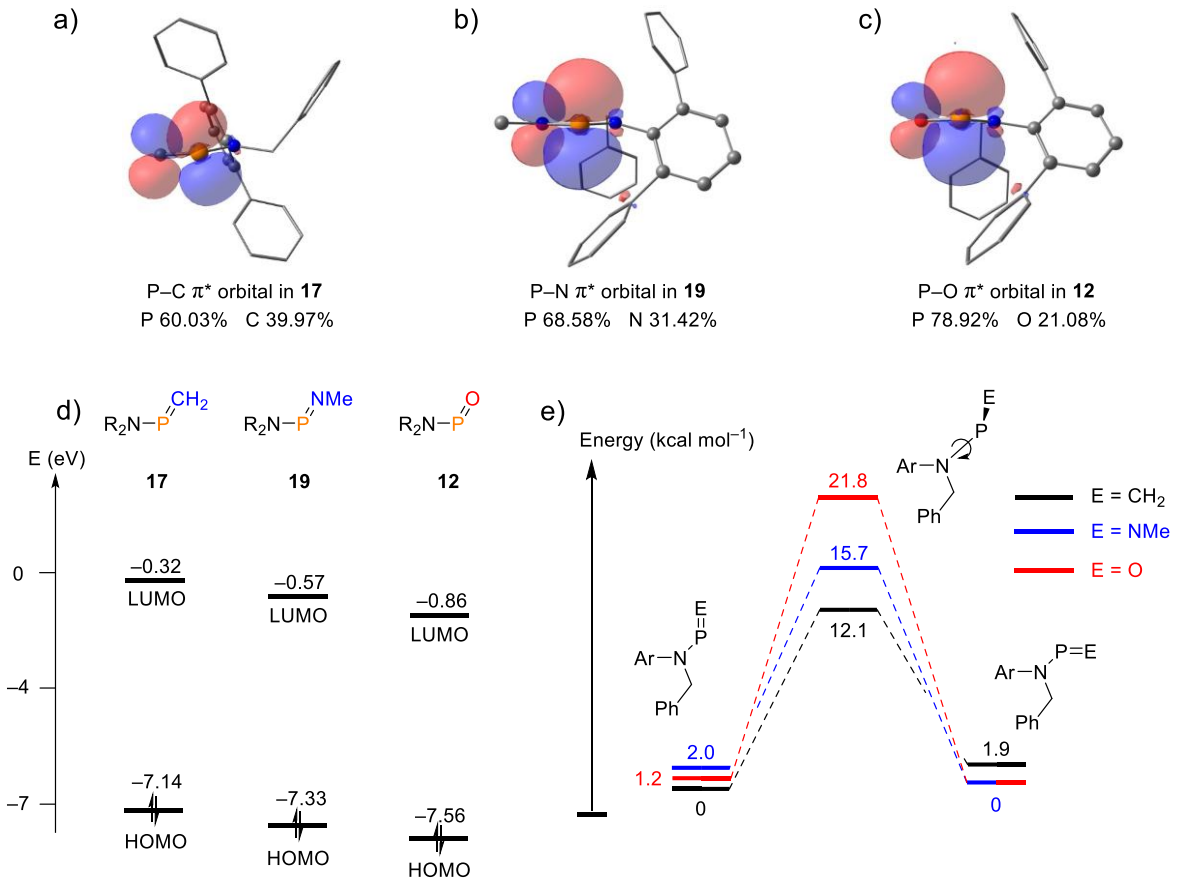

Figure 5.3. a–c) Natural Bond Orbital depictions of the π* orbital interactions for **17**, **19** and **12**; d) Comparison of relative HOMO/LUMO energies for **17**, **19** and **12**; and e) Computed energy barriers for N–P bond rotation for **17** (black), **19** (blue) and **12** (red).

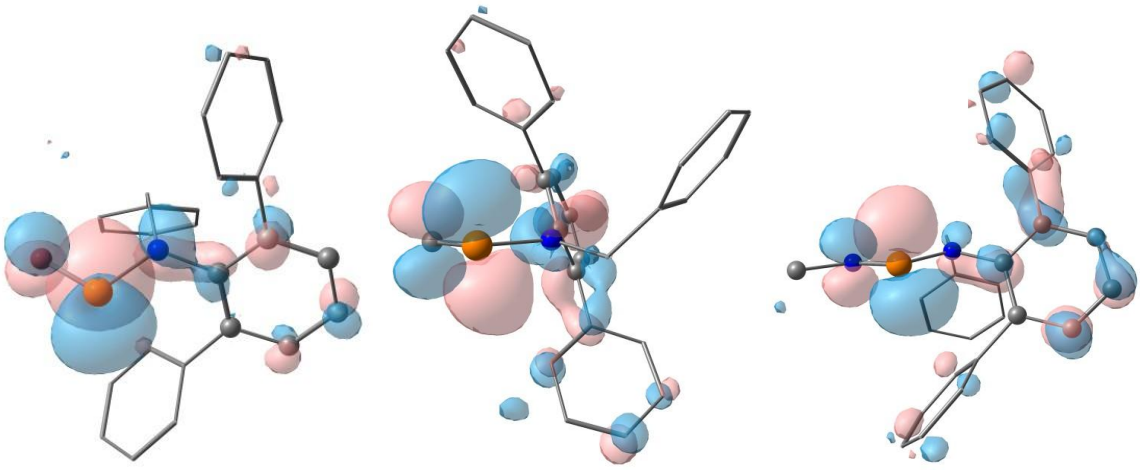

12 (-0.86 eV) **17** (-0.32 eV) **19** (-0.57 eV)

Figure 5.4. Lowest unoccupied molecular orbital (LUMO) of **12**,**17** and **19**.

5.3 A phospha-aza-Wittig reaction

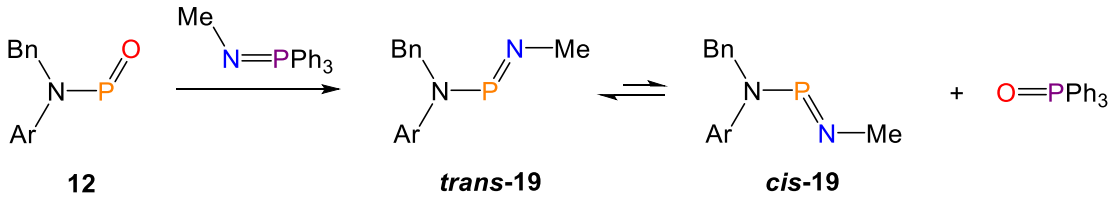

Scheme 5.3. Synthesis of compound **19** from reaction of an iminophosphorane with **12**.

The successful use of **12** as the electrophilic component in a Wittig reaction encouraged us to extend this reactivity to the phospha-aza-Wittig reaction. Thus, we investigated the reaction of **12** and *N*-(triphenylphosphoranylidene)methanamine MeN=PPh_3 (Scheme 5.3). After stirring the reaction mixture for 3 h at room temperature, generation of O=PPh_3 was once again confirmed by *in-situ* $^{31}P\{^1H\}$ NMR spectroscopy. However, no other sharp resonances were observed in the $^{31}P\{^1H\}$ NMR spectrum. Instead, two broad peaks were detected at 310.2 ppm ($W_{1/2}$ = 277.7 Hz) and 186.7 ppm ($W_{1/2}$ = 386.6 Hz). Similar to the behaviour of compound **12**, where two $^{31}P\{^1H\}$ NMR resonances arise from *cis–trans* isomerization, we attributed these broad peaks to the *cis* and *trans* isomers of the reaction product, ***cis*-19** and ***trans*-19**.

A variable temperature NMR study was performed on the isomeric mixture of **19** to investigate the observed peak broadening (Figure 5.5). Due to restricted N–P bond rotation, at low temperature the rate of exchange between ***trans*-19** and ***cis*-19** was reduced, resulting in two distinct sharp resonances. At elevated temperature, ***trans*-19** and ***cis*-19** are in fast exchange, causing the two peaks to broaden, and eventually disappear into the baseline of the $^{31}P\{^1H\}$ NMR spectra. A line shape fitting analysis was performed on the VT NMR data collected between 228 and 298 K. An Eyring plot of the data (Figure 5.6) allowed for the determination of the thermodynamic parameters for this process (ΔH^* = 47.4(22) kcal mol^{-1}, ΔS^* = 107(8) cal mol^{-1} K^{-1} and ΔG^*(298 K) = 15.6(33) kcal mol^{-1}). These data are in excellent agreement with the computed energetic barrier for N–P bond rotation (Figure

5.3; ΔG(298 K) = 15.7 kcal mol^{-1}). While heating to 358 K did not sufficiently accelerate the exchange rate to allow for resonance coalescence on the $^{31}P\{^{1}H\}$ NMR time scale, in the ^{1}H NMR spectra we were able to observe ***trans*-19** and ***cis*-19** coalesce into a time-averaged species at elevated temperatures (Figure 5.7).

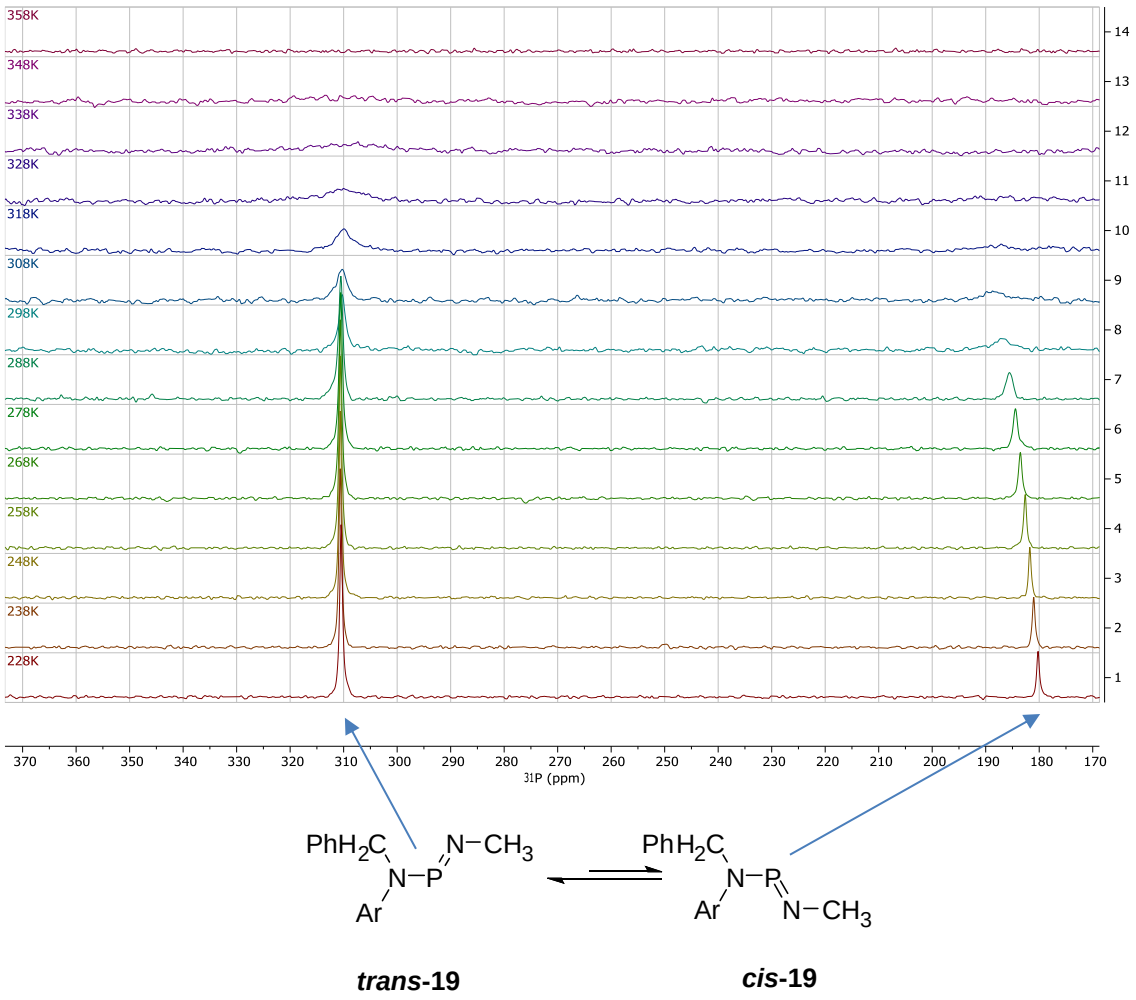

Figure 5.5. Variable-temperature $^{31}P\{^{1}H\}$ NMR spectrum of **19** in d_8-toluene from 228 K to 358 K.

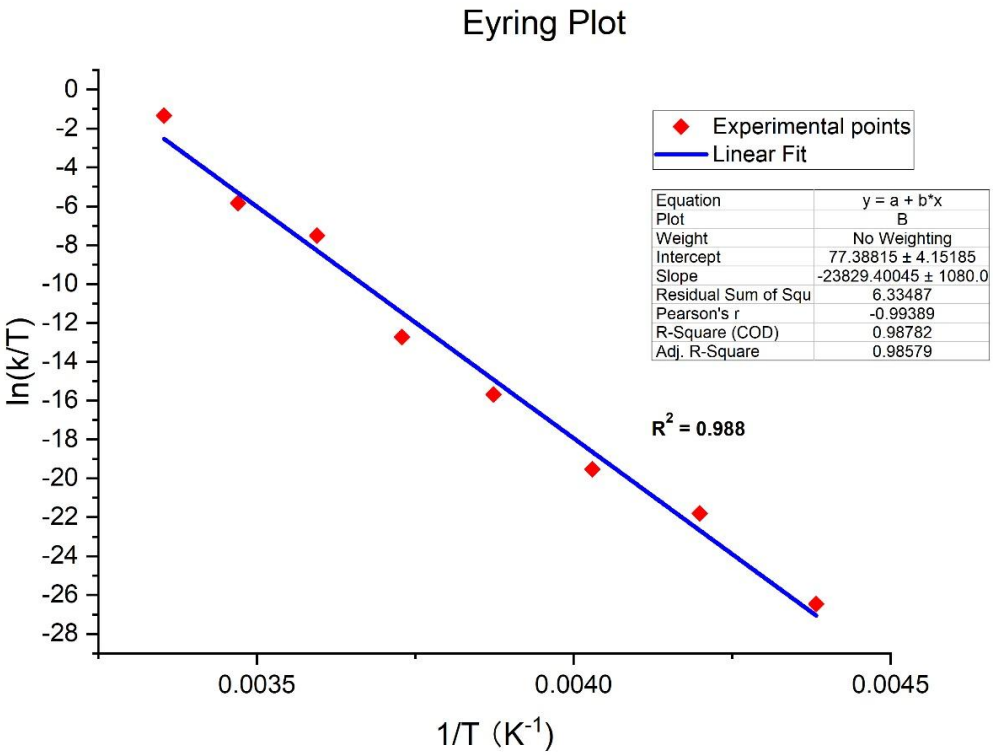

Figure 5.6. Eyring Plot of the data obtained from line shape fitting analysis for variable-temperature $^{31}P\{^{1}H\}$ NMR from 228 K to 288 K. (Line shape fitting was performed using D-NMR implanted in topspin).

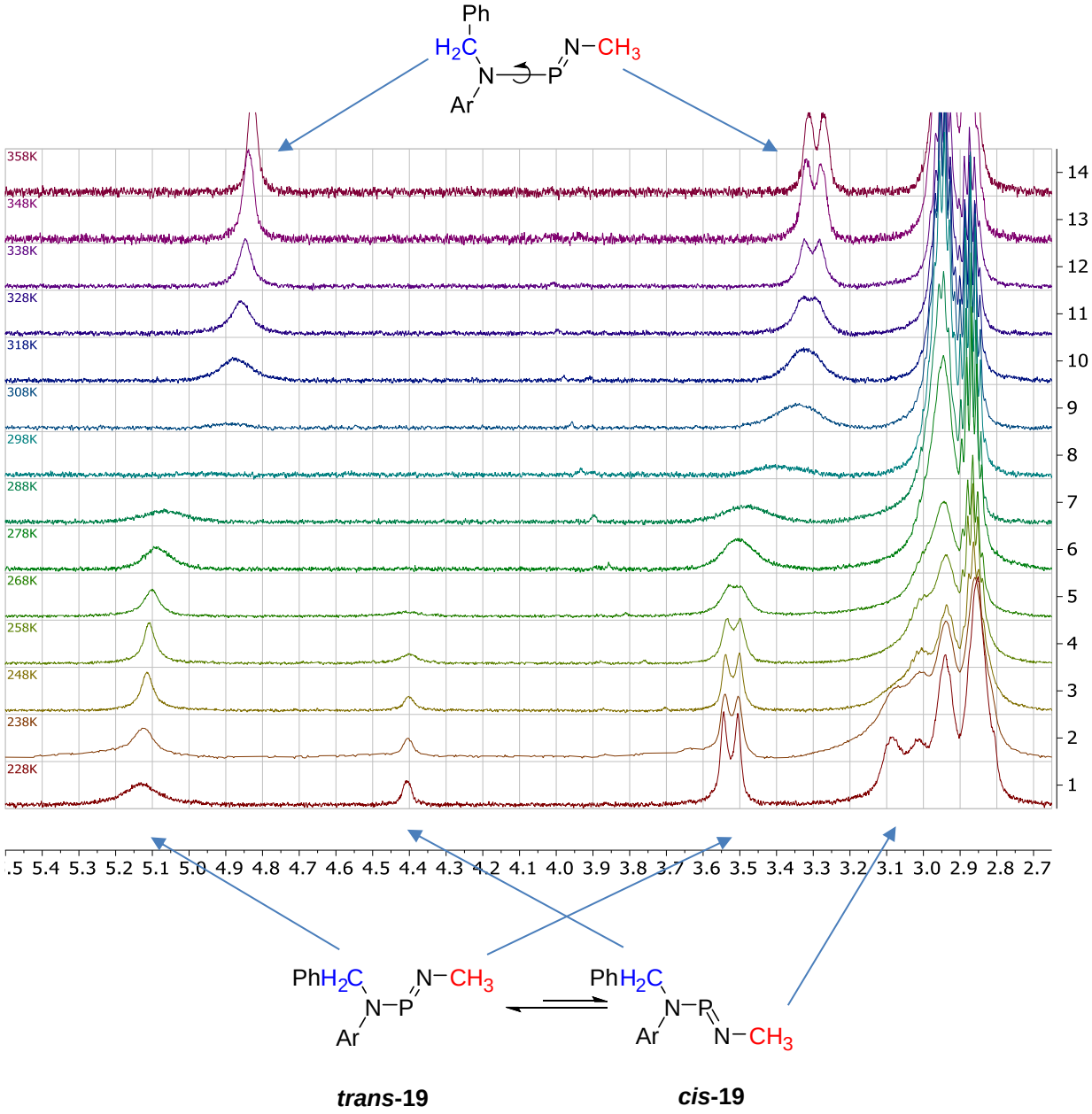

Figure 5.7. Variable-temperature ^{1}H NMR spectrum of **19** in d_8-toluene from 228 K to 358 K. Zoomed in region from 5.5 ppm to 2.6 ppm, displaying the chemical exchange process between ***trans*-19** and ***cis*-19.**

The structure of **19** was unambiguously confirmed by single-crystal X-ray diffraction (Figure 5.8). The solid-state structure reveals a *trans*-geometry along ArBnN–P bond and a *E*-configuration along the P=NMe bond. Such a configuration is common amongst iminophosphanes, a class of compounds first reported by Niecke.[31–37] Observation of a single isomer by single-crystal X-ray diffraction is postulated to arise due to steric considerations,

as the observed configuration minimizes steric hindrance. The P=NMe bond length (1.553(2) Å) is in good agreement with the expected value for a P=N double bond.[26] Consistent with the structures of **12**, **17** and **18**, the amido nitrogen atom, N2, once again exhibits a planar geometry, with a sum of bond angles ($\Sigma_N°$) of 360.0°. The N2–P1 bond length was measured to be 1.670(2) Å, which is slightly shorter than that of **18** (1.679(2) Å), but nearly identical to that in **12** (1.667(6) Å). These observations are consistent with the restricted N2–P1 bond rotation inferred from multinuclear NMR studies.

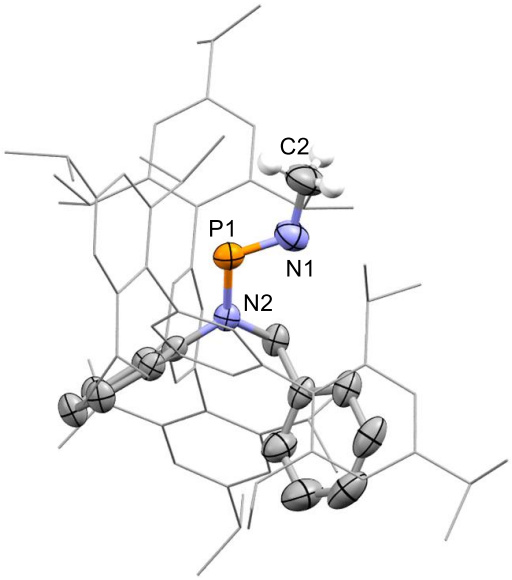

Figure 5.8. Single-crystal X-ray structures of **19**. Selected carbon atoms for backbones are depicted with wireframe mode. Thermal ellipsoids pictured at 50% probability level. Solvent of crystallization, positional disorder and hydrogen atoms are removed for clarity.

DFT calculations were carried out to gain further insight into the electronic structure of **19**. Second-order perturbation theory analysis revealed a back-donation energy of 31.7 kcal mol^{-1} from the lone pair of N2 to the P=N π* orbital. This value sits between those computed for **17** (21.2 kcal mol^{-1}) and **12** (41.1 kcal mol^{-1}), and reflects the electronegativity trends between C, N, O. Similarly, the computed phosphorus contribution to the P=N π* orbital (68.58%) and the LUMO energy (–0.57 eV; corresponding to the P=N π* orbital) are also in

between the values obtained for **12** and **17** (Figure 5.3). Furthermore, our calculations also indicated an intermediate rotational energy barrier of 15.7 kcal mol^{-1} for the N2–P1 bond, relative to those of **12** and **17**. These findings provide a coherent explanation for the observed NMR spectroscopic behaviour. For compound **12**, the high rotational barrier of the N–P bond results in slow *cis–trans* isomerization at room temperature, leading to two distinct peaks in the $^{31}P\{^{1}H\}$ NMR spectrum. In contrast, for compound **17**, the lower rotational barrier allows free rotation of the N–P bond at room temperature, giving rise to a single resonance. For compound **19**, the intermediate rotational barrier results in a moderate exchange rate between *cis* and *trans* isomers, which manifests as two broad peaks in the $^{31}P\{^{1}H\}$ NMR spectrum at room temperature.

5.4 Mechanistic studies of the phospha-Wittig reaction

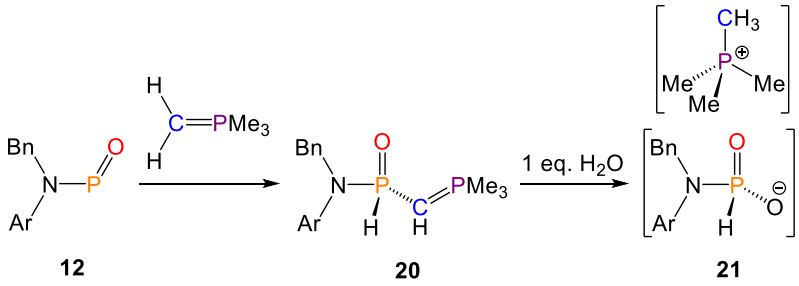

Scheme 5.4. Synthesis of **20** and **21** from reaction of **12** with $H_2C{=}PPh_3$.

To further explore the mechanistic aspects of this phospha-Wittig reaction, additional phosphorus ylides were tested. Specifically, trimethylmethylenephosphorane ($H_2C{=}PMe_3$) was selected as an alternative ylide to react with compound **12** (Scheme 5.4). To our surprise, upon mixing the two reactants at –78 °C and slowly warming up the reaction mixture to room temperature, the expected product, phosphaalkene **17**, was not detected by *in-situ* $^{31}P\{^{1}H\}$ NMR spectroscopy. Instead, the major product appeared in the form of a pair of doublets at 28.0 and 6.8 ppm, with a coupling constant of $^{2}J_{P–P}$ = 33.3 Hz. Proton-coupling revealed that the peak at 28.0 ppm split into a doublet of doublets (Figure 5.9), with a

coupling constant of $^{1}J_{P-H}$ = 530.5 Hz, suggesting the formation of a phosphorus(V) species containing a P–H bond. The second doublet at 6.8 ppm transformed into one broad resonance on ^{1}H coupling, which we attribute to interactions with the methyl groups of the PMe_3 fragment. High resolution mass spectroscopy confirmed the molecular formula of this species as $C_{89}H_{119}N_1O_1P_2$, which corresponding to the sum of **12** and $H_2C{=}PMe_3$. With this information in hand, we assigned this compound, **20**, to be a proton-migration product, where one of the protons from $H_2C{=}PMe_3$ shifted to the phosphorus center. Despite numerous attempts to obtain single-crystal diffraction data for compound **20**, no satisfactory crystals could be grown for structural confirmation.

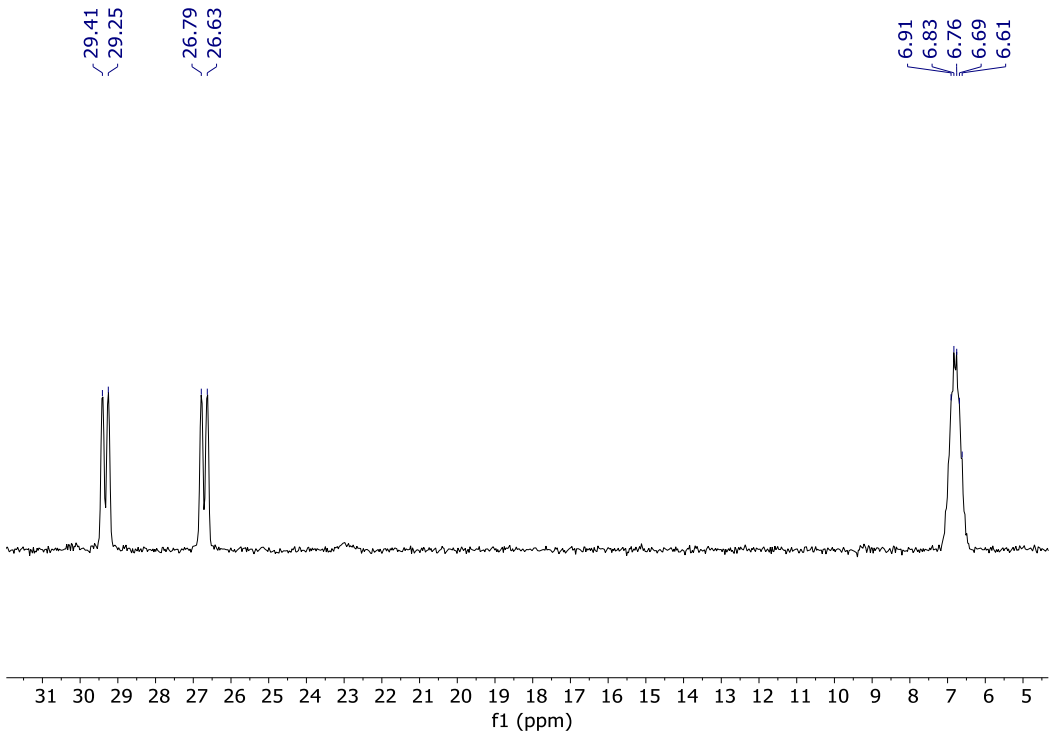

Figure 5.9. ^{31}P NMR spectrum of **20** (202 MHz, C_6D_6).

Further reaction of compound **20** with water resulted in the cleavage of the P–C bond, yielding a phosphorus acid derivative accompanied by a tetramethylphosphonium $[PMe_4]^+$ counterion, **21**. As expected for an ion pair, the P–P coupling observed in compound **20** disappeared in the $^{31}P\{^{1}H\}$ NMR spectrum of **21**, giving rise in two distinct singlets.

Compound **21** was successfully characterized by single-crystal X-ray diffraction (Figure 5.10).

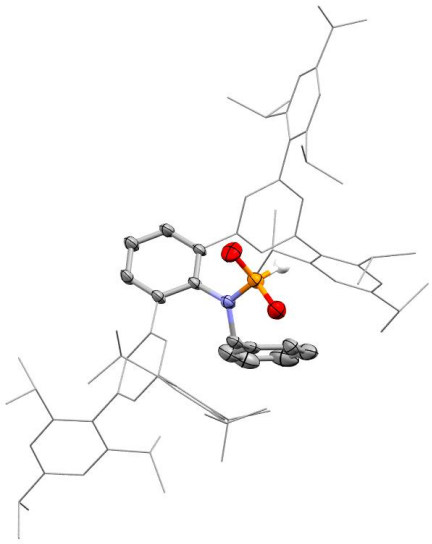

Figure 5.10. Single-crystal X-ray structures of the anionic component in **21**. Selected carbon atoms for backbones are depicted with wireframe mode. Thermal ellipsoids pictured at 50% probability level. Solvent of crystallization, positional disorder and hydrogen atoms (apart from those associated with C2 and P1A) are removed for clarity.

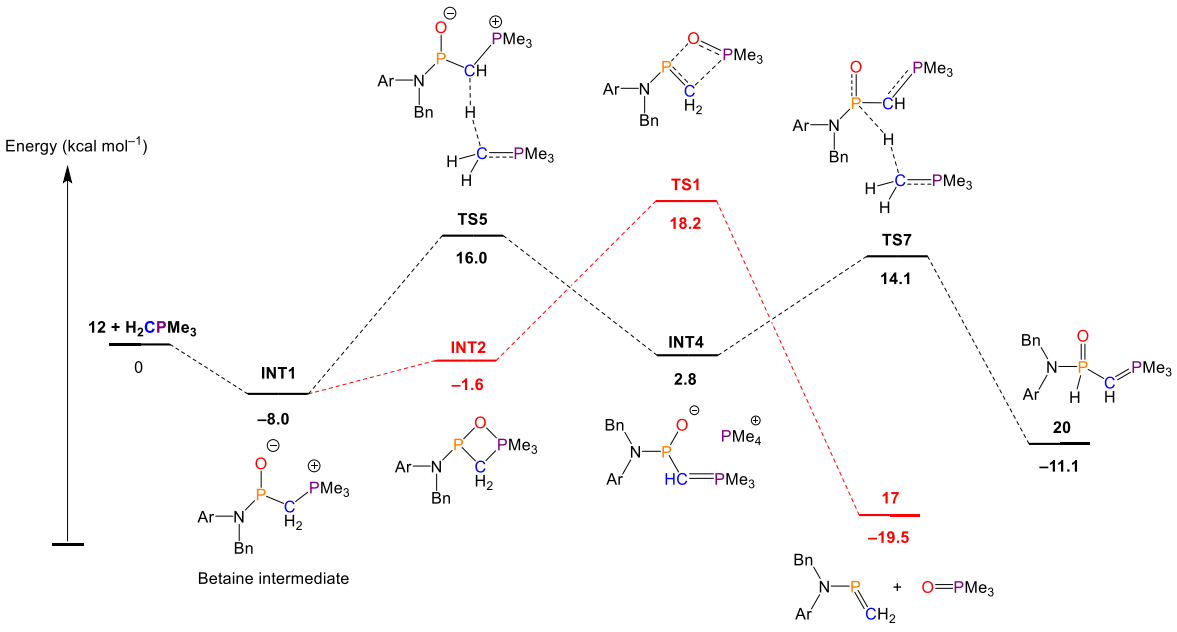

Figure 5.11. Computed reaction energy profiles for the reaction of **12** with CH_2=PMe_3.

The mechanism for this unexpected hydrogen-migration was calculated using density functional theory (DFT; Figure 5.11). Unlike the classical Wittig reaction, which involves a

concerted [2+2] cycloaddition followed by a retro-[2+2] elimination, we propose that this reaction begins with the nucleophilic addition of $H_2C{=}PMe_3$ to the P=O double bond in compound **12**, forming a betaine intermediate (**INT1**). This intermediate is energetically stabilized by 8.0 kcal mol^{-1}. Notably, similar betaine intermediates have also been proposed in the classical Wittig reaction.[13] From **INT1**, the formation of the phospha-Wittig reaction product could proceed through the retro-[2+2] elimination transition state **TS1**, which has an energy barrier of 26.2 kcal mol^{-1}. The resulting products, phosphaalkene **17** and trimethylphosphine oxide ($O{=}PMe_3$), are thermodynamically downhill by 19.5 kcal mol^{-1}. However, an alternative pathway involving a second equivalent of $H_2C{=}PMe_3$ was found to be kinetically favoured. Due to the electron-withdrawing effect of the P–O fragment in **INT1**, the α-H becomes more acidic. Thus, another molecule of $H_2C{=}PMe_3$ can react as base and deprotonate **INT1** (**TS5**, 16.0 kcal mol^{-1}), generating a stabilized phosphorus ylide **INT4** (2.8 kcal mol^{-1}). Subsequently, the tetramethylphosphonium cation PMe_4^+ can serve as a proton donor, transferring the proton back to the phosphorus center via transition state **TS7** (14.1 kcal mol^{-1}). This leads to the formation of the kinetic product **20**, which is energetically stabilized by 11.1 kcal mol^{-1}. Overall, the second equivalent of $H_2C{=}PMe_3$ functions as a proton shuttle to facilitate the hydrogen-migration from carbon to phosphorus with an energy barrier of 24.0 kcal mol^{-1}. This barrier is 2.2 kcal mol^{-1} lower than that of the retro-[2+2] transition state required for the standard phospha-Wittig reaction product. Since the reaction was performed at –78 °C, only the kinetic product **20** was observed experimentally.

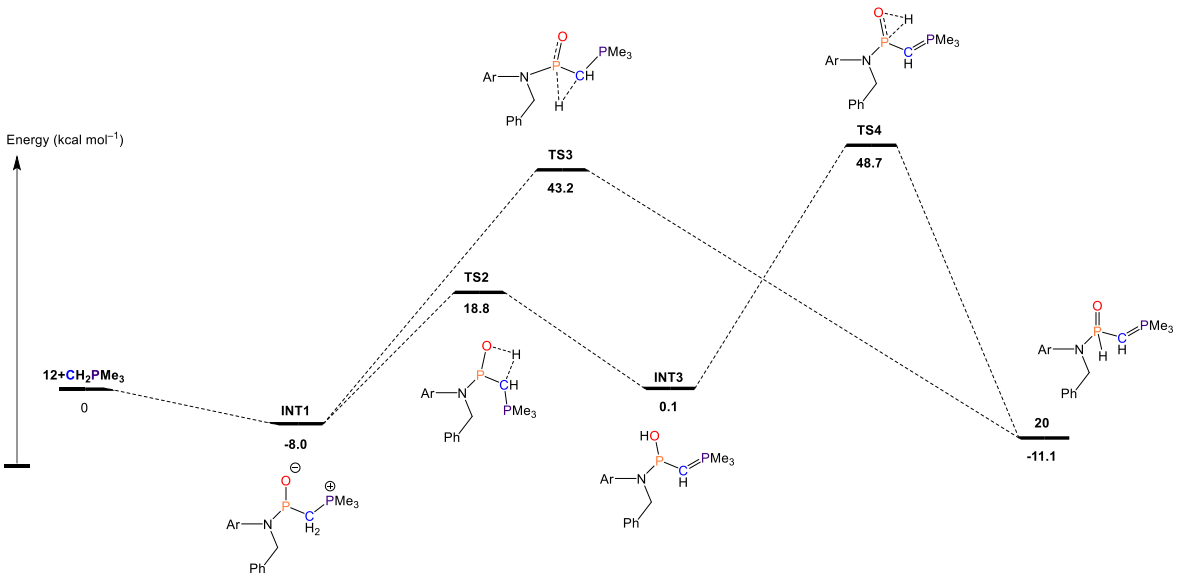

Figure 5.12. Intramolecular mechanism leading to H-migration product **20**.

The intramolecular pathway leading to H-migration product **20** was also investigated computationally. After the formation of betaine intermediate **INT1**, due to the electron withdrawing effect from P–O bond, the α-H of phosphorus shows acidic property. The acidic proton can either migrate directly to phosphorus via an energetically unachievable transition state **TS3** (43.2 kcal mol^{-1}) or shift to oxygen through a four membered ring transition state **TS2** (18.8 kcal mol^{-1}). The deprotonation process of oxygen leads to a P(III) substituted alcohol, which could further go through a H-transfer process (**TS4**, 48.7 kcal mol^{-1}) to generate **20**. However, the energy barriers for both pathways indicate this intramolecular mechanism cannot happen at room temperature condition.

5.5 Comparison between CH_2=PPh_3 and CH_2=PMe_3

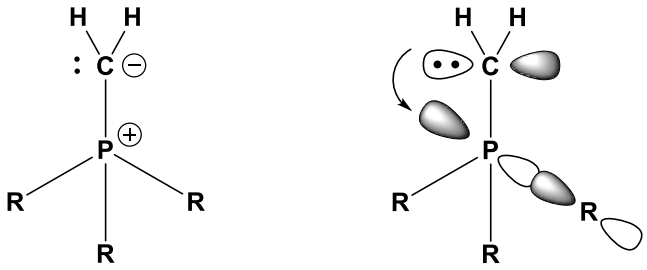

Figure 5.13. Lewis structures of phosphorus ylide and an illustration of the back-donation which takes place.

Due to the higher s-orbital character in P–Ph σ-bond in CH_2=PPh_3, the phosphorus center is more electron-deficient, as evidenced by the NPA charge calculation (Table 5.1). Additionally, the slightly more polar P–Ph bond increases the accessibility of P–Ph σ*-bond, enabling enhanced back-donation from the carbon lone pair as shown in Table 5.2. These combined electronic characteristics lead to the conclusion that CH_2=PPh_3 is a weaker base compared to CH_2=PMe_3.

Table 5.1. Calculated Natural Population Charge (NPA).

	C	P
CH_2=PPh_3	**-1.22**	**1.52**
CH_2=PMe_3	**-1.25**	**1.48**

Table 5.2. Overall back-donation from the carbon lone pair to the PR_3 fragment, calculated by Second Order Perturbation Theory Analysis (kcal mol^{-1}).

	Sum of back-donation E(2) (kcal mol^{-1})
CH_2=PPh_3	**68.7**
CH_2=PMe_3	**61.5**

The observed difference in selectivity for the phospha-Wittig reaction between H_2C=PMe_3 and H_2C=PPh_3 can be attributed to both steric and electronic differences inherent to these two phosphorus ylides. The smaller size and stronger basicity of H_2C=PMe_3 facilitates the deprotonation step with the second equivalent of the ylide reagent, enabling the formation of the H-migration product. In contrast, H_2C=PPh_3, with its electron-deficient phosphorus center, is less effective at stabilizing the betaine intermediate. This electronic property increases the tendency of an oxygen rebound process, favouring the retro-[2+2] pathway and leading to the formation of the standard phospha-Wittig reaction product.

5.6 Conclusions

In summary, we have expanded the scope of the classic Wittig reaction by employing the amino phosphinidene oxide **12** as a carbonyl analogue, reacting it with various phosphorus ylide reagents. When triphenylphosphine ylides ($E{=}PPh_3$, where E = CH_2, CHMe, or NMe) were utilized, the phospha-Wittig reaction proceeded smoothly, yielding the corresponding phosphaalkene **17**, **18** or phosphaimine **19**, alongside triphenylphosphine oxide $O{=}PPh_3$ as a byproduct. The reaction was predominantly *E*-selective. The rotational barrier for the N–P bond was investigated through multinuclear NMR spectroscopy and DFT calculations, revealing a trend that aligns with the electronegativity of the substituents C, N, and O in **17**, **19**, and **12**, respectively. Substituting $CH_2{=}PPh_3$ with $CH_2{=}PMe_3$ resulted in an unexpected H-migration product **20**. DFT calculations indicated that the formation of **20** involved a betaine intermediate, which is also proposed to be a potential intermediate in the classical Wittig reaction. This study demonstrates the potential of utilizing phosphinidene oxide as a phosphinidene synthon in double-bond metathesis reactions. Chapter 6 details the use of this strategy to access a phosphinidene sulfide P(III)=S and a phosphinidene selenide P(III)=Se.

5.7 Experimental Section

5.7.1 Synthesis of 17

To a solid mixture of **12** (30 mg, 0.025 mmol; 1.00 eq.) and $CH_2{=}PPh_3$ (10.4 mg, 0.038 mmol; 1.50 eq.), benzene (0.5 mL) was added. The mixture was stirred for 10 min at room temperature and monitored by ^{31}P NMR spectroscopy. Once the reaction reached completion, MeCN (20 mL) was added to the solution, and the mixture was left in a –35 °C freezer overnight to crystalize. The supernatant was removed and the resulting solid was

dried *in vacuo* to afford **17** (26 mg, 0.022 mmol; 87% yield) as a white powder. Single crystals of **17** suitable for X-ray diffraction were obtained by slow evaporation of a concentrated hexane solution of **17** at room temperature.

^{1}H NMR (500 MHz, C_6D_6): δ (ppm) 1.18–1.22 (m, 36H; CH(C*H*$_3$)$_2$), 1.27 (d, $^{3}J_{H–H}$ = 6.8 Hz, 12H; CH(C*H*$_3$)$_2$), 1.30 (d, $^{3}J_{H–H}$ = 6.8 Hz, 24H; CH(C*H*$_3$)$_2$), 2.89 (sept, $^{3}J_{H–H}$ = 6.8 Hz, 4H; C*H*(CH$_3$)$_2$), 3.03–3.09 (m, 8H; C*H*(CH$_3$)$_2$), 4.52 (d, $^{3}J_{P–H}$ = 6.8 Hz, 2H; NC*H*$_2$Ph), 4.94 (dd, $^{2}J_{P–H}$ = 46.7 Hz, $^{2}J_{H–H}$ = 8.1 Hz, 1H; P=C*H*$_2$), 5.34 (dd, $^{2}J_{P–H}$ = 21.2 Hz, $^{2}J_{H–H}$ = 8.1 Hz, 1H; P=C*H*$_2$), 6.70 (t, $^{3}J_{H–H}$ = 7.5 Hz, 2H; Ar*H*), 6.86 (t, $^{3}J_{H–H}$ = 7.5 Hz, 1H; Ar*H*), 6.93–6.98 (m, 3H; Ar*H*), 7.08 (t, $^{4}J_{H–H}$ = 1.6 Hz, 2H; Ar*H)*, 7.14 (s, 4H; Ar*H*), 7.19–7.22 (m, 8H; Ar*H*), 7.32 (d, $^{3}J_{P–H}$ = 7.6 Hz, 2H; Ar*H*).

^{13}C{^{1}H} NMR (125 MHz, C_6D_6): δ (ppm) 24.35, 24.48, 24.51, 24.91, 25.96 (s; CH(*C*H$_3$)$_2$), 30.86, 30.88, 34.91 (s; *C*H(CH$_3$)$_2$), 57.69 (d, $^{2}J_{P–C}$ = 30.1 Hz; N*C*H$_2$Ph), 115.53 (d, $^{1}J_{P–C}$ = 29.6 Hz; P=*C*H$_2$), 120.65, 120.70, 126.89, 129.04, 130.21, 131.04, 132.26, 137.34 (d, $J_{P–C}$ = 4.0 Hz),137.53, 138.93 (d, $J_{P–C}$ = 8.3 Hz), 141.01, 141.16, 141.29, 146.89, 146.92, 148.40 (s; Ar*C*).

^{31}P NMR (162 MHz, C_6D_6): δ (ppm) 269.6 (dd, $^{2}J_{P–H}$ = 21.2 Hz, $^{2}J_{P–H}$ = 8.1 Hz).

^{31}P{^{1}H} NMR (162 MHz, C_6D_6): δ (ppm) 269.6 (s).

HRMS (*m*/*z*): $[M+H]^+$ calcd. for $C_{86}H_{111}NP$, 1188.8449; found 1188.8436.

5.7.2 Synthesis of 18

To a solid mixture of **12** (30.0 mg, 0.025 mmol; 1.00 eq.) and $CH_3CH{=}PPh_3$ (11.0 mg, 0.038 mmol; 1.50 eq.), benzene (0.5 mL) was added. The mixture was stirred for 30 min at room temperature and monitored by ^{31}P NMR spectroscopy. Once the reaction had reached completion, MeCN (20 mL) was added to the solution, and the mixture was left in a freezer at –35 °C overnight to crystalize. The supernatant was removed and the resulting solid was

dried *in vacuo* to afford **18** (24 mg, 0.020 mmol; 80% yield) as a white powder. The *E*/*Z* ratio (94:6) was determined by ^{31}P NMR spectroscopy. Single crystals of **18-*E*** suitable for X-ray diffraction were obtained by slow evaporation of a concentrated hexane solution of **18** at room temperature.

^{1}H NMR (500 MHz, C_6D_6): δ (ppm) 1.17–1.22 (m, 36H; CH(C*H*$_3$)$_2$), 1.30 (d, $^{3}J_{H–H}$ = 6.8 Hz, 36H; CH(C*H*$_3$)$_2$), 1.59 (dd, $^{3}J_{P–H}$ = 23.3 Hz, $^{3}J_{H–H}$ = 6.5 Hz, 3H; P=CH*C*H$_3$), 2.89 (sept, $^{3}J_{H–H}$ = 6.8 Hz, 4H; C*H*(CH$_3$)$_2$), 2.99–3.13 (m, 8H; C*H*(CH$_3$)$_2$), 4.52 (d, $^{3}J_{P–H}$ = 5.6 Hz, 2H; NC*H*$_2$Ph), 6.64–6.73 (m, 3H; PC*H*CH$_3$ and Ar*H*), 6.83 (t, $^{3}J_{H–H}$ = 7.3 Hz, 1H; Ar*H*), 6.98 (t, $^{3}J_{H–H}$ = 7.3 Hz, 1H; Ar*H*), 7.02 (d, $^{3}J_{H–H}$ = 7.3 Hz, 1H; Ar*H*), 7.07 (t, $^{4}J_{H–H}$ = 1.6 Hz, 2H; Ar*H*), 6.93–6.98 (m, 3H; Ar*H*), 7.08 (t, $^{4}J_{H–H}$ = 1.6 Hz, 2H; Ar*H)*, 7.14 (s, 4H, Ar*H*), 7.19–7.22 (m, 8H; Ar*H*), 7.32 (d, $^{3}J_{P–H}$ = 7.6 Hz, 2H; Ar*H*), 7.18–7.21 (m, 12H; Ar*H*), 7.37 (d, $^{3}J_{P–H}$ = 7.3 Hz, 2H; Ar*H*)

^{13}C{^{1}H} NMR (125 MHz, C_6D_6): δ (ppm) 13.16 (d, $^{1}J_{P–C}$ = 42.8 Hz; P=CH*C*H$_3$), 24.33, 24.46, 24.59, 24.94, 24.99 (s; CH(*C*H$_3$)$_2$), 30.85, 30.91, 34.89 (s; *C*H(CH$_3$)$_2$), 57.08 (d, $^{2}J_{P–C}$ = 16.6 Hz; N*C*H$_2$Ph), 135.48 (d, $^{1}J_{P–C}$ = 28.7 Hz; P=*C*HCH$_3$), 120.69, 126.42, 129.11, 130.12, 131.07, 132.48, 137.54, 140.93, 141.20, 141.29, 141.38, 146.84, 146.94, 148.36 (s; Ar*C*).

^{31}P NMR (202 MHz, C_6D_6): δ (ppm) 252.2 (m; **18-*E***), 239.5 (m; **18-*Z***)

^{31}P{^{1}H} NMR (202 MHz, C_6D_6): δ (ppm) 252.2 (s; **18-*E***), 239.4 (s; **18-*Z***)

HRMS (*m*/*z*): [M+H]$^{+}$ calcd. for $C_{87}H_{113}NP$, 1202.8605; found 1202.8613.

5.7.3 Synthesis of 19

To a solid mixture of **12** (30.0 mg, 0.025 mmol; 1.00 eq.) and MeN=PPh$_3$ (11.1 mg, 0.038 mmol; 1.50 eq.), benzene (0.5 mL) was added. The mixture was stirred for 3 h at room temperature, and monitored by ^{31}P NMR spectroscopy. Once the reaction had reacted

completion, MeCN (20 mL) was added to the solution, and the mixture was left in at –35 °C overnight. The supernatant was removed and the resulting solid was dried *in vacuo* to afford **19** (26 mg, 0.022 mmol; 86% yield) as a white powder. Single crystals of **19** suitable for X-ray diffraction were obtained by slow evaporation of a concentrated hexane solution of **19** at room temperature.

^{1}H NMR (500 MHz, C_6D_6): δ (ppm) 1.25–1.29 (m, 36H; CH(C*H*$_3$)$_2$), 1.36–1.38 (m, 36H; CH(C*H*$_3$)$_2$), 2.96 (sept, $^{3}J_{H–H}$ = 6.8 Hz, 4H; C*H*(CH$_3$)$_2$), 3.06–3.13 (m, 8H; C*H*(CH$_3$)$_2$), 6.72 (t, $^{3}J_{H–H}$ = 7.4 Hz, 2H; Ar*H*), 6.85 (s, broad, 1H; Ar*H*), 7.01 (t, $^{3}J_{H–H}$ = 7.4 Hz, 1H; Ar*H*), 7.24 (d, $^{4}J_{H–H}$ = 2.4 Hz, 4H; Ar*H*), 7.27 (s, 4H; Ar*H*), 7.29 (s, 4H; Ar*H*), 7.39 (d, $^{3}J_{H–H}$ = 7.4 Hz, 2H; Ar*H*). P=NC*H*$_3$ and NC*H*$_2$C$_6$*H*$_5$ were not observed due to fast rotation about the N–P bond.

^{13}C{^{1}H} NMR (125 MHz, C_6D_6): δ (ppm) 24.27, 24.45, 24.47, 24.83, 25.04 (s; CH(*C*H$_3$)$_2$), 30.90, 30.95, 34.91 (s; *C*H(CH$_3$)$_2$), 120.72, 126.85, 129.19(br), 130.71(br), 131.25, 132.03(br), 137.35, 140.76, 141.44, 146.84, 146.95, 148.47 (s; Ar*C*). P=NC*H*$_3$ and NC*H*$_2$C$_6$*H*$_5$ were not observed due to fast rotation about the N–P bond.

^{31}P{^{1}H} NMR (202 MHz, C_6D_6): δ (ppm) 310.2 (br; ***trans*-19**), 186.7 (br; ***cis*-19**)

HRMS (*m*/*z*): [M+H]$^{+}$ calcd. for $C_{86}H_{112}N_2P$, 1203.8558; found 1203.8549.

5.7.4 Synthesis of 20

A THF solution CH_2=PMe_3 was prepared *in-situ* by adding THF (0.3 mL) to a solid mixture of KHMDS (1.7 mg, 0.0085 mmol; 1.01 eq.) and PMe_4Br (3.0 mg, 0.017 mmol; 2.00 eq.) and stirred for 3 h before being filtered. **12** (10.0 mg, 0.0084 mmol; 1.00 eq.) was dissolved in THF (0.3 mL) and cooled to –78 °C. At this temperature, the CH_2=PMe_3 solution was added dropwise to **12**, and the mixture was allowed to slowly warm to room temperature. The reaction mixture was stirred overnight. All volatiles were removed under vacuum, and

the solid residue was recrystallized from a THF-MeCN mixture to afford **20** (7.8 mg, 0.0061 mmol; 72% yield) as a white solid.

^{1}H NMR (500 MHz, C_6D_6): δ (ppm) 0.34 (pseudo-t, $J_{H–P}$ = 5.7 Hz, 1H; PC*H*P$(CH_3)_3$), 1.00 (d, $^{2}J_{H–P}$ = 13.1 Hz, 9H; PCHP(C*H*$_3)_3$), 1.17–1.34 (m, 72H; CH(C*H*$_3)_2$), 2.90 (sept, $^{3}J_{H–H}$ = 7.1 Hz, 4H; C*H*$(CH_3)_2$), 3.06–3.27 (m, 8H; C*H*$(CH_3)_2$), 4.57 (dd, $^{2}J_{H–H}$ = 14.3 Hz, $^{3}J_{H–P}$ = 9.3 Hz, 1H; NC*H*$_2C_6H_5$), 4.72 (dd, $^{2}J_{H–H}$ = 14.5 Hz, $^{3}J_{H–P}$ = 5.6 Hz, 1H; NC*H*$_2C_6H_5$), 6.66 (t, $^{3}J_{H–H}$ = 7.6 Hz, 2H; Ar*H*), 6.77 (t, $^{3}J_{H–H}$ = 7.4 Hz, 1H; Ar*H*), 6.98 (t, $^{3}J_{H–H}$ = 7.4 Hz, 1H; Ar*H*), 7.13 (t, $^{4}J_{H–H}$ = 1.6 Hz, 1H; Ar*H*), 7.18-7.25 (m, 12H, Ar*H*), 7.33 (dd, $^{3}J_{H–H}$ = 7.6 Hz, $^{4}J_{H–P}$ = 1.6 Hz, 1H; Ar*H*), 7.42 (dd, $^{3}J_{H–H}$ = 7.6 Hz, $^{4}J_{H–P}$ = 1.6 Hz, 1H; Ar*H*), 7.58 (dd, $^{1}J_{H–P}$ = 530.5 Hz, $^{3}J_{H–H}$ = 2.6 Hz, 1H; P*H*CHP$(CH_3)_3$)

^{13}C{^{1}H} NMR (125 MHz, C_6D_6): δ (ppm) 10.84 (dd, $^{1}J_{C–P}$ = 146.9 Hz, $^{1}J_{C–P}$ = 107.9 Hz; P*C*HP$(CH_3)_3$), 16.94 (dd, $^{1}J_{C–P}$ = 60.9 Hz, $^{3}J_{C–P}$ = 2.2 Hz; PCHP(*C*$H_3)_3$), 24.34, 24.48, 24.52, 24.54, 24.85, 25.06, 25.18 (s; CH(*C*$H_3)_2$), 30.78, 30.81, 30.84, 30.96, 34.88, 34.92, 34.98 (s; *C*H$(CH_3)_2$), 47.36 (d, $^{3}J_{C–P}$ = 5.2 Hz; N*C*$H_2C_6H_5$), 120.49, 120.59, 120.73, 120.84, 125.62, 129.49, 130.04, 130.31, 130..46, 130.80, 132.56, 133.24, 137.80, 138.14, 139.23 (d, $J_{C–P}$ = 2.3 Hz), 139.64 (d, $J_{C–P}$ = 3.0 Hz), 140.55, 140.76, 141.93 (d, $J_{C–P}$ = 3.1 Hz), 142.06, 142.36 (d, $J_{C–P}$ = 2.4 Hz), 142.65, 146.64, 147.00, 147.26, 147.32, 147.98, 148.18 (s; Ar*C*).

^{31}P NMR (202 MHz, C_6D_6): δ (ppm) 28.02 (dd, $^{1}J_{P–H}$ = 530.5 Hz, $^{2}J_{P–P}$ = 33.3 Hz; *P*HCHP$(CH_3)_3$), 6.80 (br; PHCH*P*$(CH_3)_3$)

^{31}P{^{1}H} NMR (202 MHz, C6D6): δ (ppm) 28.02 (d, $^{2}J_{P–P}$ = 33.3 Hz; *P*HCHP$(CH_3)_3$), 6.80 (d, $^{2}J_{P–P}$ = 33.3 Hz; PHCH*P*$(CH_3)_3$)

HRMS (*m*/*z*): $[M+H]^+$ calcd. For $C_{89}H_{120}NOP_2$, 1280.8845; found 1280.8854.

5.7.5 Synthesis of 21

20 (7.8 mg, 0.0061 mmol, 1.00 eq.) was dissolved in 1ml THF, and the solution was cooled to –78 °C. At this temperature, 0.05 ml (1.1 eq.) THF solution of H_2O (0.05 ml H_2O in 20.00 ml THF) was added dropwise to the mixture. The reaction was allowed to warm to room temperature over 30 min, after which all volatile was evaporated. The residual was recrystallized from a mixture of THF/MeCN to afford **21** (5.8 mg, 0.0044 mmol; 73% yield) as a white solid.

^{1}H NMR (500 MHz, C_6D_6): δ (ppm) 1.20–1.29 (m, 72H; CH(C*H*$_3$)$_2$), 1.40 (d, $^2J_{H–P}$ = 6.9 Hz, 12H; P(C*H*$_3$)$_4$), 2.87 (sept, $^3J_{H–H}$ = 6.9 Hz, 4H; C*H*(CH$_3$)$_2$), 3.13–3.23 (m, 8H; C*H*(CH$_3$)$_2$), 4.82 (d, $^3J_{H–P}$ = 6.7 Hz, 2H; NC*H*$_2$C$_6$H$_5$), 6.71 (t, $^3J_{H–H}$ = 7.0 Hz, 2H; Ar*H*), 6.77 (t, $^3J_{H–H}$ = 7.2 Hz, 1H; Ar*H*), 7.02 (d, $^1J_{H–P}$ = 581.2 Hz, 1H; P*H*), 7.04–7.07 (m, 3H; Ar*H*), 7.16–7.17 (m, 6H, overlapping with C6D6; Ar*H*), 7.21 (d, $^4J_{H–H}$ = 1.3 Hz, 4H; Ar*H*), 7.25 (d, $^3J_{H–H}$ = 7.2 Hz, 2H; Ar*H*), 7.39 (d, $^3J_{H–H}$ = 7.2 Hz, 4H; Ar*H*)

^{13}C{^{1}H} NMR (125 MHz, C_6D_6): δ (ppm) 9.37 (d, $^1J_{C–P}$ = 54.4 Hz; P(*C*H$_3$)$_4$), 24.41, 24.53, 24.57, 24.67, 25.08, 25.37 (s; CH(*C*H$_3$)$_2$), 30.81, 30.85, 34.86 (s; *C*H(CH$_3$)$_2$), 51.67 (br; N*C*H$_2$C$_6$H$_5$), 120.51, 120.64, 123.69, 126.85, 129.77, 130.20 (d, $J_{C–P}$ = 4.2 Hz), 132.09, 138.46, 140.18, 141.58, 141.83, 143.56, 143.84, 147.12, 147.49, 147.95 (s; Ar*C*).

^{31}P NMR (202 MHz, C_6D_6): δ (ppm) –0.9 (d, $^1J_{P–H}$ = 581.2 Hz; R$_2$N*P*(O)$_2$H), 23.4 (m; *P*(CH$_3$)$_4$)

^{31}P{^{1}H} NMR (202 MHz, C6D6): δ (ppm) –0.9 (s; R$_2$N*P*(O)$_2$H), 23.4 (s; *P*(CH$_3$)$_4$)

HRMS (*m*/*z*): [M]$^-$ calcd. for $C_{85}H_{109}NO_2P$, 1206.8201; found 1206.8220.

5.8 References

[1] G. Wittig, G. Geissler, *Justus Liebigs Ann. Chem.* **1953**, *580*, 44–57.

[2] G. Wittig, U. Schöllkopf, *Chem. Ber.* **1954**, *87*, 1318–1330.

[3] G. Wittig, *Science* **1980**, *210*, 600–604.

[4] Z. Wang, Wittig Reaction In *Comprehensive Organic Name Reactions and Reagents*, John Wiley & Sons, Inc., 2010; pp 3031–3042.

[5] H. Staudinger, J. Meyer, *Helv. Chim. Acta* **1919**, *2*, 635–646.

[6] H. Staudinger, W. Braunholtz, *Helv. Chim. Acta* **1921**, *4*, 897–900.

[7] S. Trippett, *Q. Rev. Chem. Soc.* **1963**, *17*, 406–440.

[8] H. Pommer, *Angew. Chem., Int. Ed. Engl.* **1977**, *16*, 423–429.

[9] M. M. Heravi, V. Zadsirjan, M. Daraie, M. Ghanbarian, *ChemistrySelect.* **2020**, *5*, 9654–9690.

[10] T. Takeda, *Modern carbonyl olefination: Methods and applications*, John Wiley & Sons, **2006**.

[11] P. J. Murphy, S. E. Lee, *J. Chem. Soc., Perkin Trans. 1* **1999**, 3049–3066.

[12] J. A. Murphy, A. G. J. Commeureuc, T. N. Snaddon, T. M. McGuire, T. A. Khan, K. Hisler, M. L. Dewis, R. Carling, *Org. Lett.* **2005**, *7*, 1427–1429.

[13] P. A. Byrne, D. G. Gilheany, *Chem. Soc. Rev.* **2013**, *42*, 6670–6696.

[14] H. Staudinger, E. Hauser, *Helv. Chim. Acta* **1921**, *4*, 861–886.

[15] F. Palacios, C. Alonso, D. Aparicio, G. Rubiales, J. M. de los Santos, *Tetrahedron* **2007**, *63*, 523–575.

[16] A. Marinetti, F. Mathey, *Angew. Chem., Int. Ed. Engl.* **1988**, *27*, 1382–1384.

[17] A. Marinetti, S. Bauer, L. Ricard, F. Mathey, *Organometallics* **1990**, *9*, 793–798.

[18] S. Shah, J. D. Protasiewicz, *Coord. Chem. Rev.* **2000**, *210*, 181–201.

[19] C. C. Cummins, R. R. Schrock, W. M. Davis, *Angew. Chem., Int. Ed. Engl.* **1993**, *32*, 756–759.

[20] T. L. Breen, D. W. Stephan, *J. Am. Chem. Soc.* **1995**, *117*, 11914–11921.

[21] B. F. Wicker, J. Scott, J. G. Andino, X. Gao, H. Park, M. Pink, D. J. Mindiola, *J. Am. Chem. Soc.* **2010**, *132*, 3691–3693.

[22] S. Shah, J. D. Protasiewicz, *Chem. Commun.* **1998**, 1585–1586.

[23] A. M. Borys, E. F. Rice, G. S. Nichol, M. J. Cowley, *J. Am. Chem. Soc.* **2021**, *143*, 14065–14070.

[24] D. Reiter, P. Frisch, T. Szilvási, S. Inoue, *J. Am. Chem. Soc.* **2019**, *141*, 16991–16996.

[25] C. Hu, N. H. Rees, M. Pink, J. M. Goicoechea, *Nat. Chem.* **2024**, *16*, 1855–1860.

[26] P. Pyykkö, M. Atsumi, *Chem. Eur. J.* **2009**, *15*, 186–197.

[27] C.-W. Tsang, C. A. Rohrick, T. S. Saini, B. O. Patrick, D. P. Gates, *Organometallics* **2004**, *23*, 5913–5923.

[28] R. Appel, C. Casser, M. Immenkeppel, F. Knoch, *Angew. Chem., Int. Ed. Engl.* **1984**, *23*, 895–896.

[29] P. Royla, K. Schwedtmann, Z. Han, J. Fidelius, D. P. Gates, R. M. Gomila, A. Frontera, J. J. Weigand, *J. Am. Chem. Soc.* **2023**, *145*, 10364–10375.

[30] R. Appel, U. Kündgen, F. Knoch, *Chem. Ber.* **1985**, *118*, 1352–1370.

[31] E. Niecke, D. Gudat, *Angew. Chem., Int. Ed. Engl.* **1991**, *30*, 217–237.

[32] E. Niecke, W. Flick, *Angew. Chem., Int. Ed. Engl.***1973**, *12*, 585–586.

[33] O. J. Scherer, N. Kuhn, *Angew. Chem., Int. Ed. Engl.* **1974**, *13*, 811–812

[34] K. Miqueu, J.-M. Sotiropoulos, G. Pfister-Guillouzo, V. L. Rudzevich, H. Gornitzka, V. Lavallo, V. D. Romanenko, *Eur. J. Inorg. Chem.* **2004**, *2004*, 2289–2300

[35] D. Barion, C. Gärtner-Winkhaus, M. Link, M. Nieger, E. Niecke, E. *Chem. Ber.* **1993**, *126*, 2187–2195.

[36] T. Böttcher, C. Jones, *Dalton Trans.* **2015**, *44*, 14842–14853.

[37] J. Vrána, V. Němec, M. A. Samsonova, A. Růžička, *Dalton Trans.* **2021**, *50*, 14352–14361.

Chapter 6
Isolation of a Phosphinidene Sulfide and Selenide

6.1 Introduction

Phosphinidenes (R–P) are often regarded as the phosphorus analogues of carbenes (R_2C), due to the diagonal relationship between phosphorus and carbon.[1–12] Their oxidized phosphorus(III) counterparts, phosphinidene chalcogenides (R–PCh; where E = group 16 element), have also been shown to exhibit carbene-like reactivity.[13,14] That being said, the reactivity of phosphinidene chalcogenides is poorly understood, in large part due to their instability under ambient conditions. Recently, our group reported the first example of an isolable phosphinidene oxide using an extremely bulky amido supporting ligand for kinetic stabilization of the highly reactive P(III)=O bond (Figure 6.1b).[15] Despite this advancement, the structural characterization of the heavier chalcogen derivatives, namely phosphinidene sulfides, selenides, and tellurides has yet to be achieved. This is largely attributed to the high polarity of the phosphorus–chalcogen bond, and its weak π-bonding character, which typically leads to deleterious dimerization or oligomerization reactions. Given the inherent difficulties in isolating heavier phosphinidene chalcogenides, they have thus far only been observed at extremely low temperatures (3–15 K) in inert gas matrices.[16] As an alternative approach, the trapping of *in-situ* generated phosphinidene chalcogenides has been extensively investigated (Figure 6.1a).[13, 17–26] However, isolable phosphinidene sulfides and selenides have yet to be achieved.

The successful isolation of a phosphinidene oxide stabilized by an extremely bulky amido ligand **12** motivated us to explore the feasibility of employing the same ligand to support heavier phosphinidene chalcogenides. The phospha-Wittig reaction described in Chapter 5 between **12** and phosphorus ylide reagents has demonstrated the potential of this compound as an electrophilic phosphinidene precursor for accessing various phosphorus–main group element double bonds. Herein, we further expand this strategy and report the transformation

from phosphinidene oxide **12** to its sulfide and selenide analogues using Lawesson's and Woollin's reagents, respectively.

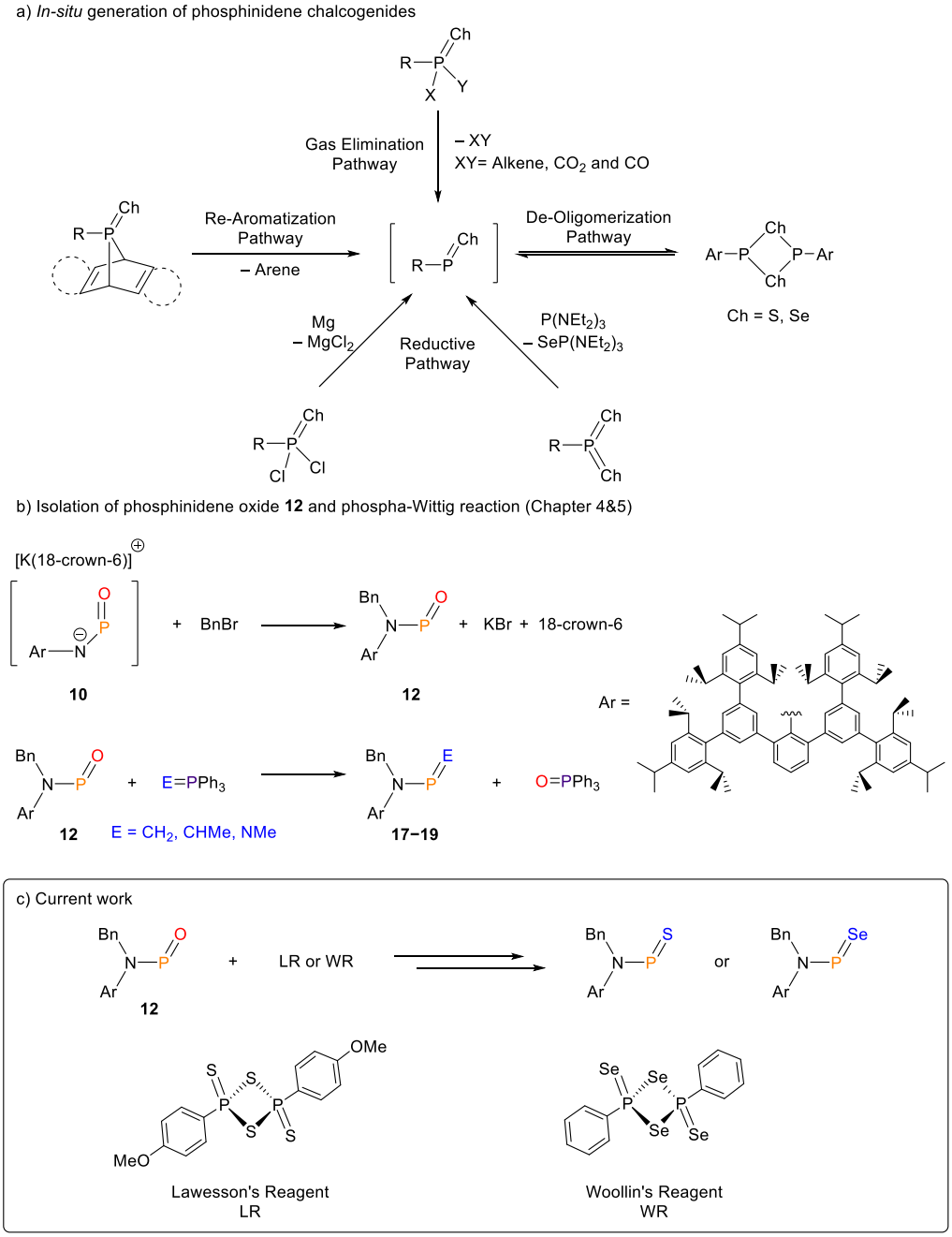

Figure 6.1. a) *In-situ* generated phosphinidene sulfides; b) previously reported isolation of a phosphinidene oxide **12** and its phospha-Wittig reactivity; c) current work: isolation of a phosphinidene sulfide and selenide.

6.2 A phosphinidene sulfide

Inspired by the phospha-Wittig reaction (detailed in Chapter 5), we initiated our studies by reacting triphenylphosphine sulfide ($S{=}PPh_3$) and trimethylphosphine sulfide ($S{=}PMe_3$) with phosphinidene oxide **12** (Scheme 6.1). We reasoned that given $S{=}PR_3$ shares a similar electronic structure with phosphorus ylides, these reagents should allow chalcogen atom transfer to the phosphorus atom in **12**. To our surprise, unlike phosphorus ylides, which react with **12** instantly, no reaction was observed between $S{=}PPh_3$ or $S{=}PMe_3$ and **12**, even at elevated temperatures. This suggests that phosphine sulfides lack the requisite nucleophilicity to undergo reactions with phosphinidene oxides. Similarly, no Wittig-type reactions between phosphine sulfides and carbonyl compounds have been reported to date, further supporting the inert nature of phosphine sulfides in such transformations.

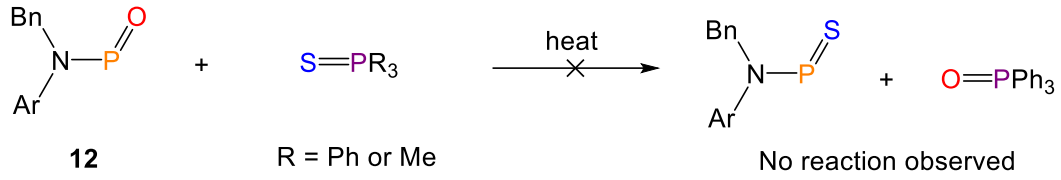

Scheme 6.1. Attempted synthesis of a phosphinidene sulfide using phosphine sulfide.

Given the structural and electronic similarity between phosphinidene oxide **12** and carbonyl compounds as described in Chapter 4, we trialled other strategies which have been shown to be effective in the chalcogenation of carbonyl compounds. Lawesson's reagent (LR) is well established as a versatile thionation reagent. The proposed mechanism which gives rise to its effective reactivity, involves the dissociation of the dimeric structure and the *in-situ* generation of a dithioxophosphorane.[27] We envisioned that the use of Lawesson's reagent could facilitate the conversion of our phosphinidene oxide, **12**, to its sulfide analogue, mirroring the thionation reactivity observed towards carbonyl compounds.

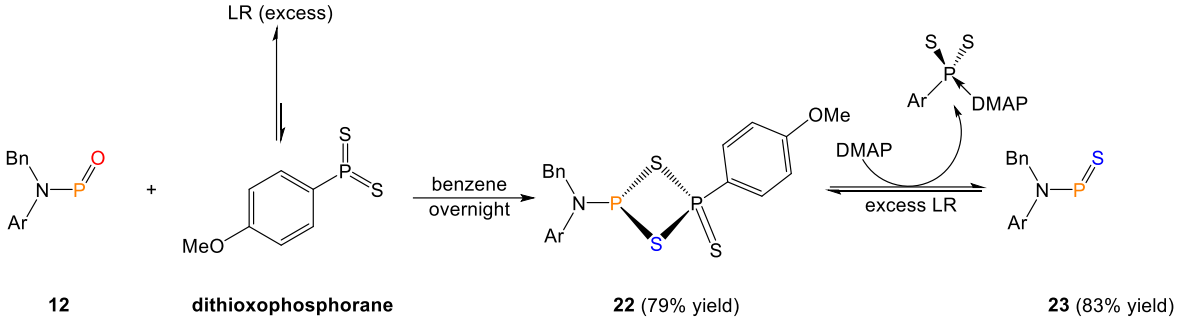

Scheme 6.2. Synthesis of compounds **22** and **23**.

The reaction of 0.5 equivalents of LR with 1 equivalent of compound **12** (Scheme 6.2) gave rise to multiple products, as observed via *in-situ* $^{31}P\{^{1}H\}$ NMR spectroscopy. Addition of excess LR drove conversion to a major product which features a set of doublets at 42.5 and 47.8 ppm with a $^{3}J_{P-P}$ coupling constant of 93.2 Hz. The proton-coupled NMR spectrum revealed that the resonance at 42.5 ppm splits into a doublet of triplets, with a $^{3}J_{P-H}$ coupling constant of 15.2 Hz, indicating that it originates from the LR fragment. Collectively, we propose that product **22** is a dimeric phosphinidene sulfide, incorporating a dithioxophosphorane unit derived from LR dissociation. Similar dimeric structures have been reported previously for germanium and tin, formed via the reaction of germylenes, stannylenes or stannylene sulfides with LR.[28]

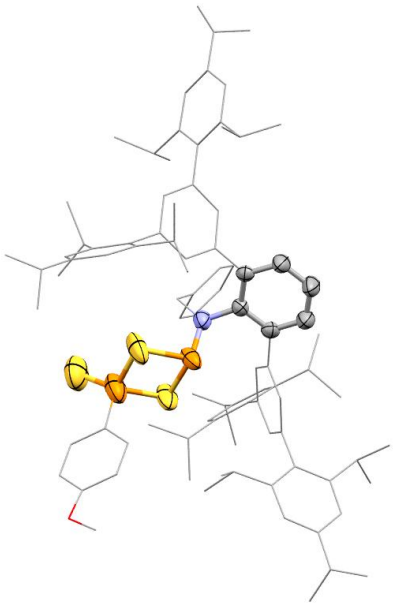

Figure 6.2. Single-crystal X-ray structure of **22**. Selected carbon atoms for backbones are depicted with wireframe mode. Thermal ellipsoids pictured at 50% probability level. Solvent of crystallization, positional disorder and hydrogen atoms are removed for clarity.

The structure of compound **22** was confirmed by single crystal X-ray diffraction. As expected, it revealed a P_2S_2 four membered ring core with one phosphours(III) center and one phosphorus(V) center. However, due to heavy positional disorder within the asymmetric unit and poor crystal quality, a more nuanced analysis of bond metric data for **22** is not viable.

During the purification of compound **22**, a minor product caught our attention. Upon removal of the excess LR from the reaction mixture through washing with MeCN, a set of new resonances appeared at 477.0 and 472.1 ppm in the $^{31}P\{^{1}H\}$ NMR spectrum in a 4.28:1 ratio. These two peaks exhibit a pattern analogous to that of phosphinidene oxide **12**, which also displays two $^{31}P\{^{1}H\}$ NMR signals arising from the *cis-trans* isomer pair. Based on this spectral similarity, we assigned these peaks to phosphinidene sulfide **23**. A dynamic equilibrium exists between compounds **22**, **23** and LR, with the equilibrium favouring the formation of compound **22**. Notably, while the removal of excess LR shifts the equilibrium toward compound **23**, washing with MeCN alone was insufficient to eliminate all residual LR. We hypothesized that introducing an additional reaction capable of consuming the LR

while leaving compound **23** intact would provide an external thermodynamic driving force towards the generation of compound **23**. LR and its analogues are known to react with Lewis bases, forming four-coordinate monomeric adducts.[29,30] For this purpose, 4-dimethylaminopyridine (DMAP) was selected as an external Lewis base to neutralize LR. Satisfactorily, upon the addition of excess DMAP to compound **22**, *in situ* $^{31}P\{^{1}H\}$ NMR spectroscopy revealed the complete consumption of compound **22**, an increased signal intensity for compound **23**, together with a new singlet at 109.4 ppm. Independent reaction of LR with DMAP in THF confirmed that the new $^{31}P\{^{1}H\}$ signal corresponds to the monomeric LR-DMAP adduct. These findings provide strong support for the success of our synthetic strategy. Subsequently, a one-pot synthesis of compound **23** was performed by sequential addition of LR and DMAP to compound **12**, affording compound **23** in excellent yields (83 %) on a 50 mg scale (Scheme 6.2). Addition of excess LR to **23** leads to the reformation of **22** again, further confirming the equilibrium nature of this transformation.

The solid-state molecular structure of compound **23** was determined by single crystal X-ray diffraction. The crystal structure reveals a *trans*-arrangement of the $R_2N{-}P{=}S$ moiety, consistent with the solid-state structure of **12**. The P=S bond length is 1.9167(15) Å, which is slightly shorter than the computed standard P=S double bond length (1.96 Å)[31] and the P(V)=S double bond in $S{=}PPh_3$ (1.9554 Å).[32] It is worth noting at this stage that the short phosphorous(V)=S multiple bond in $S{=}PPh_3$ arises from hyperconjugation of the sulfur atom lone pairs into a doubly degenerate set of P−C σ* antibonding orbitals. In contrast, in compound **23**, the P=S bond shortening is attributed to a strong π-interaction between phosphorus and sulfur, reinforcing the P=S double bond character. Notably, the nitrogen atom still retains its planar geometry (Σ°: 360.0°), consistent with **12** and previously reported amido phosphaalkenes and phosphaimines.[33-35] The N−P bond length (1.672(3) Å) falls between that of single and double bond, closely resembling previously reported N−P bond length in amido phosphoaalkenes **17**, **18-*E*** and phosphaimines ***trans*-19**. These structural

features indicate that the nitrogen atom lone pair is delocalized into P−S π* orbital, which aligns with the restricted N−P bond rotation observed in NMR studies.

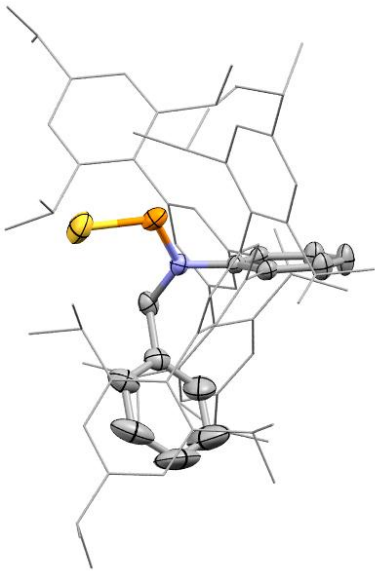

Figure 6.3. Single-crystal X-ray structure of **23**. Selected carbon atoms for backbones are depicted with wireframe mode. Thermal ellipsoids pictured at 50% probability level. Solvent of crystallization, positional disorder and hydrogen atoms are removed for clarity.

To gain deeper insight into the electronic structure of **23**, density functional theory (DFT) calculations were performed at the M06-2X/Def2-SVP level of theory. The optimized geometry is in good agreement with that obtained by X-ray crystallography (e.g. P–S: 1.941 Å; N–P: 1.689 Å; N Σ°: 359.7°). While the LUMO orbital reveals a highly localized P−S π* orbital, the P−S π orbital is diffuse and low in energy, observed as the HOMO−12 (Figure 6.4a). Additionally, one of the lone pairs on sulfur is distinctly characterized in the HOMO−1. Natural bond orbital (NBO) analysis further confirmed the presence of a well-defined σ-bond and π-bond within the P=S moiety (Figure 6.5). The π-interaction is predominantly composed of p-orbital overlap between phosphorus (97.0% p-character) and sulfur (98.1% p-character), with a significant polarization toward sulfur (70.5%). Second-order perturbation theory analysis revealed a back-donation energy of 36.0 kcal mol^{-1} from the nitrogen atom lone pair to the P−S π* orbital, which is comparable to that of **12** (41.1 kcal

mol^{-1}). The back-donation was also evidenced by the low occupancy of nitrogen lone pair (1.70 e^{-}) and the partially filled P−S π* orbital (0.23 e^{-}). Mayer bond indices corroborates these findings, indicating a bond order of 1.09 for N−P and 1.81 for P=S. Since the electronic structure of **23** closely resembles that of **12**, a similar energy barrier for N−P bond rotation should also be expected. Energy calculations at SMD-M062X/def2-TZVP//M062X/def2-SVP level revealed a rotation barrier of 20.7 kcal mol^{-1}, closely matching that of **12** (21.8 kcal mol^{-1}). The *trans*-isomer of **23** is thermodynamically favoured by 0.6 kcal mol^{-1}, agreeing with the crystallographic observed *trans*-geometry for N−P bond (Figure 6.4b).

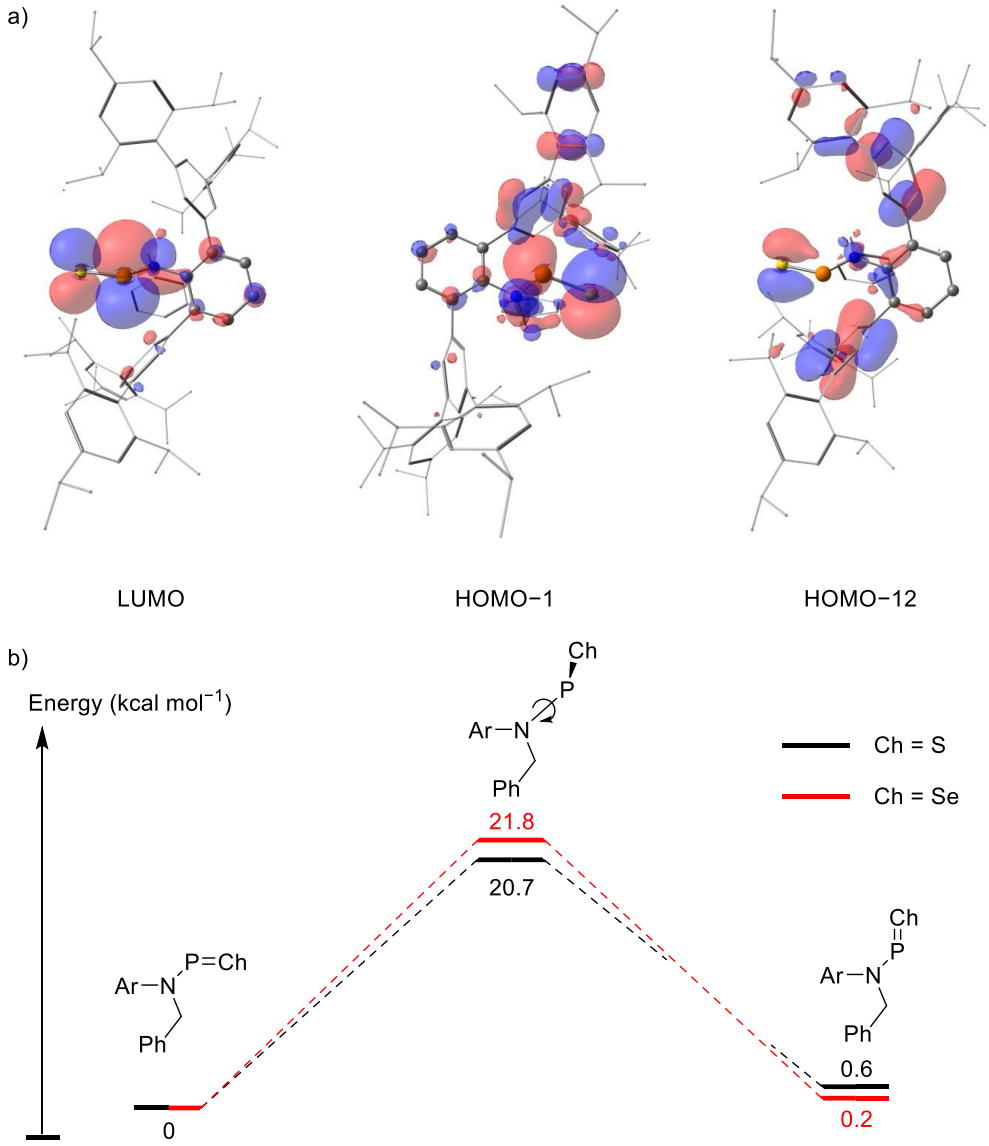

Figure 6.4. a) Selected molecular orbital diagram for compound **23**; b) Calculated N−P bond rotation energy profiles for **23** and **25**.

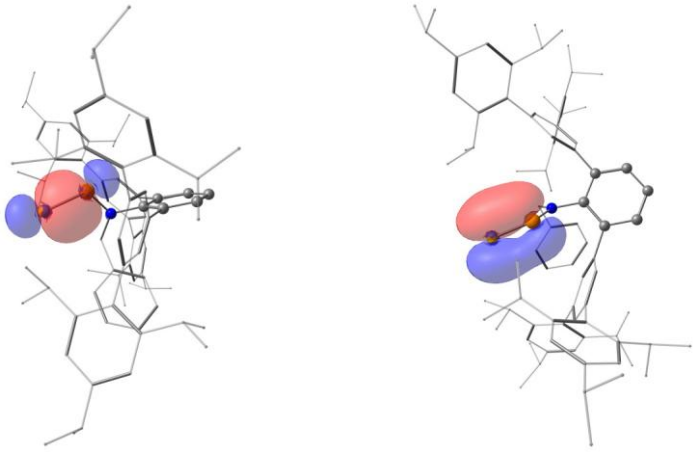

Figure 6.5. σ- (left) and π-NBO (right) orbitals of **23**.

The thermodynamic of the equilibrium between **22**, **23** and LR was further investigated using DFT calculation (Scheme 6.3). Reaction of compound **23** with 0.5 equivalents of LR to generate compound **22** (Reaction 1) was found to be spontaneous and thermodynamically favored by 2.9 kcal mol^{-1}, which aligns well with experimental observations, as compound **22** is the predominant species in the equilibrium. DMAP induced LR cleavage (Reaction 2) is determined to be an exothermic reaction (−6.5 kcal mol^{-1}). By coupling Reaction 1 and Reaction 2, the overall transformation (Reaction 3) favours the formation of compound **23**, with an overall free energy change of −3.6 kcal mol^{-1}. These computational results are in strong agreement with experimental observations, where the addition of DMAP effectively shifts the equilibrium between compounds **22**, **23** and LR, favouring the formation of compound **23**.

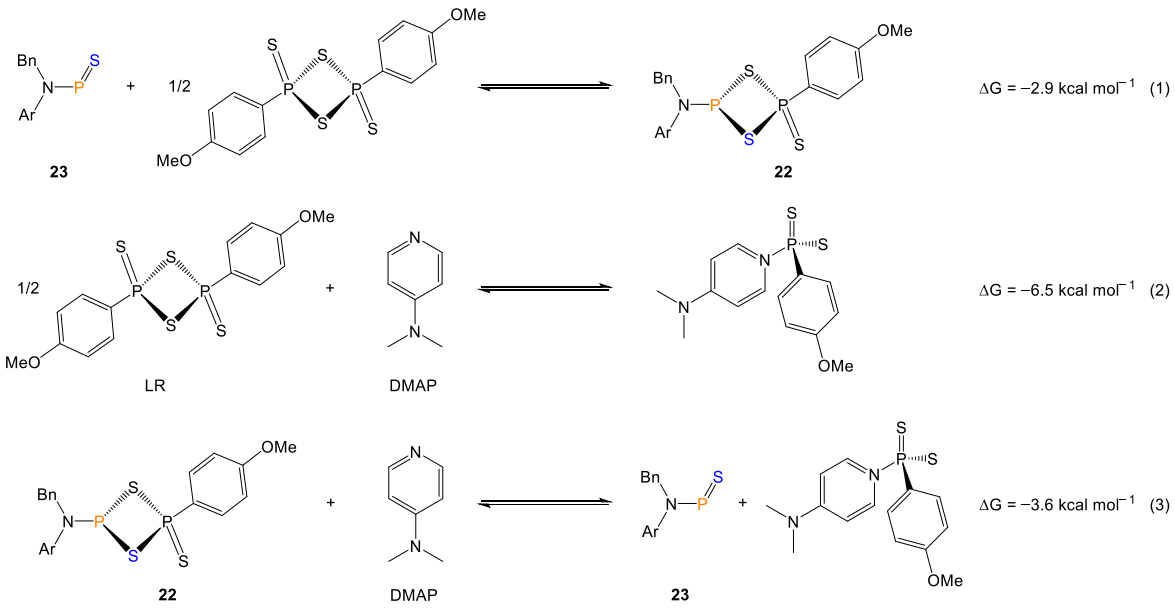

Scheme 6.3. DFT calculated energy profile for the equilibrium between **22**, **23** and LR.

6.3 A phosphinidene selenide

The successful thionation of phosphinidene oxide **12** prompted us to explore the use of Woollin's reagent (WR) to access phosphinidene selenide. Woollin's reagent is the selenium analogue of Lawesson's reagent and is widely used in organic synthesis for the selenation of carbonyl compounds.[36] Building on insights gained from the reaction between compound **12** and LR, we treated **12** with excess WR in benzene (Scheme 6.4). After stirring overnight, a bright-yellow solution was obtained, and *in-situ* ^{31}P NMR spectroscopy revealed a doublet at 46.0 ppm with a $^{3}J_{P–P}$ coupling constant of 80.6 Hz, and a doublet of triplets at −46.0 ppm with coupling constants $^{3}J_{P–P}$ = 80.6 Hz and $^{3}J_{P–H}$ = 17.0 Hz. The similarity of this ^{31}P NMR spectrum to that of compound **22** suggests the formation of the dimeric structure **24**. Since Woollin's reagent can also be cleaved using a Lewis base,[37] we envisioned that addition of DMAP can promote the formation of phosphinidene selenide **25**, following a mechanism analogous to the generation of compound **23**. Indeed, upon the addition of excess DMAP to the reaction mixture (Scheme 6.4), the solution rapidly changed colour to light red. *In-situ* ^{31}P{^{1}H} NMR spectroscopy revealed two singlets at 535.4 and 528.6 ppm in a 4.81:1 ratio,

closely resembling the $^{31}P\{^{1}H\}$ NMR spectrum of compounds **12** and **23**. Extended $^{31}P\{^{1}H\}$ scans further revealed the presence of selenium satellites, with a $^{31}P–^{77}Se$ coupling constant of 788.1 Hz, confirming the formation of phosphinidene selenide **25**. While no signals were observed in the ^{77}Se NMR spectrum at room temperature, a broad doublet appeared at 1081.6 ppm when the ^{77}Se NMR spectrum was recorded at –45 °C. These observations are tentatively attributed to the chemical exchange process between the *cis-trans* isomers at room temperature, leading to broad and weak signals. Upon cooling, the chemical exchange process is effectively frozen, resulting in enhanced spectral resolution and signal intensity in the ^{77}Se NMR spectrum. Upon re-addition of excess Woollin's reagent, **25** can cleanly convert back to **24**.

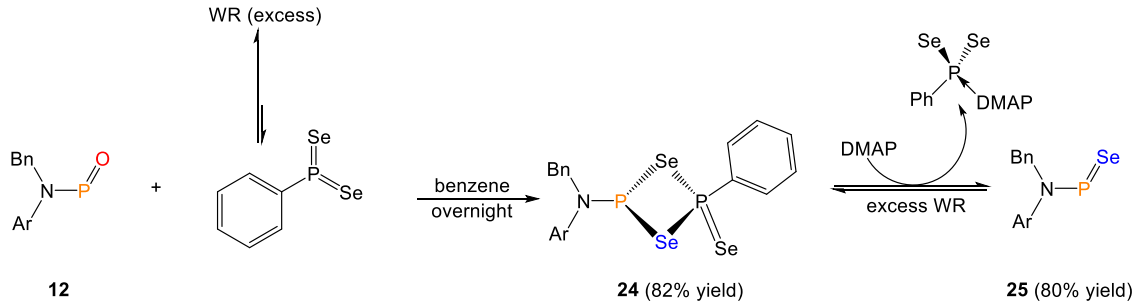

Scheme 6.4. Synthesis of compound **24** and **25**.

The structures of **24** and **25** were authenticated via single crystal X-ray diffraction. The crystal structures for both **24** and **25** are comparable to those of **22** and **23**, demonstrating structural consistency across the series. Similar to its sulfur analogue, phosphinidene selenide **25** adopts a *trans*-geometry in solid state. The P=Se bond length in **25** was determined to be 2.066(2) Å, which is shorter than the phosphorus(V)=Se bond (2.106(1) Å) in $Se=PPh_3$, [38] likely due to presence of P–Se π interaction. The planar geometry of the nitrogen atom (Σ°: 360.0°) and short N–P bond length (1.669(4) Å) are consistent those observed for **12** and **23**, indicating the back-donation from the nitrogen lone pair to P–Se σ* antibonding orbital.

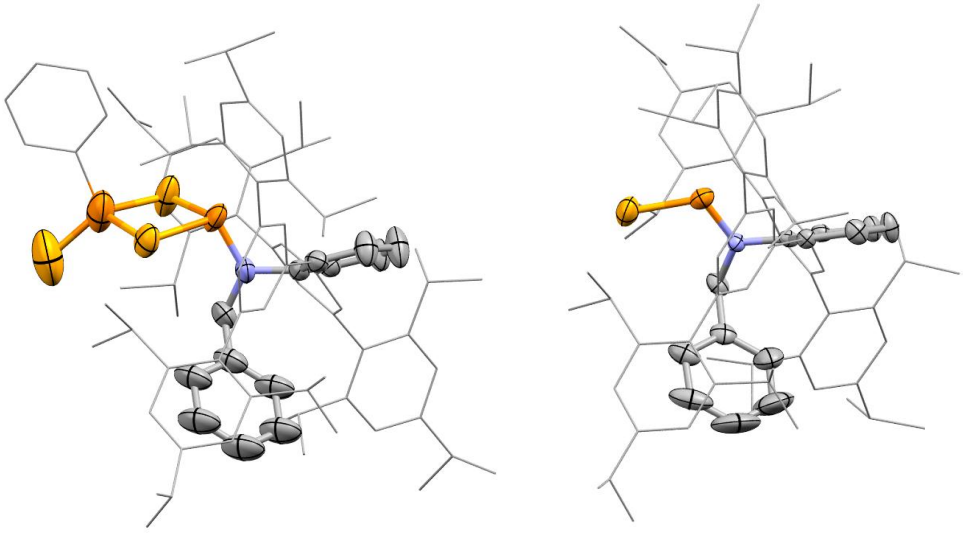

Figure 6.6. Single-crystal X-ray structures of **24** (left) and **25** (right). Selected carbon atoms for backbones are depicted with wireframe mode. Thermal ellipsoids pictured at 50% probability level. Solvent of crystallization, positional disorder and hydrogen atoms are removed for clarity.

DFT calculations were conducted to elucidate the electronic structure of **25**. While the LUMO of **25** is predominantly composed from the P–Se π* orbital, the HOMO represents the lone pair of the selenium atom (Figure 6.7). The P–Se π bond is highly delocalized and is observed in HOMO–3 and HOMO–12. Natural bond orbital (NBO) analysis confirmed the presence of both σ- and π-bonding orbital between phosphorus and selenium (Figure 6.8). Due to the similar electronegativity of selenium (2.55) and sulfur (2.58), the p-type π orbital remains polarized, with selenium contributing 64.7% and phosphours contributing 35.3%, which is comparable to the values determined for **23**. Second-Order Perturbation Theory analysis revealed a back-donation energy of 19.0 kcal mol^{-1} for nitrogen lone pair donating to the P–Se π* bond and 12.5 kcal mol^{-1} to σ* bond, in agreement with the crystal structure of **25**. Notably, while the back-donation to π* bond is weaker than calculated for **23** (36.1 kcal mol^{-1}), the σ* back-donation is much stronger in **25** (12.5 kcal mol^{-1} versus 3.5 kcal mol^{-1} in **23**). We attribute this difference to the lower electronegativity and larger atomic orbital size of Se. The P–Se π-bond in **25** is less polar, which disfavours the π* back-donation, whereas the orbital mismatch between P and Se weakens σ-bond, thereby enhancing the σ*

back-donation. Energy calculations determined a *cis-trans* isomerization barrier of 21.8 kcal mol^{-1}, with the *trans*-isomer being energetically favoured by 0.2 kcal mol^{-1}, consistent with the crystallographic structure of **25**. While the back-donation in **25** is weaker than that in **23**, it may seem counterintuitive that the rotation barrier is higher in **25** (21.8 kcal mol^{-1} versus 20.7 kcal mol^{-1} in **23**). This can be rationalized by the longer P–Se bond length in **25** (2.066(2) Å) compared to the P–S bond in **23** (1.917(2) Å), which introduces additional steric hindrance in the transition state. This energy barrier also matches the observed $^{31}P\{^{1}H\}$ NMR spectrum of **25**, which is similar to those observed for **12** and **23**. Mayer bond indices revealed a bond order of 1.11 for the N–P bond and 1.75 for the P=Se bond, reinforcing the proposed bonding model.

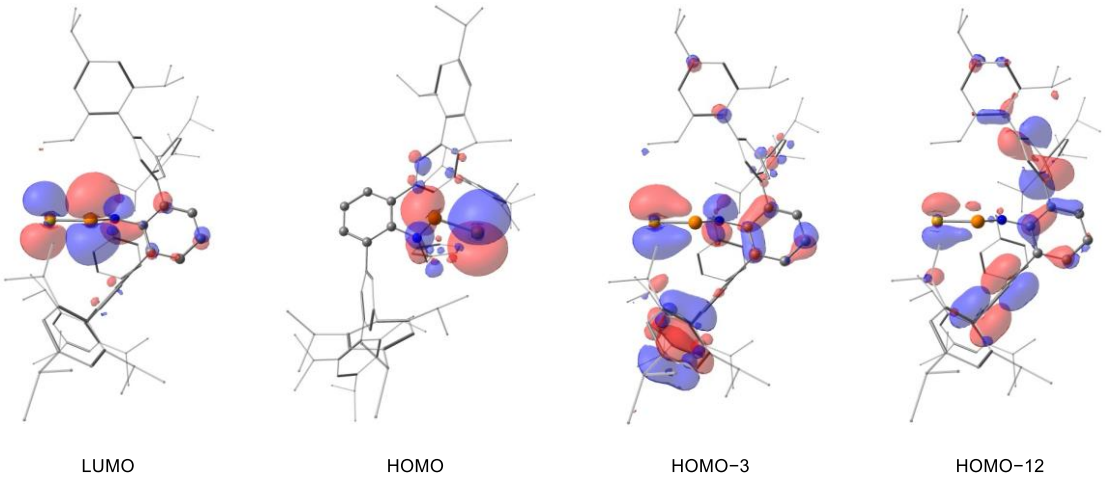

Figure 6.7. Selected molecular orbital diagram for compound **25**.

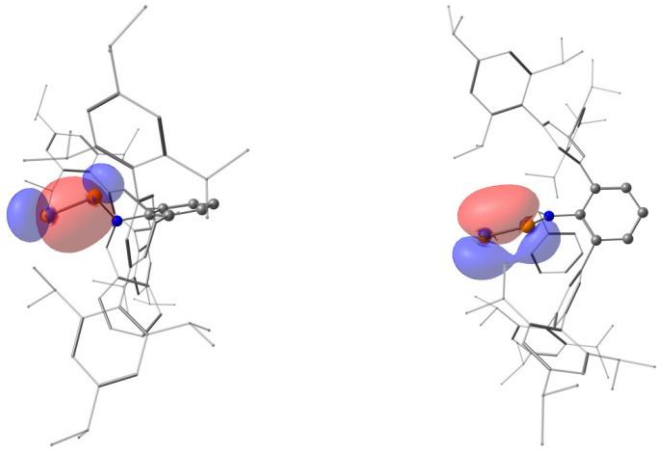

Figure 6.8. σ- (left) and π-NBO (right) orbitals of **25**.

6.4 Conclusions

Following the first successful isolation of free phosphinidene oxide **12** discussed in Chapter 4, we herein report the isolation of its heavier analogues, phosphinidene sulfide, **23**, and phosphinidene selenide, **25**, further expanding the chemistry of phosphorus(III)–chalcogen double bonds. Lawesson's reagent (LR) and Woollin's reagent (WR) are widely employed in organic synthesis for the transformation of carbonyl compounds into corresponding thio- and seleno-carbonyl derivatives. Given the similarity between carbonyl compounds and phosphinidene oxide **12**, we have shown that these reagents are also effective in converting phosphinidene oxide **12** to the corresponding sulfide and selenide. Upon reaction of phosphinidene oxide **12** with excess LR or WR, the *in-situ* generated phosphinidene chalcogenide overreacted with LR or WR, forming dimeric structure **22** and **24**, which features a P–Ch–P–Ch four membered ring motif. The addition of excess DMAP to **22** or **24** introduces an external thermodynamic driving force, facilitating the generation of monomeric phosphinidene sulfide **23** and selenide **25**. Crystal structures of both **23** and **25** revealed a *trans*-geometry within the R_2N–P=Ch moiety and back-donation from the nitrogen atom lone pair to P–Ch π^* orbital, which is also observed in **12**. DFT calculations further support the presence of significant back-donation, and an energetically significant rotation barrier was determined for **23** (20.7 kcal mol^{-1}) and **25** (21.8 kcal mol^{-1}), which is comparable to that observed in **12**.

6.5 Experimental Section

6.5.1 Synthesis of 22 from 12

To a solid mixture of **12** (30 mg, 0.025 mmol, 1.00 eq.) and Lawesson's reagent (20 mg, 0.049 mmol, 2 eq.), benzene (0.5 mL) was added. The mixture was stirred overnight at room temperature, and monitored with $^{31}P\{^{1}H\}$ NMR spectrum. Once compound **12** is fully consumed, the mixture is filtered, and MeCN (20 ml) was added to the filtrate. The mixture was left in a –35 °C freezer overnight to crystalize. Supernatant was removed and the resulting solid was dried *in vacuo* to afford **22** (28 mg, 0.020 mmol; 79% yield) as a colorless powder. Single crystals of **22** suitable for X-ray diffraction were obtained by slow evaporation of a concentrated hexane solution of **22** under room temperature.

^{1}H NMR (500 MHz, C_6D_6): (accurate integration is not possible due to extensive overlapping with residual compound **23** and LR) δ (ppm) 1.12 (d, $^{3}J_{H–H}$ = 6.8 Hz, 12H; CH(C*H*$_3$)$_2$), 1.15 (d, $^{3}J_{H–H}$ = 6.8 Hz, 18H; CH(C*H*$_3$)$_2$), 1.24–1.29 (m, 42H; CH(C*H*$_3$)$_2$), 2.85 (sept, $^{3}J_{H–H}$ = 6.8 Hz, 4H; C*H*(CH$_3$)$_2$), 3.04–3.10 (m, 8H; C*H*(CH$_3$)$_2$), 3.12 (s, 3H; OC*H*$_3$), 5.44 (s, 2H; NC*H*$_2$Ph), 6.59–6.62 (m, 2H; Ar*H*), 6.68–6.75 (m, 3H; Ar*H*), 7.00 (t, $^{3}J_{H–H}$ = 7.8 Hz, 1H; Ar*H*), 7.16 (s, overlapping with C_6D_6, 8H, Ar*H*), 7.17 (d, $^{4}J_{H–H}$ = 1.7 Hz, 2H; Ar*H*), 7.19 (d, $^{4}J_{P–H}$ = 1.7 Hz, 2H; Ar*H*), 7.22 (d, $^{4}J_{H–H}$ = 1.7 Hz, 2H; Ar*H*), 7.30 (d, $^{3}J_{H–H}$ = 7.8 Hz, 2H; Ar*H*), 7.56 (d, $^{3}J_{H–H}$ = 8.6 Hz, 2H; Ar*H*), 8.26 (dd, $^{3}J_{H–P}$ = 15.2 Hz $^{3}J_{H–H}$ = 8.6 Hz, 2H; Ar*H*).

^{13}C{^{1}H} NMR (125 MHz, C_6D_6): δ (ppm) 24.40, 24.43, 24.68, 25.04, 25.23, (s; CH(*C*H$_3$)$_2$) 30.71, 30.99, 31.11, 34.84, 34.93 (s; *C*H(CH$_3$)$_2$), 52.80 (br; N*C*H$_2$Ph) 54.88 (s; O*C*H$_3$), 113.81 (d, $^{1}J_{P–C}$ = 16.7 Hz), 120.89, 128.59, 129.63, 131.53, 131.72, 132.39, 133.49, 133.54, 133.61, 135.20 (d, $^{1}J_{P–C}$ = 17.1 Hz), 136.39, 137.07, 137.38, 140.28, 141.39, 141.90, 142.39 (d, $^{2}J_{P–C}$ = 6.6 Hz), 147.00, 148.53, 163.07 (s; Ar*C*).

^{31}P NMR (162 MHz, C_6D_6): δ (ppm) 42.5 (dt, $^3J_{P–P}$ = 93.2 Hz $^3J_{P–H}$ = 15.2 Hz; PS*P*(S)Ar), 47.8 (d, $^3J_{P–P}$ = 93.2 Hz; *P*SP(S)Ar).

^{31}P{^{1}H} NMR (162 MHz, C_6D_6): δ (ppm) 42.5 (d, $^3J_{P–P}$ = 93.2 Hz; PS*P*(S)Ar), 47.8 (d, $^3J_{P–P}$ = 93.2 Hz; *P*SP(S)Ar).

HRMS (*m*/*z*): $[M+H]^+$ calcd. For $C_{92}H_{116}NOP_2S_3$, 1408.7689; found 1408.7670.

6.5.2 One-pot synthesis of 23

To a solid mixture of **12** (50 mg, 0.042 mmol, 1.00 eq.) and Lawesson's reagent (40 mg, 0.099 mmol, 2.3 eq.), benzene (0.7 mL) was added. The mixture was stirred overnight at room temperature, and monitored with ^{31}P{^{1}H} NMR spectrum. Once compound **12** is fully consumed, the mixture is filtered, DMAP (20 mg, 0.164 mmol, 3.9 eq.) was added to the filtrate. After stirring the mixture for 30 min at room temperature, formation of precipitate was observed. The mixture is filtered again, and MeCN (20 ml) was added to the filtrate. The mixture was left in a –35 °C freezer overnight to crystalize. Supernatant was removed and the resulting solid was dried *in vacuo* to afford **23** (42 mg, 0.035 mmol; 83% yield) as a light-green powder. Single crystals of **23** suitable for X-ray diffraction were obtained by slow evaporation of a concentrated hexane solution of **23** under room temperature.

^{1}H NMR (500 MHz, C_6D_6): (accurate integration is not possible due to extensive overlapping with **23**-*cis*) δ (ppm) 1.16 (d, $^3J_{H–H}$ = 6.8 Hz, 12H; CH(C*H*$_3$)$_2$), 1.20–1.22 (m, 24H; CH(C*H*$_3$)$_2$), 1.28–1.32 (m, 36H; CH(C*H*$_3$)$_2$), 2.87 (sept, $^3J_{H–H}$ = 6.8 Hz, 4H; C*H*(CH$_3$)$_2$), 2.93–3.06 (m, 8H; C*H*(CH$_3$)$_2$), 5.46 (s, 2H; NC*H*$_2$Ph), 6.61 (t, $^3J_{H–H}$ = 7.6 Hz, 2H; Ar*H*), 6.74 (t, $^3J_{H–H}$ = 7.6 Hz, 2H; Ar*H*), 6.79–6.83 (m, 1H; Ar*H*), 6.95 (t, $^3J_{H–H}$ = 7.8 Hz, 1H; Ar*H*), 7.10 (t, $^4J_{H–H}$ = 1.6 Hz, 2H; Ar*H*), 7.16–7.17 (m, overlapping with C_6D_6, 8H; Ar*H*), 7.19 (t, $^4J_{H–H}$ = 1.6 Hz, 2H; Ar*H*), 7.21 (t, $^4J_{H–H}$ = 1.6 Hz, 2H; Ar*H*), 7.31 (t, $^3J_{H–H}$ = 7.8 Hz, 2H; Ar*H*).

$^{13}C\{^1H\}$ NMR (125 MHz, C_6D_6): δ (ppm) 24.17, 24.37, 24.41, 24.45, 24.70, 24.81, 25.02, 25.09 (s; $CH(CH_3)_2$), 30.86, 30.89, 30.99, 31.00, 31.11, 34.88 (s; $CH(CH_3)_2$), 51.02 (br; NCH_2Ph), 120.72, 120.78, 128.59, 129.37, 130.53, 131.19, 131.37, 131.81, 131.91, 132.10, 135.78, 137.06, 137.24, 139.86, 140.61 (d, J_{P-C} = 5.2 Hz), 140.94, 141.57, 146.78, 146.90, 148.60 (s; Ar*C*).

$^{31}P\{^1H\}$ NMR (202 MHz, C_6D_6): δ (ppm) 477.0 (s; **23**-*trans*), 472.1 (s; **23**-*cis*) **23**-*trans*:**23**-*cis* = 4.28:1.

HRMS (*m*/*z*): $[M+H]^+$ calcd. For $C_{85}H_{109}NPS$, 1206.8013; found 1206.8017.

6.5.3 Synthesis of 22 from 23

To a solid mixture of **23** (10 mg, 0.0083 mmol, 1.00 eq.) and Lawesson's reagent (10 mg, 0.025 mmol, 3 eq.), benzene (0.5 mL) was added. The mixture was stirred overnight at room temperature, and monitored with $^{31}P\{^1H\}$ NMR spectrum. Once compound **23** is fully consumed, the mixture is filtered, and MeCN (20 ml) was added to the filtrate. The mixture was left in a –35 °C freezer overnight to crystalize. Supernatant was removed and the resulting solid was dried *in vacuo* to afford **22** (9 mg, 0.0064 mmol; 77% yield) as a colorless powder. All characteristic data is identical to previously reported data.

6.5.4 Independent synthesis of $ArPS_2$(DMAP)

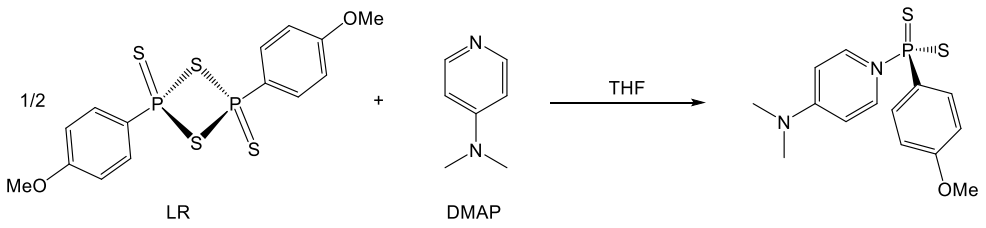

Scheme 6.5. Synthesis of $ArPS_2$(DMAP).

To a solid mixture of Lawesson's reagent (20 mg, 0.049 mmol, 1.00 eq.) and DMAP (12 mg, 0.098 mmol, 2 eq.), THF (1 mL) was added (Scheme 6.5). The mixture was stirred overnight at room temperature, after which all volatiles were removed *in vacuo*. The residual was washed with benzene for three times (0.5 ml × 3) and then n-hexane for three times (0.5 ml × 3) before dried under vacuum to afford $ArPS_2$(DMAP) (24 mg, 0.074 mmol; 75% yield) as a colorless powder.

^{1}H NMR (500 MHz, $CDCl_3$): δ (ppm) 3.19 (s, 6H; N(C*H*$_3$)$_2$), 3.80 (s, 3H; OC*H*$_3$), 6.60 (d, $^3J_{H–H}$ = 7.9 Hz, 2H; Ar*H*), 6.85 (dd, $^3J_{H–H}$ = 9.1 Hz, $^3J_{H–P}$ = 2.6 Hz, 2H; Ar*H*), 8.10–8.15 (m, 2H; Ar*H*), 9.10–9.14 (m, 2H; Ar*H*).

^{13}C{^{1}H} NMR (125 MHz, $CDCl_3$): δ (ppm) 40.34 (s; N(*C*H$_3$)$_2$), 55.54 (s; OCH$_3$), 106.01 (d, $^3J_{C–P}$ = 4.0 Hz; Ar*C*), 113.41 (d, $^2J_{C–P}$ = 15.5 Hz; Ar*C*), 132.76 (d, $^2J_{C–P}$ = 14.5 Hz; Ar*C*), 132.98 (d, $^1J_{C–P}$ = 101.5 Hz; Ar*C*), 141.12 (d, $^3J_{C–P}$ = 6.0 Hz; Ar*C*), 156.46 (s; Ar*C*), 161.96 (d, $^4J_{C–P}$ = 3.1 Hz; Ar*C*).

^{31}P NMR (202 MHz, $CDCl_3$): δ (ppm) 109.4 (s).

^{31}P{^{1}H} NMR (202 MHz, $CDCl_3$): δ (ppm) 109.4 (s).

6.5.5 Synthesis of 24 from 12

To a solid mixture of **12** (30 mg, 0.025 mmol, 1.00 eq.) and Woollin's reagent (26 mg, 0.049 mmol, 2 eq.), benzene (0.5 mL) was added. The mixture was stirred overnight at room temperature, and monitored with ^{31}P{^{1}H} NMR spectrum. Once compound **12** is fully consumed, the mixture is filtered, and MeCN (20 ml) was added to the filtrate. The mixture was left in a –35 °C freezer overnight to crystalize. Supernatant was removed and the resulting solid was dried *in vacuo* to afford **24** (31 mg, 0.020 mmol; 82% yield) as a bright-yellow powder. Single crystals of **24** suitable for X-ray diffraction were obtained by slow evaporation of a concentrated hexane solution of **24** under room temperature.

^{1}H NMR (500 MHz, C_6D_6): (accurate integration is not possible due to extensive overlapping with residual compound **25** and other unidentified impurity) δ (ppm) 1.11 (d, $^{3}J_{H–H}$ = 6.9 Hz, 18H; CH(C*H*$_3$)$_2$), 1.17 (d, $^{3}J_{H–H}$ = 6.9 Hz, 18H; CH(C*H*$_3$)$_2$), 1.24–1.30 (m, 36H; CH(C*H*$_3$)$_2$), 2.85 (sept, $^{3}J_{H–H}$ = 6.9 Hz, 4H; C*H*(CH$_3$)$_2$), 3.01–3.14 (m, 8H; C*H*(CH$_3$)$_2$), 5.53 (s, 2H; NC*H*$_2$Ph), 6.69–6.75 (m, 3H; Ar*H*), 6.97–7.02 (m, 3H; Ar*H*), 7.16 (s, overlapping with C_6D_6, 8H; Ar*H*), 7.18 (d, $^{4}J_{H–H}$ = 1.7 Hz, 2H; Ar*H*), 7.20 (d, $^{4}J_{H–H}$ = 1.7 Hz, 2H; Ar*H*), 7.25 (t, $^{4}J_{H–H}$ = 1.7 Hz, 2H; Ar*H*), 7.29 (d, $^{3}J_{H–H}$ = 7.7 Hz, 2H; Ar*H*), 7.53–7.58 (m, 3H; Ar*H*), 8.42 (dd, $^{3}J_{H–P}$ = 17.0 Hz $^{3}J_{H–H}$ = 7.2 Hz, 2H; Ar*H*).

^{13}C{^{1}H} NMR (125 MHz, C_6D_6): δ (ppm) 24.40, 24.44, 24.68, 25.04, 25.32 (s; CH(*C*H$_3$)$_2$), 30.77, 30.84, 30.90, 31.05, 31.11, 34.84, 34.88 (s; *C*H(CH$_3$)$_2$), 55.24 (br; N*C*H$_2$Ph), 120.71, 120.82, 120.96, 128.59, 129.63, 131.46, 131.56, 131.62, 131.82, 132.39, 136.26, 136.95, 137.05, 137.17, 137.38, 138.87 (d, $^{1}J_{C–P}$ = 25.3 Hz), 140.13, 140.88, 141.40, 141.54, 141.90, 142.40 (d, $^{2}J_{C–P}$ = 6.2 Hz) 143.84 (br), 146.79, 146.91, 146.96, 147.05, 147.10, 148.56, 148.63 (s; Ar*C*).

^{31}P NMR (202 MHz, C_6D_6): δ (ppm) –46.0 (dt, $^{3}J_{P–P}$ = 80.6 Hz $^{3}J_{P–H}$ = 17.0 Hz; PSe*P*(Se)Ar), 46.0 (d, $^{3}J_{P–P}$ = 80.6 Hz; PSe*P*(Se)Ar).

^{31}P{^{1}H} NMR (202 MHz, C_6D_6): δ (ppm) –46.0 (d, $^{3}J_{P–P}$ = 80.6 Hz; PSe*P*(Se)Ar), 46.0 (d, $^{3}J_{P–P}$ = 80.6 Hz; PSe*P*(Se)Ar).

HRMS (*m*/*z*): [M+H]$^{+}$ calcd. For $C_{91}H_{114}NP_2Se_3$, 1520.5925; found 1520.5954.

6.5.6 One-pot synthesis of 25

To a solid mixture of **12** (50 mg, 0.042 mmol, 1.00 eq.) and Woollin's reagent (40 mg, 0.075 mmol, 1.8 eq.), benzene (0.7 mL) was added. The mixture was stirred overnight at room temperature, and monitored with ^{31}P{^{1}H} NMR spectrum. Once compound **12** is fully consumed, the mixture is filtered, DMAP (20 mg, 0.164 mmol, 3.9 eq.) was added to the

filtrate. After stirring the mixture for 30 min at room temperature, formation of precipitate was observed. The mixture is filtered again, and MeCN (20 ml) was added to the filtrate. The mixture was left in a –35 °C freezer overnight to crystalize. Supernatant was removed and the resulting solid was dried *in vacuo* to afford **25** (42 mg, 0.033 mmol; 80% yield) as a light-red powder. Single crystals of **25** suitable for X-ray diffraction were obtained by slow evaporation of a concentrated hexane solution of **25** under room temperature.

^{1}H NMR (500 MHz, C_6D_6): (accurate integration is not possible due to extensive overlapping with **25**-*cis*) δ (ppm) 1.15 (d, $^{3}J_{H–H}$ = 6.8 Hz, 12H; CH(CH_3)$_2$), 1.18 (d, $^{3}J_{H–H}$ = 6.8 Hz, 12H; CH(CH_3)$_2$), 1.21 (d, $^{3}J_{H–H}$ = 6.8 Hz, 12H; CH(CH_3)$_2$), 1.28 (d, $^{3}J_{H–H}$ = 6.8 Hz, 24H; CH(CH_3)$_2$), 1.30–1.32 (m, 12H; CH(CH_3)$_2$), 2.86 (sept, $^{3}J_{H–H}$ = 6.8 Hz, 4H; CH(CH$_3$)$_2$), 2.92–3.07 (m, 8H; CH(CH$_3$)$_2$), 5.49 (s, 2H; NCH_2Ph), 6.61 (t, $^{3}J_{H–H}$ = 7.5 Hz, 2H; ArH), 6.72–6.75 (m, 2H; ArH), 6.79–6.81 (m, 1H; ArH), 6.94 (t, $^{3}J_{H–H}$ = 7.7 Hz, 1H; ArH), 7.09 (t, $^{4}J_{H–H}$ = 1.5 Hz, 2H; ArH), 7.16–7.17 (m, overlapping with C_6D_6, 8H; ArH), 7.19 (d, $^{4}J_{H–H}$ = 1.5 Hz, 4H; ArH), 7.29 (d, $^{3}J_{H–H}$ = 7.7 Hz, 2H; ArH).

^{13}C{^{1}H} NMR (125 MHz, C_6D_6): δ (ppm) 24.17, 24.41, 24.45, 24.71, 24.81, 25.05, 25.10 (s; CH(*C*H$_3$)$_2$), 30.84, 30.86, 30.95, 31.01, 31.11, 34.88 (s; *C*H(CH$_3$)$_2$), 54.14 (br; N*C*H$_2$Ph), 120.71, 120.80, 128.77, 129.01, 129.35, 130.55, 131.23, 131.38, 131.83, 132.05, 135.47, 137.05, 137.23, 139.80, 140.15, 140.54, 140.71, 141.54, 141.90, 146.77, 146.80, 146.86, 146.91, 148.49, 148.59 (s; Ar*C*).

^{31}P{^{1}H} NMR (202 MHz, C_6D_6): δ (ppm) 535.4 (s, $^{1}J_{P–Se}$ = 788.1 Hz; **25**-*trans*), 528.6 (s; **25**-*cis*) **25**-*trans*:**25**-*cis* = 4.81:1.

^{77}Se NMR (95.4 MHz, d8-Tol, –45 °C): δ (ppm) 1081.62 (d, $^{1}J_{P–Se}$ = 875.03 Hz; **25**-*trans*).

HRMS (*m*/*z*): [M+H]$^{+}$ calcd. For $C_{85}H_{109}NPSe$, 1254.7457; found 1254.7473.

6.5.7 Synthesis of 24 from 25

To a solid mixture of **25** (10 mg, 0.0080 mmol, 1.00 eq.) and Woollin's reagent (10 mg, 0.019 mmol, 2.3 eq.), benzene (0.5 mL) was added. The mixture was stirred overnight at room temperature, and monitored with $^{31}P\{^{1}H\}$ NMR spectrum. Once compound **25** is fully consumed, the mixture is filtered, and MeCN (20 ml) was added to the filtrate. The mixture was left in a –35 °C freezer overnight to crystalize. Supernatant was removed and the resulting solid was dried *in vacuo* to afford **24** (9 mg, 0.0059 mmol; 74% yield) as a bright-yellow powder. All characteristic data is identical to previously reported data.

6.6 References

[1] G. Fritz, T. Vaahs, H. Fleischer, E. Matern, *Angew. Chem., Int. Ed. Engl.* **1989**, *28*, 315−316.

[2] F. Mathey, *Angew. Chem., Int. Ed. Engl.* **1987**, *26*, 275−286.

[3] X. Li, S. I. Weissman, T.-S. Lin, P. P. Gaspar, A. H. Cowley, A. I. Smirnov, *J. Am. Chem. Soc.* **1994**, *116*, 7899−7900.

[4] S. Shah, M. C. Simpson, R. C. Smith, J. D. Protasiewicz, *J. Am. Chem. Soc.* **2001**, *123*, 6925−6926.

[5] A. H. Cowley, *Acc. Chem. Res.* **1997**, *30*, 445−451.

[6] K. Lammertsma, Mark J. M. Vlaar, *Eur. J. Org. Chem* **2002**, *2002*, 1127−1138.

[7] K. Lammertsma, in *New Aspects in Phosphorus Chemistry III* (Ed.: J.-P. Majoral), Springer Berlin Heidelberg, Berlin, Heidelberg, **2003**, pp. 95-119.

[8] F. Mathey, *Dalton Trans.* **2007**, 1861−1868.

[9] H. Aktaş, J. C. Slootweg, K. Lammertsma, *Angew. Chem. Int. Ed.* **2010**, *49*, 2102−2113.

[10] L. Liu, David A. Ruiz, D. Munz, G. Bertrand, *Chem* **2016**, *1*, 147−153.

[11] M. C. Neben, N. Wegerich, T. A. Al Said, R. R. Thompson, S. Demeshko, K. Dollberg, I. Tkach, G. P. Van Trieste, III, H. Verplancke, C. von Hänisch, M. C. Holthausen, D. C. Powers, A. Schnegg, S. Schneider, *J. Am. Chem. Soc.* **2025**.

[12] Q. Luo, T. Liu, L. Huang, C. Yang, W. Lu, *Angew. Chem. Int. Ed.* **2024**, *63*, e202405122.

[13] P. P. Gaspar, H. Qian, A. M. Beatty, D. A. d'Avignon, J. L. F. Kao, J. C. Watt, N. P. Rath, *Tetrahedron* **2000**, *56*, 105−119.

[14] C. M. E. Graham, C. L. B. Macdonald, P. D. Boyle, J. A. Wisner, P. J. Ragogna, *Chem. Eur. J.* **2018**, *24*, 743−749.

[15] C. Hu, N. H. Rees, M. Pink, J. M. Goicoechea, *Nat. Chem.* **2024**, *16*, 1855−1860.

[16] A. Mardyukov, F. Keul, P. R. Schreiner, *Angew. Chem. Int. Ed.* **2020**, *59*, 12445−12449.

[17] P. P. Gaspar, A. M. Beatty, X. Li, H. Qian, N. P. Rath, J. C. Watt, *Phosphorus, Sulfur, Silicon Relat. Elem.* **1999**, *144*, 277−280.

[18] C. M. E. Graham, T. E. Pritchard, P. D. Boyle, J. Valjus, H. M. Tuononen, P. J. Ragogna, *Angew. Chem. Int. Ed.* **2017**, *56*, 6236−6240.

[19] W. J. Transue, M. Nava, M. W. Terban, J. Yang, M. W. Greenberg, G. Wu, E. S. Foreman, C. L. Mustoe, P. Kennepohl, J. S. Owen, S. J. L. Billinge, H. J. Kulik, C. C. Cummins, *J. Am. Chem. Soc.* **2019**, *141*, 431−440.

[20] L. Wang, R. Ganguly, F. Mathey, *Organometallics* **2014**, *33*, 5614−5617.

[21] S. Nakayama, M. Yoshifuji, R. Okazaki, N. Inamoto, *J. Chem. Soc. D* **1971**, 1186−1187.

[22] H. Tomioka, S. Takata, Y. Kato, Y. Izawa, *J. Chem. Soc., Perkin Trans. 2* **1980**, 1017−1021.

[23] S. Nakayama, M. Yoshifuji, R. Okazaki, N. Inamoto, *Bull. Chem. Soc. Jpn.* **2006**, *48*, 546−548.

[24] S. Holand, F. Mathey, *J. Org. Chem.* **1981**, *46*, 4386−4389.

[25] H. Tomioka, S. Miura, Y. Izawa, *Tetrahedron Lett.* **1983**, *24*, 3353−3356.

[26] C. C. Santini, J. Fischer, F. Mathey, A. Mitschler, *J. Am. Chem. Soc.* **1980**, *102*, 5809−5815.

[27] T. Ozturk, E. Ertas, O. Mert, *Chem. Rev.* **2007**, *107*, 5210−5278.

[28] C. J. Carmalt, *Chem. Commun.* **1998**, 243−244.

[29] E. Soleimani, K. N. Robertson, C. C. Pye, J. A. C. Clyburne, *Dalton Trans.* **2018**, *47*, 6299−6303.

[30] L. E. English, A. Pajak, C. L. McMullin, J. P. Lowe, M. F. Mahon, D. J. Liptrot, *Chem. Eur. J.* **2022**, *28*, e202200376.

[31] P. Pyykkö, M. Atsumi, *Chem. Eur. J.* **2009**, *15*, 12770−12779.

[32] C. Foces-Foces, A. L. Llamas-Saiz, *Acta Crystallogr. C* **1998**, *54*.

[33] P. Royla, K. Schwedtmann, Z. Han, J. Fidelius, D. P. Gates, R. M. Gomila, A. Frontera, J. J. Weigand, *J. Am. Chem. Soc.* **2023**, *145* (18), 10364–10375.

[34] R. Appel, U. Kündgen, F. Knoch, *Chem. Ber.* **1985**, *118* (4), 1352–1370.

[35] E. Niecke, D. Gudat, *Angew. Chem., Int. Ed. Engl.* **1991**, *30* (3), 217–237.

[36] J. V. X. da Silva, I. C. Chipoline, S. B. Ferreira, *SynOpen* **2024**, *08*, 223−231.

[37] L. Ascherl, A. Nordheider, K. S. A. Arachchige, D. B. Cordes, K. Karaghiosoff, M. Bühl, A. M. Z. Slawin, J. D. Woollins, *Chem. Commun.* **2014**, *50*, 6214−6216.

[38] P. W. Codding, K. A. Kerr, *Acta Crystallogr. B* **1979**, *35*, 1261−1263.

Chapter 7
Conclusions and Future Work

7.1 Conclusions

This thesis explored the concept of using electrostatic repulsion to stabilize compounds with multiple bonds between the heavier main group elements. The synthesis of two novel phosphorus-containing anionic compounds is described: the cyapho(dicyano)methanide salt $[C(CN)_2CP]^-$, and the anionic imine supported phosphinidene oxide $ArNPO^-$.

(Cyapho)dicyano-methanide $[C(CN)_2CP]^-$ was synthesized from the reaction of 1,1-diethoxy-2,2-dicyanoethylene $(EtO)_2C=C(CN)_2$ with [Na(18-crown-6)][PH_2]. An intermediate, $[HP\{C(OEt)=C(CN)_2\}]^-$, was isolated after the first Michael addition-elimination step, and with the help of a non-nucleophilic base (KHMDS), this intermediate could further be converted to the target anion. DFT calculations revealed that the cyaphide moiety is just as (if not more) effective at negative charge stabilization than a nitrile group. The parent acid, (cyapho)dicyanomethane could also be synthesized and characterized at −60 °C by multi-element NMR spectroscopic studies. Further reactivities studies indicated that the cyapho moiety adopted phosphaalkyne-like reactivities.

After the successful synthesis of a cyapho(dicyano)methanide salt, we applied both an electrostatic repulsion stabilization strategy and steric protection to the synthesis of a phosphinidene oxide, which contains one of the most challenging main group element multiple bonds. The imine supported phosphinidene oxide $ArNPO^-$ was synthesized by the reaction of chloro(imino)phosphane ArNPCl and excess KOTMS. As the heavier analogue of NO_2^-, a three-center-four-electron (3c-4e) interaction was detected within the N–P–O moiety through crystallographic analysis and DFT calculations.

Selective functionalization was achieved for all three atoms in the N–P–O moiety. When reacting with small electrophiles such as BnBr, the nitrogen atom is functionalized, affording an amino phosphinidene oxide. Alternatively, when reacted with a bulky silyl

group, *O*-functionalization occurs. Oxidants selectively react with the phosphorus(III) center, leading to phosphorus(V) compounds. The *N*-functionalized amino phosphinidene oxide was found to adopt a similar electronic structure to its lighter isolobal analogue, organo-amides.

Based on the isolobal relationship between organo-amides and an amino phosphinidene oxide, the phospha-(aza)-Wittig reaction was proposed. Our amino phosphinidene oxide was found to be able to replace the role of carbonyl compounds in Wittig reactions and react with phosphorus ylides, affording the corresponding phosphaalkenes or phosphaimines. This reaction showed the potential of our phosphinidene oxide as a phosphinidene synthon through double bond metathesis.

The use of an amino phosphinidene oxide as phosphinidene synthon was further explored. Through double bond metathesis with Lawesson's or Woollin's reagents, a dimer between phosphinidene sulfide or selenide and a monomer of LR or WR was isolated. Addition of DMAP leads to the cleavage of the dimer, affording the phosphinidene chalcogenide monomers. These two compounds represent the first isolated acid- or base-free P(III)=S and P(III)=Se double bonds.

7.2 Future work

The isolation of a phosphinidene sulfide and selenide proved that the amino phosphinidene oxide is a versatile phosphinidene transfer reagent through double bond metathesis. More underexplored main group multiple bonding can be expected from such double bond metathesis.

A phosphinidene telluride is the only compound left that has not been characterized in the phosphinidene chalcogen family using our *meta*-substituted terphenyl ligand. Due to the

lack of a phosphorus(V) telluride reagent such as Lowesson's reagent and Woollin's reagent, we cannot replicate the reaction of the synthesis of phosphinidene sulfide and selenide.

However, looking back at the phospha-Wittig reaction, while the phosphorus ylide is able to react with a phosphinidene oxide because of its high nucleophilicity, the phosphine sulfide is inert towards the phosphinidene oxide, as the P=S bond in $Ph_3P=S$ is not polar enough. We postulate that using a more nucleophilic chalcogenide reagent with polar E=Ch and an oxophilic E center would facilitate the exchange between P=O and E=Ch. As silicon fits both requirement for such E=Ch reagent, the silylene chalcogenide shown in Scheme 7.1 may be used for the synthesis of phosphinidene telluride through double bond metathesis.

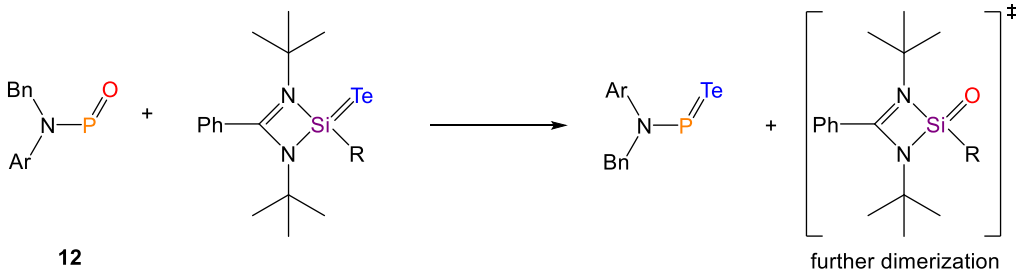

Scheme 7.1. Proposed reaction to access a phosphinidene telluride.

Several reasons led us to choose Roesky's amidinate ligand stablized silylene as candidate. Firstly, this silylene platform is well-established, and the synthesis of the silylene telluride is reported.[1] Secondly, the silicon center is relatively naked compared to other reported silylenes, which makes it feasable for the Si=Te double bond to fit in the pocket of our *meta*-substituted terphenyl ligand and react with the P=O double bond. Lastly, if the reaction were to proceed as expected, a silylene oxide would be formed, which happens to be a reported compound. Due to the high polarity of such Si=O double bond, the amidinate silylene oxide is not stable and undergoes dimerization.[2]

Since our *meta*-substituted terphenyl ligand demostrated great potential in proventing dimerization or oligomerization of species with multiple bonds between heavier main group elements, it would also be disirable to use such ligand to stablize other highly reactive main

group multiple bonds with terminal atoms. For example, arsenidene oxide may be synthesized through a similar route to the phosphinidene oxide. Another interesting target would be an anionic borylene oxide, $ArN{=}B{=}O^{-}$, which is isoelectronic to carbon dioxide CO_2. Recent research indicated another isoelectronic counterpart of such structure, $[RN{=}B{=}NR]^{-}$ is isolable,[3] further supporting that anionic borylene oxide $ArN{=}B{=}O^{-}$ can also be synthesized, through the right conditions.

7.3 Publications

The work contained in this thesis can be found in the following publications:

1. C. Hu, J. M. Goicoechea, *Angew. Chem. Int. Ed.* **2022**, *61*, e202208921.
2. C. Hu, N. H. Rees, M. Pink, J. M. Goicoechea, *Nat. Chem.* **2024**, *16*, 1855–1860.

A further publication is currently under review, and two manuscripts are in preparation.

7.4 References

[1] Y. -C. Chan, Y. Li, R. Ganguly, C.-W. *Eur. J. Inorg. Chem.* **2015**, *23*, 3821–3824.

[2] R. Azhakar, K. Pröpper, B. Dittrich, H. W. Roesky, *Organometallics* **2012**, *31*, 7586–7590.

[3] J. Tang, C. Hu, A. E. Crumpton, M. Dietz, D. Sarkar, L. P. Griffin, J. M. Goicoechea, S. Aldridge, *J. Am. Chem. Soc.* **2024**, *146*, 30778–30783.

Chapter 8
Experimental Details

8.1 General synthetic procedures

All reactions and product manipulations were carried out under an inert atmosphere of argon or dinitrogen using standard Schlenk or glovebox techniques (MBraun UNILab glovebox maintained at <0.1 ppm O_2 and <0.1 ppm H_2O) unless otherwise noted.

Tetrahydrofuran (THF; Fisher, HPLC grade), diethyl ether (Et_2O; Fisher, pesticide residue grade), and 1,4-dioxane (Alfa Aesar, 99+%, stab. 5-10 ppm BHT) were distilled from a sodium/benzophenone mixture. Pyridine (Alfa Aesar, 99+%) and 1,2-difluorobenzene (1,2-DFB; Fluorochem, 98%) were distilled from CaH_2. Hexane (Sigma Aldrich, HPLC grade), pentane (Sigma Aldrich, HPLC grade) and toluene (Sigma Aldrich, HPLC grade) were purified using an MBraun SPS-800 solvent system. d_8-THF (Eurisotop, >99.5%), d_5-pyridine (Eurisotop, >99.5%) were dried over CaH_2, vacuum distilled, and degassed before use. D_8-toluene (tol; Alfa Aesar, 99% (isotopic)) was dried over activated 3 Å molecular sieves and degassed before use. All dry solvents were stored under argon in gas-tight ampoules over 3 Å molecular sieves. Deionised water was obtained from a Millipore Milli-Q machine.

The following compounds were prepared according to literature procedures: [Na(18-crown-6)][PH_2],[1] $(EtO)_2C=C(CN)_2$,[2] [Ni(COD)(^{Me}IPr)$_2$],[3] Brookhart's acid [$H(OEt_2)]_2$][$BAr^F{}_4$] ($BAr^F{}_4$ = B{$C_6H_3(CF_3)_2$}$_4$),[4] 5′-Bromo-2,2″,4,4″,6,6″-hexakis(1-methylethyl)-1,1′:3′,1″-terphenyl (HIPTBr),[5] Benzylpotassium BzK,[6] $CH_2=PPh_3$ and $CH_3CH=PPh_3$,[7] MeN=PPh_3.[8]

8.2 Characterisation techniques

8.2.1 Single crystal X-ray diffraction

Single-crystal X-ray diffraction data for compounds from Chapter 2–4 were collected using an Oxford Diffraction Supernova dual-source diffractometer equipped with a 135 mm Atlas CCD area detector. Crystals were selected under Fomblin-y oil, mounted on micromount loops and quench-cooled using an Oxford Cryosystems open flow N_2 cooling device. Data were collected at 150 K using mirror monochromated Cu Kα radiation (λ = 1.5418 Å; Oxford Diffraction Supernova) and processed using the CrysAlisPro package, including unit cell parameter refinement and inter-frame scaling (which was carried out using SCALE3 ABSPACK within CrysAlisPro).[9] Equivalent reflections were merged and diffraction patterns processed with the CrysAlisPro suite.

Single-crystal X-ray diffraction data for compounds from Chapter 5–6 were collected using a Bruker Venture D8 diffractometer equipped with a PhotonIII detector at 123 or 173 K. The data collection was carried out using Cu Kα radiation (multilayer mirror monochromator) with various frame times (between 1 and 80 seconds) and a detector distance of 4.00 cm. A collection strategy was calculated and complete data to a resolution of 0.83 Å (twelve sets of frames) were collected with 0.5 or 1º ω and ϕ scans. The frames were integrated with the SAINT V8.41 package using a narrow-frame algorithm.[10] The final cell constants are based upon the refinement of the XYZ-centroids of observed reflections. Data were corrected for absorption effects using the Multi-Scan method in SADABS 2016/2.[11] The calculated minimum and maximum transmission coefficients (based on crystal size) were calculated.

Structures were subsequently solved using direct methods and refined on F^2 using the SHELXL package.[12–14]

Table 8.1. Selected X-ray data collection/refinement parameters for [Na(18-crown-6)]**1**·THF, [K(18-crown-6)]**2**·THF, [K(18-crown-6)]**4**·1.5tol and [K(18-crown-6)]**5**.

	[Na(18-crown-6)]**1**·THF	[K(18-crown-6)]**2**·THF	[K(18-crown-6)]**4**·1.5tol	[K(18-crown-6)]**5**
Formula	$C_{22}H_{38}N_2NaO_8P$	$C_{20}H_{32}KN_2O_7P$	$C_{48.5}H_{76}KN_6NiO_6P$	$C_{26}H_{39}KN_5O_6P$
CCDC	2179806	2179807	2179808	2179809
Fw [g mol^{-1}]	512.50	482.54	967.93	587.69
Crystal system	triclinic	triclinic	monoclinic	triclinic
Space group	$P\bar{1}$	$P\bar{1}$	$P2_1/n$	$P\bar{1}$
a (Å)	9.0861(3)	8.0042(5)	11.1847(1)	10.1564(3)
b (Å)	9.1743(3)	9.8316(4)	33.9741(2)	10.7107(3)
c (Å)	16.4208(4)	16.1020(8)	13.9174(1)	15.3083(4)
α (°)	87.976(2)	95.380(4)	90	75.303(2)
β (°)	82.419(2)	100.530(4)	91.247(1)	82.672(2)
γ (°)	89.177(2)	91.780(4)	90	65.466(3)
V (Å^3)	1355.94(7)	1238.80(11)	5287.22(7)	1464.89(8)
Z	2	2	4	2
Radiation, λ (Å)	Cu Kα, 1.54184	Cu Kα, 1.54184	Cu Kα, 1.54184	Cu Kα, 1.54184
Temp (K)	150(2)	150(2)	150(2)	150(2)
ρ_{calc} (g cm^{-3})	1.255	1.294	1.216	1.332
μ (mm^{-1})	1.446	2.837	1.915	2.503
Reflections collected	31042	21813	92959	31548
Independent reflections	5617	5658	10987	6082
Parameters	312	353	650	439
R(int)	0.0389	0.0424	0.0458	0.0315
R1/wR2, $I \geq 2\sigma I$ (%)	4.34/12.27	4.39/10.04	3.16/8.54	3.00/7.47
R1/wR2, all data (%)	5.23/13.08	6.69/11.21	3.66/8.93	3.50/7.86
GOF	1.064	1.040	1.031	1.037

Table 8.2. Selected X-ray data collection/refinement parameters for **9**, **10**, **11** and **12**.

	9	**10**	**11**	**12**
Formula	$C_{84}H_{115}ClNP$	$C_{104}H_{141}KNO_7P$	$C_{106}H_{159}KNO_{10}P$	$C_{88}H_{115}NOP$
CCDC	2339507	2339509	2339508	2339510
Fw [g mol^{-1}]	1205.18	1587.24	1677.40	1233.77
Crystal system	triclinic	monoclinic	monoclinic	triclinic
Space group	$P\bar{1}$	$P2_1/c$	Cc	$P\bar{1}$
a (Å)	10.8284(2)	12.6495(2)	18.3672(1)	17.9057(8)
b (Å)	17.3676(4)	19.3622(3)	20.3124(1)	18.2358(8)
c (Å)	21.7267(4)	40.1290(6)	28.4218(1)	28.0067(15)
α (°)	76.291(2)	90	90	83.449(4)
β (°)	89.186(2)	98.989(2)	108.357(1)	77.074(4)
γ (°)	81.360(2)	90	90	68.082(4)
V (Å^3)	3923.57(14)	9707.8(3)	10064.06(10)	8264.2(7)
Z	2	4	4	4
Radiation, λ (Å)	Cu Kα, 1.54184	Cu Kα, 1.54184	Cu Kα, 1.54184	Cu Kα, 1.54184
Temp (K)	150(2)	150(2)	150(2)	150(2)
ρ_{calc} (g cm^{-3})	1.020	1.086	1.107	0.992
μ (mm^{-1})	0.913	1.031	1.038	0.597
Reflections collected	86968	88768	131464	38711
Independent reflections	16297	20094	20225	17754
Parameters	918	1241	1215	1748
R(int)	0.0380	0.0718	0.0245	0.0882
R1/wR2, I ≥ 2σI (%)	7.75/22.89	5.95/15.30	5.13/13.59	10.59/24.40
R1/wR2, all data (%)	9.35/24.76	9.17/18.13	5.25/13.72	23.73/29.80
GOF	1.040	1.023	1.060	0.952

Table 8.3. Selected X-ray data collection/refinement parameters for **13**, **14**, **15** and **16**.

	13	**14**	**15**	**16**
Formula	$C_{93}H_{136}NOPSi$	$C_{118}H_{142}N_2O_3P_3$	$C_{96}H_{139}I_2KNO_7P$	$C_{138}H_{165}N_2O_4P_3Se_2$
CCDC	2339511	2339512	2339513	2339514
Fw [g mol^{-1}]	1343.08	1729.24	1742.94	2166.54
Crystal system	triclinic	monoclinic	monoclinic	orthorhombic
Space group	$P\bar{1}$	$P2_1/c$	$P2_1/n$	$P2_12_12_1$
a (Å)	10.9370(4)	20.0566(2)	22.1567(6)	11.6624(1)
b (Å)	19.8302(9)	34.5871(3)	12.4108(4)	29.5823(1)
c (Å)	21.5571(8)	17.4123(1)	36.1453(11)	35.2891(1)
α (°)	76.643(4)	90	90	90
β (°)	83.450(3)	97.495(1)	103.880(3)	90
γ (°)	74.530(4)	90	90	90
V (Å^3)	4377.2(3)	11975.71(17)	9649.1(5)	12174.76(12)
Z	2	4	4	4
Radiation, λ (Å)	Cu Kα, 1.54184	Cu Kα, 1.54184	Cu Kα, 1.54184	Cu Kα, 1.54184
Temp (K)	150(2)	150(2)	150(2)	150(2)
ρ_{calc} (g cm^{-3})	1.019	0.959	1.200	1.182
μ (mm^{-1})	0.721	0.788	6.040	1.535
Reflections collected	73507	150324	157402	307967
Independent reflections	18081	24932	17019	25427
Parameters	1024	1265	1033	1554
R(int)	0.0726	0.0543	0.1713	0.0486
R1/wR2, I ≥ 2σI (%)	6.75/17.71	8.56/23.08	7.82/20.96	3.74/9.86
R1/wR2, all data (%)	11.25/21.09	10.08/24.32	10.06/22.64	3.88/9.99
GOF	1.024	1.081	1.040	1.067

Table 8.4. Selected X-ray data collection/refinement parameters for **17**, **18**, **19** and **21**.

	17	**18**	**19**	**21**
Formula	$C_{86}H_{109}NP$	$C_{87}H_{112}NP$	$C_{86}H_{111}N_2P$	$C_{92}H_{129}NO_{2.5}P_2$
CCDC	2424217	2424218	2424219	2424220
Fw [g mol^{-1}]	1187.71	1202.74	1203.73	1350.89
Crystal system	monoclinic	monoclinic	monoclinic	triclinic
Space group	*C2/c*	$P2_1/n$	$P2_1/n$	$P\bar{1}$
a (Å)	33.8379(10)	22.2964(2)	22.268(4)	12.8556(5)
b (Å)	13.0435(3)	15.59490(10)	15.567(3)	22.1688(9)
c (Å)	38.1134(12)	24.0387(2)	24.034(5)	34.4367(13)
α (°)	90	90	90	108.431(3)
β (°)	105.491(3)	94.5805(5)	94.473(11)	93.443(2)
γ (°)	90	90	90	97.050(2)
V (Å^3)	16210.8(8)	8331.80(12)	8306(3)	9189.3(6)
Z	8	4	4	4
Radiation, λ (Å)	Cu Kα, 1.54184	Cu Kα, 1.54184	Cu Kα, 1.54184	Cu Kα, 1.54184
Temp (K)	173(2)	173(2)	173(2)	123(2)
ρ_{calc} (g cm^{-3})	0.973	0.959	0.963	0.976
μ (mm^{-1})	0.585	0.574	0.579	0.742
Reflections collected	155684	118502	104240	149510
Independent reflections	14842	15168	15203	33372
Parameters	947	868	893	1926
R(int)	0.1068	0.1333	0.1110	0.1488
R1/wR2, I ≥ 2σI (%)	7.96/21.76	7.77/21.40	6.42/17.36	10.56/21.76
R1/wR2, all data (%)	8.96/22.99	9.43/22.79	7.68/18.70	15.49/24.40
GOF	1.035	1.037	1.029	1.088

Table 8.5. Selected X-ray data collection/refinement parameters for **22**, **23**, **24** and **25**.

	22	**23**	**24**	**25**
Formula	$C_{92}H_{115}NOP_2S_3$	$C_{85}H_{108}NPS$	$C_{92}H_{113}NP_2Se_3$	$C_{85}H_{108}NPSe$
CCDC	N.A.	N.A.	N.A.	N.A.
Fw [g mol^{-1}]	1408.46	1206.75	1531.14	1253.65
Crystal system	trigonal	monoclinic	trigonal	monoclinic
Space group	$R\bar{3}$	$P2_1$	$R\bar{3}$	$P2_1$
a (Å)	62.7993(16)	15.2779(7)	62.496(4)	15.2938(5)
b (Å)	62.7993(16)	15.5539(8)	62.496(4)	15.5419(6)
c (Å)	13.0734(5)	16.9138(8)	13.0753(7)	16.9381(7)
α (°)	90	90	90	90
β (°)	90	92.609(3)	90	92.737(2)
γ (°)	120	90	120	90
V (Å^3)	44651(3)	4015.1(3)	44228(6)	4021.5(3)
Z	18	2	18	2
Radiation, λ (Å)	Cu Kα, 1.54184	Cu Kα, 1.54184	Cu Kα, 1.54184	Cu Kα, 1.54184
Temp (K)	173(2)	173(2)	173(2)	173(2)
ρ_{calc} (g cm^{-3})	0.943	0.998	1.035	1.035
μ (mm^{-1})	1.270	0.834	1.944	1.107
Reflections collected	129694	69244	239336	49746
Independent reflections	18214	14702	18085	14027
Parameters	1059	817	1046	817
R(int)	0.0877	0.0929	0.2789	0.0937
R1/wR2, I ≥ 2σI (%)	17.37/49.27	5.68/15.24	17.95/46.13	7.19/19.04
R1/wR2, all data (%)	19.38/51.60	6.15/15.78	24.07/50.23	7.94/20.02
GOF	2.238	1.0071	1.746	1.042

8.2.2 NMR spectroscopy

NMR spectra were acquired on a Bruker NEO 600 MHz NMR spectrometers (^{1}H 600 MHz, ^{13}C 150 MHz, ^{31}P 243 MHz), Bruker AVIII 500 MHz NMR spectrometer (^{1}H 500 MHz, ^{13}C 125 MHz, ^{31}P 202 MHz, ^{77}Se 95 MHz), Bruker AVIII 400 MHz NMR spectrometer (^{1}H 400 MHz, ^{31}P 162 MHz), Bruker 500 MHz Avance Neo spectrometer (^{1}H 500 MHz, ^{13}C 125 MHz, ^{31}P 202 MHz) and a Varian 500 MHz Inova spectrometer (^{1}H 500 MHz, ^{31}P 202 MHz, ^{77}Se 95 MHz). ^{1}H and ^{13}C NMR spectra were referenced to the most downfield solvent resonance (^{1}H NMR C_6D_6: δ (ppm) 7.16 ppm; ^{13}C NMR C_6D_6: δ (ppm) 188.06 ppm, ^{1}H NMR d_8-toluene: δ = 2.08 ppm). ^{31}P, ^{77}Se spectra were externally referenced to an 85% solution of H_3PO_4 in H_2O, and Me_2Se respectively.

8.2.3 Elemental analysis

Elemental analysis were carried out by Elemental Microanalyses Ltd. (Devon, U.K.) or London Metropolitan University. Samples (approx. 5 mg) were submitted in sealed Pyrex ampoules.

8.2.4 IR spectroscopy

IR data were obtained by using Fourier Transform Infrared Spectroscopy (FTIR) method, spectra were recorded on a Shimadzu Plastic Analyzer spectrometer.

8.2.5 High-resolution Mass spectroscopy

High-resolution mass spectra were recorded on a Thermo Q-Exactive Plus (ESI-TOF, positive ion mode) instrument at the Mass Spectrometry Facility of the Department of Chemistry of Indiana University.

8.2.6 Computational detail

Geometry optimizations were carried out using the Gaussian 16 package with the M06-2X functional.[15,16] The def2-SVP basis set was used for all the atoms.[17,18] Frequency calculations at the same level of theory were performed to identify the number of imaginary frequencies (zero for local minimum and one for transition states), and provide the thermal corrections of Gibbs free energy. Single-point energy calculations were performed at the M06-2X/def2-TZVP level of theory for the modelling of compounds in corresponding solution. The gas-phase geometry was used for all the solution phase calculations. The SMD method was used with the corresponding solvent, while Bondi radii were chosen as the atomic radii to define the molecular cavity.[19] The corrections of Gibbs free energy from frequency calculations were added to the single-point energies to obtain the Gibbs free energy in solution. All the energies reported in the paper correspond to the reference state of 1 mol L^{-1}, 298 K. Natural bond orbital (NBO) calculations were carried out using NBO 7.0 program at the M06-2X/def2-TZVP level of theory for Chapter 2, and at the M06-2X/def2-SVP level of theory for Chapter 3-6.[20] Natural Resonance Theory was used as implemented in NBO 7.0. Isotropic shifts for **3** were computed at the GIAO-PBE1PBE/6-311G(d,p)[21-25] level of theory using the phosphorus (−69.2 ppm) and carbon atoms (184.8 ppm) of ^{t}BuCP as reference.[26] No solvent corrections were applied. Optimized structures were visualized using Chemcraft.[27]

8.3 References

[1] D. Ergöçmen, J. M. Goicoechea, *Angew. Chem. Int. Ed.* **2021**, *60*, 25286−25289.

[2] F. Thétiot, S. Triki, J. S. Pala, C. J. Gómez-García, *J. Chem. Soc., Dalton Trans.* **2002**, 1687−1693.

[3] L. Tendera, M. Helm, M. J. Krahfuss, M. W. Kuntze-Fechner, U. Radius, *Chem. Eur. J.* **2021**, *27*, 17849−17861.

[4] M. Brookhart, B. Grant, A. F. Volpe, *Organometallics* **1992**, *11*, 3920−3922.

[5] D. V. Yandulov, R. R. Schrock, *J. Am. Chem. Soc.* **2002**, 124, 6252−6253.

[6] P. J. Bailey, R. A. Coxall, C. M. Dick, S. Fabre, L. C. Henderson, C. Herber, S. T. Liddle, D. Loroño-González, A. Parkin, S. Parsons, *Chem. Eur. J.* **2003**, 9, 4820−4828.

[7] W. J. Transue, J. Yang, M. Nava, I. V. Sergeyev, T. J. Barnum, M. C. McCarthy, C. C. Cummins, *J. Am. Chem. Soc.* **2018**, 140 (51), 17985−17991.

[8] H. Zimmer, G. Singh, *J. Org. Chem.* **1963**, 28 (2), 483−486.

[9] *CrysAlisPro*, Agilent Technologies, Version 1.171.35.8.

[10] SAINT V8.41 (2024), Bruker AXS, Madison, WI.

[11] L. Krause, R. Herbst-Irmer, G. M. Sheldrick, D. Stalke, *J. Appl. Cryst.* **2015**, *48*, 3–10.

[12] G. M. Sheldrick in SHELXL97, *Programs for Crystal Structure Analysis (Release 97-2)*, Institut für Anorganische Chemie der Universität, Tammanstrasse 4, D-3400 Göttingen, Germany, 1998;

[13] G. M. Sheldrick, *Acta Crystallogr. Sect. A Found. Crystallogr.* **2008**, *64*, 112–122.

[14] G. M. Sheldrick, *Acta Crystallogr. Sect. A* **1990**, *46*, 467–473.

[15] M. J. Frisch, G. W. Trucks, H. B. Schlegel, G. E. Scuseria, M. A. Robb, J. R. Cheeseman, G. Scalmani, V. Barone, G. A. Petersson, H. Nakatsuji, X. Li, M. Caricato, A. V. Marenich, J. Bloino, B. G. Janesko, R. Gomperts, B. Mennucci, H. P. Hratchian, J. V. Ortiz, A. F. Izmaylov, J. L. Sonnenberg, Williams, F. Ding, F.

Lipparini, F. Egidi, J. Goings, B. Peng, A. Petrone, T. Henderson, D. Ranasinghe, V. G. Zakrzewski, J. Gao, N. Rega, G. Zheng, W. Liang, M. Hada, M. Ehara, K. Toyota, R. Fukuda, J. Hasegawa, M. Ishida, T. Nakajima, Y. Honda, O. Kitao, H. Nakai, T. Vreven, K. Throssell, J. A. Montgomery Jr., J. E. Peralta, F. Ogliaro, M. J. Bearpark, J. J. Heyd, E. N. Brothers, K. N. Kudin, V. N. Staroverov, T. A. Keith, R. Kobayashi, J. Normand, K. Raghavachari, A. P. Rendell, J. C. Burant, S. S. Iyengar, J. Tomasi, M. Cossi, J. M. Millam, M. Klene, C. Adamo, R. Cammi, J. W. Ochterski, R. L. Martin, K. Morokuma, O. Farkas, J. B. Foresman, D. J. Fox, Wallingford, CT, **2016**.

[16] Y. Zhao, D. G. Truhlar, *Theor. Chem. Acc.* **2008**, *120*, 215−241.

[17] F. Weigend, *Phys. Chem. Chem. Phys.* **2006**, *8*, 1057−1065.

[18] F. Weigend, R. Ahlrichs, *Phys. Chem. Chem. Phys.* **2005**, *7*, 3297−3305.

[19] A. Bondi, *J. Phys. Chem.* **1964**, *68*.

[20] E. D. Glendening, J. K. Badenhoop, A. E. Reed, J. E. Carpenter, J. A. Bohmann, C. M. Morales, P. Karafiloglou, C. R. Landis, F. Weinhold, NBO 7.0, University of Wisconsin: Madison, WI, 2018.

[21] J. P. Perdew, K. Burke, M. Ernzerhof, *Phys. Rev. Lett.* **1997**, *78*, 1396−1396.

[22] J. P. Perdew, K. Burke, M. Ernzerhof, *Phys. Rev. Lett.* **1996**, *77*, 3865−3868.

[23] C. Adamo, V. Barone, *J. Chem. Phys.* **1999**, *110*, 6158−6170.

[24] A. D. McLean, G. S. Chandler, *J. Chem. Phys.* **1980**, *72*, 5639−5648.

[25] R. Krishnan, J. S. Binkley, R. Seeger, J. A. Pople, *J. Chem. Phys.* **1980**, *72*, 650−654.

[26] G. Becker, G. Gresser, W. Uhl, *Z. Naturforsch. B* **1981**, *36*, 16−19.

[27] Chemcraft − Graphical Software for Visualization of Quantum Chemistry Computations. https://www.chemcraftprog.com